

UNCLASSIFIED

Copy No. 122  
*Melvin K. Gough*

*Declassified per auth. RA 1/7/58*

*JSP 2/15/79*

# NATIONAL ADVISORY COMMITTEE FOR AERONAUTICS

*6505  
NACA-1947/4*

## NACA CONFERENCE ON AERODYNAMIC PROBLEMS OF TRANSONIC AIRPLANE DESIGN

### A COMPILATION OF THE PAPERS PRESENTED

Ames Aeronautical Laboratory  
Moffett Field, Calif.

November 5-6, 1947

(NASA-TN-804-2) NACA CONFERENCE ON AERODYNAMIC PROBLEMS OF TRANSONIC AIRPLANE DESIGN (National Advisory Committee for Aeronautics.) 281 p	N79-79427 THRU N79-79448 Unclas 00/01 35403
--	---



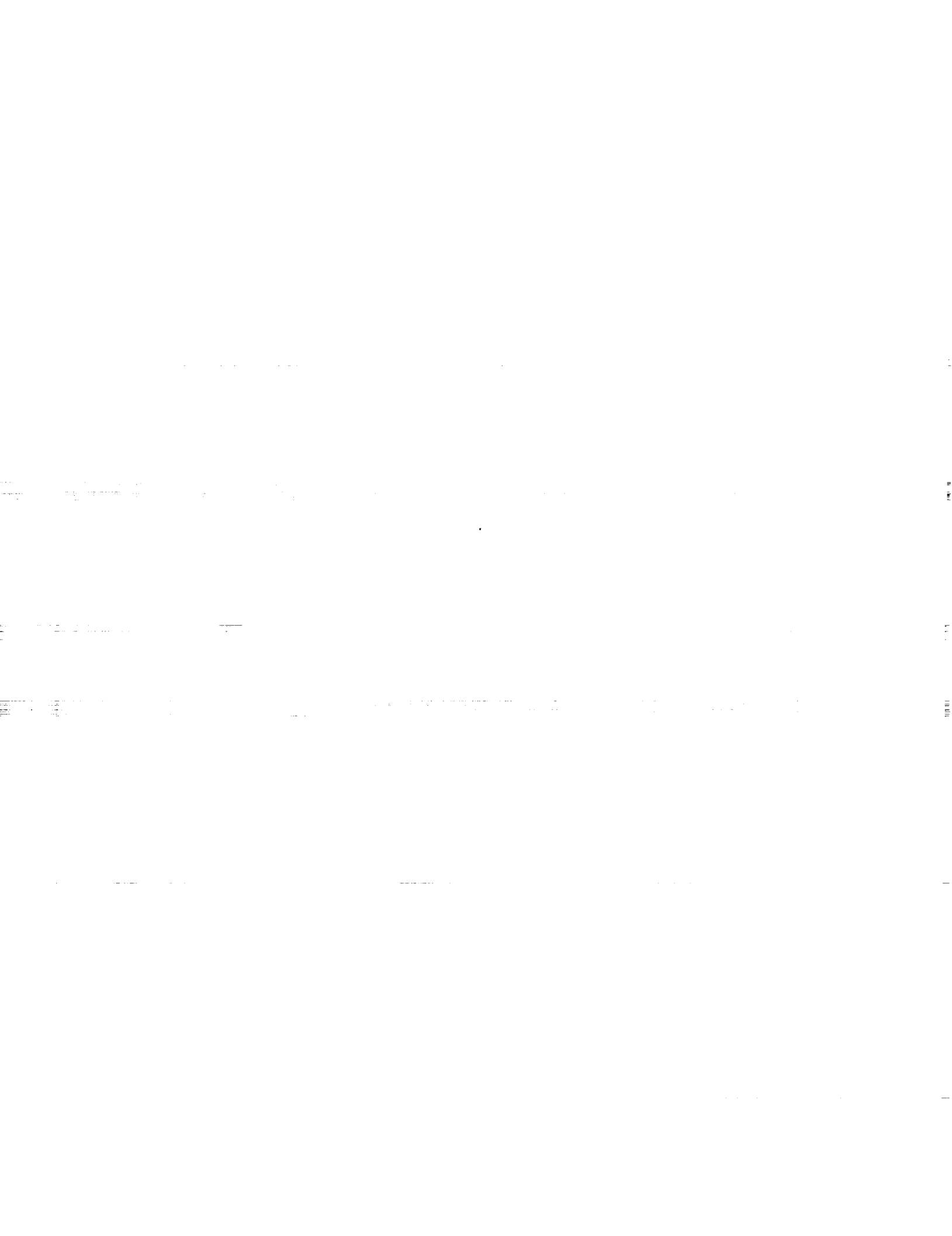
REPRODUCED BY  
NATIONAL TECHNICAL  
INFORMATION SERVICE  
U.S. DEPARTMENT OF COMMERCE  
SPRINGFIELD, VA 22161



CLASSIFIED DOCUMENT

This document contains classified information affecting the National Defense of the United States within the meaning of the Espionage Act, USC 50:31 and 32. Its transmission or the revelation of its contents in any manner to an unauthorized person is prohibited by law. Information so classified may be imparted only to persons in the military and naval services of the United States, appropriate civilian officers and employees of the Federal Government who have a legitimate interest therein, and to United States citizens of known loyalty and discretion who of necessity must be informed thereof.

~~CONFIDENTIAL~~  
UNCLASSIFIED



UNCLASSIFIED

N79-79427

NACA CONFERENCE ON AERODYNAMIC PROBLEMS  
OF TRANSONIC AIRPLANE DESIGN

A Compilation of the Papers Presented

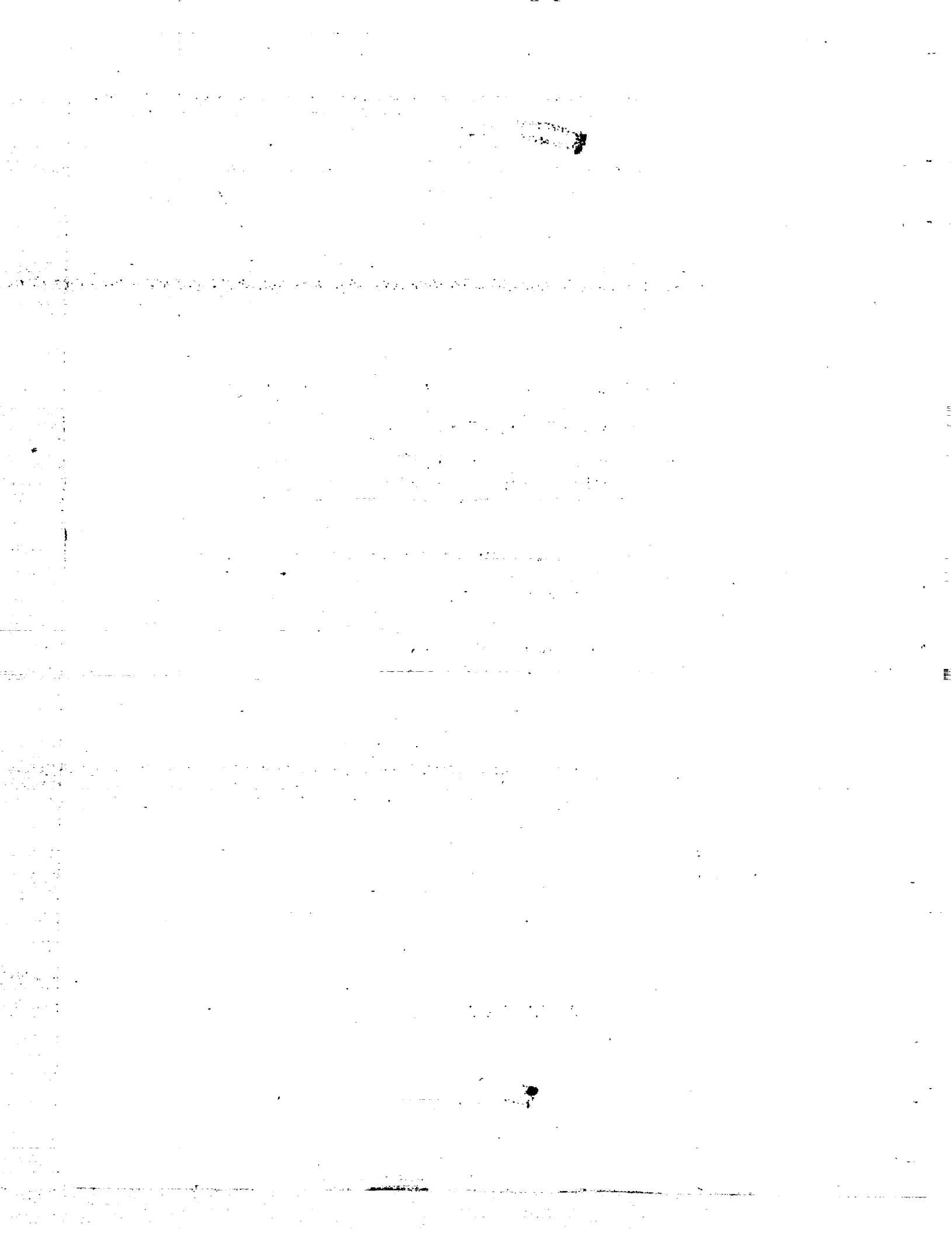
Ames Aeronautical Laboratory  
Moffett Field, Calif.

November 5 - 6, 1947

UNCLASSIFIED

REPRODUCED BY  
NATIONAL TECHNICAL  
INFORMATION SERVICE  
U.S. DEPARTMENT OF COMMERCE  
SPRINGFIELD, VA. 22161

251



**ATTENTION**

PORTIONS OF THIS REPORT ARE NOT LEGIBLE.  
HOWEVER, IT IS THE BEST REPRODUCTION  
AVAILABLE FROM THE COPY SENT TO NTIS.

CONFIDENTIAL

	Page
Transonic Flutter of Control Surfaces . . . by Albert L. Erickson . . . . .	89
STABILITY AND CONTROL . . . . .	93
Prediction of the Aerodynamic Characteristics of Wings of Arbitrary Plan Form . . . by Victor I. Stevens . . . . .	95
Current Status of Longitudinal Stability . . . by Charles J. Donlan . . . . .	101 ✓
Effects of Sweep on Controls. I - Effectiveness . . . by John G. Lowry and Harold I. Johnson . . . . .	113 ✓
Effects of Sweep on Controls. II - Hinge Moments . . . by John A. Axelson . . . . .	127 ✓
Factors Affecting Lateral Stability and Controllability . . . by John P. Campbell and Thomas A. Toll . . . . .	133 ✓
Low-Speed Flight Investigation of an Airplane with Sweptback Wings . . . by W. H. Phillips . . . . .	145
Flight Characteristics at Transonic Speeds. I - P-80A Airplane Investigation . . . by H. H. Brown . . . . .	153
Flight Characteristics at Transonic Speeds. II - Research Airplanes . . . by Walter C. Williams . . . . .	157
CONFIGURATIONS WITH EXTREME SWEEP . . . . .	163
Characteristics of a Configuration with a Large Angle of Sweepback . . . by Robert T. Jones . . . . .	165
Characteristics of a Triangular-Winged Aircraft. I - Performance Data . . . by Donald J. Graham . . . . .	169
Characteristics of a Triangular-Winged Aircraft. II - Stability and Control . . . by Robert M. Crane . . . . .	173



**CONFIDENTIAL**

**INTRODUCTION**

This document contains reproductions of technical papers on some of the recent research results from the NACA Laboratories on aerodynamic problems pertinent to the design of transonic airplanes. These papers were presented at the NACA conference held at the Ames Aeronautical Laboratory November 5 and 6, 1947. The purpose of this conference was to convey to those involved in the study of the aerodynamic problems of transonic aircraft these recent research results and to provide those attending an opportunity for discussion of the results.

The papers in this document are in the same form in which they were presented at the conference so that distribution of them might be prompt. The original presentation and this record are considered as complementary to, rather than as substitutes for, the Committee's system of complete and formal reports.

A list of the conferees is included.

SECRET

... ..  
... ..  
... ..  
... ..  
... ..

... ..  
... ..  
... ..  
... ..  
... ..

... ..  
... ..  
... ..  
... ..  
... ..

... ..  
... ..  
... ..  
... ..  
... ..

... ..  
... ..  
... ..  
... ..  
... ..



[REDACTED]

LIST OF CONFEREES

The following were registered at the NACA Conference on Aerodynamic Problems of Transonic Airplane Design, Ames Aeronautical Laboratory, Moffett Field, Calif., Nov. 5-6, 1947:

Abbott, I. H.	NACA
Allen, H. J.	NACA
Ames, M. B., Jr.	NACA
Anderson, H. L.	AAF, Air Materiel Command
Ashkenas, Irving L.	Northrop Aircraft Corp.
Axelson, John A.	NACA
Babberger, Carl	Hughes Aircraft
Baker, Paul S.	Chance-Vought Aircraft
Beeler, D. E.	NACA
Bell, Richard W.	North American Aviation, Inc.
Belsky, Steven E.	NACA
Bennett, T. C.	Naval Air Development Station
Bioletti, Carlton	NACA
Bitner, J.	Glenn L. Martin Co.
Blom, Trygve	AAF, Air Materiel Command
Bowman, R. G.	Republic Aviation Corp.
Brown, H. H.	NACA
Burstein, A.	Consolidated-Vultee Aircraft Corp.
Campbell, John P.	NACA
Carley, H.	Glenn L. Martin Co.
Cerny, Walter J.	Northrop Aircraft Corp.
Chambers, Comdr. L. S.	U. S. Navy, David Taylor Model Basin
Chandler, H. C., Jr.	NACA
Chapman, Comdr. S.	U. S. Navy, David Taylor Model Basin
Cherry, H. A.	Douglas Aircraft Co.
Clousing, L. A.	NACA
Cohen, Doris	NACA
Cohn, Benedict	Boeing Aircraft Co.
Cook, W. H.	Boeing Aircraft Co.
Crane, Robert M.	NACA
Dannenberg, Robert E.	NACA
Davis, F. W.	Consolidated-Vultee Aircraft Corp.
Davis, Wallace F.	NACA
DeFrance, S. J.	NACA
Dernbach, A. F.	AAF, Air Materiel Command
Dickey, D. A.	AAF, Air Materiel Command
Diehl, Capt. W. S.	U. S. Navy, Bureau of Aeronautics

Dill, D. G.  
Donlan, Charles J.  
Drake, Hubert M.  
Draley, Eugene C.  
Dryden, Dr. H. L.  
Dunn, O. R.

Ellis, F. E., Jr.  
Emmons, P. C.  
Enos, Louis H.  
Erickson, Albert L.  
Erickson, Miles

Frick, Charles

Garrick, I. E.  
Gavin, Joseph  
Goett, Harry J.  
Gough, Melvin N.  
Graham, Donald J.  
Gregory, E. G.

Halpern, Herman  
Hardum, W.  
Harper, William  
Harris, T. A.  
Hartman, E. P.  
Hayes, Lt. R. G.  
Head, Richard M.  
Heald, E. R.  
Heaslet, Max A.  
Helms, C. H.  
Hibbard, Hall L.  
Hood, Manley J.  
Horkey, Edward W.  
Huntzberger, R. F.  
Hutton, Richard  
Hyatt, A.

Jacob, John B.  
Jessen, Henry  
Johnson, Clarence L.  
Johnston, R. B.  
Jones, Alun  
Jones, Robert T.

Douglas Aircraft Co.  
NACA  
NACA  
NACA  
NACA  
Douglas Aircraft Co.

U. S. Navy, Bureau of Aeronautics  
Bell Aircraft  
Curtiss-Wright Corp.  
NACA  
NACA

NACA

NACA  
Grumman Aircraft  
NACA  
NACA  
NACA  
NACA

Fairchild Aircraft Co.  
Sperry Gyroscope Co.  
NACA  
NACA  
NACA  
AAF, Air Materiel Command  
North American Aviation, Inc.  
Douglas Aircraft Co.  
NACA  
NACA  
Lockheed Aircraft Corp.  
NACA  
North American Aviation, Inc.  
NACA  
Grumman Aircraft  
AAF, Air Materiel Command

Joint Research and Development Board  
NACA  
Lockheed Aircraft Corp.  
Ryan Aeronautical Corp.  
NACA  
NACA

Kaufman, H.  
Kayten, G. C.  
Kinghorn, George  
Knopf, G. S.

Lambert, A. A.  
Lefebber, G.  
Levin, D. H.  
Lewis, D. S.  
Liepmann, Dr. H. W.  
Lilly, Howard  
Loftin, Laurence K., Jr.  
Louden, F. A.  
Lowry, John G.  
Lunn, Rose  
Luskin, H.  
Lyman, C. B.

Maggin, Bernard  
Mastrocola, N.  
McAvoy, W. H.  
McHugh, J. G.  
McLaughlan, W. H.

Metsger, Comdr. A. B.  
Milliken, W. F., Jr.  
Morkovin, M. V.  
Mossman, Emmet A.  
Murray, Maj. J. L.  
Myers, Dale

Northrop, John K.

Outman, Vernon

Pappas, G.  
Pearson, E. O.  
Pierce, Dr. C. J.  
Perkins, G. D.  
Pettinghall, C. E.  
Phillips, W. H.  
Pierce, E. W.  
Purser, Paul E.

Robinson, R. G.  
Rumph, L. B.

Naval Air Development Station  
U. S. Navy, Bureau of Aeronautics  
NACA  
Fairchild Aircraft Co.

McDonnell Aircraft  
Consolidated-Vultee Aircraft Corp.  
Consolidated-Vultee Aircraft Corp.  
McDonnell Aircraft  
California Institute of Technology  
NACA  
NACA  
U. S. Navy, Bureau of Aeronautics  
NACA  
North American Aviation, Inc.  
Douglas Aircraft Co.  
U. S. Navy, Bureau of Aeronautics

NACA  
Naval Air Missile Test Center  
NACA  
NACA  
Hughes Aircraft

U. S. Navy, Bureau of Aeronautics  
Cornell Aeronautical Laboratory  
Univ. of Michigan  
NACA  
Air Materiel Command, Liaison Office, AAL  
North American Aviation, Inc.

Northrop Aircraft Corp.

McDonnell Aircraft

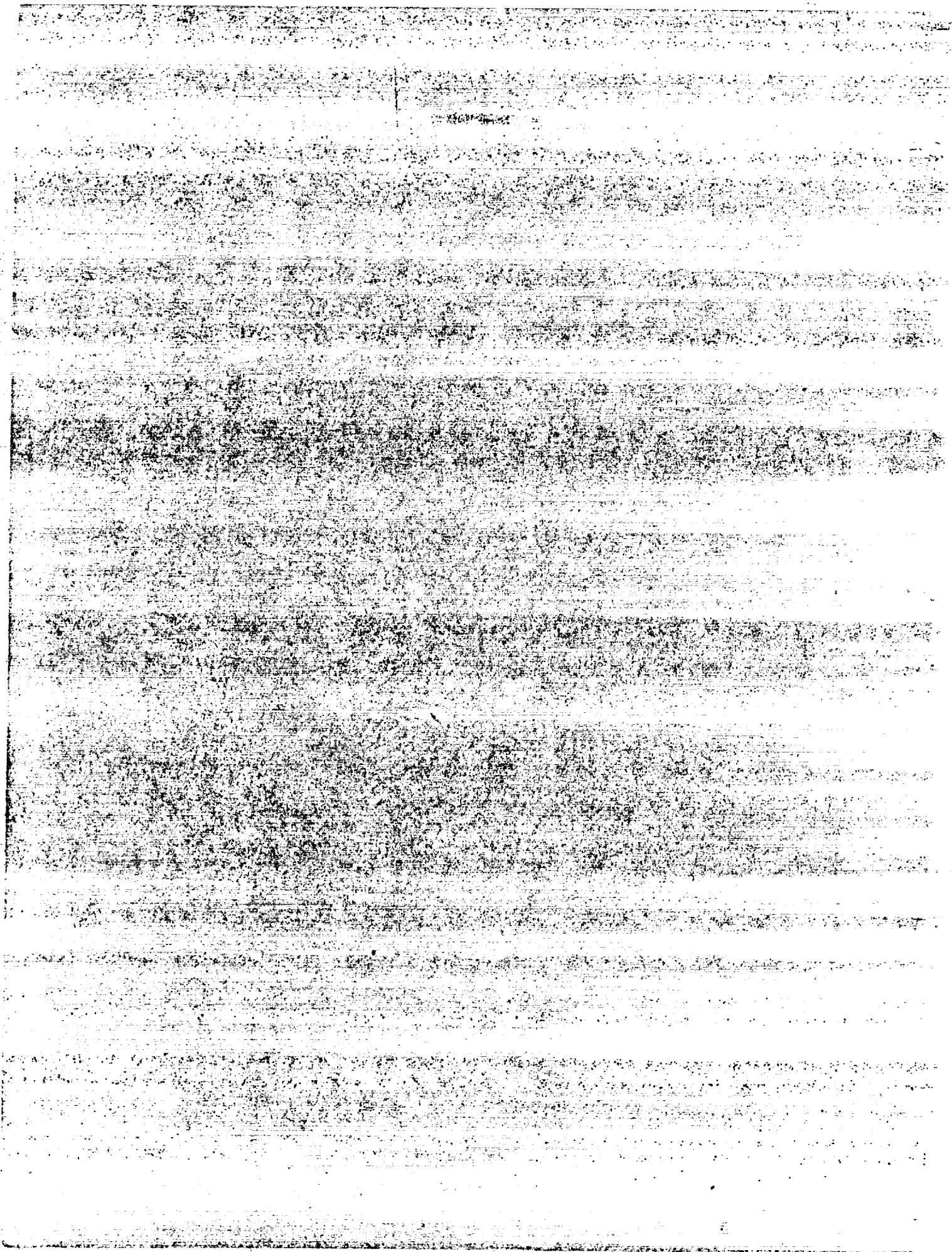
Republic Aviation Corp.  
NACA  
AAF, Air Materiel Command  
Princeton Univ.  
Douglas Aircraft Co.  
NACA  
Douglas Aircraft Co.  
NACA

NACA  
Curtiss-Wright Corp.

~~XXXXXXXXXX~~

Sandstrom, R. J.	Bell Aircraft
Schamberg, Richard	North American Aviation, Inc.
Sears, R. I.	Chance-Vought Aircraft
Sherby, Comdr. S. S.	Naval Air Test Center
Shick, R. S.	Consolidated-Vultee Aircraft
Shorr, Melvin	AAF, Air Materiel Command
Sibila, A. I.	Chance-Vought Aircraft
Silverstein, A.	NACA
Smith, Norman E.	NACA
Smith, R. B.	Douglas Aircraft Co.
Snodgrass, R. P.	Consolidated-Vultee Aircraft Corp.
Springer, Burdell L.	CAA
Soulé, H. A.	NACA
Stevens, Victor I.	NACA
Stirling, Comdr. C. W.	U. S. Navy, Bureau of Aeronautics
Stivers, Louis S., Jr.	NACA
Swann, W. H.	NACA
Tilgner, Charles, Jr.	Grumman Aircraft
Trimble, G. S.	Glenn L. Martin Co.
Tusch, Carl W.	Air Materiel Command, Liaison Office, AAL
Vincenti, Walter	NACA
Voyles, Capt. J. H.	AAF, Air Materiel Command
Walter, D. L.	Douglas Aircraft Co.
Wasserman, L. S.	AAF, Air Materiel Command
Wetmore, J. W.	NACA
Whitcomb, Richard T.	NACA
Williams, Walter C.	NACA
Wilson, Herbert A., Jr.	NACA
Withington, Holden W.	Boeing Aircraft Co.
Wood, Donald H.	NACA
Wood, Col. F. D.	AAF, Air Materiel Command
Worley, G. F.	Douglas Aircraft Co.
Yeager, D. M.	Air Materiel Command, Liaison Office, AAL

LIFT AND DRAG



A REVIEW OF RECENT INFORMATION RELATING  
TO THE DRAG RISE OF AIRPLANES

By J. W. Wetmore

Langley Memorial Aeronautical Laboratory

INTRODUCTION

The airplane, of conventional design as we know it today, has very nearly attained its limit in practical operating speed at about 500 miles per hour. With the large drag increase attending the formation of shock waves at these speeds, pushing the airplane to appreciably greater speeds results in a prohibitive loss in efficiency or L/D and the airplane is no longer capable of performing its primary function of carrying a payload a reasonable distance. Consider, for example, the case of a representative modern jet airplane having a wing loading of about 50 pounds per square foot and operating at an altitude of 30,000 feet.

In figure 1 the upper solid curve shows the variation of drag coefficient with speed or Mach number (reference 1) and the lower curve, the corresponding variation in range (based on assumption of constant specific fuel consumption in terms of thrust). For an increase in speed of about 100 miles per hour or in Mach number of 0.15 above the speed at which the drag rise starts, the range would decrease about 75 percent and would be too small to be useful. The dashed curves show that if the drag rise could be delayed sufficiently, or eliminated, the speed could be increased 100 miles per hour with only a 10-percent loss in range or 200 miles per hour with about 20-percent decrease in range. (This small loss in range results from the condition of constant altitude assumed here: the effect of decreasing L/D, resulting from the decreasing lift coefficient with increasing speed, somewhat more than offsets the effect of the increasing speed.)

With the development of more concentrated fuels and efficient power plants to utilize them, the effect of the drag rise will no doubt be less critical from this standpoint, but for the present, at least, it seems clear that further increase in the speeds at which airplanes may operate efficiently will be accomplished by changes in aerodynamic design required to avoid any substantial drag rise up to these speeds.

The purpose of this paper is to point out briefly the information relating to drag in the transonic range which is available to guide designers in planning efficient higher speed airplanes of the immediate future and to indicate some of the trends in these data. The principal

sources of the information that will be presented are the high-speed tunnels, covering the lower end of the transonic range up to Mach numbers of 0.9 to 0.95, tests of free-fall models dropped from high altitudes covering practically the whole transonic range, and tests of rocket-propelled models dealing with the upper end of the range from Mach numbers of 1.0 to 1.2.

#### WING CONFIGURATIONS

The wing which is, of course, the major source of the drag rise of present airplane configurations will be considered first. Figure 2 indicates the increase in the Mach number of the drag rise that can be obtained with unswept wings by using thinner wing sections. The solid lines actually represent the Mach numbers at which the drag coefficient has increased 0.005 above the sub-critical value. The use of this value provides a better indication of the trends than the use of the value at which the drag rise actually begins since the latter value is not always clearly defined. The start of the drag rise occurs in the region between the solid line and the dashed line which defines the theoretical critical Mach number of the wing sections. The Mach number of the drag rise is shown as a function of the thickness-chord ratio of the wing: in the left hand figure for a tapered and cambered wing at a lift coefficient of 0.2 as tested in the high-speed tunnel (reference 2); and in the right-hand figure for a straight, symmetrical wing at zero lift from the results of free-fall tests (reference 3). It is indicated that in both cases the Mach number of the drag rise increases by 0.015 to 0.02 or between 10 and 15 miles per hour for each percent reduction in thickness ratio.

The effects of sweepback and aspect ratio on the Mach number of the drag rise, defined as before, are illustrated in figure 3. In this figure, the Mach number of the drag rise is shown plotted against the inverse of the aspect ratio from the results of high-speed tunnel tests of two series of unswept wings of different airfoil section, and a series of wings of 30° sweep (references 4 and 5), and from the results of free-fall tests of two wings of 45° sweep (reference 6). The indicated values of the drag-rise Mach number at infinite aspect ratio for the swept conditions were estimated from two-dimensional high-speed tunnel data using the simple cosine law for infinite yawed wings. The results indicate that the benefits of sweep are increased as the aspect ratio increases particularly for large sweep angles. Conversely, although decreasing the aspect ratio provides a substantial increase in the Mach number of the drag rise for the unswept wings, it has little effect when the wings are sweptback 30° and becomes adverse for 45° sweepback. It may be noted that in order to avoid a substantial



drag rise up to or through sonic velocity with the wing thicknesses considered a sweepback of at least  $45^\circ$  is required.

A considerable amount of data on the drag of wings at the upper end of the transonic range has been obtained by the rocket technique and although these results do not define the conditions of the drag rise, they, together with the free-fall data, do show the extent of the drag rise and provide an indication of the wing configurations that will be required to extend speeds for reasonably efficient airplane operation to Mach numbers above 1.0. Figure 4 shows the variation with thickness ratio of the drag coefficient of unswept wings at a Mach number of 1.15. Data from both rocket and free-fall tests (references 3 to 7) are included and although there is considerable scatter due to the different test techniques and different aspect ratios, which will be discussed later, the trend is well defined. The large reduction in drag at this speed afforded by decreasing the wing thickness is clearly shown. As an indication of what the drag data at Mach number 1.15 shown in this and subsequent figures mean in relation to thrust available from present turbojet power plants or those in immediate prospect, it is estimated that the drag coefficient for a complete single-engine airplane of representative dimensions operating at altitudes of 30,000 to 40,000 feet could not exceed about 0.02. According to this figure then, the thickness ratio of an unswept wing would have to be something less than 4 percent to permit attainment of Mach number 1.15.

The effects of sweep and aspect ratio on the drag at Mach number 1.15 are shown in figure 5 which again includes data from both rocket and free-fall tests (references 6 and 8). Here the drag coefficients are plotted against the inverse of the aspect ratio for sweep angles from  $0^\circ$  to  $52^\circ$ . All the wings are of NACA 65-009 section in planes normal to the leading edge. The trends indicated in this figure are generally similar to those of figure 3. That is, the effect of sweep in decreasing the drag becomes greater with increasing aspect ratio and the effect of reducing the aspect ratio, although favorable with no sweep, disappears at moderate sweep angles and becomes adverse with greater sweep. The results shown here do not of course give the complete story, which would require consideration of structural requirements and space requirements for fuel storage and so forth. For example, the beneficial effect indicated for reduced aspect ratio of the unswept wings, is due to aspect ratio alone and does not take account of the reduction in drag due to the thinner wing sections that could probably be used with the smaller aspect ratios. Furthermore, the indicated advantage of sweep is not entirely realistic since it applies to constant wing thickness in planes normal to the leading edge; whereas for structural reasons the thickness would probably have to be increased considerably with increasing sweep and the benefits would

thereby be reduced. Consider again the value of drag coefficient 0.02, representing, as before, the probable limit for a single-engine airplane with the jet engines that will be available in the near future: it appears that to attain a Mach number of 1.15 within this limitation the wing would have to be swept at least  $45^\circ$  and probably more to allow for the drag of fuselage and other elements of the airplane.

There has been some interest, for various reasons, in the possibilities of using forward sweep rather than sweepback. In figure 6 the variations of drag with Mach number through the transonic range for a sweptback and a sweptforward wing are compared from the results of free-fall tests (reference 9 and data not yet published). The wings are similar in all respects except taper, and it is shown that the results are very similar. These results may be influenced to some extent by effects on the wings due to the flow fields of the bodies used in these tests. In this connection it might be of interest to mention that the sweptforward wing was found to have a considerably more adverse effect on the drag of the body, at Mach numbers of 1.0 and above, than the sweptback wing. However, the indication that the direction of sweep has little effect on either the Mach number or the extent of the drag rise of the wing alone is supported by other data from wind-tunnel tests (reference 10) and rocket tests (reference 11).

As part of the investigation of wing-plan-form effects on drag at high transonic speeds, rocket tests have been made of several configurations incorporating variations in taper as well as sweep (references 12 and 13). Figure 7 shows the drag coefficients at a Mach number of 1.15 in relation to the taper ratio, grouped for approximately constant sweep angles of either the mean line or the leading edge of the wing. The thickness chord ratio in the stream direction is approximately constant for each group. With the mean line unswept, tapering the wing to a pointed configuration provides a substantial reduction in drag over that of the untapered wing. The second group indicates that with the leading edge held constant at  $45^\circ$ , tapering the wing tends to be unfavorable and this trend appears to continue to the inverse-taper condition shown by the third group. These results apparently indicate simply that sweep of the leading edge is not the determining factor for tapered wings. Perhaps, the most interesting feature of these data is shown by the fourth group where the result of tapering the wing about a  $45^\circ$  swept mean line is indicated. The taper in itself has practically no effect in this case which suggests that it should be possible to take full advantage of the benefits of large sweep and thin sections with considerably less difficulty from structural problems than in the case of untapered wings.

Investigation of the effects of airfoil section on the transonic drag characteristics of finite wings has been limited mainly to determining the effects of sharp leading edges, with the thought that they might provide some benefit in the transonic range as well as at supersonic speeds. Figure 8 shows the variation of drag with Mach number from free-fall tests (reference 14) of a six-percent-thick, unswept wing with a sharp-edge circular-arc section and one with NACA 65-series section. Little difference is indicated and such as there is favors the 65-series airfoil. Similar comparisons from rocket tests with thicker unswept wings and with swept wings, including double-wedge as well as circular-arc sections (reference 7) lead to the same conclusions - that wings with supersonic-type sections tend to have somewhat poorer drag characteristics in the transonic range than wings with more conventional high-speed sections.

#### BODIES

With the delay and reduction in the drag rise of wings that appear possible from the foregoing results the drag characteristics of the body or fuselage of the airplane may well become the critical factor in determining the limiting normal operating speed of the airplane. An investigation of body drag through the transonic range has been undertaken by the free-fall method (reference 15) and the results to date are shown in figure 9 in which the drag coefficients, based on frontal area, of four simple bodies of revolution, varying in fineness ratio and in thickness distribution are compared over the Mach number range from 0.85 to 1.08. The drag values shown include the drag of the stabilizing tail surfaces which were identical in all cases. The body of fineness ratio 12 had a similar thickness distribution to that of the fineness ratio 6 body, with the maximum diameter at half the body length. The start of the drag rise of the fineness ratio 12 body appears to occur at a considerably higher Mach number than for the fineness ratio 6 body although this advantage is more than offset at Mach numbers below 0.94 by the greater skin friction drag of the longer body. The extent of the drag rise is also much less - on the order of one-third - for the slender body so that at Mach numbers around 1.0 its drag coefficient is only about 60 percent of that of the fineness ratio 6 body. The other two bodies were formed by combinations of the forebody and afterbody shapes of the fineness ratio 6 and fineness ratio 12 bodies. Of these two bodies, the one with the blunter forebody and more slender afterbody has a lower drag at Mach numbers above 0.92. Although the drags of both these bodies lie generally between the curves for the fineness ratio 6 and 12 bodies, the values are somewhat higher at Mach numbers above 1.0 than would be expected for a fineness ratio 9 body of similar shape to the 6 and 12 bodies.

This will be indicated more clearly in another figure. A further point of interest in the data in this figure is in the similarity of the drag variation above Mach number 1.0 for the bodies of similar nose shape: for the two bodies having the more slender forebody the curves flatten out, whereas with the blunter nose shape the drag coefficient continues to increase, suggesting that the nose shape becomes the dominant factor in determining the character of the drag variation of bodies very shortly after Mach number 1.0 has been exceeded.

In figure 10 the drag coefficients of the four bodies at a Mach number of 1.08 are plotted to logarithmic scale as a function of the inverse of fineness ratio. The drag values shown have been reduced to represent approximately the pressure or wave drag by subtracting the measured drag of the stabilizing tail and estimated skin friction from the values shown in figure 9. The values for the fineness ratio 6 and fineness ratio 12 bodies, which may be considered as belonging to the same shape family, fall very close to a line which defines the drag as a function of the square of the inverse fineness ratio, or, in effect, the square of the thickness ratio. This result is in accord with the theory for the wave drag of slender bodies of revolution at supersonic speeds and in fact the complete

relation  $C_{D_{FF}} = 10.7 \left( \frac{1}{F.R.} \right)^2$  defined by this line is almost exactly

the same as that derived theoretically by Lighthill for slender parabolic bodies (reference 16). The fact that the data for the two fineness ratio 9 bodies with maximum diameter forward and aft of the midlength of the body lie above this line, indicates that these departures from the shape family represented by the fineness ratio 6 and 12 bodies are both unfavorable.

In connection with a study of the sources of the drag rise of bodies in the transonic range, pressure-distribution measurements on a body of revolution have been obtained by the wing-flow method over the range of Mach number from 0.85 to 1.05 (reference 17). Some of these results are shown in figure 11. The body was of parabolic shape in longitudinal section with a fineness ratio of 6 and was sting supported as indicated in the sketch in the left hand figure. The pressure-orifice locations are also shown in the sketch. The pressure distributions along the body are shown for four Mach numbers from 0.92 to 1.05 in the left hand figure and the variation of pressure-drag coefficient with Mach number determined from these data is plotted in the right hand figure. The pressure distribution for Mach number 0.92 is typical of the results obtained at lower Mach numbers and gave no appreciable pressure drag. With increasing Mach number, the suction peak moves back of the maximum diameter of the body and the pressure

drag rises accordingly. The greatest rearward movement of the suction peak in relation to change of Mach number occurs between Mach number 0.96 and 1.00 and the drag rise is also most abrupt over this range. At Mach numbers from 1.00 to 1.05, the change in pressure distribution and in drag coefficient is relatively small. Although the pressures over the forebody increase somewhat as the Mach number increases and thereby contribute to the drag rise, the greater part of the effect up to Mach number 1.0 arises from the growth and rearward movement of the suction on the afterbody. As an indication that the pressure measurements and their interpretation in terms of the drag rise are probably not greatly influenced by the low Reynolds number of these tests, the drag curve from the free-fall tests of a fineness ratio 6 body of generally similar shape is given by the dashed line in the right-hand figure. The Reynolds number of these tests was some twenty times that of the wing-flow tests but the shapes of the curves are remarkably similar.

#### WING-BODY INTERACTION

A final interpretation of the results of investigations of airplane components requires, of course, some understanding of the effects of combining these components in the complete airplane configuration. Figures 12 and 13 indicate some of the tendencies that have been observed in the effects of wing-fuselage interaction on the drag rise. Figure 12 shows the variation of drag coefficient with Mach number through the beginning of the drag rise for three unswept wings of varying thickness from high-speed tunnel tests (reference 2). The solid lines apply to the wings alone, and the dashed lines to the combinations of wing and fuselage. For these cases, the Mach number of the drag rise and the rate of increase in the drag coefficient beyond the start of the drag rise appear to be practically unaffected by the addition of the fuselage. A similar absence of effects of adding a fuselage to the wing was noted in the results of high-speed tunnel tests of an airplane configuration incorporating a 35° sweptback wing (reference 18).

A considerably different result was indicated from free-fall tests of wing-body configurations incorporating wings of greater sweepback (reference 19). Figure 13 compares the drag-coefficient variation with Mach number for two combinations of identical 45° swept wings and fineness ratio 12 bodies, differing only in the position of the wings on the body. With the wing located 1/8 of the body length back of its maximum diameter, the drag rise apparently did not occur until the Mach number was at least 0.05 greater than for the arrangement with the wing a similar distance forward of the maximum diameter,

and the drag throughout the Mach number range covered was markedly less. From the simultaneous measurements of total drag and wing drag obtained in these tests it was evident that the greater part of the difference shown here arose from the effect of the wing position on the body drag: With the wing in the rearward position, the presence of the wing apparently reduced the drag of the body appreciably below the values obtained with a similar body without wings, whereas with the wing in the forward position, the body drag was increased. It appears from these results that considerable attention should be given to the arrangement of the wing on the fuselage, at least when large sweep angles are used, to avoid the possibility of rather large unfavorable interaction effects.

#### CONCLUSION

By way of conclusion, figure 14 was prepared to provide a somewhat more direct indication of the advances in operating speeds that may be expected from some of the changes in airplane configuration that have been discussed. This figure shows the variation of drag coefficient with Mach number for three simple body-wing-tail configurations incorporating fineness ratio 12 bodies varying in wing sweep and thickness (reference 19 and data not yet published) compared with that for the representative modern jet fighter discussed earlier (reference 1). The curve designated  $T/sq$  represents the probable thrust capabilities that can be expected of a turbojet engine in the immediate future in terms of a representative wing area and dynamic pressure for comparison with the drag coefficients. The speed of the conventional airplane, with unswept wings, 13-percent thick, is limited by the intersection of the thrust and drag curves to a Mach number of 0.80 with the highest speed for reasonably efficient cruising probably not greater than 0.70 in Mach number. It was found that the drags of models of three projected high-speed airplanes with wings of around  $35^\circ$  sweep and 10- to 12-percent thickness (references 18, 20, and 21) fell generally between the two drag curves for the  $35^\circ$  configurations shown here. It appears therefore that maximum speeds up to Mach number of 0.9 to 0.95 and reasonable range up to Mach numbers of almost 0.9 can be realized with the moderate sweep and thickness that are being incorporated in a number of new high-speed jet airplanes now in design, construction, or prototype stages. The  $45^\circ$  swept-wing arrangement shown on the right attained the highest Mach number before the drag rise and gave the most gradual drag rise of any wing-body-tail combination for which free-fall test data are available. From these results it appears that with wings having sweep angles of  $45^\circ$  and sufficiently slender bodies, arranged to avoid unfavorable interaction effects, airplanes cruising at Mach numbers up to 0.95 and with top speed around Mach number 1.0 are

quite possible, with turbojet engines that are or probably soon will be available. This does not constitute the limit, of course: more extreme sweep should permit further advances in airplane operating speeds and an indication of the results that can be expected with sweep angles up to  $63^\circ$  will be given in a paper by Robert T. Jones.

## REFERENCES

1. Cleary, Joseph W., and Gray, Lyle J.: High-Speed Wing-Tunnel Tests of a Model of the Lockheed XP-80A Airplane Including Correlation with Flight Tests and Tests of Dive-Recovery Flap. NACA RM No. A7A29, Army Air Forces, 1947.
2. Hamilton, William T., and Nelson, Warren H.: Summary Report on the High-Speed Characteristics of Six Model Wings Having NACA 65<sub>1</sub>-series Sections. NACA MR No. A5J19, Army Air Forces, 1945.
3. Thompson, Jim Rogers, and Mathews, Charles W.: Measurements of the Effects of Thickness Ratio and Aspect Ratio on the Drag of Rectangular-Plan-Form Airfoils at Transonic Speeds. NACA RM No. L7E08, 1947.
4. Adler, Alfred A.: Effects of Combinations of Aspect Ratio and Sweepback at High Subsonic Mach Numbers. NACA RM No. L7C24, 1947.
5. Stack, John, and Lindsey, W. F.: Characteristics of Low-Aspect-Ratio Wings at Supercritical Mach Numbers. NACA MR No. L5H27a, Army Air Forces and Bur. Aero., 1945.
6. Mathews, Charles W., and Thompson, Jim Rogers: Drag Measurements at Transonic Speeds of NACA 65-009 Airfoils Mounted on a Freely Falling Body to Determine the Effects of Sweepback and Aspect Ratio. NACA RM No. L6K08c, 1947.
7. Katz, Ellis: Flight Tests to Determine the Effect of Airfoil Section Profile and Thickness Ratio on the Zero-Lift Drag of Low Aspect Ratio Wings at Supersonic Speeds. (Prospective NACA paper)
8. Tucker, Warren A., and Nelson, Robert L.: Drag Characteristics of Rectangular and Swept-Back NACA 65-009 Airfoils Having Various Aspect Ratios as Determined by Flight Tests at Supersonic Speeds. NACA RM No. L7C05, 1947.
9. Thompson, Jim Rogers, and Mathews, Charles W.: Drag of Wing-Body Configuration Consisting of a Swept-Forward Tapered Wing Mounted on a Body of Fineness Ratio 12 Measured during Free Fall at Transonic Speeds. NACA RM No. L6L24, 1947.
10. Whitcomb, Richard T.: An Investigation of the Effects of Sweep on the Characteristics of a High-Aspect-Ratio Wing in the Langley 8-Foot High-Speed Tunnel. NACA RM No. L6J01a, 1946.



11. Alexander, Sidney R.: Drag Measurements of a  $34^\circ$  Swept-Forward and Swept-Back NACA 65-009 Airfoil of Aspect Ratio 2.7 as Determined by Flight Tests at Supersonic Speeds. NACA RM No. L6I11, 1946.
12. Alexander, Sidney R., and Nelson, Robert L.: Flight Tests to Determine the Effect of Taper on the Zero-Lift Drag of Wings at Low Supersonic Speeds. NACA RM No. L7E26, 1947.
13. Alexander, Sidney R.: Drag Measurements of a Swept-Back Wing Having Inverse Taper as Determined by Flight Tests at Supersonic Speeds. NACA RM No. L6L30, 1946.
14. Thompson, Jim Rogers, and Marschner, Bernard W.: Comparative Drag Measurements at Transonic Speeds of an NACA 65-006 Airfoil and a Symmetrical Circular-Arc Airfoil. NACA RM No. L6J30, 1946.
15. Thompson, Jim Rogers, and Kurbjun, Max C.: Measurements of Effect of Location of Maximum Diameter on Drag of Bodies at Transonic Speeds. (Prospective NACA paper)
16. Lighthill, M. J.: Supersonic Flow Past Bodies of Revolution. R. & M. No. 2003, British A.R.C., 1943.
17. Danforth, Edward C. B., and Johnston, J. Ford: Pressure Distribution over a Sharp-Nose Body of Revolution at Transonic Speeds by the NACA Wing-Flow Method. (Prospective NACA paper)
18. Kuhn, Richard E., and Myers, Boyd C., II: An Investigation of the Aerodynamic Characteristics of an 0.08-Scale Model of the Chance Vought XF7U-1 Airplane in the Langley High-Speed 7- by 10-Foot Tunnel. Part V - Wing Alone Tests and Effect of Modifications to the Vertical Fins, Speed Brakes, and Fuselage. TED No. NACA DE308, NACA RM No. L7J09, Bur. Aero., 1947.
19. Mathews, Charles W., and Thompson, Jim Rogers: Comparison of the Transonic Drag Characteristics of Two Wing-Body Combinations Differing Only in the Location of the  $45^\circ$  Sweptback Wing. NACA RM No. L7I01, 1947.
20. Wright, John B., and Loving, Donald L.: High-Speed Wind-Tunnel Tests of a 1/16-Scale Model of the D558 Research Airplane Lift and Drag Characteristics of the D-588-1 and Various Wing and Tail Configurations. NACA RM No. L6J09, 1946.
21. Alexander, Sidney: Flight Tests to Determine the Aerodynamic Characteristics of a  $\frac{1}{9}$ -Scale Model of the Republic XP-91 Airplane (MX-809) with Controls Undelected and Short Tail Length. NACA RM No. L7G16, Army Air Forces, 1947.

Wetmore

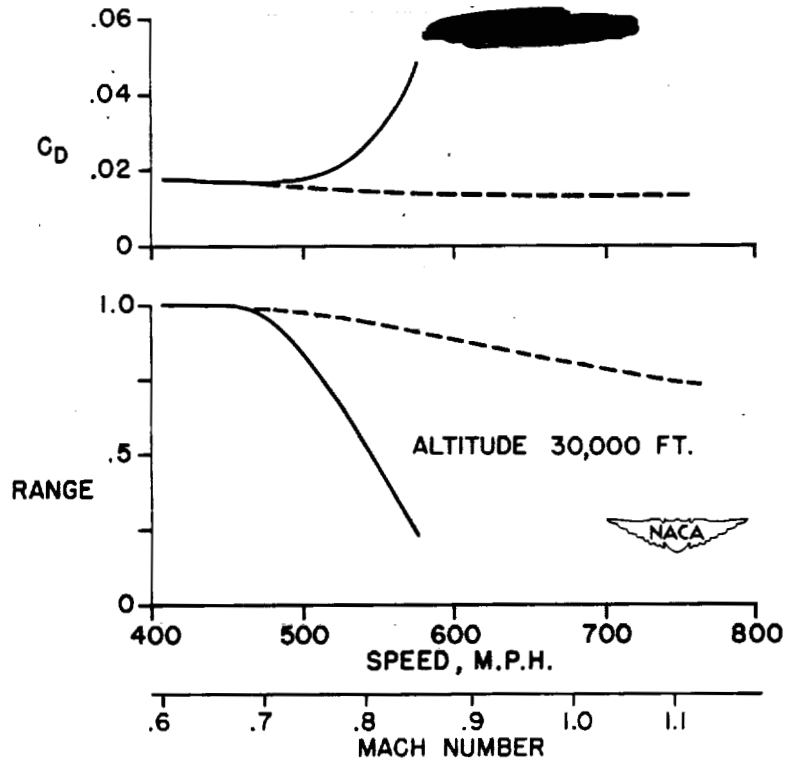


Figure 1.- Effect of drag rise on range of representative modern turbojet airplane.

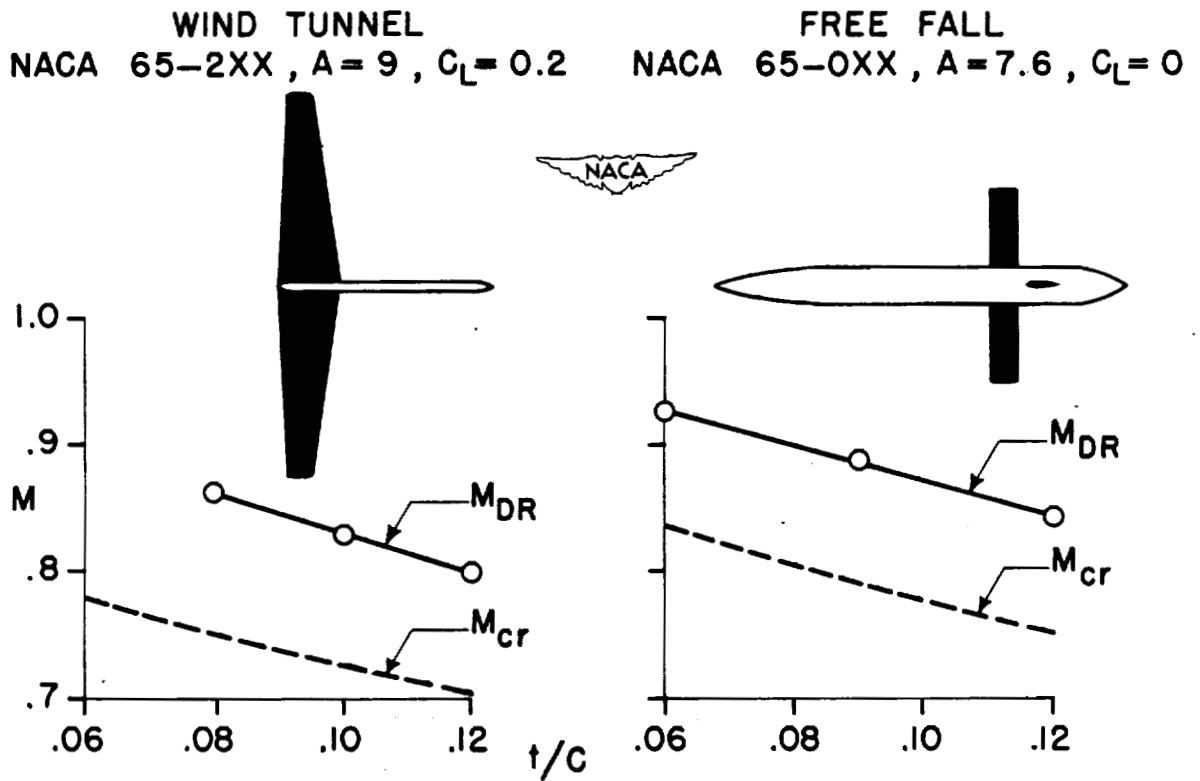


Figure 2.- Effect of wing thickness ratio on Mach number of the drag rise.

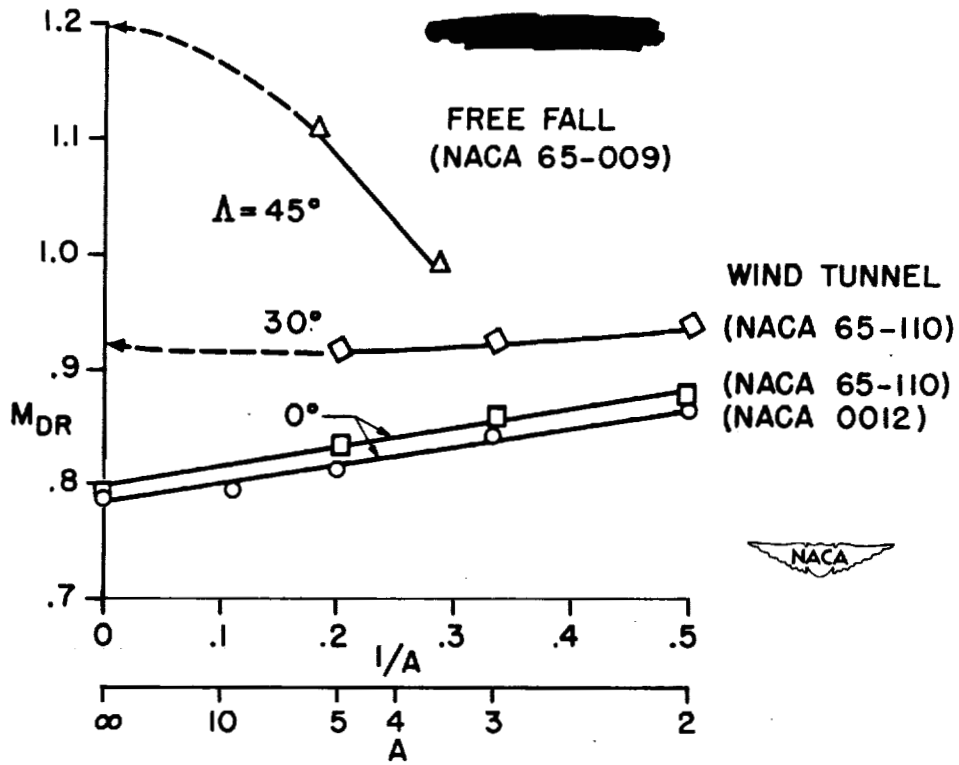


Figure 3.- Effects of aspect ratio and sweep of wings on the Mach number of the drag rise;  $\alpha = 0^\circ$ .

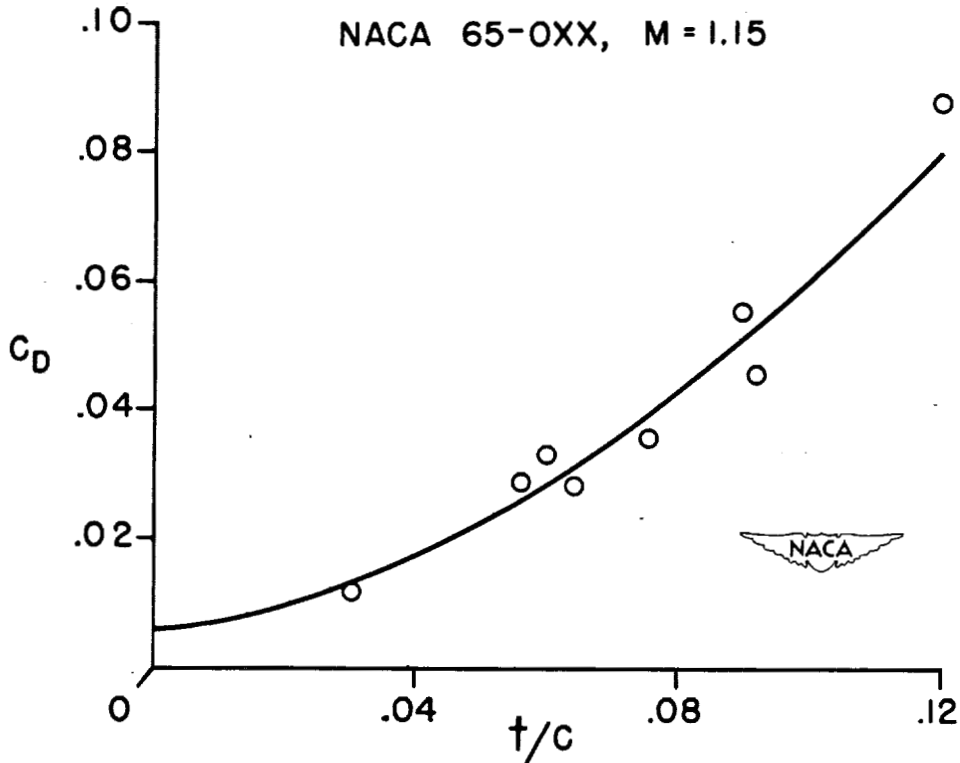


Figure 4.- Variation of drag coefficient of unswept wings with thickness ratio.  $M = 1.15$ ;  $C_L = 0$ .

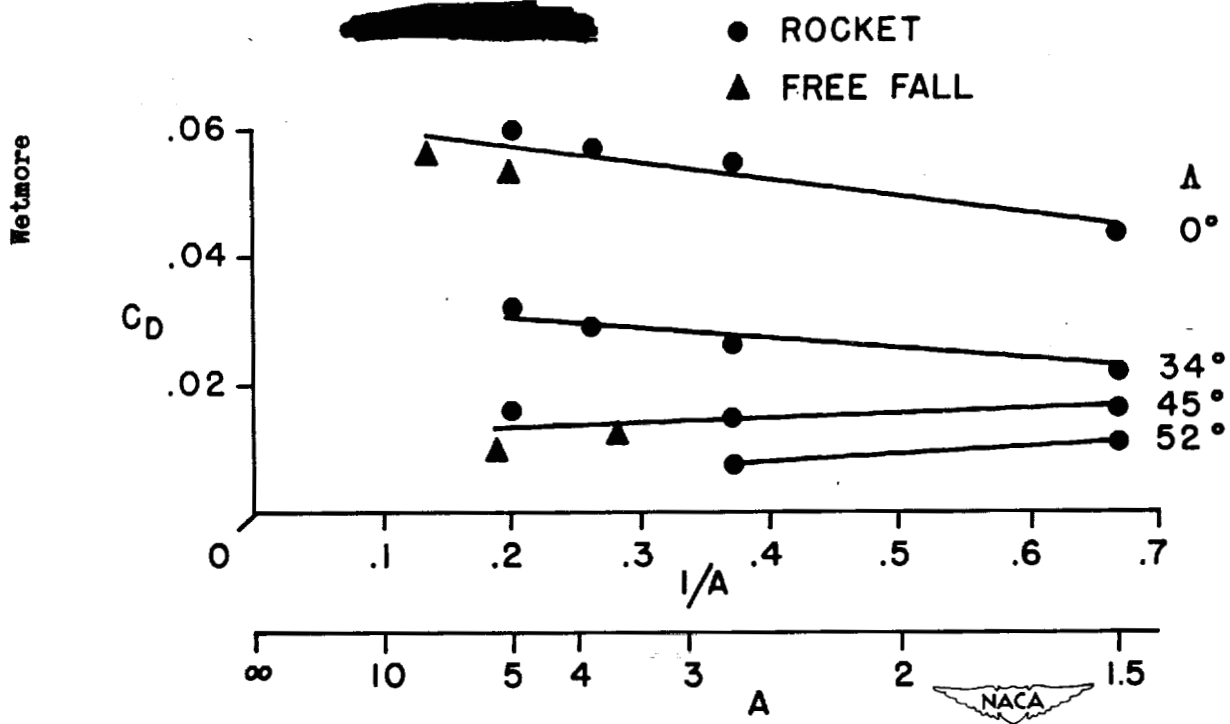


Figure 5.- Variation of wing drag coefficient with aspect ratio and sweepback.  $M = 1.15$ ;  $C_L = 0$ .

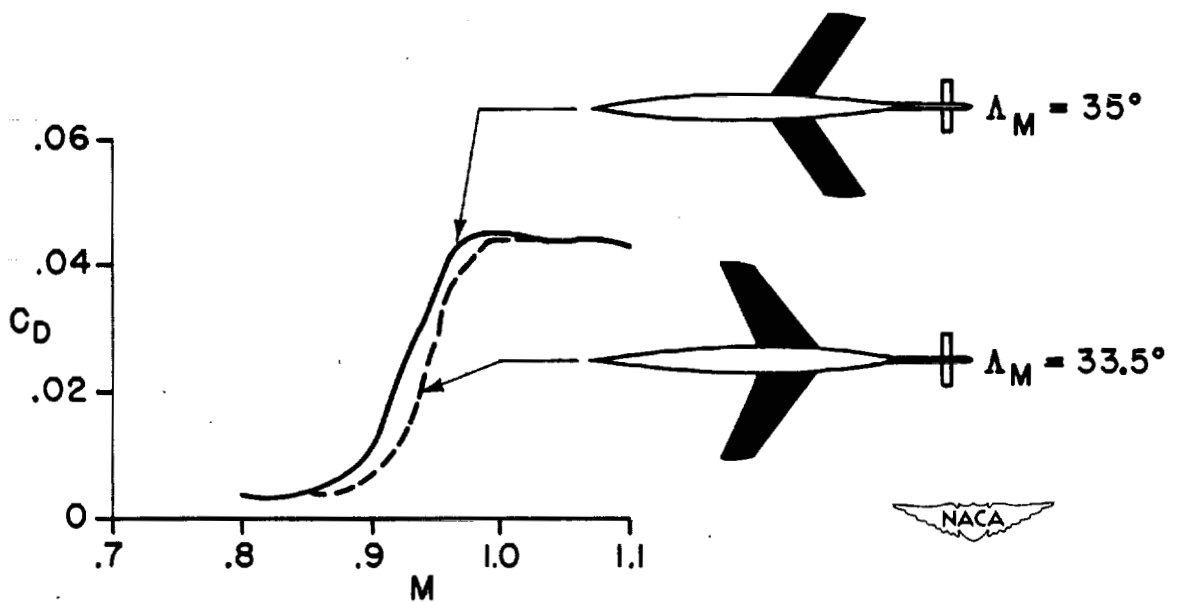


Figure 6.- Comparison of drag of sweptforward and sweptback wings through the transonic range.  $C_L = 0$ ;  $t/c = 0.12$ .

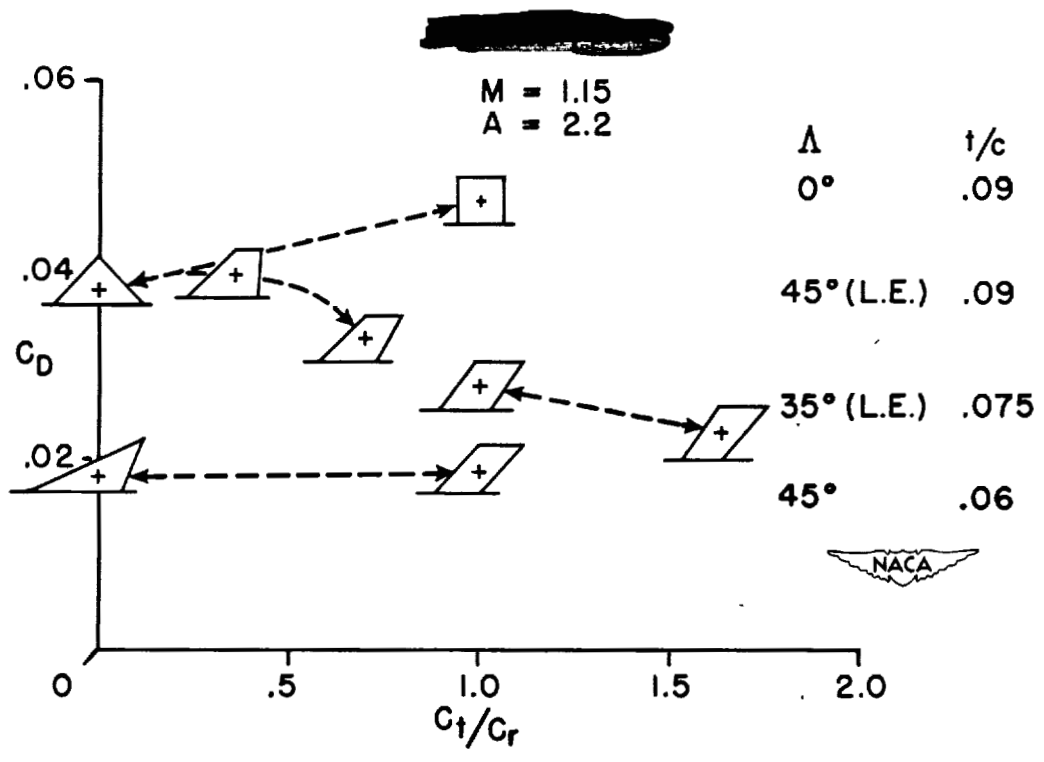


Figure 7.- Effects of various combinations of taper and sweep on the drag of wings at Mach number 1.15.  $C_L = 0$ .

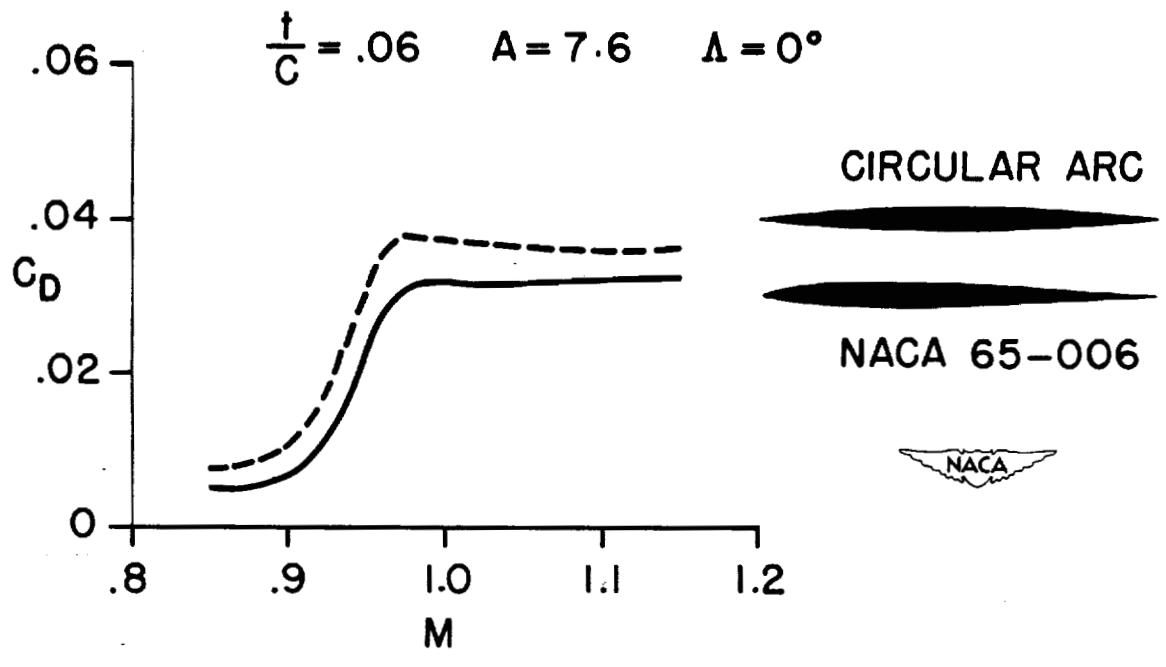


Figure 8.- Comparison of drag of wings with sharp-leading-edge and conventional NACA airfoil sections through the transonic range.  $C_L = 0$ .

Wetmore

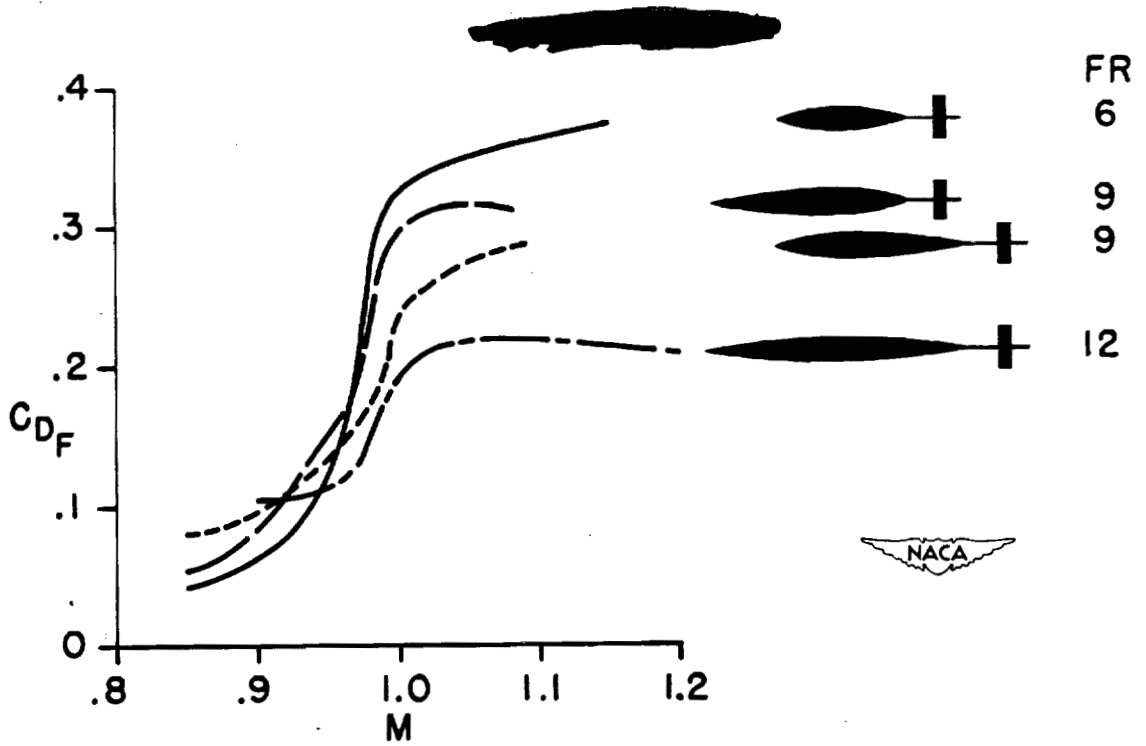


Figure 9.- Effects of fineness ratio and thickness distribution on the drag of bodies of revolution at transonic speeds.

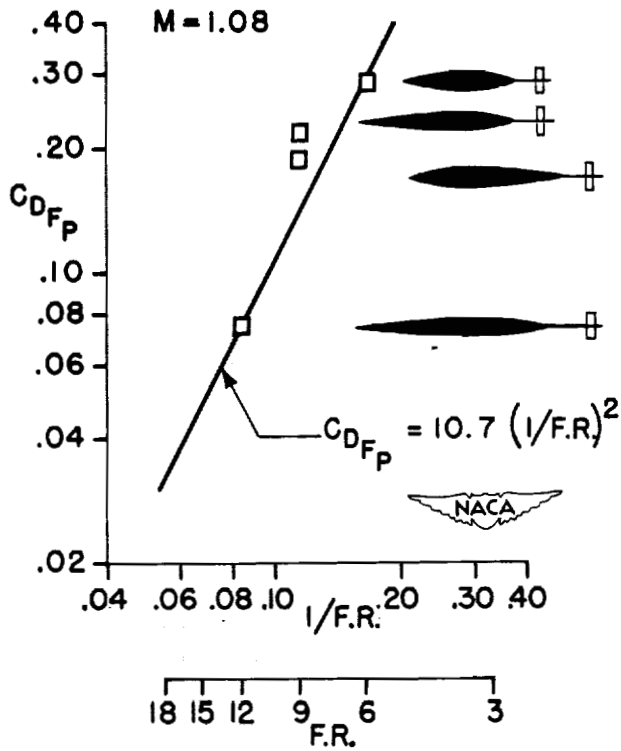


Figure 10.- Logarithmic plot of variation of pressure drag with inverse of fineness ratio for four bodies of revolution.

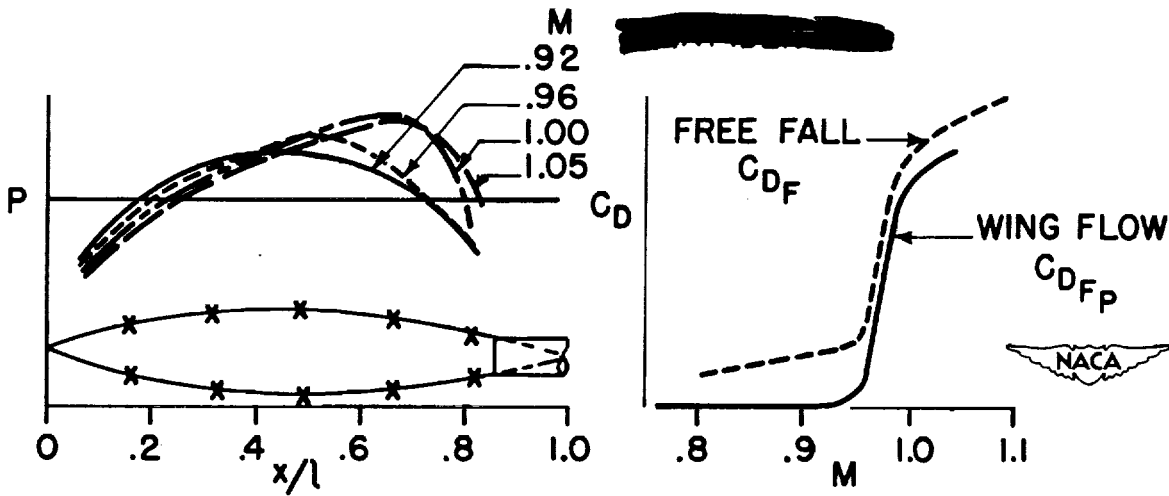


Figure 11.- Pressure distributions from wing-flow tests through the speed of sound on a fineness ratio 8 body of revolution, and comparison of the corresponding pressure drag with the total drag measured in free-fall tests of a similar body.

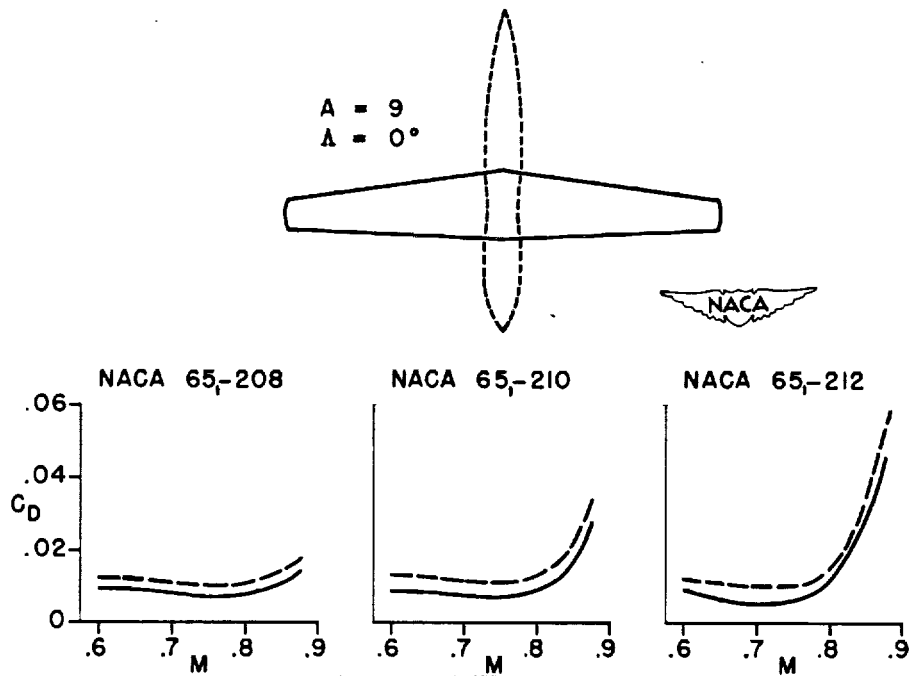


Figure 12.- Comparison of initial drag rise of wing alone and wing-fuselage combination for three wings of different thickness ratio.

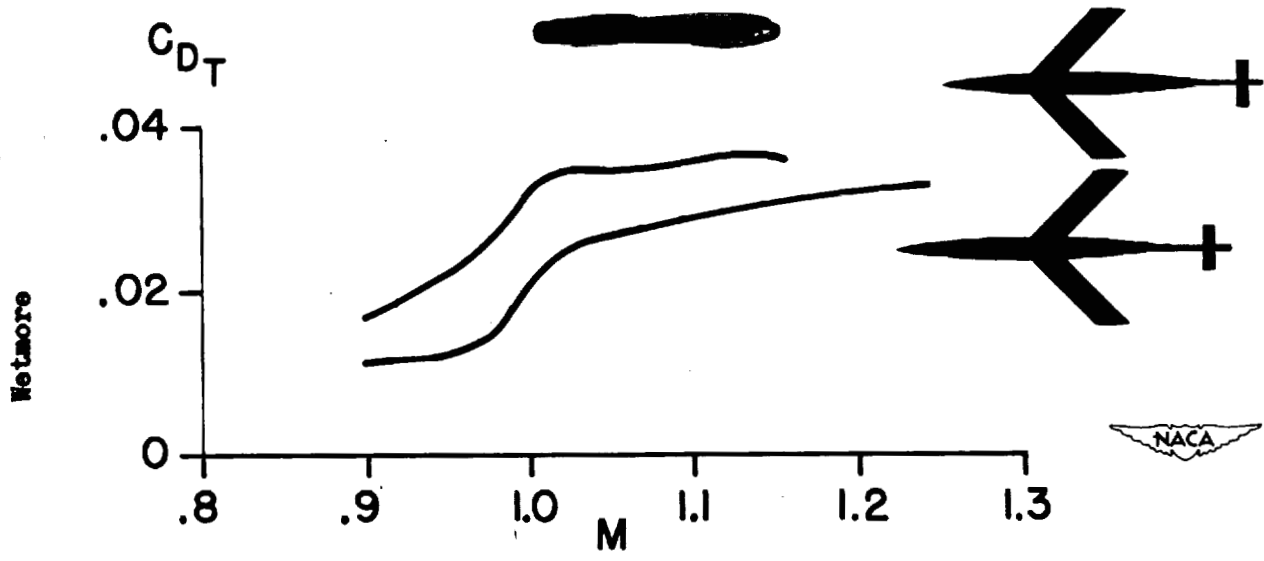


Figure 13.- Effect on drag of wing-body-tail combination through transonic range due to fore-and-aft position of 45° swept wing.

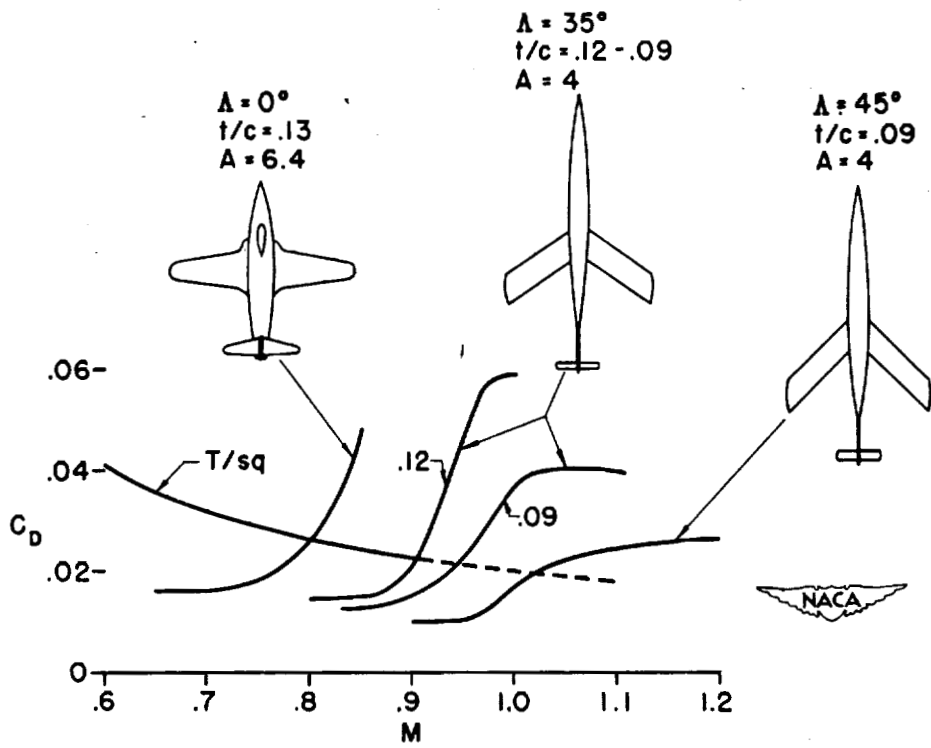


Figure 14.- Comparison of drag rise of three wing-body-tail combinations varying in wing sweep and thickness and of representative, modern turbojet airplane. Thrust available from turbojet engine at 30,000 to 40,000 feet altitude shown in form corresponding to drag coefficient for comparison.



AIRFOIL SECTION CHARACTERISTICS

AT HIGH SUBSONIC SPEEDS

By Louis S. Stivers, Jr.

AMES Aeronautical Laboratory

The design of airplane lifting surfaces and the prediction of their aerodynamic characteristics have always depended, to a great extent, on airfoil section data. The drag data are of particular significance from the standpoint of airplane performance, whereas the lift and pitching-moment data are of appreciable importance from the point of view of airplane stability and control. It was first believed, nevertheless, that airfoil section data would be of limited value for swept wings. Recent theoretical work of V. V. Struminsky and also of R. T. Jones reported in references 1 and 2, however, have indicated that airfoil section data should have a wider scope of application in the design of high-aspect-ratio swept wings. In such use, the aerodynamic characteristics of the airfoil section normal to the swept leading edge are used together with the Reynolds and Mach numbers corresponding to the normal component of the free-stream velocity. According to the present knowledge, this is the most logical procedure for the selection of airfoil sections of a high-aspect-ratio wing either straight or swept. Although the qualitative use of airfoil section data is made in the design of swept wings, it should not be inferred that such data may be used quantitatively. In view of the aforementioned application it was thought that a review of important high-speed properties of several NACA 6-series airfoils would be of interest. A large part of the data which will be presented has already been reported in references 3 and 4.

It is generally known that the reduction in the lift and the abrupt increase in the drag of an airfoil section (in other words, the divergence of forces) occur at speeds somewhat greater than the airfoil critical speed. Since the force-divergence Mach numbers for a given airfoil are of particular interest in the design of wings for high-speed aircraft, it has been suggested that the critical Mach number might be used as a conservative indication of these Mach numbers. In figure 1 is shown a calculated curve of critical Mach number for the NACA 64-210 airfoil section. This curve was determined from the Karman-Tsien relationship between the critical Mach numbers and the peak incompressible pressure coefficients of the airfoil. The extremities of the curve are determined by the peak pressures at the airfoil leading edge, whereas the center part is determined by the peak pressures which are, for this airfoil, at 0.4 chord. For comparison, curves of lift- and drag-divergence Mach numbers determined from experimental results are also shown.

It can be seen in figure 1 that the critical Mach number curve is entirely inadequate in indicating the range of lift coefficient over which the lift- and drag-divergence Mach numbers are the highest. Only in the center part does the curve of critical Mach number approximate the force-divergence Mach number curves. This center part of the critical Mach number curve is quite close to the curve of drag-divergence Mach number, but the curve of lift-divergence Mach number is about 0.025 Mach number higher. For every lift coefficient shown in this figure, the Mach numbers of lift divergence are greater than the Mach numbers of drag divergence. A comparison of experimental and calculated critical Mach number curves has shown very good agreement between the center part of the curves; the extremities of the experimental curve, however, came between those of the curves of calculated critical Mach number and the curves of force-divergence Mach numbers. It is apparent, then, that the Karman-Tsien relation overestimates the increases in peak pressures at the airfoil leading edge. It is quite significant to note that there are greater differences between the force-divergence Mach numbers and the critical Mach numbers when the critical Mach numbers have been determined from peak pressures at the airfoil leading edge than when they are determined from peak pressures located somewhat behind the leading edge. This is explained by the fact that at a given increment in Mach number above the critical the extent of the region of supersonic flow at the leading edge is much less than the corresponding region of flow at a position on the airfoil somewhat behind the leading edge. These remarks are also applicable to other airfoils besides the NACA 6-series type.

The disposition of these curves of calculated critical Mach numbers and experimental lift- and drag-divergence Mach numbers for other thin NACA 6-series airfoils can be expected to be similar to that shown in figure 1. At low lift coefficients the cambered airfoils have lift-divergence Mach numbers that are 0.02 to 0.06 greater than the drag-divergence Mach numbers. In general, the differences between these force-divergence Mach numbers appear to be the greatest for the NACA 64- and 65-series airfoils. The ranges of lift coefficients over which the force-divergence Mach numbers are the highest also appear to be somewhat greater for these series of airfoils.

Associated with the divergence of airfoil lift at supercritical Mach numbers is the variation of angle of attack required to maintain a given lift coefficient and the reduction in airfoil lift-curve slope. Shown in figure 2 for several NACA 64-series airfoils is the effect of airfoil thickness ratio and camber on the section angle of attack required to maintain a lift coefficient of 0.1. Variations in this angle of attack are significant in that they lead

to corresponding changes in airplane trim. This figure shows that for the cambered airfoils the Mach number of the abrupt change in angle of attack increases with a decrease in airfoil thickness ratio. It appears, also, that the large variation in angle of attack is not alleviated by a reduction in thickness ratio but is delayed to higher Mach numbers. The advantage of the symmetrical airfoil is clearly evident when the curves for the NACA 64-210 and 64-010 airfoils are compared. Up to the highest Mach numbers shown, the data indicate that the symmetrical airfoil can maintain a constant lift coefficient of 0.1 with only very small changes in angle of attack.

In figure 3 are shown the effects of thickness ratio and extent of favorable pressure gradient on the section lift-curve slopes per degree of several NACA 6-series airfoils. From the standpoint of the static longitudinal stability of an airplane, the variations of the lift-curve slope of the wing are of appreciable importance. When the lift-curve slope of the wing increases, the downwash at the tail plane increases correspondingly, leading to a decrease in airplane stability; and for a decrease in the lift-curve slope the converse is true. The thickness effect for several NACA 64-series airfoils is indicated in the upper group of curves in figure 3. It can be seen that the Mach numbers at which the lift-curve slopes begin to decrease and the values of the lift-curve slopes at these Mach numbers increase as the thickness ratio decreases. It is of interest to note that the maximum value of the lift-curve slope for the airfoil with a 6-percent thickness is nearly three times as large as the value at low speeds. The effect of a change in the extent of favorable pressure gradient from 0.4 chord to 0.6 chord for 10-percent thick NACA 6-series airfoils is indicated in the lower group of curves in this figure. The data show that the maximum values of lift-curve slope decrease as the region of favorable pressure gradient becomes more extensive or as the position of maximum thickness moves rearward. (The positions of maximum thickness for the NACA 64-, 65-, and 66-series airfoils are at approximately 38-, 41-, and 45-percent chord, respectively.) The Mach numbers at which the lift-curve slopes begin to decrease seem to be the least for the airfoil having the greatest extent of favorable pressure gradient. The preceding remarks can be expected to apply only to airfoils with small trailing-edge angles such as those of the NACA 6-series airfoils.

Data of reference 4 show that the lift-curve slopes for the NACA 63-210 airfoil are practically identical with those for the NACA 64-210 airfoil. Unpublished data indicate that camber has very little effect on the lift-curve slopes of the thin NACA 6-series airfoils.

Presented in figure 4 are the section drag characteristics of several NACA 64-series airfoils as affected by camber and thickness ratio. The lower group of curves indicate the effect of thickness at a section lift coefficient of 0.2. These data show that the Mach number of drag divergence increases as the thickness ratio decreases. Above this Mach number the increases in drag coefficient appear to be independent of thickness ratio. The upper two curves of this figure show the variation of section drag coefficient at a lift coefficient of 0.2 for the NACA 64-210 and 64-010 airfoils. Even though a comparison at this lift coefficient is disadvantageous for the symmetrical airfoil, the data show that it has a slightly higher drag-divergence Mach number. At Mach numbers just above those for drag divergence the data show that the NACA 64-010 airfoil has the least drags; hence, the lift-drag ratios are the highest for this airfoil at these Mach numbers.

Pitching-moment data for the NACA 6-series airfoils show, in general, no large changes until a Mach number in the vicinity of the lift- and drag-divergence Mach numbers has been reached. Corresponding data for other types of airfoils having trailing-edge angles considerably larger than those for the NACA 6-series airfoils, however, have shown abrupt changes in the pitching moments at high lift coefficients which have indicated rearward shifts of the center-of-pressure position. Even at low lift coefficients, the latter type of airfoil has shown forward movements of the position of center of pressure. For these airfoils with large trailing-edge angles, there is appreciable variation of flow separation near the trailing edge with small changes in airfoil angle of attack. The action is effectively the same as if there were a flap at the trailing edge deflected in opposition to the airfoil angle of attack.

The data which have been presented thus far have been obtained at Mach numbers as high as 0.9. It is noteworthy that in the Langley transonic tunnel, which is now in operation, airfoil pressure-distribution measurements may be made at a Mach number of approximately unity. Shown in figure 5 is a schematic diagram of this tunnel. The tunnel working section is actually a 3-inch annulus between two concentric circular cylinders. The airfoil models are fixed to the rim of a rotor having a diameter equivalent to that of the inner cylinder. The model rotates within the annulus at speeds which correspond to Mach numbers as high as 1.4. Since the ratio of tunnel height to model thickness for this tunnel is almost infinite, the choking effects of the usual subsonic tunnel are eliminated. In order to prevent the model from operating in its own wake and to control the model angle of attack, a low axial velocity is induced through the annulus. In order to reduce the effects of the boundary

layer on the tunnel walls in the vicinity of the model, air from the boundary layer is removed at three annular slots upstream of the test section.

Shown in figure 6 are preliminary pressure-distribution data obtained in the Langley transonic tunnel at a Mach number of approximately unity for the NACA 66-006 airfoil at zero angle of attack. The data are presented as pressure ratios: the ratio of the local pressure  $p$  on the surface of the airfoil to the stagnation pressure  $p_s$ . For comparison, the Prandtl-Meyer expansion was computed for the supersonic region of the airfoil. A comparison of these curves shows that the pressure ratios given by the Prandtl-Meyer expansion are somewhat lower than the corresponding pressure ratios shown by the test data. There is a very good agreement, however, in the shapes of the curves and the chordwise position of the peak pressures. This agreement is remarkable in view of the fact that the Prandtl-Meyer expansion is based on the assumptions that no boundary layer exists on the airfoil and that the sonic flow field extends from the airfoil surface to infinity. The magnitude of the experimental peak pressure corresponds to approximately 80 percent of the calculated Prandtl-Meyer increment, whereas at about the 25-percent-chord position the experimental pressure corresponds to approximately 40 percent. An analysis of the local supersonic region of NACA airfoil sections tested up to Mach numbers of approximately 0.9 has been made by Nitzberg and Sluder in reference 5. It was shown that values of the Prandtl-Meyer increments from 40 to 60 percent, depending upon the conditions at the beginning of the sonic region, occur on the forward parts of the airfoils. A comparison of the calculated value of pressure drag, from the experimental data presented in figure 6, with corresponding data obtained from a freely falling body shows good agreement.

Data from the Langley 24-inch high-speed tunnel for NACA 16-series airfoil sections (reference 6) indicate that the camber for best lift-drag ratio  $L/D$  decreases rapidly as the Mach number increases beyond the point of force divergence. Figure 7 presents typical results for the NACA 16-X09 airfoil family at  $M = 0.775$ . For this particular speed best  $L/D$  at  $c_l = 0.5$ , for example, was obtained with a section cambered for a design lift coefficient  $c_{l_1}$  of only 0.2. The results indicated that at somewhat higher Mach numbers best  $L/D$  would probably occur with zero camber. Reduction in camber also reduced the angle-of-attack variations required to maintain a given lift coefficient throughout the transonic-speed range.

## REFERENCES

1. Struminsky, V. V.: Glissement d'une aile dans un gaz visqueux compressible. Comptes Rendus Acad. Sci. USSR, vol. LIV, 1946, pp. 765-768.
2. Jones, Robert T.: Effects of Sweepback on Boundary Layer and Separation. NACA TN No. 1402, 1947.
3. Van Dyke, Milton D., and Wibbert, Gordon A.: High-Speed Aerodynamic Characteristics of 12 Thin NACA 6-Series Airfoils. NACA MR No. A5F27, Army Air Forces, 1945.
4. Ilk, Richard J.: High-Speed Aerodynamic Characteristics of Four Thin NACA 63-Series Airfoils. NACA RM No. A7J23, 1947.
5. Nitzberg, Gerald E., and Sluder, Loma E.: An Empirically Derived Method for Calculating Pressure Distributions over Airfoils at Supercritical Mach Numbers and Moderate Angles of Attack. NACA RM No. A7B07, 1947.
6. Lindsey, W. F., Stevenson, David B., and Daley, Bernard N.: The Aerodynamic Characteristics of 24 NACA 16-Series Airfoils at Mach Numbers between 0.3 and 0.8. (Prospective NACA paper)

NACA 64-210 AIRFOIL SECTION

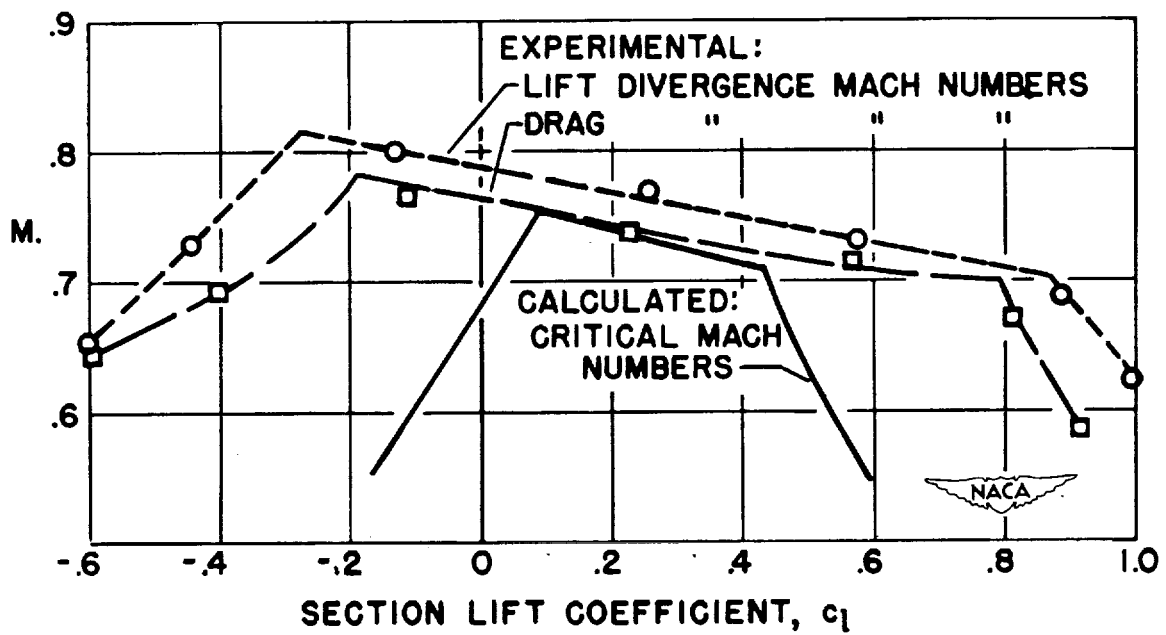


Figure 1.- Variation of the force-divergence and critical Mach numbers with section lift coefficient for the NACA 64-210 airfoil.

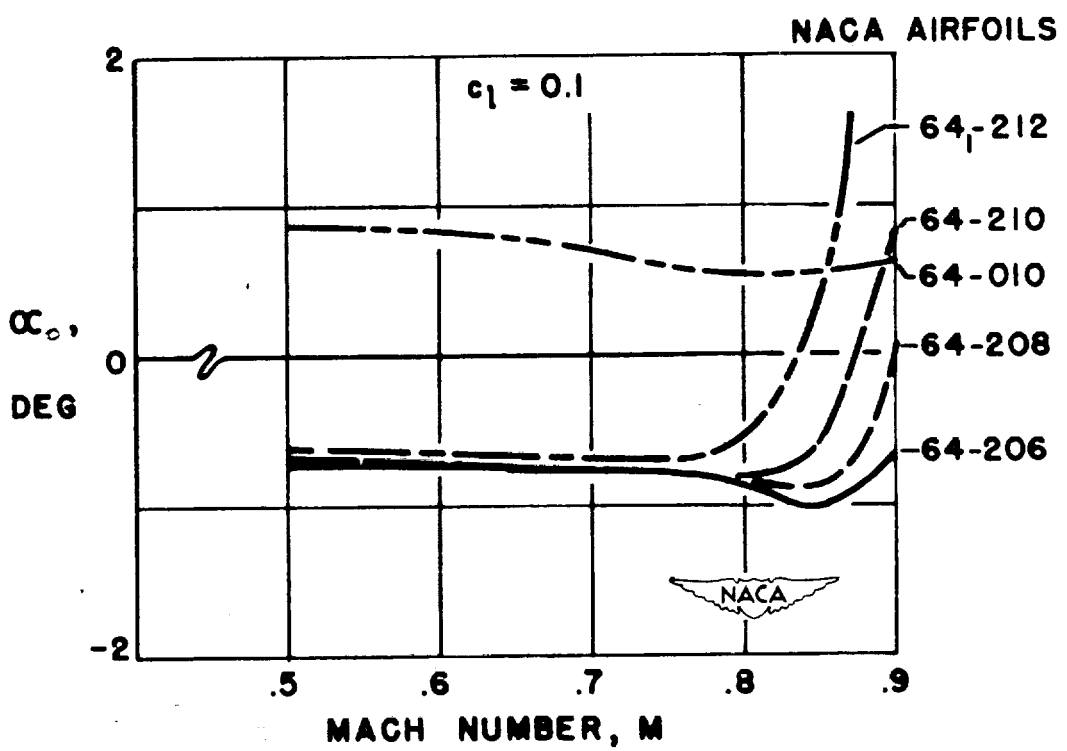


Figure 2.- Variation with Mach number of the angle of attack required to maintain a section lift coefficient of 0.1 for several NACA 64-series airfoils.

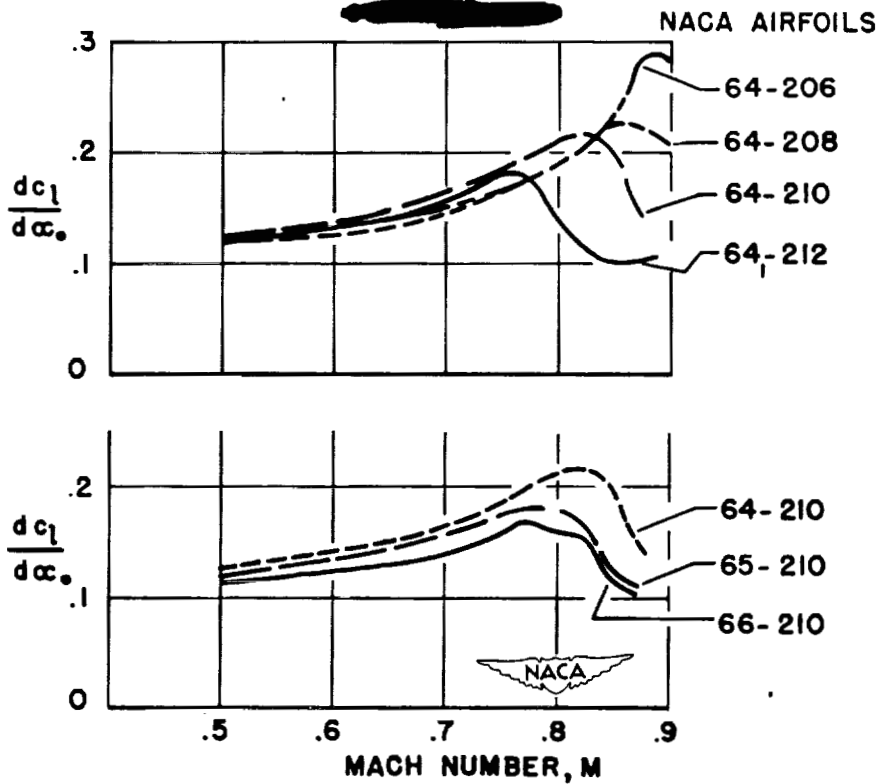


Figure 3.- Variation with Mach number of section lift-curve slope per degree for several NACA 6-series airfoils.

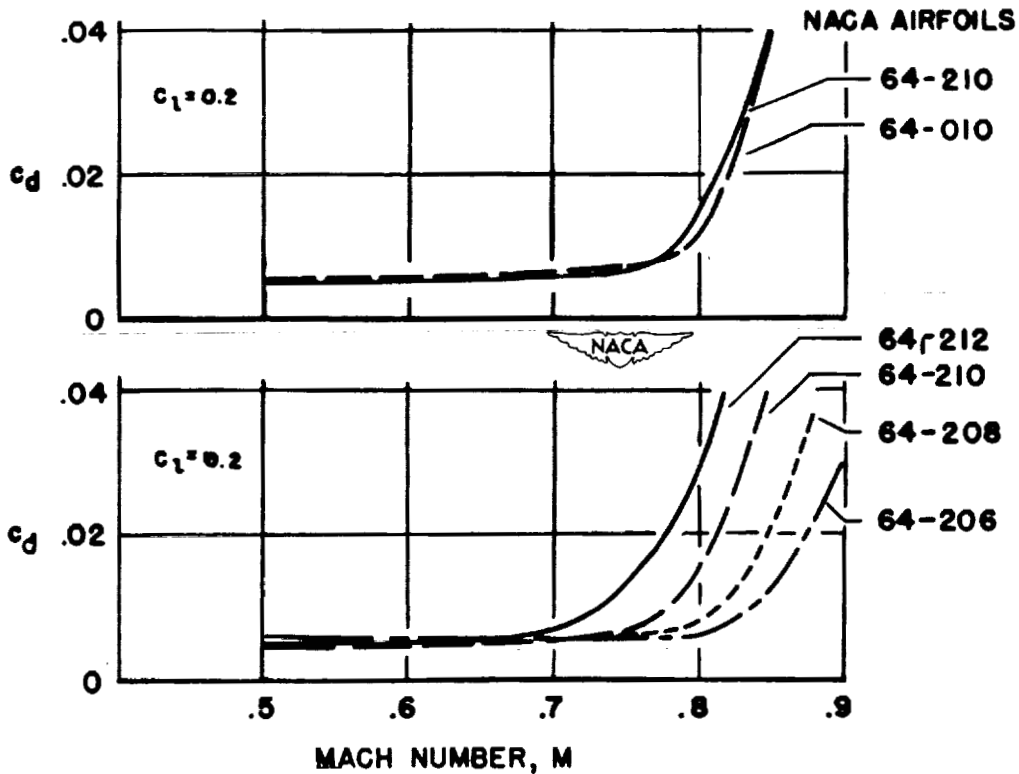


Figure 4.- Variation with Mach number of section drag coefficient at a lift coefficient of 0.2 for several NACA 64-series airfoils.



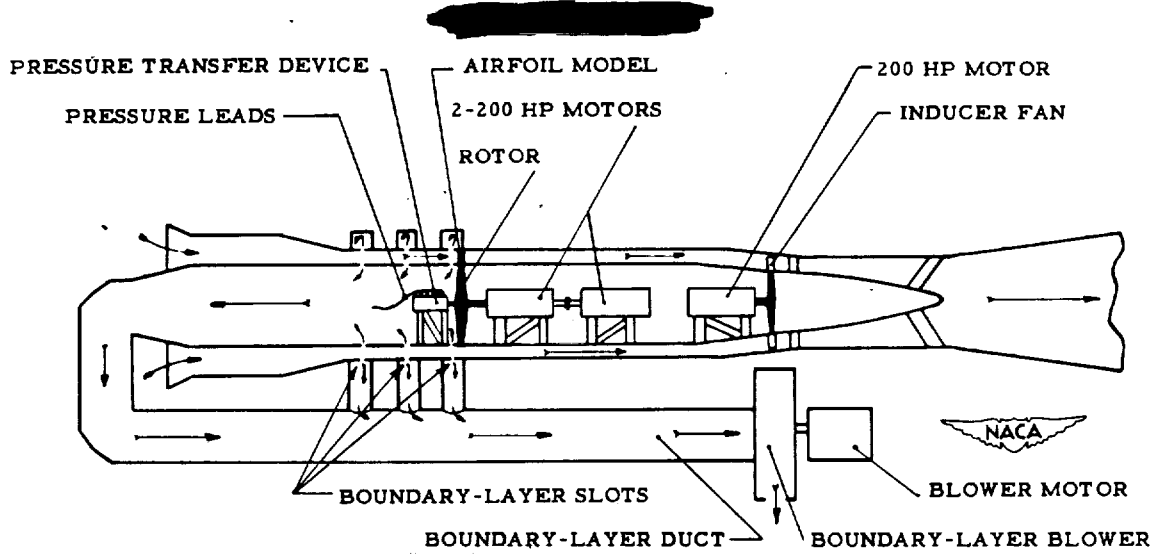


Figure 5.- Schematic diagram of the Langley transonic tunnel.

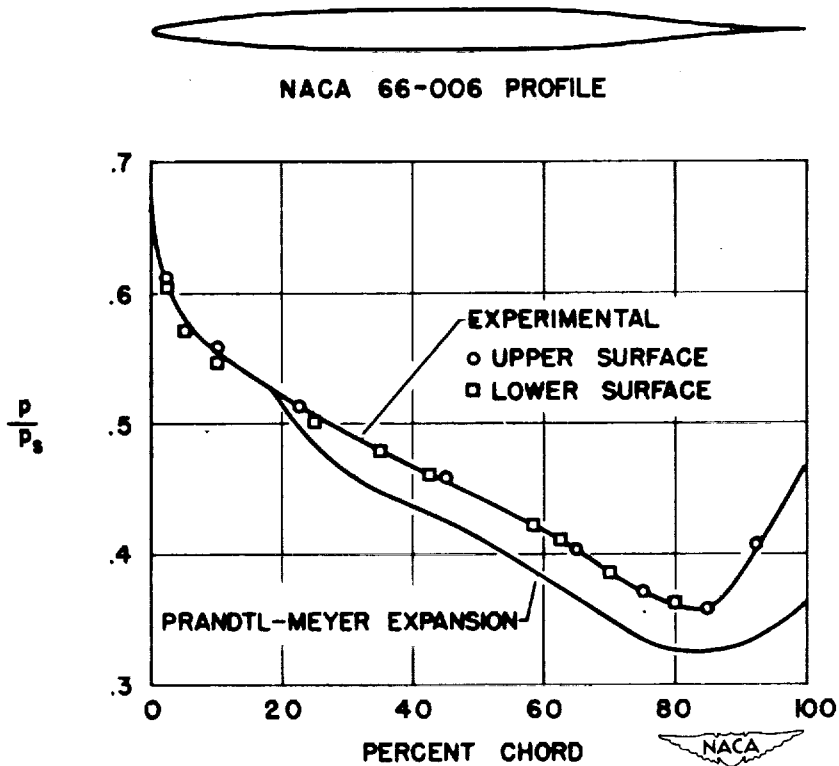


Figure 6.- Preliminary pressure-distribution data obtained in the Langley transonic tunnel at a Mach number of approximately unity for the NACA 66-006 airfoil at zero angle of attack.

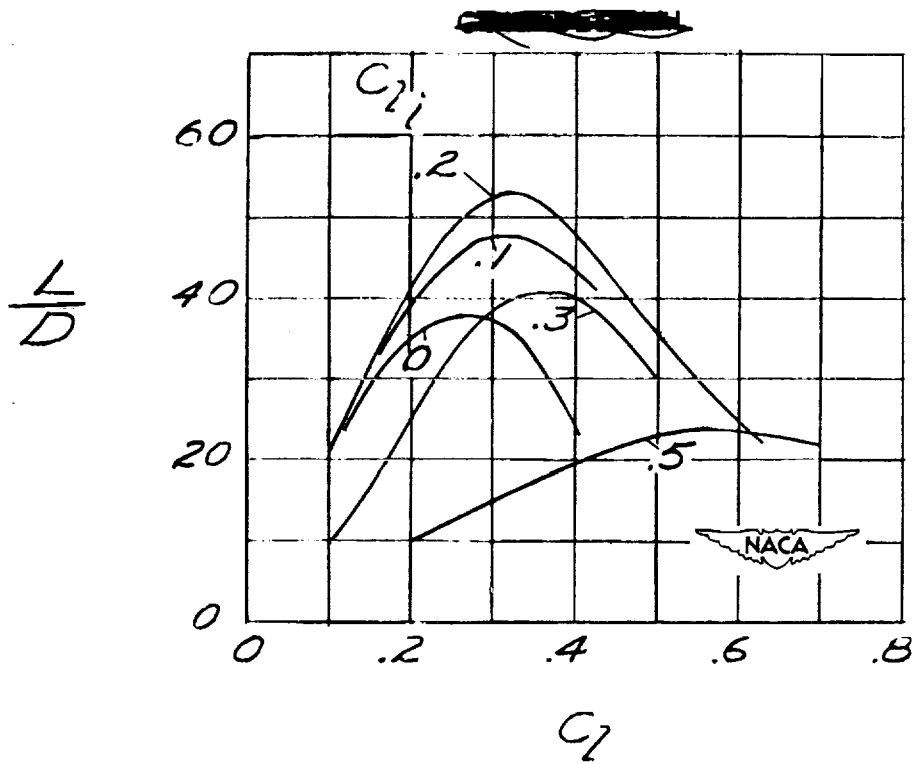


Figure 7.- Lift-drag ratios for NACA 16-X09 airfoils at  $M = 0.775$ .

D<sub>3</sub>

LIFT AND DRAG CHARACTERISTICS OF A WING WITH SEVERAL ANGLES OF SWEEP AT HIGH SUBSONIC SPEEDS

By Richard T. Whitcomb

Langley Memorial Aeronautical Laboratory

To obtain detailed information on flow around swept and unswept wings at high subsonic speeds, very extensive pressure measurements have been made on and behind a thin, high-aspect-ratio wing with no sweep and with 30° and 45° of sweepback and sweepforward at Mach numbers from 0.60 to 0.96 in the Langley 8-foot high-speed tunnel. Measurements have been made with and without aileron deflections; and for unswept condition they have been made with and without spoilers, dive recovery flaps, and brakes. For the swept configurations measurements have been made with a midwing fuselage present, whereas for the unswept condition they have been made with and without the fuselage present.

The measurements have included static-pressure readings at chordwise rows of orifices at eight stations along the span of the wing and at one station on the fuselage, total pressure measurements at various vertical stations behind the wing, and measurements of the average and fluctuating downwash at the probable horizontal tail location. From these measurements the normal-force, drag, and moment coefficients, the spanwise and chordwise pressure and load distributions, and wake patterns have been obtained for the various configurations. The major portion of the results is now available in NACA classified publications (references 1 to 9). The remainder of the results will be made available in the near future.

Because of the limited amount of time available even a summary discussion of all the results obtained cannot be given. Instead, some of the more interesting published and unpublished results pertaining to the normal force and drag of the unswept and swept wing without aileron or spoiler deflections are discussed briefly in the present paper and some of the other results obtained with aileron deflections are presented in the paper entitled "Effects of Sweep on Controls. I - Effectiveness" by Lowry and Johnson. The present paper includes a brief discussion of some of the variations of the over-all normal-force and profile-drag coefficients with Mach number presented in reference 5, but will deal primarily with a discussion of the section lift and drag characteristics. These factors indicate where the most severe changes in lift and drag occur at high Mach numbers and how the lift and drag characteristics of a wing with a given amount of sweep may be improved. The discussion will be limited to results obtained for conditions which usually occur during level flight at high speeds, but the results presented indicate the general nature of the changes that occur for other conditions.

The model used in this investigation without sweep or fuselage is shown in figure 1. The unswept wing has an NACA 65-210 section, an aspect ratio of 9.0, and a taper ratio of 0.4. The span of the model is 37.8; the mean chord is 4.2. The model was supported in the tunnel by a vertical steel plate as shown in figure 1. The model extended from both sides of the plate which completely spanned the tunnel and effectively produced two semicircular test sections. The advantages of such a support are described in reference 1.

Sweep was obtained by rotating the wing with respect to the support plate. Pressure measurements made on the tunnel wall indicate that the model on one side of the strut had little effect on the flow on the other side of the strut. A given over-all configuration represents, therefore, not a yawed model but sweptback and sweptforward semispan models. The semispan model with  $30^\circ$  of sweepback is shown in figure 2. The locations of the chordwise rows of pressure orifices are indicated in the same figure. The fuselage was placed in the midwing location. The tip was revised for each sweep to be parallel with the airstream. With these tips the aspect ratios of the wing with  $30^\circ$  and  $45^\circ$  of sweep were approximately 7.5 and 5, respectively. Sweep is based on the quarter-chord line.

With the model in place the tunnel choked at Mach numbers of 0.945, 0.975, and 0.985, approximately, for no sweep,  $30^\circ$ , and  $45^\circ$  of sweep, respectively. The data obtained at these choking Mach numbers are not applicable to the prediction of the wing characteristics in free air and these data are not presented. The data obtained at Mach numbers of 0.925 and 0.96 for the unswept and swept conditions, respectively, are affected to only a slight degree by choking tendencies, and pressure data obtained at these Mach numbers are presented. With the wake-survey support strut in place the tunnel choked at a Mach number of 0.89. Pressure measurements indicate that the tunnel choked at the support strut behind the model and this choking did not affect the field of flow at the model but merely limited the maximum test Mach number. Data obtained at this Mach number are, therefore, presented.

Presented in figure 3 are variations of the wing normal-force coefficients obtained from the pressure measurements with Mach number for the various sweeps at an angle of attack of  $2^\circ$ . The normal-force coefficient for the unswept wing started to decrease due to the onset of shock at a Mach number of approximately 0.75. The normal-force coefficients for the wing with  $30^\circ$  of sweepforward and sweepback started to decrease at a Mach number approximately 0.1 greater than the Mach number at which the coefficient for the wing with no sweep started to decrease. There are no losses in the normal-force coefficients for the wings with  $45^\circ$  of sweepforward and sweepback. Not only is the Mach number at which the normal-force coefficients decrease delayed

for  $30^\circ$  of sweepforward and sweepback but more important the magnitude of the changes is reduced. The magnitude of the change for the swept-forward condition is less than that for the sweptback condition.

Part of these variations are due to changes in the aspect ratio. However, it is believed that the major portion of the changes is due to the effects of sweep. For the angle of attack for which data are presented, the normal-force coefficients are generally very nearly equal to the lift coefficients and it may be assumed that the variations of the normal-force coefficient with Mach number presented are the same as the variations of the lift coefficient with Mach number.

Presented in figure 4 are variations of the wing profile-drag coefficients obtained from the wake-survey measurements with Mach number for the various sweeps at an angle of attack of  $2^\circ$ . The wing profile-drag coefficient for the wing with no sweep increased rapidly due to the onset of shock at a Mach number of approximately 0.75. The wing profile-drag coefficient for the wing with  $30^\circ$  of sweepback increased rapidly at a Mach number approximately 0.08 greater than the Mach number at which the drag increase occurred on the wing with no sweep. The wing profile-drag coefficient for the wing with sweepforward started to increase gradually at approximately the same Mach number as that at which the rapid increase in drag coefficient occurred for the wing without sweep and increased abruptly at the Mach number at which the similar abrupt increase occurred for the wing with  $30^\circ$  of sweepback. The wing with  $45^\circ$  sweepback experienced no large increase in the profile-drag coefficient.

A comparison of the measured loss in normal-force coefficient and increase in profile-drag coefficient produced by the occurrence of shock for a sweep angle of  $30^\circ$  and an angle of attack of  $2^\circ$  with the changes predicted for the same condition by use of the characteristics of the unswept wing and the simple sweep theory is presented in figure 5. The measured changes are shown as heavy lines, the predicted as dashed lines. The measured loss in normal-force coefficient is almost exactly the same as the predicted loss. The measured increase in drag coefficients occurs initially at about the same Mach number as does the predicted increase but is more severe than the predicted increase. The agreement between the measured and predicted variations is much closer than any previous similar comparison has shown. The closer agreement is believed to be due to the relieving effect of the midwing fuselage on the flow around the root of the swept wing.

Presented in figure 6 are spanwise variations of the section normal-force and section profile-drag coefficients for the wing without sweep at an angle of attack of  $2^\circ$  at various Mach numbers, obtained from the pressure and wake measurements. Because of the asymmetrical, three-dimensional flow around the wing, the spanwise variations

of section profile-drag coefficient obtained from wake measurements made behind the wing are not exactly the same as the actual spanwise variations of the coefficients at the wing. The variations for all sweeps are believed to be very nearly correct, however. The spanwise variation of section normal force at a Mach number of 0.6 is very nearly the same as that predicted by use of potential-flow theory. The section profile-drag coefficients for the various sections are very nearly the same value for a Mach number of 0.6.

When the Mach number is increased beyond the critical value, the normal-force coefficients for the various sections decrease and generally the section profile-drag coefficients increase. The increase in normal-force coefficient and the decrease in drag coefficient occur at higher Mach numbers and are much less severe for the sections near the tip and root, however. The delay in the Mach number at which the increase in drag coefficient occurs on the tip is so great that no drag increase occurs at this region up to the highest test Mach numbers.

The delays and reductions of the changes at the tip may be attributed to the three-dimensional flow around the tip. This flow reduces the induced velocities over the tip sections, thus increasing the Mach numbers at which severe shock occurs on these sections. Also, because of this flow the air is directed inward over the upper surface of the tip sections and the tip effectively has sweepforward. The delay and reductions of the changes at the root sections may be attributed to the relieving effect of the midwing fuselage.

Similar spanwise variations of the section normal-force coefficient and the section profile-drag coefficient for the wing with  $30^\circ$  of sweepforward for an angle of attack of  $2^\circ$  at various Mach numbers are presented in figure 7. The spanwise variation of section normal-force coefficient at a Mach number of 0.6 is very nearly the same as that predicted by use of potential-flow theory. The section profile-drag coefficients for the various sections are very nearly the same across the semispan. This spanwise uniformity of section profile-drag coefficient indicates that there is very little spanwise flow of air in the boundary layer on a sweptforward wing at the angle of attack for which these data are presented. When the Mach number is increased beyond a Mach number of 0.8, the section profile-drag coefficients for the root sections increase. The gradual increase in the over-all drag coefficient for the sweptforward wing, which occurs at approximately the same Mach number as shown in figure 4, may be attributed to this rise in the coefficients for the root. When the Mach number is increased up to the highest test value, the section profile-drag coefficients for the root sections become very large. The section profile-drag coefficients for the outboard sections rise only slightly, however. In fact, the increases in the section profile-drag coefficient with Mach number for these outboard sections are less than those predicted

by use of the simple sweep theory. As a result, the abrupt increase in the over-all drag coefficient for the sweptforward wing, which occurs at a Mach number of approximately 0.85, may be attributed primarily to the increase in the section profile-drag coefficients at the root sections. There is no severe reduction in the section normal-force coefficients for the root sections associated with the increases in the section profile-drag coefficients for these sections. Similar early and severe changes in the section profile-drag coefficients at the wing-fuselage juncture occur with  $45^\circ$  of sweepforward.

Because of the severe separation of the flow near the wing-fuselage juncture associated with the large increases in drag at these sections, the wake behind this juncture is very large at the higher Mach numbers; and due to the large wake, the downwash at the probable tail location changes by very large amounts at relatively low Mach numbers in comparison with the Mach numbers at which the changes occur behind the wing with a similar amount of sweepback.

The reason for the early abrupt separation of the flow at the root sections is shown by the pressure measurements made on the surface of the wing. Presented in figure 8 are contour maps of the pressures measured on the upper surface of the wing with  $30^\circ$  of sweepforward for an angle of attack of  $2^\circ$  at a Mach number of 0.6. The solid lines show the lines of constant pressure coefficient; the dashed lines indicate the lines of peak pressure. The contours indicate very high negative pressures or high induced velocities at the leading edge of the root sections. Because of these high induced velocities, the critical Mach numbers for the root sections are much lower than the critical Mach numbers for the sections further outboard and it would be expected that severe shock would occur on the root sections and that the flow over these sections would separate at much lower Mach numbers than it would at the outboard sections.

The high negative pressures on the leading edge of the root sections may be attributed to the induced flow associated with sweptforward wings. It is believed that the pressure peaks may be reduced, and thus the critical Mach number and the Mach number at which shock occurs may be increased, by reshaping the fuselage and by washing out the root sections. Reshaping the fuselage alone would probably not completely eliminate the pressure peaks since the effect of such a reshaping would be local, while the pressure peaks extend over a considerable region of the wing leading edge.

Spanwise variations of the section normal-force coefficients and section profile-drag coefficients for the wing with  $30^\circ$  of sweepback for an angle of attack of  $2^\circ$  at several Mach numbers are presented in figure 9. The spanwise variation of section normal-force coefficient

for a Mach number of 0.6 is again very nearly the same as that predicted by use of potential-flow theory. The section profile-drag coefficients are very nearly the same for each of the sections along the semispan. When the Mach number is increased from 0.6 to the highest test value, the various sections experience reductions in the normal-force coefficients and increases in the profile-drag coefficients as would be expected. The reductions in the normal-force coefficients and the increases in the profile-drag coefficients occur at lower Mach numbers and are much more severe at the outboard sections than at the inboard sections. The increases in the profile-drag coefficient for the tip sections are so severe that at the highest test Mach number, a Mach number of 0.89, the section profile-drag coefficient for these sections for the sweptback wing are greater than those for the tip sections of the unswept wing. Near the wing-fuselage juncture the drag coefficients measured at the highest test Mach number are the same as those measured at a Mach number of 0.6. These data indicate spanwise variations of the changes in the section characteristics associated with the onset of shock which are exactly opposite to those which were thought to occur on sweptback wings. Instead of the initial and most severe changes occurring at the root, they occur at the tip.

With  $45^\circ$  of sweepback, the spanwise variations of section normal-force and section profile-drag coefficients are nearly the same for all Mach numbers up to the highest test value. However, the wake measurements made behind this wing at a Mach number of 0.89 indicate a slight initial increase in the drag coefficients for the tip sections.

The early and severe changes in the characteristics of the tip sections may be attributed to three factors: Lower critical Mach numbers for the tip sections, the distribution of pressures on the tip sections, and the inflow over the upper surface of the tip section. The contour map of the pressure coefficients for the upper surface of the wing with  $30^\circ$  of sweepback for an angle of attack of  $2^\circ$  at a Mach number of 0.6 is presented in figure 10. Because of the relieving effect of the fuselage, the maximum pressure coefficients at the root sections are less than the maximum pressure coefficients for the sections further outboard. Due to the induced flow, peculiar to sweptback wings, pressure peaks occur on the leading edge of the sections near the tip. As a result of this spanwise variation in peak pressures, the critical Mach numbers for the tip sections are less than those for the root sections. Near the tip the distribution of pressure is changed in such a manner that the region of maximum pressure coefficients slopes forward with respect to the swept span of the wing. Assuming that shock occurs initially in the region of maximum pressure coefficients it may be deduced that the effective sweep of the tip sections is less than the geometric sweep of the wing. Because of the flow around the tip, the flow over the upper surface of the tip sections is directly



inward and the effective sweepback of the tip sections is further reduced. Each of these factors would lead to earlier and more severe separation and changes in the section normal-force coefficients and section profile-drag coefficients near the tip.

None of the previously mentioned factors explains the extraordinary delay in the increases of section profile-drag coefficients for the root sections. The contour map of the pressures measured on the upper surface of the wing with  $30^\circ$  of sweepback for an angle of attack of  $2^\circ$  at a Mach number of 0.89 (fig. 11) indicates the probable reason for this delay. At this Mach number, there is a severe shock along the entire semispan of the wing as indicated by the very severe adverse pressure gradient near the trailing edge. This shock appears to be normal to the stream and very near the trailing edge at the wing-fuselage juncture. It would be expected that such a strong normal shock would lead to severe separation at the wing-fuselage juncture. The pressure recovery behind the shock indicates, however, that very little separation is produced by the shock.

Since the initial and most severe changes in the section characteristics occur at the tip, it might be expected that the changes in the over-all normal-force and profile-drag coefficient for the wing with sweepback could be delayed and perhaps reduced by washing out the tip sections to reduce the angle of attack of these sections which experience the most severe changes. No data have been obtained to show the effects of washout on the changes in the normal-force and profile-drag coefficients; however, pressure data have been obtained on the wing of the present discussion with aileron deflection of  $-5^\circ$  which should simulate to a certain extent a washout condition. The normal-force results obtained with this aileron deflection indicate that a definite reduction in the changes of the normal-force coefficient with Mach number for the wing with  $30^\circ$  of sweepback is produced by such a deflection. Washout applied to the wing to improve the high-speed characteristics would also probably improve the landing characteristics of the wing but might produce adverse changes in the lateral stability and control characteristics of the wing.

The results of detailed pressure measurements made on and behind a high-aspect-ratio wing with and without sweep at high subsonic Mach numbers indicate that the initial and most severe changes in the normal-force and profile-drag characteristics occur at the tip for sweptback wings and at the root for sweptforward wings. The results also indicate means of improving the high-speed normal-force and profile-drag characteristics of a wing with a given amount of sweep.

## REFERENCES

1. Whitcomb, Richard T.: Investigation of the Characteristics of a High-Aspect-Ratio Wing in the Langley 8-Foot High-Speed Tunnel. NACA RM No. L6H28a, 1946.
2. Ferri, Antonio: Preliminary Investigation of Downwash Fluctuations of a High-Aspect-Ratio Wing in the Langley 8-Foot High-Speed Tunnel. NACA RM No. L6H28b, 1946.
3. Mattson, Axel T.: Investigation of Dive Brakes and a Dive-Recovery Flap on a High-Aspect-Ratio Wing in the Langley 8-Foot High-Speed Tunnel. NACA RM No. L6H28c, 1946.
4. Luoma, Arvo A.: An Investigation of a High-Aspect-Ratio Wing Having 0.20-Chord Plain Ailerons in the Langley 8-Foot High-Speed Tunnel. NACA RM No. L6H28a, 1946.
5. Whitcomb, Richard T.: An Investigation of the Effects of Sweep on the Characteristics of a High-Aspect-Ratio Wing in the Langley 8-Foot High-Speed Tunnel. NACA RM No. L6J01a, 1946.
6. Luoma, Arvo A., and Liccini, Luke L.: An Investigation of the Hinge-Moment Fluctuations of 0.20-Chord Plain Ailerons on a High-Aspect-Ratio Wing in the Langley 8-Foot High-Speed Tunnel. NACA RM No. L6L10a, 1947.
7. Whitcomb, Richard T.: An Investigation of the Downwash at the Probable Tail Location behind a High-Aspect-Ratio Wing in the Langley 8-Foot High-Speed Tunnel. NACA RM No. L7B12, 1947.
8. Luoma, Arvo A.: An Investigation of the Lateral-Control Characteristics of Spoilers on a High-Aspect-Ratio Wing of NACA 65-210 Section in the Langley 8-Foot High-Speed Tunnel. NACA RM No. L7D21, 1947.
9. Luoma, Arvo A., Bielat, Ralph P., and Whitcomb, Richard T.: A Wind-Tunnel Investigation of the Lateral Control Characteristics of Plain Ailerons on a Wing with Various Amounts of Sweep. NACA RM No. L7I15, 1947.

Whitcomb

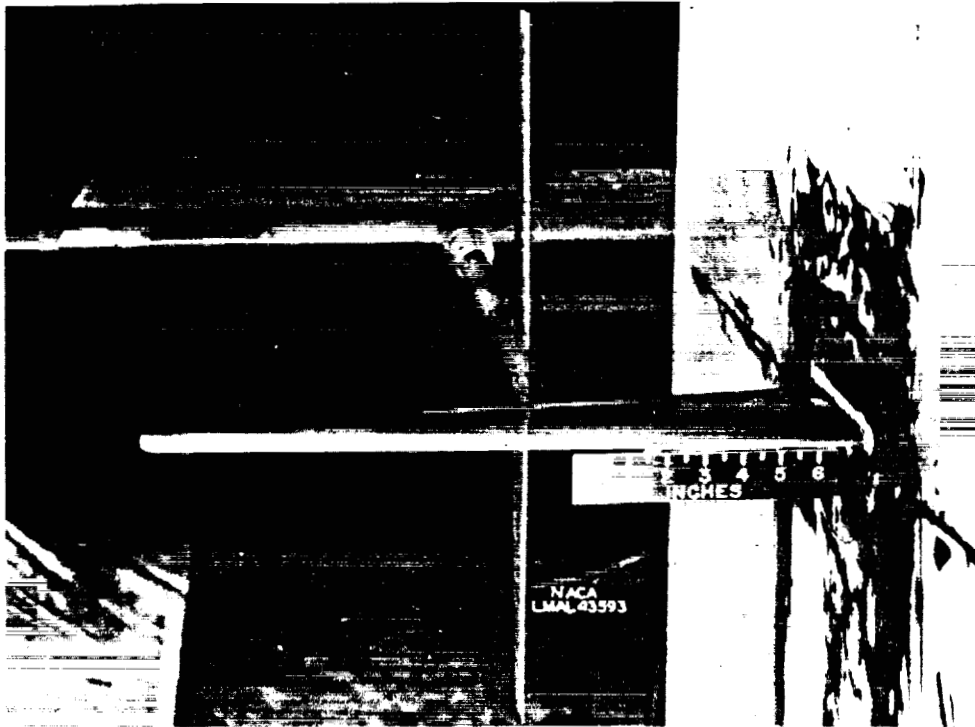


Figure 1.- Photographs of unswept wing without fuselage.

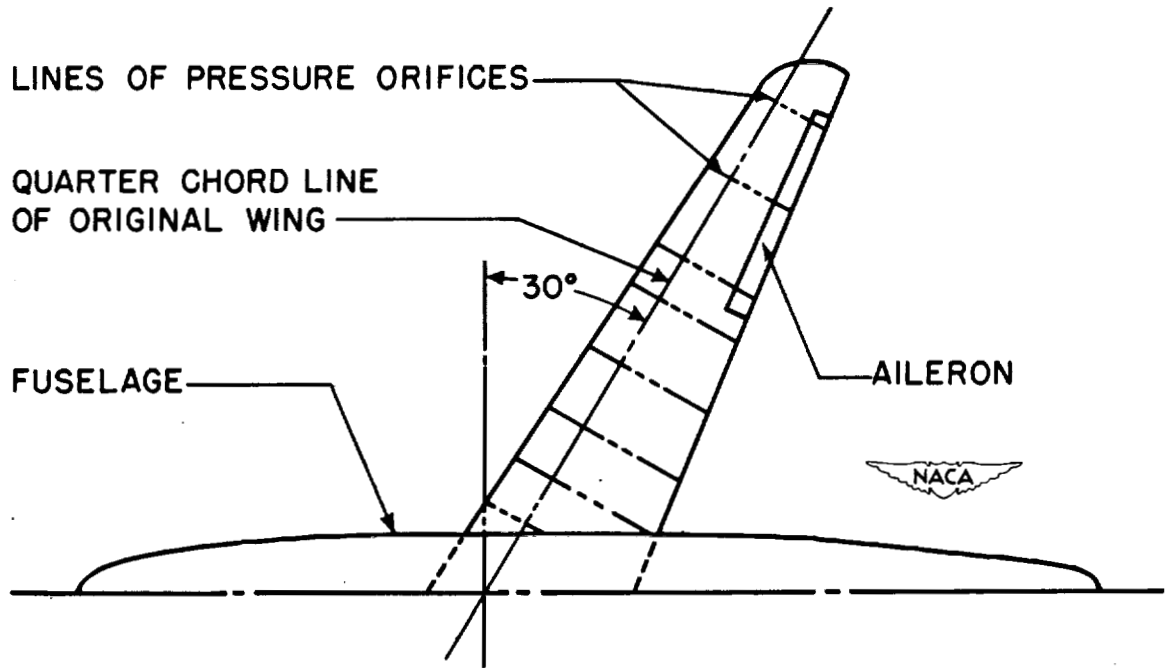


Figure 2.- Plan view of wing with 30° of sweepback.

23(a)

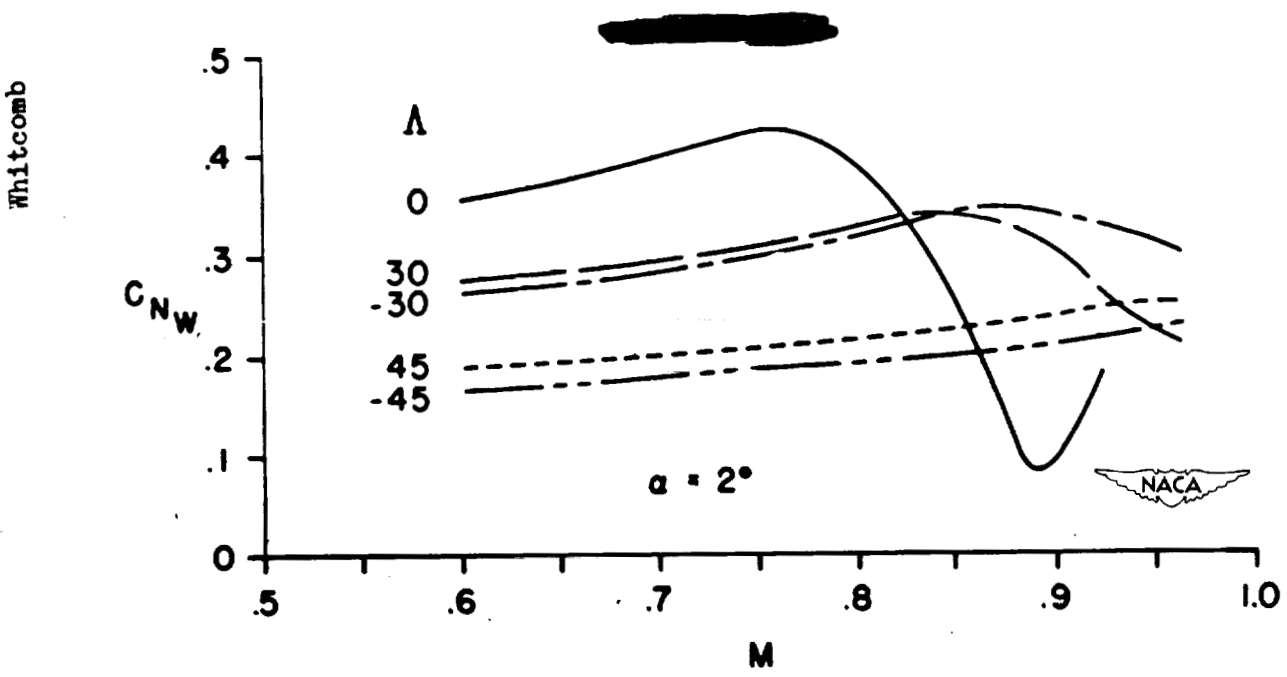


Figure 3.- Variations of wing normal-force coefficient with Mach number for  $\alpha = 2^\circ$ .

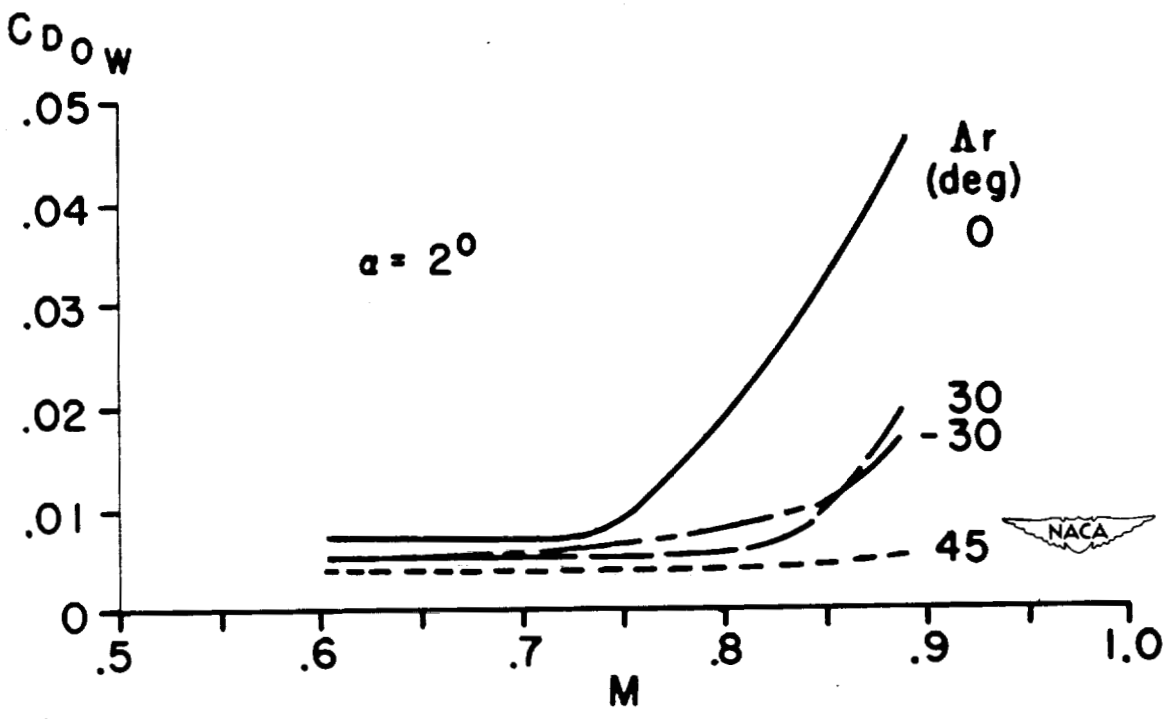


Figure 4.- Variations of wing profile-drag coefficient with Mach number for  $\alpha = 2^\circ$ .

28(b)

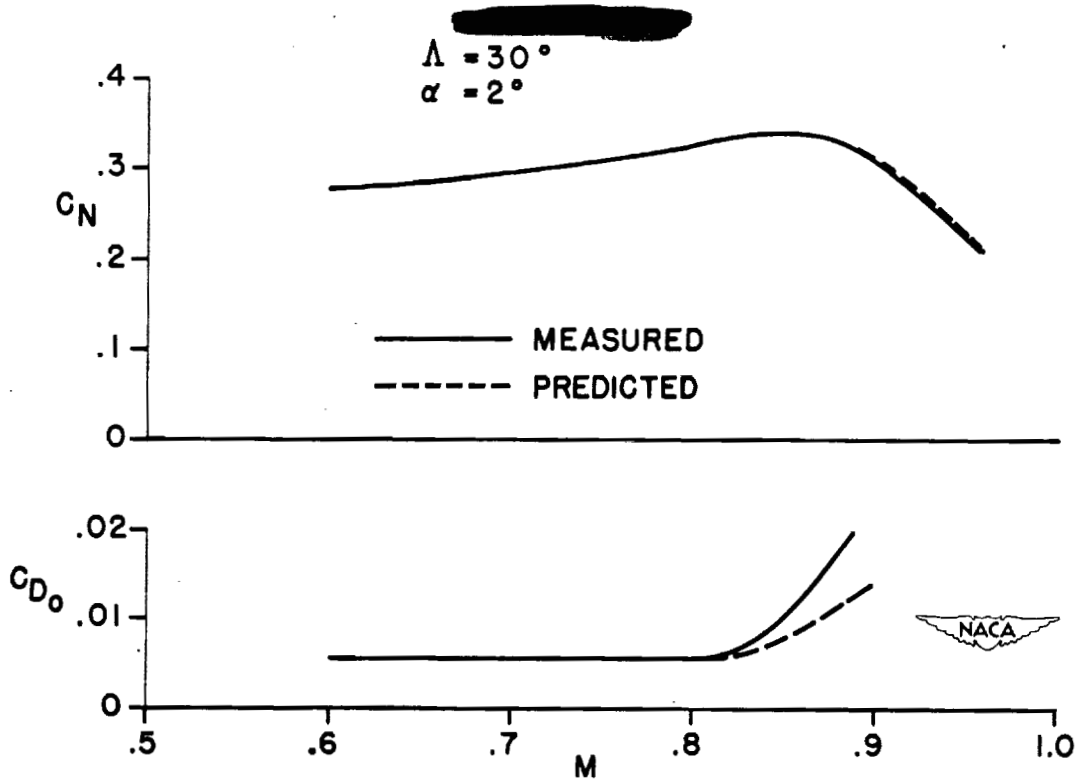


Figure 5.- Comparisons of measured and predicted variations of wing normal-force coefficient and wing profile-drag coefficient with Mach number for  $\Lambda = 30^\circ$ .

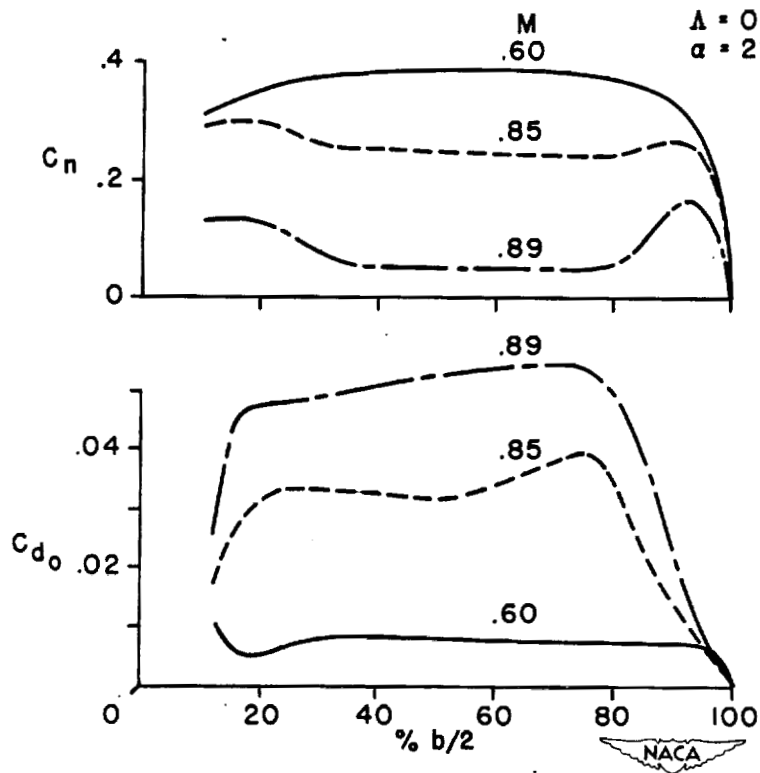


Figure 6.- Spanwise variations of section normal-force coefficient and section profile-drag coefficient for  $\Lambda = 0^\circ$  and  $\alpha = 2^\circ$ .

Whitcomb

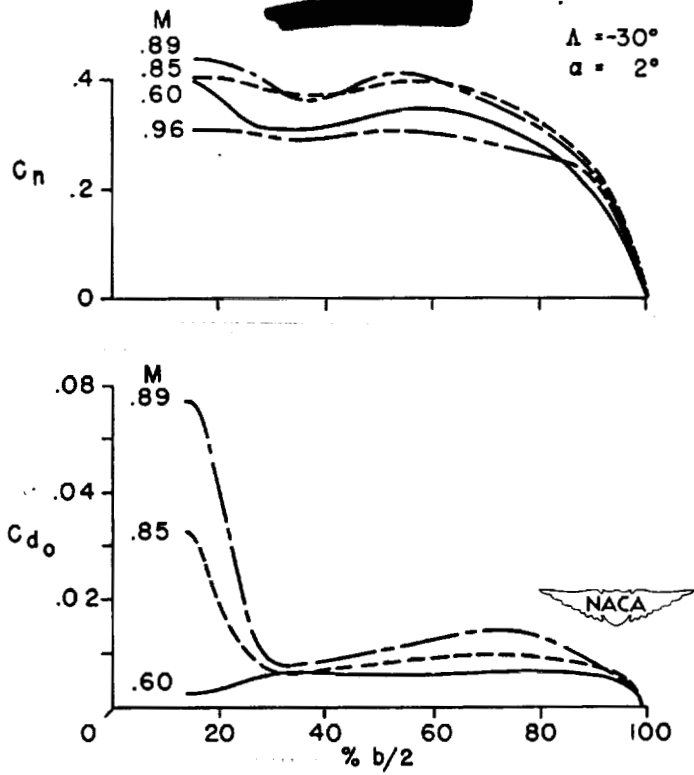


Figure 7.- Spanwise variations of section normal-force coefficient and section profile-drag coefficient for  $\Lambda = -30^\circ$  and  $\alpha = 2^\circ$ .

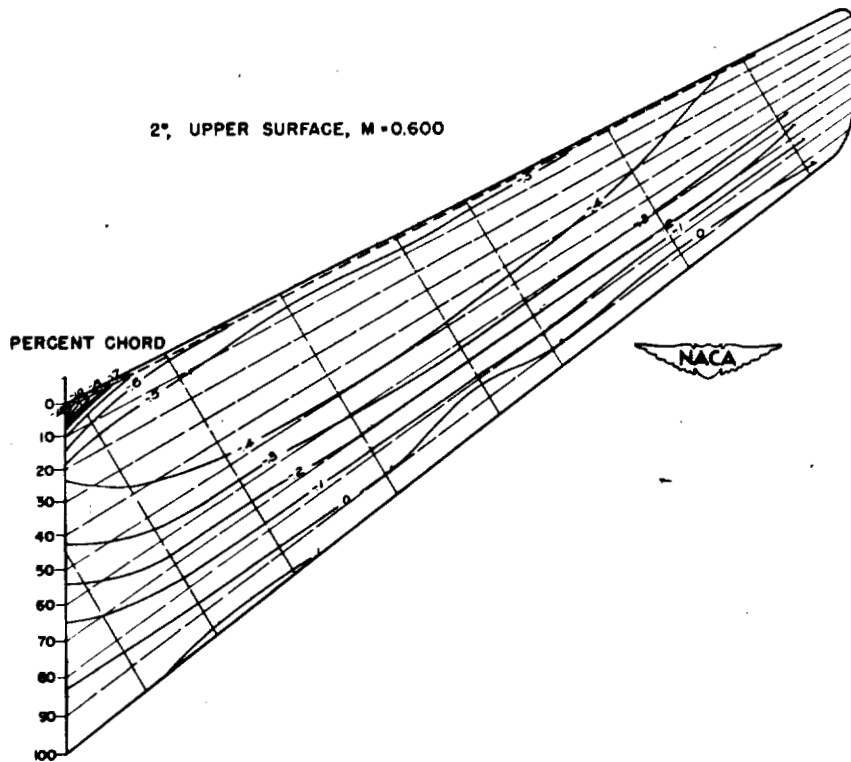


Figure 8.- Equal pressure-coefficient contours for  $\Lambda = -30^\circ$ ,  $\alpha = 2^\circ$ , and  $M = 0.60$ .

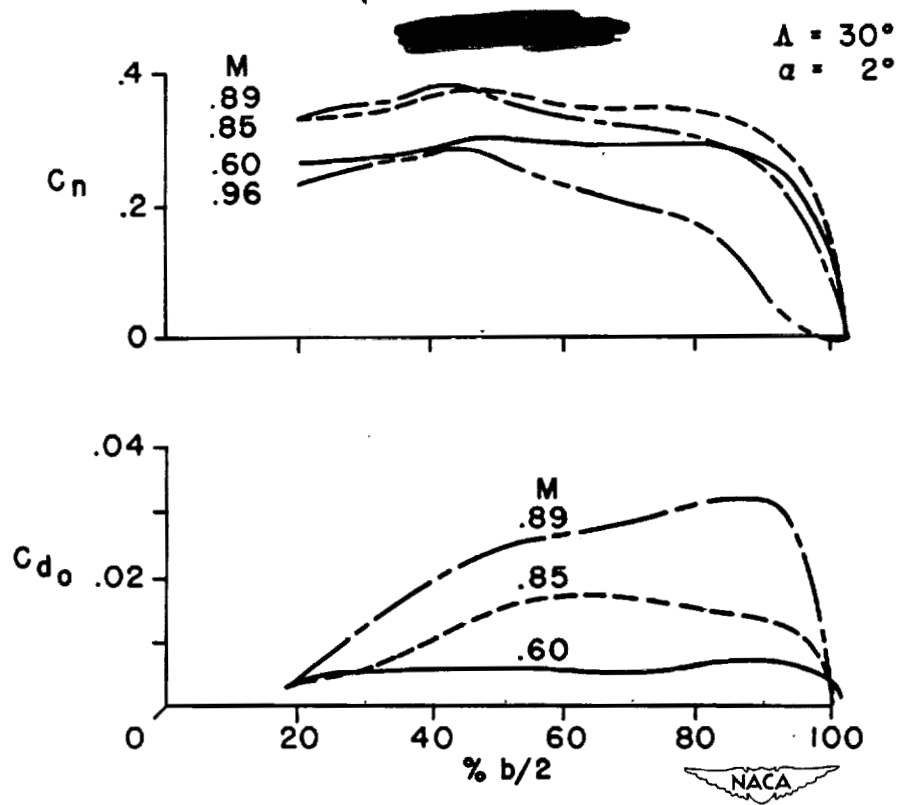


Figure 9.- Spanwise variations of section normal-force coefficient and section profile-drag coefficient for  $\Lambda = 30^\circ$  and  $\alpha = 2^\circ$ .

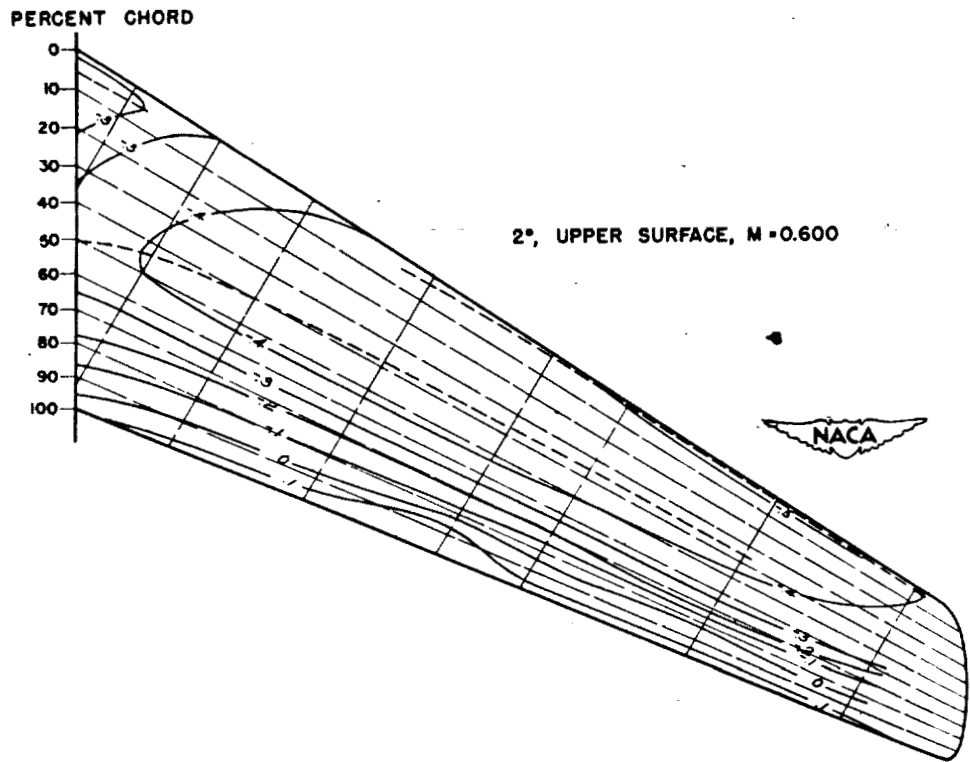
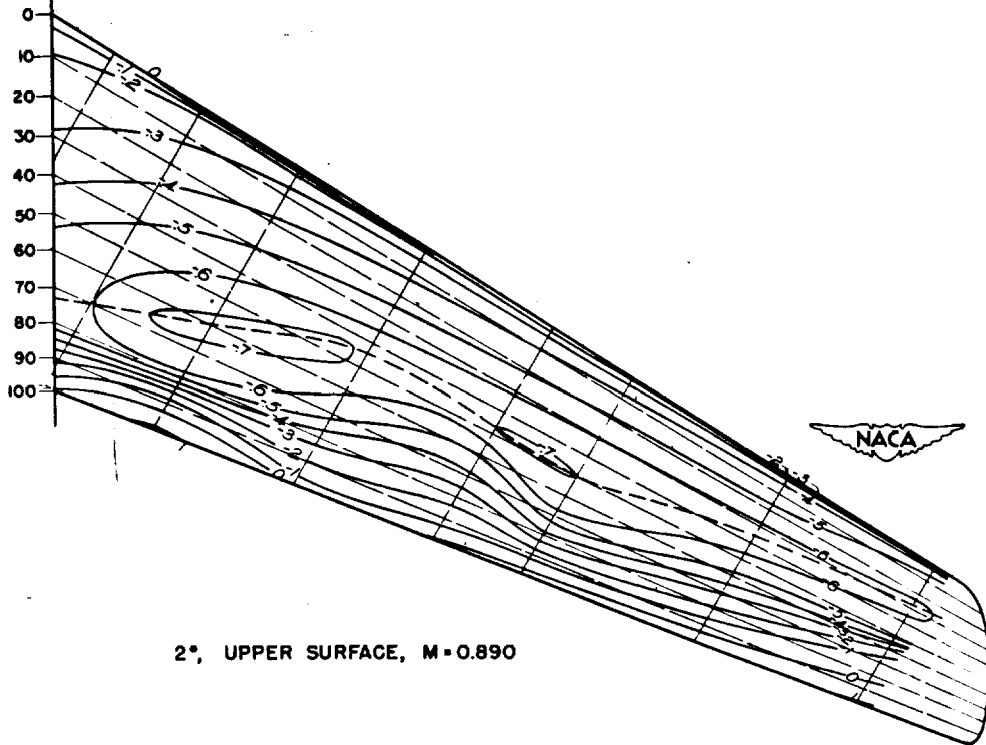


Figure 10.- Equal pressure-coefficient contours for  $\Lambda = 30^\circ$ ,  $\alpha = 2^\circ$ , and  $M = 0.60$ .

Whitcomb

PERCENT CHORD



2°, UPPER SURFACE, M = 0.890

Figure 11.- Equal pressure-coefficient contours for  $\Lambda = 30^\circ$ ,  
 $\alpha = 2^\circ$ , and  $M = 0.89$ .



## LANDING CHARACTERISTICS OF HIGH-SPEED WINGS

By Herbert A. Wilson, Jr. and Laurence K. Loftin, Jr.

Langley Memorial Aeronautical Laboratory

The wings of aircraft designed to fly at transonic Mach numbers are usually characterized by thin airfoil sections and, in most cases, low aspect ratio and considerable sweep. The poor maximum lift characteristics of such wings and the difficulties associated with the prediction of their characteristics have greatly complicated the problem of designing high-speed aircraft to land at speeds within the capabilities even of highly skilled pilots. Considerable effort is therefore being directed toward the improvement of the maximum lift characteristics of wings suitable for high-speed applications. The present paper first reviews the development of high-lift devices in two dimensions; second, surveys the available large scale data of the characteristics of three-dimensional wings; and third, indicates briefly the correlation between the characteristics of swept and unswept wings.

The high-lift devices investigated are in the following two classes: those which are applied to the trailing edge of the airfoil and those which are applied to the leading edge of the airfoil. For airfoils which are only moderately thin, a section maximum lift sufficiently high often can be obtained by the use of a suitable trailing-edge device alone. For thin airfoils or for airfoils having sharp leading edges, however, the large peak negative pressures near the leading edge and the subsequent highly adverse pressure gradient cause laminar separation near the leading edge. Accordingly, it is necessary to use a leading-edge device designed to lower this peak and reduce the adverse pressure gradient in order to obtain large increases in the section maximum lift coefficient with these airfoil sections.

Double slotted flaps have long been known to provide about the largest gains in lift of all types of trailing-edge flaps. In figure 1 are shown results obtained with the NACA 65-210 airfoil equipped with such a flap and also with single slotted and with split flaps. (See reference 1.) The results herein shown and those for figures 2 to 4 have been obtained with a two-dimensional setup at a Reynolds number of  $6 \times 10^6$ , which corresponds approximately to that for an airplane with a 6-foot-chord wing landing at 100 miles per hour. The relative merit of the types of flap is clearly shown. The highest maximum lift coefficient obtained was about 2.80 with the double slotted flap. The values shown for the two types of slotted flap are for the optimum locations of flap and vane and, if such flaps were applied to a three-dimensional swept wing, some further experimentation might be required to insure that the optimum location remains the same.

The effects of section thickness ratio and the location of minimum pressure at the design lift coefficient have been investigated for a number of NACA 6-series airfoils with double slotted flaps (reference 2). In figure 2 the left side shows the variation of maximum lift coefficient with thickness ratio for airfoils with a design lift coefficient of 0.2. The variation is seen to be approximately linear for both smooth and rough airfoils over the test range. On the right side data indicating the effect of minimum pressure location at the design lift coefficient are shown for 10-percent-thick airfoils with a design lift coefficient of 0.2. The maximum lift coefficient is seen to decrease linearly as the position of minimum pressure moves rearward. (See curve for smooth airfoils in fig. 2.) For rough airfoils the minimum-pressure location is unimportant.

It should be pointed out herein that these high maximum lift coefficients are also accompanied by high negative pressure peaks at the leading edge. Inasmuch as high landing speeds are being considered for many high-speed aircraft, it is altogether possible that maximum lift coefficients different from those shown might be obtained because of Mach number effects (reference 3).

The effectiveness of leading-edge devices in increasing the maximum lift is shown in figure 3. These results were obtained with a NACA 641-012 airfoil section equipped with a split flap, with a nose flap of the type that is hinged out from the lower surface, and with a nose flap extending tangentially from the upper surface at the leading edge (reference 4). It is seen that the maximum effectiveness of the nose flaps is only realized when they are used in conjunction with the trailing-edge flap. Also, the tangential type of flap is seen to give somewhat better results than the lower surface type.

The leading-edge devices discussed herein are not the only ones that could be made effective. Any leading-edge device which tends to reduce the negative pressure peak and the adverse pressure gradient at the leading edge should be effective in increasing the maximum lift of a thin airfoil.

An indication of what can be accomplished on thin biconvex airfoils with another such device is shown in figure 4. A droop nose of 0.15c and a plain trailing-edge flap of 0.20c have been investigated on a biconvex airfoil 6-percent thick. (See reference 5.) The highest maximum lift coefficient of nearly 2.00 was obtained with the leading and trailing flaps at their optimum deflections of  $30^\circ$  and  $60^\circ$ , respectively. Substantially the same results were obtained with the 10-percent-thick biconvex section and with a 6-percent-thick NACA 64-series section between Reynolds numbers of  $3 \times 10^6$  and  $9 \times 10^6$ . Recent tests of an NACA 63-006 airfoil indicate a favorable scale effect between Reynolds numbers of  $9 \times 10^6$  and  $25 \times 10^6$ ; whereas over the same range the biconvex sections show no scale effect. These results indicate that at 6-percent thickness as well as at about 9-to

10-percent thickness the conventional section may have some slight advantage from a maximum lift standpoint.

The discussion has thus far dealt only with two-dimensional results. At present no adequate method has been developed for predicting the high-angle-of-attack characteristics of swept wings. Such studies as the ones by Sivells and Neely (reference 6) and Sivells (reference 7) in which nonlinear section data have been applied to the calculation of the characteristics of unswept wings and those described in references 8 and 9 in which lifting-line and lifting-surface theories have been applied to the calculation of swept-wing characteristics at low and moderate angles of attack together with the section data form a valuable background upon which to base conjectures as to the probable effect of various modifications to swept wings. It is necessary however to rely on large scale experiment for the final quantitative evaluation of the characteristics of wings having any considerable amount of sweep.

In answer to the need for an organization of the data pertaining to the maximum lift characteristics of swept wings Sweberg and Lange have summarized the existing data (reference 10). The principal emphasis in this report was on the effects of Reynolds number and the importance of obtaining swept-wing results at the highest possible scale was established. Since the investigation of reference 10 was made, a number of large Reynolds number investigations of the high-lift-range characteristics of wings for high-speed aircraft have been completed in the Langley 19-foot pressure tunnel, the Langley full-scale tunnel and in the Ames 40- by 80-foot tunnel. These investigations have been closely correlated but the configurations have not in general been sufficiently systematized to allow the isolation of the effects of sweep angle from those of aspect ratio and taper ratio. It is possible at this time, however, to draw a number of useful conclusions from these results.

The information of the characteristics of three-dimensional wings presented in figures 5 to 14 is only a very brief summary of the total of the information that is available. The detailed test results and analysis are contained in references 11 to 22 and a few other prospective reports.

The first effect to be discussed is that of Reynolds number. Figure 5 shows the maximum-lift-coefficient variation with Reynolds number obtained with four swept wings. Generally speaking the effects are small. The most significant result is a small increase in the maximum lift coefficient between Reynolds numbers of  $4.2 \times 10^6$  and  $5.5 \times 10^6$  for the wing having  $42^\circ$  sweep and NACA 64<sub>1</sub>-112 airfoil sections. This increase is rather unimportant in itself but is accompanied by significant improvements in the longitudinal stability.

Adding standard roughness to the wing as shown by the dashed curve decreases the lift coefficient over the entire range and eliminates the favorable scale effect. The same wing with biconvex airfoil sections shows no scale effect within the test range just as was the case for the two-dimensional airfoil results.

The wing with  $48^\circ$  sweep had lower scale effect even than the  $42^\circ$  swept wing and the changes still occur below a Reynolds number of  $5 \times 10^6$ . All of the results shown hereinafter were obtained above this critical range.

Inasmuch as the experimental information obtained herein has been obtained both with and without fuselage, it is desirable first to examine the effect of the fuselage on the maximum lift characteristics so that both types of results can be used later. Figure 6 shows the results of a series of tests made with a  $42^\circ$  swept wing of aspect ratio 4 with a fuselage in the high-wing, the midwing, and the low-wing locations. The fuselage had a relatively small effect on the maximum lift. The drag of the fuselage likewise is an unimportant factor in the high-lift-coefficient range. The vertical location of the wing on the fuselage made no difference for the plain-wing results and in the high-lift-coefficient range made no difference with the flapped wing. The same conclusions do not, however, apply to the longitudinal stability characteristics at the stall. In this connection a few stability effects, where they are of first-order importance, will be pointed out during the discussion of the results. However, the stability of swept wings in the low-speed ranges is the subject of a paper to be presented at this conference by Mr. Donlan entitled "Current Status of Longitudinal Stability."

The next variable discussed is that of airfoil section. Results are shown in figure 7 for three wings - one with  $42^\circ$  sweep, one with  $48^\circ$  sweep, and a  $60^\circ$  delta wing. Airfoils of conventional section and shape are represented by the NACA 641-112 airfoil sections (perpendicular to quarter-chord line) in the first two cases and by the NACA 0015-64 airfoil (root section) in the third case. The very thin sections are represented by biconvex sections 10-percent thick and in the case of the delta wing are also represented by adding a sharp leading edge to promote separation. For the  $42^\circ$  swept wing, representative of the moderate sweep case, it is seen that the airfoil section makes a large difference in the maximum lift characteristics. The decrease in maximum lift resulting from the use of the biconvex or thin sections is, likewise, accompanied by extremely undesirable changes in the longitudinal stability. In the higher sweep range represented by the  $48^\circ$  swept wing the effects of airfoil section are much less marked, and in the extremely high sweep range represented by the delta wing it would appear that sharp-leading-edge airfoil sections may have some slight advantages over the conventional sections although

it is suspected that more favorable results might have been obtained by the use of a thinner conventional section.

Throughout the investigations summarized herein, split flaps or plain flaps of about 20 percent chord have been used with the wings to give an index of the lift producing capacity of the wing with trailing-edge high-lift devices in general.

The results obtained by applying semispan split flaps to the  $42^\circ$  and the  $48^\circ$  swept wings with NACA 64-series airfoil sections are shown in figure 8. With the  $42^\circ$  swept wing a lift increment of 0.20 was obtained which was about two-thirds of the lift increment due to these flaps below the angle for maximum lift. The maximum lift increment for the  $48^\circ$  swept wing was considerably smaller although the increment in lift below the stall was about the same as for the  $42^\circ$  swept wing with due consideration taken of the differences in sweep of the two wings. It would appear from these results that the effectiveness of flaps in increasing the maximum lift falls off rapidly as the sweep increases. This is in accord with the data obtained by McCormack and Stevens in the Ames 40- by 80-foot tunnel (reference 11). These results indicate that at a sweep angle of about  $60^\circ$  flaps will be ineffective in increasing the maximum lift.

Also, shown in this figure are key letters designating the longitudinal stability characteristics at the stall for each configuration. These letters, G for good, M for marginal, and P for poor, will be used in figures 8 to 11. A curve of pitching-moment coefficient against lift coefficient which has no abrupt slope changes in a positive direction and which either breaks in a negative direction or does not change at the stall is considered to be good. A pitching-moment curve which has sharp changes in slope in an unstable (positive) direction below the stall or which breaks in a positive direction at the stall is considered poor. It must be realized, of course, that the tail geometry and location will also affect the stability of the final airplane. All of the wings shown in figure 8 had poor longitudinal stability at the stall, arising from tip stalling which caused unstable breaks.

The biconvex wing results are shown in figure 9. For the case of  $0^\circ$  sweep the increment obtained from the trailing-edge flap is very large. But as the sweep is increased the lift increment becomes progressively smaller even though reasonably large increments in lift coefficient are produced below the stall. The failure of the flaps to give substantial increases in maximum lift coefficient is a consequence of early tip stall, and it has become quite evident that in order to produce satisfactory lift characteristics on these wings it will be necessary to provide the wing tip with a leading-edge stall

control aid or high-lift device. An additional phenomenon shown herein is the beneficial effect of sweep on the maximum lift coefficient of these thin sections. For the unswept case the maximum lift coefficient of 0.58 measured for the basic wing is below the section value of about 0.7 by about the amount that would be calculated from standard methods of applying section data to three-dimensional wings. As the sweep increases, however, the maximum lift of the wing increases and exceeds the section value. This result is associated with a strong spanwise flow at the leading edge of the wing which enables the flow over the bubble of separation at the leading edge to reestablish itself at higher angles of attack than for the two-dimensional case (references 12 and 13).

The longitudinal stability characteristics of the unswept wing and of the delta wing are good. For the swept wings the pitching-moment curves have a highly unstable slope as maximum lift is approached and even though the eventual break is in a stable direction, the characteristics below the stall are sufficiently undesirable to warrant the poor classification.

The results obtained with leading-edge high-lift devices installed on these four wings are shown in figure 10. Two kinds of flap have been used - the droop nose and the extended type with a rounded leading edge (fig. 10). Drooping the nose of the rectangular wing increased the maximum lift coefficient by about 0.30; adding the extended type of nose flap gives an additional increment of almost 0.30 since, in this case, a rounded leading edge is provided for the airfoil as well as an increase in the forward camber. These improvements are additive to the increments that can be obtained by the use of trailing-edge flaps as shown by the top curve. A similar picture is presented for the  $42^\circ$  swept wing, and it appears that once the tip stalling is controlled by the use of the leading-edge device relatively large increases in the maximum lift can be obtained. The two flapped arrangements shown (fig. 10) are for partial-span leading-edge flaps. These arrangements are shown in preference to arrangements having a greater spanwise extent of the leading-edge flaps because they have favorable longitudinal stability characteristics, whereas some others which give slightly greater maximum lifts have unfavorable pitching-moment characteristics. On the  $48^\circ$  swept wing the leading-edge droop was also effective, but as noted in figure 9 with the plain trailing-edge flaps the greatest maximum lift coefficient attainable at this sweep was considerably smaller. On the delta wing a small increment in maximum lift was obtained by deflecting the small leading-edge droop indicated and an additional small increase in maximum lift coefficient was obtained by deflecting the trailing-edge flap. The increment in lift obtained below the stall for this arrangement may perhaps be useful for maintaining a more satisfactory attitude during the landing approach. For the  $42^\circ$  and  $48^\circ$  swept wings which had poor longitudinal stability at the stall

for the basic wing deflecting the nose flap had a distinctly beneficial effect. This is particularly true of the  $42^\circ$  swept-wing case in which the addition of the optimum configuration of nose flap provides excellent longitudinal characteristics.

The data from this figure show that the use of an optimum leading-edge high-lift device on any wing having a thin or sharp leading-edge airfoil section will improve significantly both its maximum lift characteristics and its longitudinal stability at the stall.

Similar results for the wings of NACA 64-series airfoil sections are shown in figure 11. The addition of the nose flap to the  $42^\circ$  swept wing increased the maximum lift coefficient about 0.20 and made the wing stable at the stall. (See fig. 11.) This lift increment is somewhat lower than that obtained with the biconvex wing principally because the maximum lift of the basic wing is much higher. The addition of split flaps gave a further increase in  $C_{L_{max}}$  to 1.58, still maintaining stable longitudinal characteristics at the stall. This maximum lift value was only slightly higher than the one shown in figure 10 for the biconvex wing.

The addition of nose and split flaps to the  $43^\circ$  swept wing gave smaller increases than for the  $42^\circ$  swept wing as was noted earlier for split flaps and, moreover, the wing still remained unstable at the stall. On the extreme right in figure 11 are shown results that were obtained by the use of boundary-layer suction applied at the 0.20c, 0.40c, and 0.70c locations on the  $48^\circ$  swept wing with nose flaps and with both nose and split flaps. The lift increments obtained were relatively small but the stability was greatly improved. The maximum lift coefficient of almost 1.25 obtained for this configuration is the highest thus far obtained with this wing plan form.

This paper has, thus far, discussed only the changes in the maximum lift produced by these high-lift devices. If power-off landings are to be expected of the airplane or if the thrust available during the landing phase is limited, the drag near maximum lift is of great importance inasmuch as it determines the vertical speed during the landing approach. It has been found that a sinking speed in excess of about 25 to 30 feet per second will probably lead to erratic landings even on the part of highly skilled pilots (reference 23). This fact seems to be relatively independent of the forward speed at which the landing is made. In figure 12 some lift-drag polar curves for various configurations of the  $42^\circ$  swept wing have been shown. Superimposed upon these curves are contours of the forward speed and the vertical speed for a power-off glide at a wing loading of 40 pounds per square foot. In order to show the significance of these forward speed-sinking speed charts, a point is indicated that represents the forward speed and

sinking speed for a reference airplane for which flight test data were available (reference 23). This airplane was of the two-engine medium-bomber class and was only landed power off in emergency.

For the most favorable configurations the landing conditions appear to be no worse than those for the reference airplane. Certain changes from these conditions, however, such as increasing the wing loading, increasing the sweep, and increasing the roughness, make this picture appear less favorable. The effect of the high drag due to roughness on the basic wing, for example, is shown by the dashed curve. Not only is the maximum lift decreased but the sinking speed in the high-lift range is more than doubled. Split flaps, as pointed out earlier, give some increase in maximum lift, in this case enough to reduce the landing speed by 10 miles per hour. This is partially offset by an increase of about 5 feet per second in the sinking speed. Leading-edge flaps alone on account of their high drag at the higher lift do not appear to have any particular advantages. The combination of leading- and trailing-edge flaps, however, is quite effective in decreasing the landing speed provided that the increases in the rate of descent or alternately the amount of power required for landing can be tolerated.

The corresponding results for the biconvex wing (fig. 13) show that in general the higher drag of the biconvex sections will cause their rates of descent to be higher. In this case minor improvements only result from the deflection of split flaps alone; whereas deflecting the nose flaps greatly decreases the drag with some increase in the maximum lift. Deflecting the trailing-edge flaps in combination with the leading-edge flaps allows speeds almost as low as with conventional sections but with somewhat higher rates of descent. On account of the generally higher rates of descent shown for these sections, power-off landings will be distinctly more hazardous than for the NACA 64-series section wing in figure 12.

The problem of calculating the maximum lift of swept wings, as pointed out earlier, has thus far defied theoretical efforts. It is possible, however, to correlate some of the data that have been obtained on swept wings to get a guide in estimating the maximum lift. In figure 14 experimental values of maximum lift divided by the maximum lift of the wing rotated back to zero sweep have been plotted against sweep angle  $\Lambda$ . A plot of  $\cos^2\Lambda$  is also shown for comparison. The data of McCormack and Stevens from the Ames 40- by 80-foot tunnel and of Anderson from some tests in the old Langley variable density tunnel (references 11 and 24) in which the sweep of the wing was varied systematically were particularly useful in forming this curve. Experimental values of  $C_{L_{max}}$  for the  $0^\circ$  sweep conditions of the  $42^\circ$  swept



wing tested in the Langley 19-foot pressure tunnel and of the 48° swept wing tested in the Langley full-scale tunnel were not available, and hence were calculated by the method of Sivells and Neely (reference 6) which has been shown to give excellent agreement for unflapped unswept wings. The correlation curve shows a gradual decrease in maximum lift that is only about one-half that indicated by the simple  $\cos^2\Lambda$  approximation.



In conclusion the results of the investigations of maximum lift characteristics discussed herein can be summarized as follows:

Maximum lift coefficients of the order of 1.3 to 1.6, depending upon the angle of sweep, have been obtained with the best combinations of split flaps and leading-edge devices investigated. The importance of the airfoil section has been shown to decrease as the sweep increases and as the thickness of the airfoil decreases, the characteristics of all sections tending to approach the characteristics of flat plates at high sweeps and low-aspect ratios. The drag is shown to be of great importance in determining the power-off rate of descent or alternately the amount of power required during the landing. Leading-edge high-lift devices of the types investigated are extremely effective in reducing the drag and improving the stability in the high-lift range for wings having biconvex or other thin airfoil sections and would thus be desirable for wings having these sections.

## REFERENCES

1. Cahill, Jones F.: Two-Dimensional Wind-Tunnel Investigation of Four Types of High-Lift Flaps on an NACA 65-210 Airfoil Section. NACA TN No. 1191, 1947.
2. Cahill, Jones F., and Racisz, Stanley F.: Wind-Tunnel Development of Optimum Double-Slotted-Flap Configurations for Seven Thin NACA Airfoil Sections. NACA RM No. L7B17, 1947.
3. Furlong, G. Chester, and Fitzpatrick, James E.: Effects of Mach Number and Reynolds Number on the Maximum Lift Coefficient of a Wing of NACA 230-Series Airfoil Sections. NACA TN No. 1299, 1947.
4. Fullmer, Felicien F., Jr.: Two-Dimensional Wind-Tunnel Investigation of the NACA 641-012 Airfoil Equipped with Two Types of Leading-Edge Flap. NACA TN No. 1277, 1947.
5. Underwood, William J., and Nuber, Robert J.: Two-Dimensional Wind-Tunnel Investigation at High Reynolds Numbers of Two Symmetrical Circular-Arc Airfoil Sections with High-Lift Devices. NACA RM No. L6K22, 1947.
6. Sivells, James C., and Neely, Robert H.: Method for Calculating Wing Characteristics by Lifting-Line Theory Using Nonlinear Section Lift Data. NACA TN No. 1269, 1947.
7. Sivells, James C.: Experimental and Calculated Characteristics of Three Wings of NACA 64-210 and 65-210 Airfoil Sections with and without 2° Washout. NACA TN No. 1422, 1947.
8. Falkner, V. M.: The Calculation of Aerodynamic Loading on Surfaces of Any Shape. R. & M. No. 1910, British A.R.C., 1943.
9. Van Dorn, Nicholas H., and DeYoung, John: A Comparison of Three Theoretical Methods of Calculating Span Load Distribution on Swept Wings. NACA TN No. 1476, 1947.
10. Sweberg, Harold H., and Lange, Roy H.: Summary of Available Data Relating to Reynolds Number Effects on the Maximum Lift Coefficients of Swept-Back Wings. NACA RM No. L6L20a, 1946.
11. McCormack, Gerald M., and Stevens, Victor I., Jr.: An Investigation of the Low-Speed Stability and Control Characteristics of Swept-Forward and Swept-Back Wings in the Ames 40- by 80-Foot Wind Tunnel. NACA RM No. A6K15, 1947.

12. Wilson, Herbert A., Jr., and Lovell, J. Calvin: Full-Scale Investigation of the Maximum Lift and Flow Characteristics of an Airplane Having Approximately Triangular Plan Form. NACA RM No. L6K20, 1946.
13. Proterra, Anthony J.: Aerodynamic Characteristics of a  $45^\circ$  Swept-Back Wing with Aspect Ratio of 3.5 and NACA 2S-50(05)-50(05) Airfoil Sections. NACA RM No. L7C11, 1947.
14. Conner, D. William: Effect of Reflex Camber on the Aerodynamic Characteristics of a Highly Tapered Moderately Swept-Back Wing at Reynolds Numbers up to 8,000,000. NACA TN No. 1212, 1947.
15. Graham, Robert R., and Conner, D. William: Investigation of High-Lift and Stall-Control Devices on an NACA 64-Series  $42^\circ$  Sweptback Wing with and without Fuselage. NACA RM No. L7G09, 1947.
- 15a. Conner, D. William, and Foster, Gerald V.: Investigation of Pressure Distribution over an Extended Leading-Edge Flap on a  $42^\circ$  Swept-back Wing. NACA RM No. L7J03, 1947.
16. Neely, Robert H., and Koven, William: Low-Speed Characteristics in Pitch of a  $42^\circ$  Sweptback Wing with Aspect Ratio 3.9 and Circular-Arc Airfoil Sections. NACA RM No. L7E23, 1947.
17. Neely, Robert H., and Conner, D. William: Maximum Lift and Pitching-Moment Characteristics of a  $40^\circ$  Swept-Back Wing of Aspect Ratio 4 at Reynolds Numbers up to 9.5 Million. NACA MR No. L6G23, 1946.
18. Lange, Roy H.: Langley Full-Scale-Tunnel Investigation of the Maximum Lift and Stalling Characteristics of a Trapezoidal Wing of Aspect Ratio 4 with Circular-Arc Airfoil Sections. NACA RM No. L7H19, 1947.
19. Salmi, Reino J., Conner, D. William, and Graham, Robert R.: Effects of a Fuselage on the Aerodynamic Characteristics of a  $42^\circ$  Swept-back Wing at Reynolds Numbers to 8,000,000. NACA RM No. L7E13, 1947.
20. Conner, D. William, and Cancro, Patrick A.: Low-Speed Characteristics in Pitch of a  $34^\circ$  Sweptforward Wing with Circular Arc Airfoil Sections. NACA RM No. L7F04a, 1947.
21. Lovell J. Calvin, and Wilson, Herbert A., Jr.: Langley Full-Scale-Tunnel Investigation of Maximum Lift and Stability Characteristics of an Airplane Having Approximately Triangular Plan Form (DM-1 Glider). NACA RM No. L7F16, 1947

- 
22. Hieser, Gerald: Tuft Studies of the Flow over a Wing at Four Angles of Sweep. NACA RM No. L7C05a, 1947.
  23. Gustafson, F. B., and O'Sullivan, William J., Jr.: The Effect of High Wing Loading on Landing Technique and Distance, with Experimental Data for the B-26 Airplane. NACA ARR No. L4K07, 1945.
  24. Anderson, Raymond F.: Determination of the Characteristics of Tapered Wings. NACA Rep. No. 572, 1936.
- 

Wilson

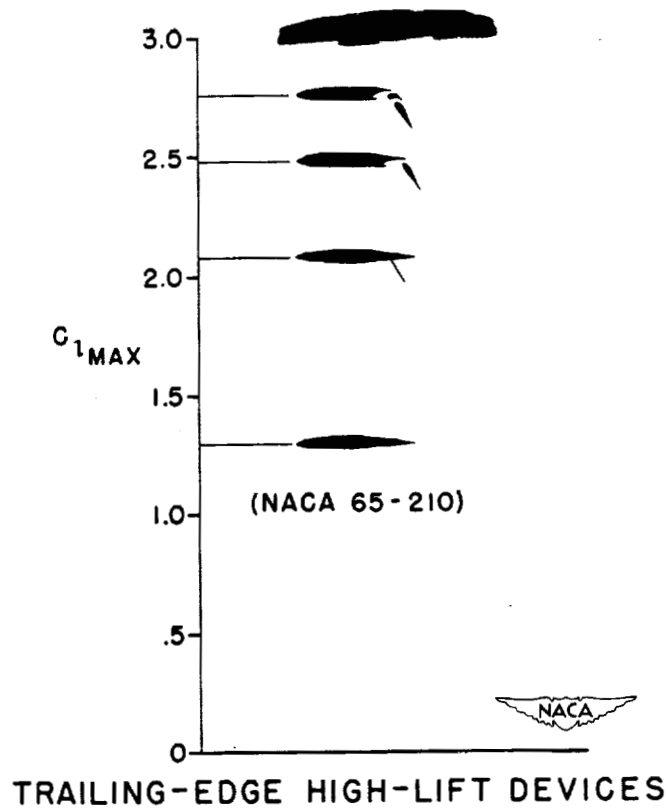
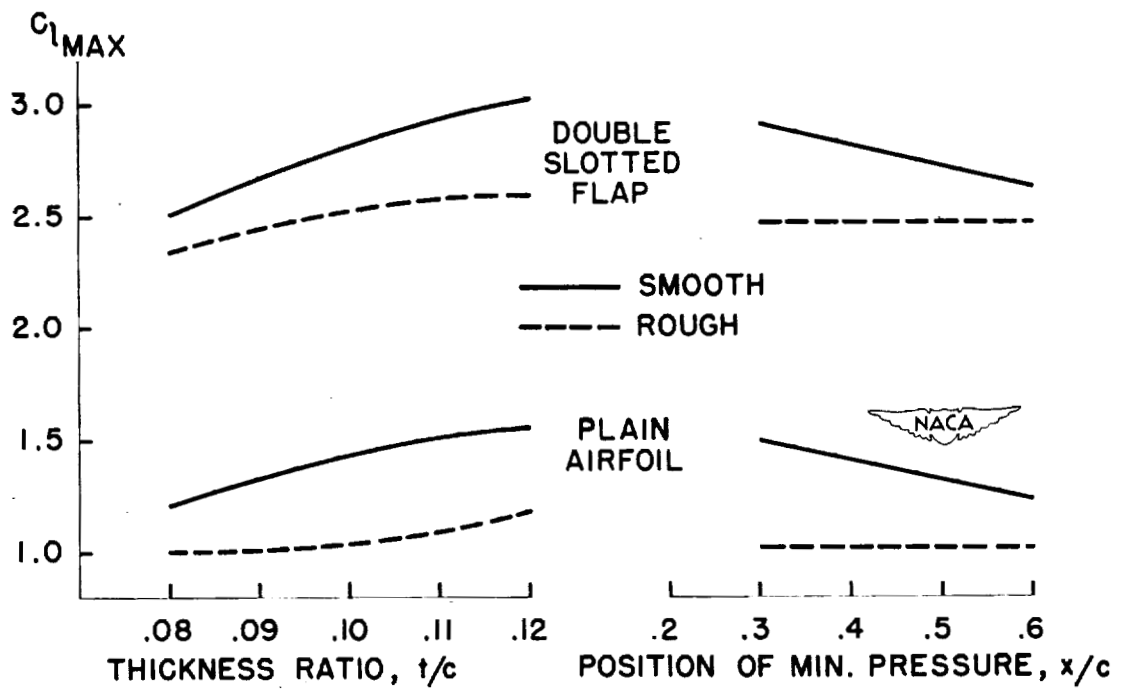


Figure 1.



EFFECTS OF AIRFOIL SHAPE ON MAXIMUM LIFT

Figure 2.

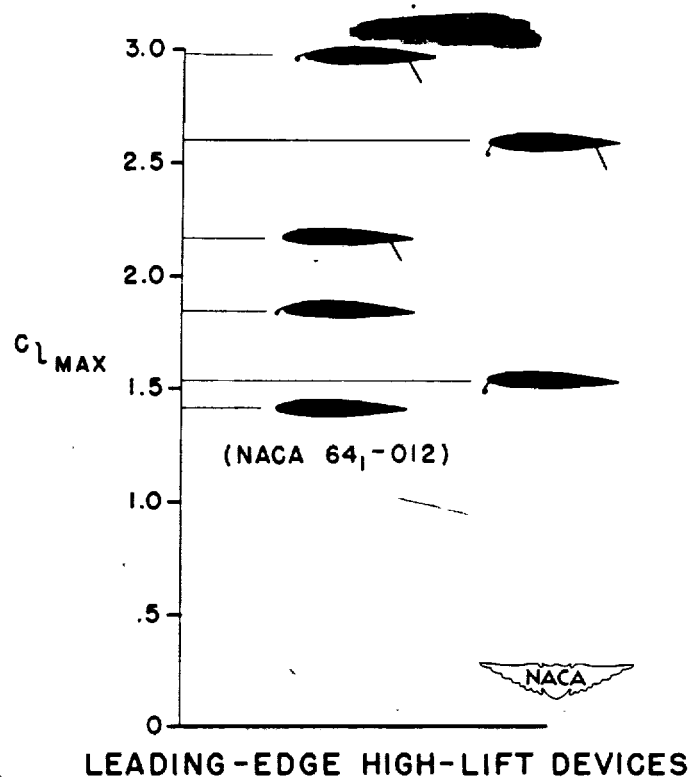
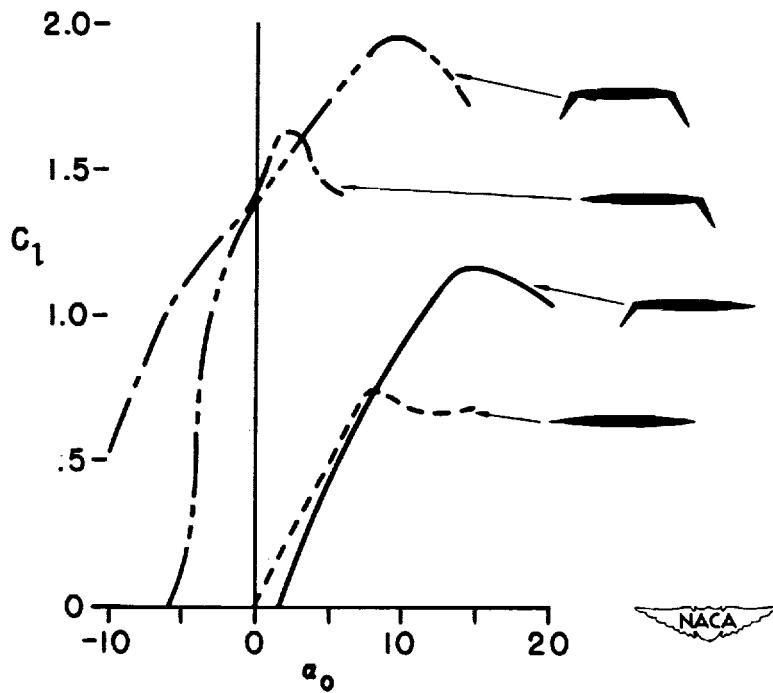


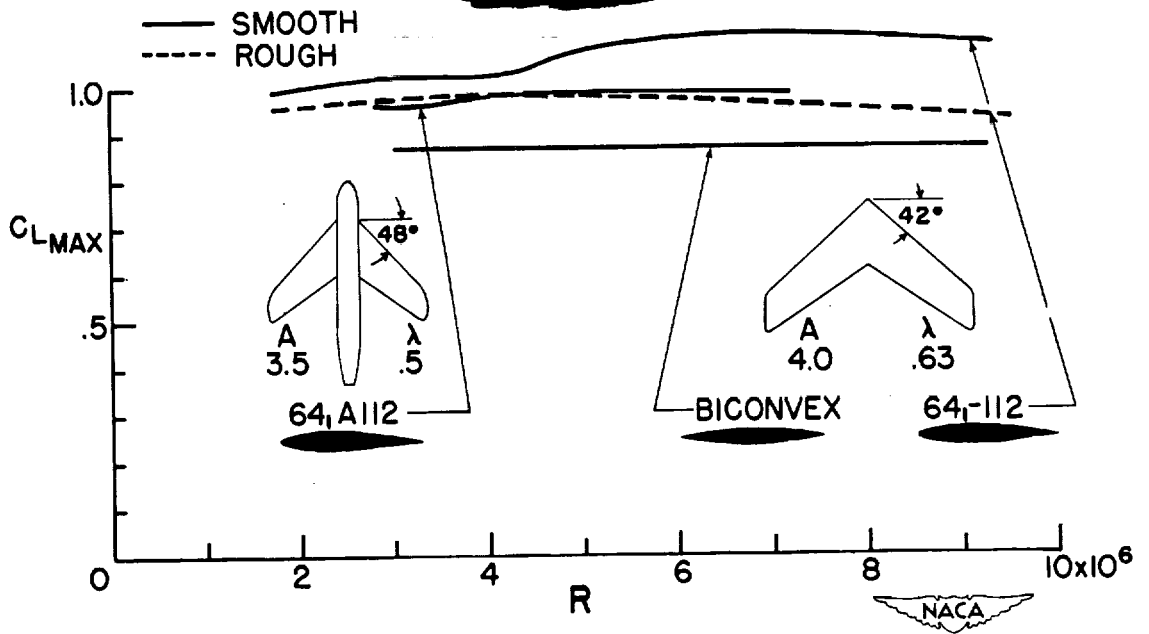
Figure 3.



HIGH-LIFT DEVICES ON A 6% THICK BICONVEX AIRFOIL

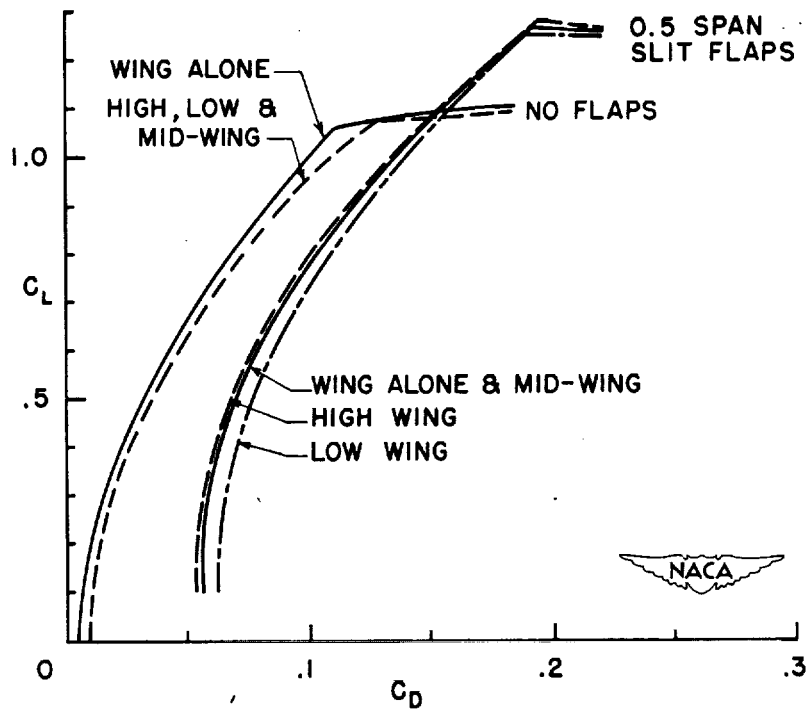
Figure 4.

Wilson



SCALE EFFECT ON MAXIMUM LIFT

Figure 5.



EFFECT OF FUSELAGE ON MAXIMUM LIFT

Figure 6.

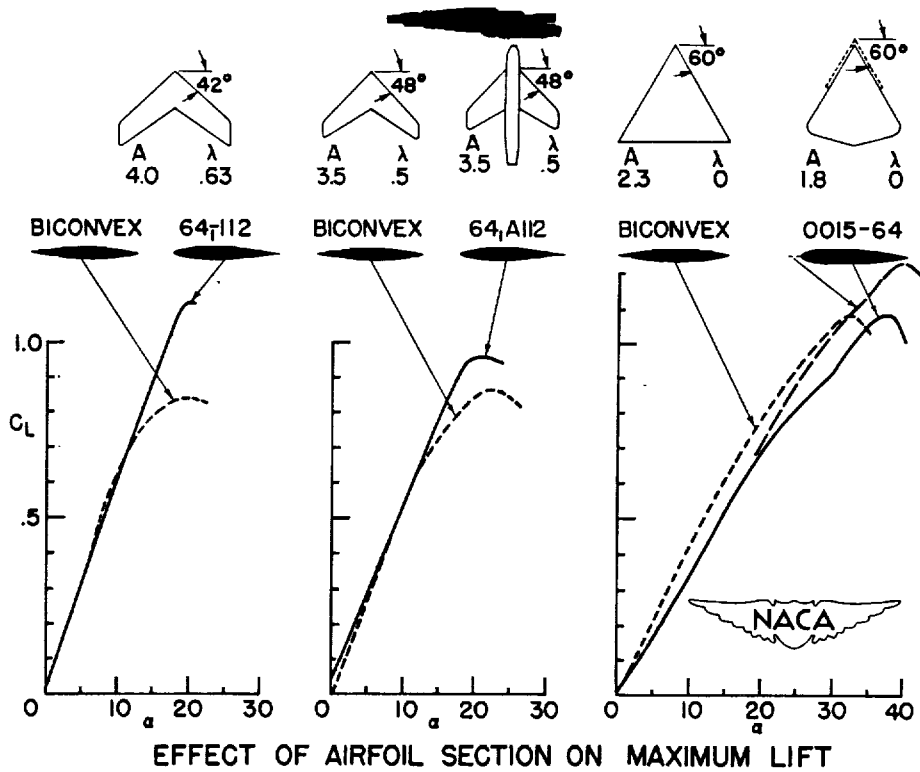


Figure 7.

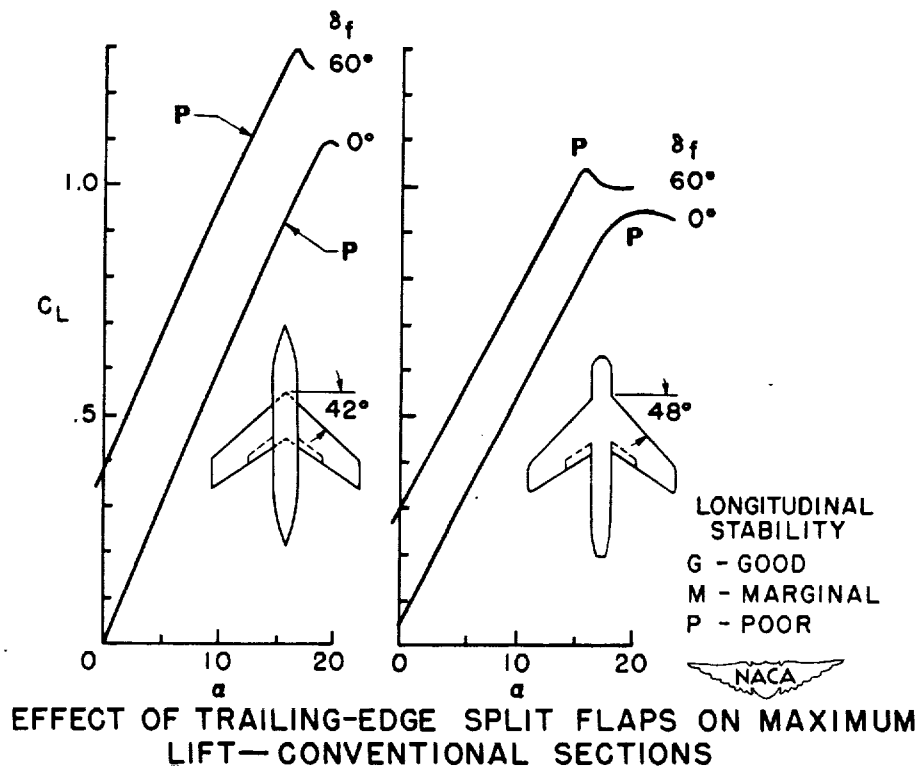


Figure 8.



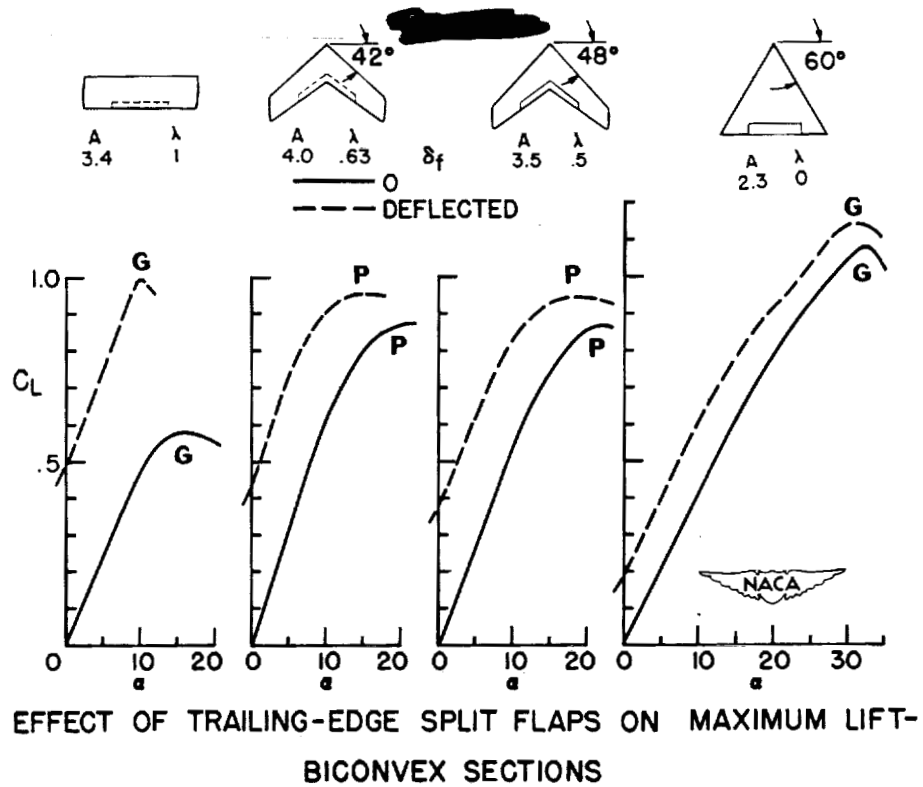


Figure 9.

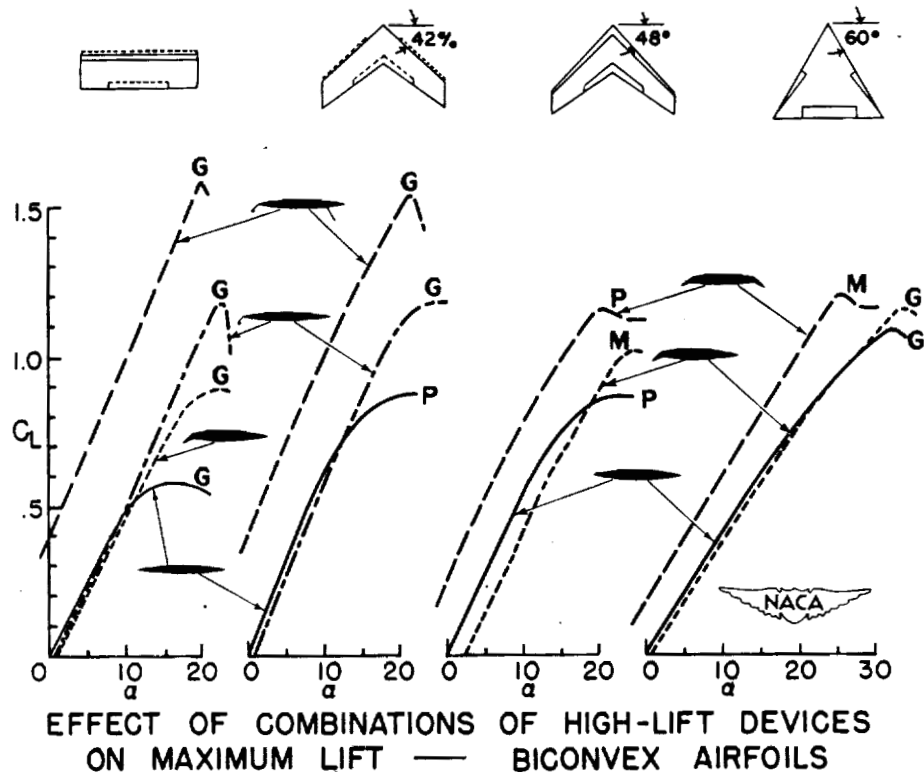


Figure 10.

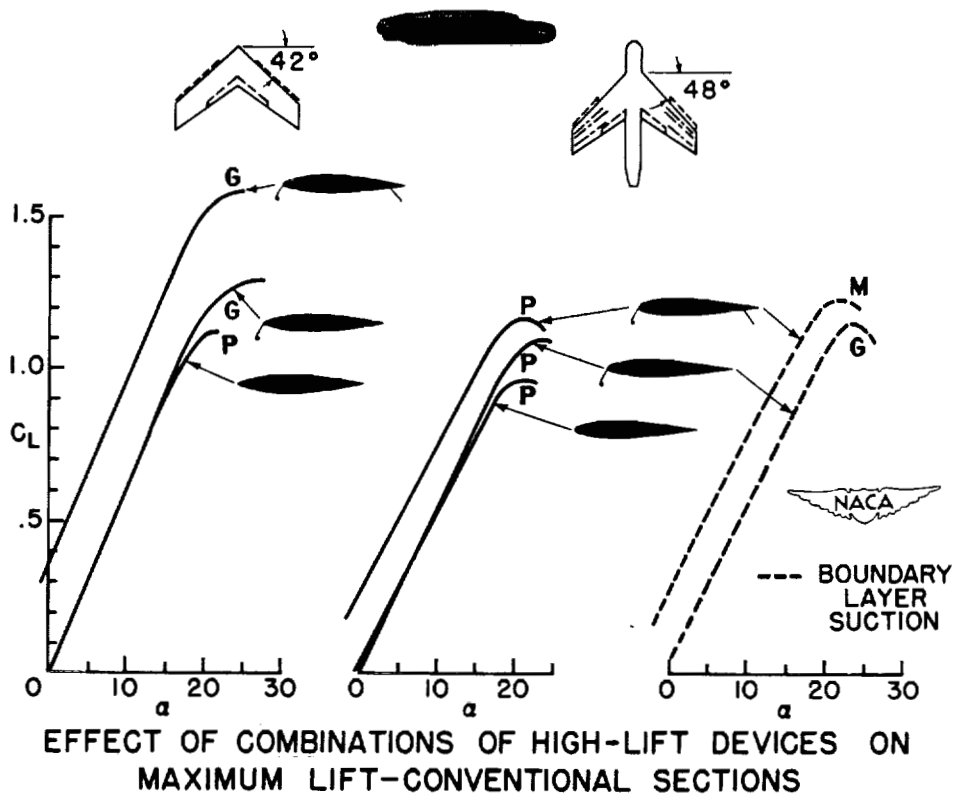


Figure 11.

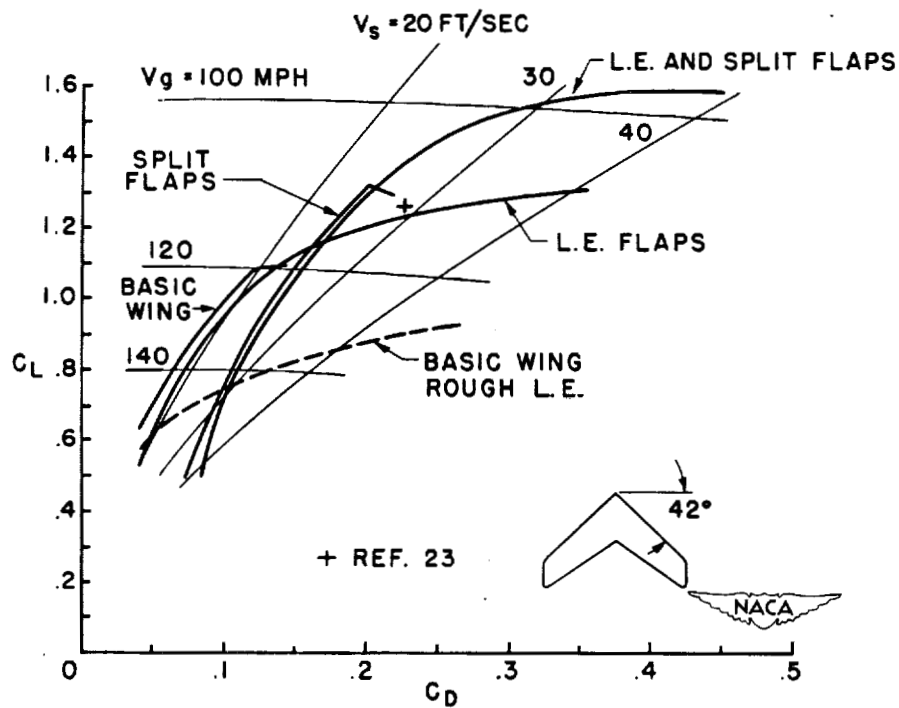
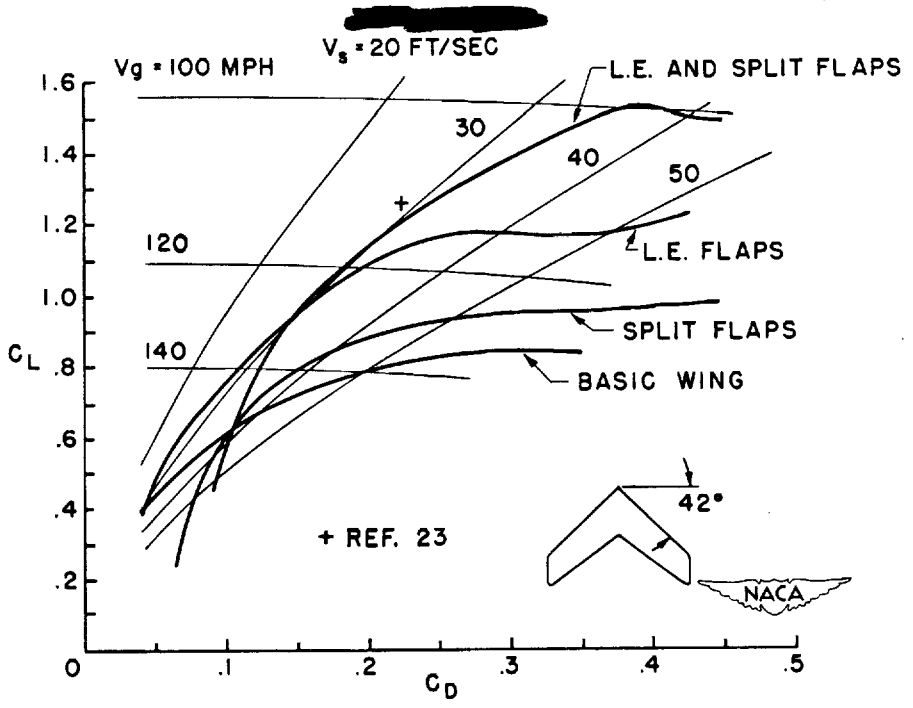


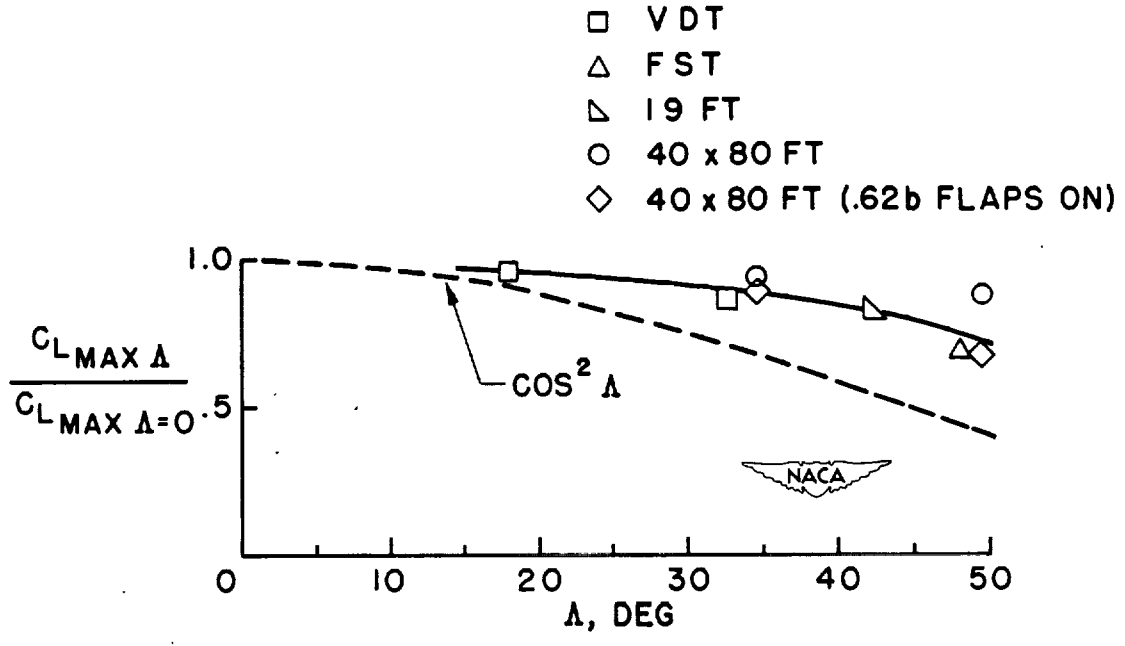
Figure 12.

Wilson



EFFECT OF HIGH-LIFT DEVICES ON LIFT AND DRAG - BICONVEX AIRFOIL SECTIONS

Figure 13.



EFFECT OF SWEEPBACK ON  $C_{L \text{ MAX}}$

Figure 14.

40(2)

AIR INLETS AND NACELLES

## NOSE INLETS

43

By Norman F. Smith

Langley Memorial Aeronautical Laboratory

For some years the NACA has had in operation a continuous research program on air inlets. The most recent developments and applications of the nose inlet work will be presented in this paper. First, however, some of the past work will be briefly reviewed because of its importance as background.

The basis of much of the high-critical speed inlet work originated with the development of NACA cowl "C" and nose "B" (references 1 and 2). These two inlets were derived on a basis similar to that for optimum critical speed airfoils: namely, a flat pressure distribution with no pressure peaks. It was found that although these two inlets were of greatly different proportions and critical speeds, the basic ordinates were essentially identical. The ordinates were consequently applied to a large family of nose inlets which were tested at medium and high speeds to determine the effects of proportions. The results were published (reference 3) in the form of design selection charts, a simplified version of which is shown in figure 1.

The selection procedure is shown by the arrows; starting at the bottom with the desired value of mass flow coefficient and proceeding vertically to the value of critical Mach number desired, the  $d/D$  or entrance diameter ratio is obtained. Continuing to the top of the chart, the  $X/D$  or length ratio is obtained. Application of the 1-series ordinates to those proportions yields a nose inlet of the required characteristics. Sample selections are shown for three values of critical Mach number and show that the higher critical Mach numbers involve cowlings of greater length.

These NACA 1-series charts are directly applicable to the design of open-nose inlets and were used in the design of the external lines of the D-558 airplane installation. The charts are also applicable to the design of rotating cowlings, such as the NACA "E" cowling (reference 4).

In addition, the applicability to the design of a protruding fuselage scoop has been demonstrated and reported in an NACA paper (reference 5). Recent tests of NACA 1-series cowlings with protruding propeller spinners (reference 6) have corroborated an analysis included in reference 3 by showing that the effects of spinners of reasonable size are small and predictable, and that cowlings for propeller-driven airplanes can be designed from NACA 1-series data.

The spinner shape has been found to have important effects upon the flow into a cowling (reference 6). It is usually desirable to admit air at a low value of inlet velocity ratio, since external compression is accomplished at an efficiency of one-hundred percent, while internal compression is accomplished at a somewhat lower value. At values of inlet velocity less than unity, an adverse pressure gradient exists into which the spinner boundary layer must advance. This pressure gradient, coupled with the pressure field of the spinner, may be sufficient to separate the flow at a relatively high value of inlet velocity ratio, thus making it impossible to obtain stable inlet flow with low losses at low values of inlet-velocity ratio. Pressure distributions measured without propeller on two shapes of spinners ahead of a 1-series cowling operating at a medium value of inlet-velocity ratio are shown in figure 2. The curved spinner was designed using the 1-series inlet profile and is approximately elliptical in section. The conical spinner is a straight-sided cone ahead of the inlet. The spinner with the curved surface evinces a higher peak pressure and a consequently greater adverse pressure gradient ahead of the inlet than does the conical spinner.

The effect of this gradient on spinner boundary layer is shown in the right half of figure 2. As the inlet velocity ratio is decreased, an abrupt increase in boundary layer thickness, indicating separation, occurs for both spinner shapes. The inlet velocity ratios for separation are of the order of 0.53 for the curved spinner and approximately 0.12 lower, or 0.41, for the conical. It is believed that the permissible value of inlet-velocity ratio can be still further lowered by modifying this conical spinner. If the cone angle is increased, for example, the pressure gradient can be expected to further diminish, thus permitting a lower value of inlet-velocity ratio to be obtained before separation occurs.

With regard to the general effect of spinners on the critical speed of cowlings, an extension of work by Ruden and Kucheman in Germany has provided an interesting analysis. The theory considers the average forces (obtained by integration of surface pressures) on the cowling and spinner and states that the average force on the cowling plus the average force on the spinner, if present, is equal to the change of momentum of the air entering the cowling. Simultaneous solution of equations for the conditions with and without a spinner gives the spinner force required for zero effect upon the critical Mach number of the cowling. A plot of this spinner force or pressure against inlet-velocity ratio is shown in figure 3. Values above this line indicate a decreased critical Mach number due to the spinner. Variations of average spinner pressure with inlet-velocity ratio obtained by integrating measured pressure

distributions are shown for the conical and curved spinners of reference 6. The intersection of the curves shows the values of inlet-velocity ratio below which the particular spinner can be used without affecting the cowling critical Mach number. This figure shows that the plain conical spinner can be used in the low inlet-velocity ratio range where its use is desirable from the standpoint of boundary-layer separation. The curved spinner should be used for medium values of inlet-velocity ratio, but its use, at least in the "short" condition, appears to be limited to values of the order of 0.6.

The effect of using a conical spinner at too high a value of inlet-velocity ratio is shown in the pressure distribution on the right of figure 3. A peak is produced at the lip by the conical spinner, whereas the curved spinner has virtually no effect upon the flat cowling pressure distribution at this value of  $V_1/V_0$ .

The conical spinner shown in figures 2 and 3 remains conical to the inlet, making the transition to axial aft of the inlet. It has been found from experimental data that the principal influence of the inlet extends to a distance  $1\frac{1}{2}$  to 2 times the inlet height ahead of the inlet for spinners of reasonable size. It therefore appears probable that a curved surface might be used in this region to bring the spinner surface axial at the entrance with little or no adverse effect upon the pressure gradient. The advantage of this is that a spinner of smaller maximum-diameter is obtained for given propeller hub clearances. Also, the more axial flow at the entrance may have less tendency to produce pressure peaks at the cowling lip.

The problem of designing air inlets for transonic military airplanes is complicated by simple military requirements such as good visibility downward and space in the nose of the airplane for armament. These two requirements in some cases tend to rule out the nose inlet, which usually represents the optimum from the standpoint of pressure recovery at the inlet, and make necessary some sort of fuselage side inlet, with sufficient fuselage volume ahead of the inlet to house the pilot and armament. The problem which exists in the design of any such configuration is that the fuselage ahead of the inlet must be shock-free in order to avoid shock-separated flow into the air intake. This means that, for a transonic airplane, the flow velocities on the fuselage ahead of the inlet must be substream. A theoretical analysis showed that in order to obtain the required substream velocities, the fuselage forward of the inlet must be very nearly conical in shape. In figure 4 is shown such a configuration which has been tested at low speeds (reference 7). It consists of an NACA 1-series cowling,

an approximately conical nose, and two canopies whose sections are approximately wedge-shaped forward of the inlet. The low-speed tests showed that substream velocities are obtained ahead of the inlet on all surfaces, thus indicating that shock-free flow can be obtained up to a Mach number of 1.0. Above a Mach number of 1.0, a small shock, first unattached then conical, can be expected to compress the flow on the cone to subsonic up to flight Mach numbers of the order of 1.2. This configuration therefore appears to have characteristics which merit consideration for transonic military aircraft.

In all of the foregoing material, the critical Mach number is defined in the usual fashion: the Mach number at which sonic velocity is first attained at some point on the surface of the body. Numerous tests of airfoils have indicated this criterion to be conservative by showing that clearance exists between critical Mach number and the Mach number at which significant changes occur in the aerodynamic forces. A similar clearance might reasonably be expected in the case of three-dimensional bodies. The amount of clearance available and the nature of the supercritical drag rise are of considerable interest with regard to transonic aircraft.

A preliminary investigation now underway at the Langley 8-foot high-speed tunnel has provided some information on this subject. The results of the tests of one fuselage shape are shown in figure 5. The body consists of an NACA 1-50-100 nose inlet one diameter in length, a cylindrical center section four diameters in length, and a tail section three diameters in length, making an overall fineness ratio of eight. The model was supported by a sting at the tail, with provisions for ducting the internal flow through the sting. The drag of the model was measured by a wake survey rake located on the sting as shown in the figure.

The drag curve for the body at  $\alpha = 0^\circ$  is shown in the lower left portion of figure 5. The measured critical Mach number is about 0.8, very close to that predicted by low speed data and from the design chart shown previously. At a Mach number 0.05 to 0.07 above the critical a slight drag rise appears, which continues to increase very slowly up to the highest test Mach number, 0.93 where the drag coefficient reaches a value 27 percent above the lowest value obtained.

Some explanation of the cause of this drag rise and the reason for its small magnitude is found by examination of the pressure distributions and the wake profiles.



Pressure distributions are shown for three Mach numbers: 0.6, 0.8 (approximately the critical Mach number), and 0.93, the highest Mach number obtained. For the last case, a large area of supersonic velocities is shown to exist, followed by a shock of considerable pressure rise. The pressure recovery at each Mach number is, however, essentially identical over the cylindrical section and at the tail of the body, indicating that no significant separation has occurred.

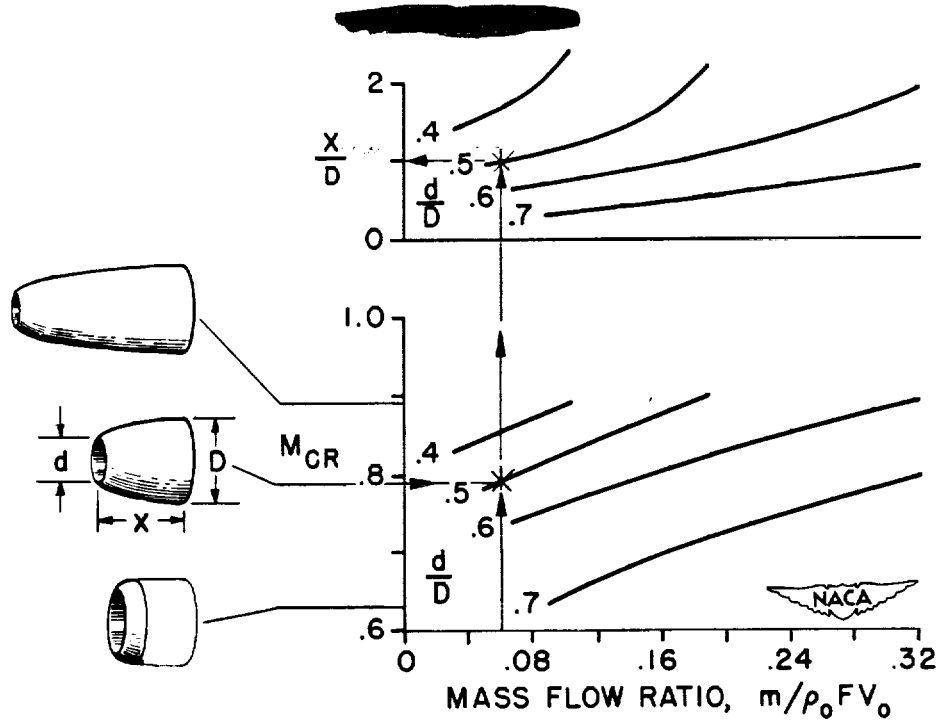
The wake profile (right half of fig. 5), plotted as point drag coefficient against distance from the surface of the body, also shows no significant separation. Instead a moderate thickening of the boundary layer is shown to occur. A direct shock loss is also measured just outside the boundary layer but is too small to be seen on the plot shown. The contribution of this area to the total drag is therefore negligible.

In conclusion: Data are available for the design of various types of nose inlets, including cowlings with propeller spinners. Also, a type of fuselage side inlet which appears useful through the transonic range has been developed. Tests of a nose inlet at supercritical speeds have shown that, as in the case of airfoils, significant clearance exists between the critical Mach number and the Mach number at which a drag rise occurs. The moderate drag rise which occurs up to a Mach number of 0.93 is due to thickening of the boundary layer by the increased adverse pressure gradient rather than to direct shock losses and shock-induced separation.

## REFERENCES

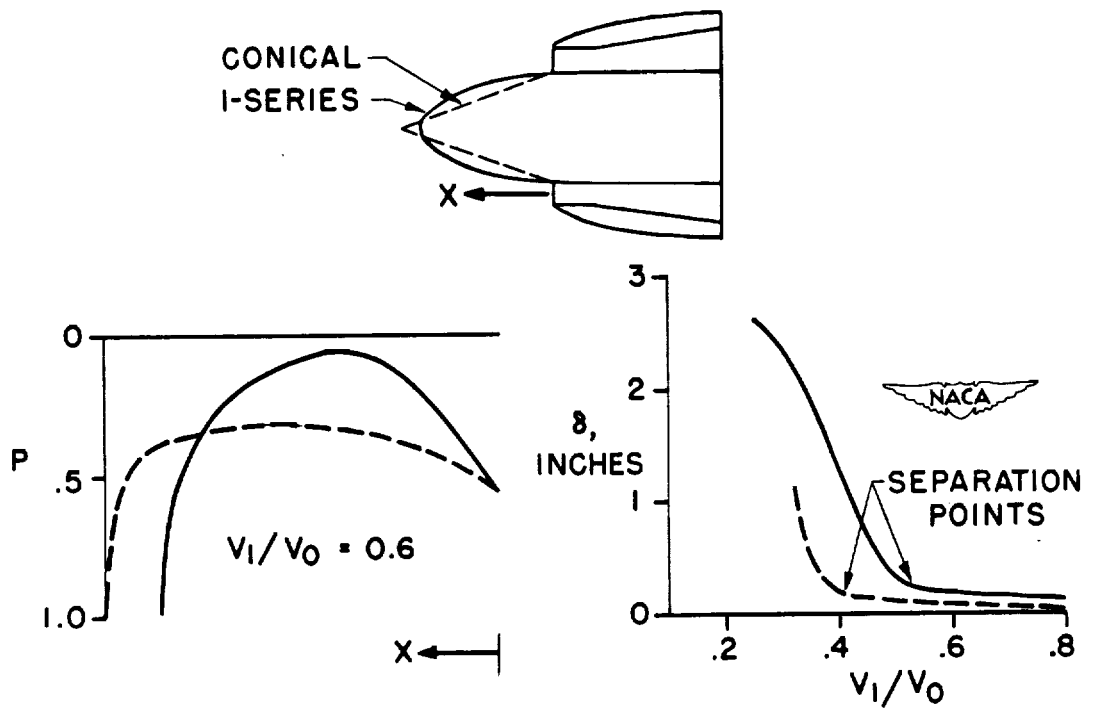
1. Robinson, Russell G., and Becker, John V.: High-Speed Tests of Conventional Radial-Engine Cowlings. NACA Rep. No. 745, 1942.
2. Becker, John V.: Wind-Tunnel Tests of Air Inlet and Outlet Openings on a Streamline Body. NACA ACR, Nov. 1940.
3. Baals, Donald D., Smith, Norman F., and Wright, John B.: The Development and Application of High-Critical-Speed Nose Inlets. NACA ACR No. L5F30a, 1945.
4. McHugh, James G.: Progress Report on Cowlings for Air-Cooled Engines Investigated in the NACA 19-Foot Pressure Wind Tunnel. NACA ARR, July 1941.
5. Smith, Norman R., and Baals, Donald D.: Wind-Tunnel Investigation of a High-Critical-Speed Fuselage Scoop Including the Effects of Boundary Layer. NACA ACR No. L5B01a, 1945.
6. Nichols, Mark R., and Keith, Arvid L., Jr.: Investigation of a Systematic Group of NACA 1-Series Cowlings with and without Spinners. (Prospective NACA paper)
7. Nichols, Mark R., and Goral, Edwin B.: A Low-Speed Investigation of a Fuselage-Side Air Inlet for Use at Transonic Flight Speeds. NACA RM No. L7A06, 1947.

Smith



### NACA I-SERIES DESIGN CHART

Figure 1.

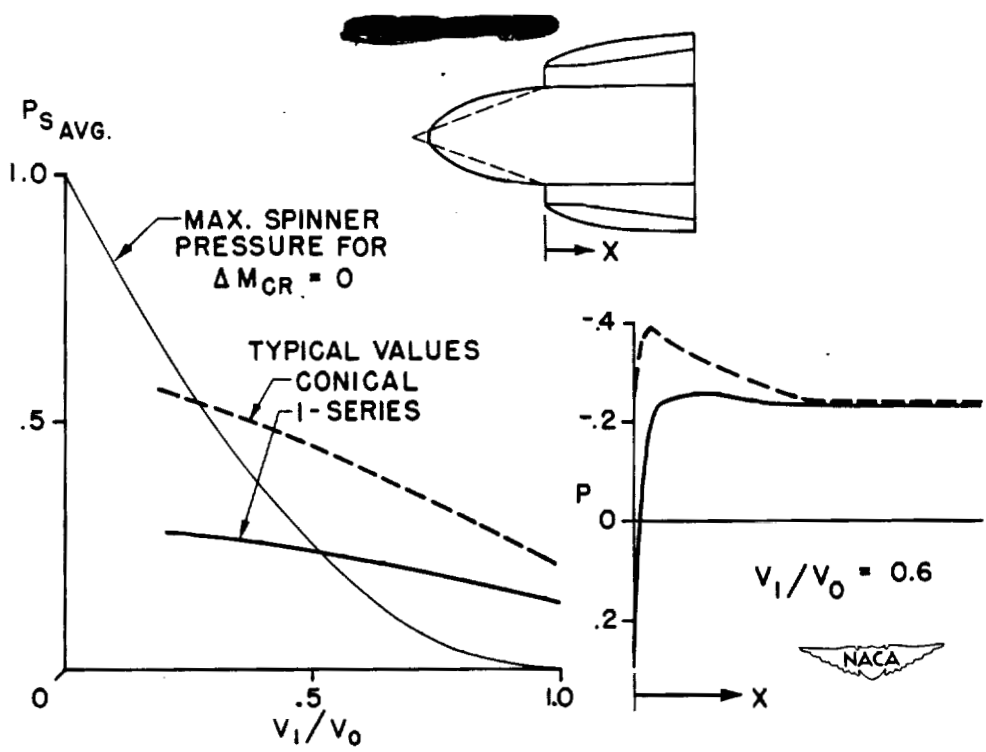


### EFFECTS OF SPINNER SHAPE ON INTERNAL FLOW

Figure 2.

48(a)

Smith



EFFECTS OF SPINNER SHAPE ON EXTERNAL FLOW

Figure 3.

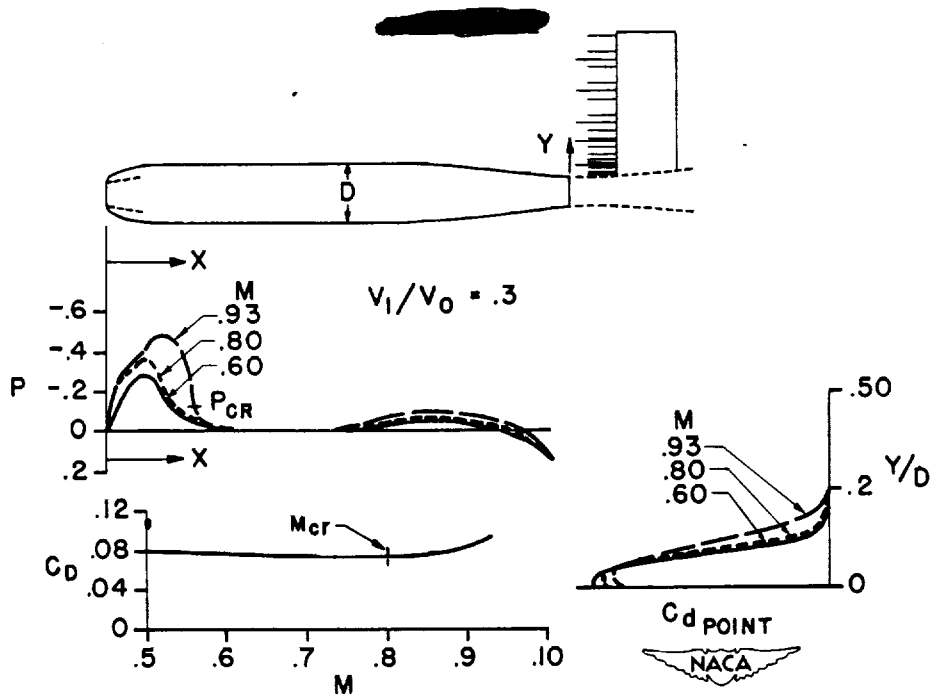


NACA TRANSONIC INLET

Figure 4.

42(b)

Smith



SUPERCritical CHARACTERISTICS OF NACA 1-50-100 NOSE INLET

Figure 5.

48(c)

## SUMMARY OF NACA SUBMERGED-INLET INVESTIGATIONS

By Emmet A. Mossman

Ames Aeronautical Laboratory

On many existing and proposed airplanes the fuselage shape is assuming a greater importance. A dominant factor determining the shape of the fuselage for a pursuit-type turbojet airplane may be the ducting system. The general fundamental requirements to be satisfied by jet airplane ducting systems are high efficiency of the impact or ram pressure conversion and small external drag coefficient. The importance of ram recovery can be visualized by considering its effect on a typical pursuit-type airplane, powered by a jet engine and traveling 650 miles per hour at sea level. Analysis shows that for every 10 percent decrease in ram recovery at this speed the net thrust decreases 7 percent and the specific fuel consumption increases about 5 percent. The resultant adverse effects on range, climb, and maximum speed are quite large.

Recognizing the need for a new type inlet which would combine the good qualities of the nose inlet with the short internal ducting of the external scoop, the National Advisory Committee for Aeronautics has developed what is known as a "submerged air inlet". This intake is shown in figure 1 and the component parts are noted in this figure. The entrance is completely submerged below the contour of the fuselage or wall into which it is placed. The air travels down an inclined surface, which we have termed the ramp. Ramp angle is the angle of the intersection of the ramp floor with the fuselage skin, ramp wall divergence is the divergence of the ramp side wall from the parallel, and width-to-depth ratio is simply the ratio of the corresponding dimensions of the inlet. This paper summarizes the results of research on NACA submerged inlets in the 7- by 10-foot, the 40- by 80-foot, and the 16-foot high-speed tunnel sections at the Ames Aeronautical Laboratory.

An entry with parallel ramp walls was the first to be investigated, these tests having been conducted in a small wind channel. As expected, the pressure recovery with this parallel-walled entry was not very good, especially at the low mass flow ratios. It was then reasoned that shaping the walls to conform to the streamlines at some desired mass flow ratio might result in better duct characteristics. Such an entry with divergent ramp walls was designed and tested.

A comparison of the pressure recovery for this inlet with that for a parallel-walled intake is shown in figure 2. These data were obtained from a full-scale duct installation in the Ames 40- by 80-foot tunnel. The ordinate for these curves is ram-recovery ratio, which is the ratio of the ram pressure recovered to the ram pressure

available. This ratio was selected because it is relatively constant for subsonic Mach numbers and is readily measurable. The abscissa is mass flow ratio, which in the incompressible case is equivalent to inlet velocity ratio. Comparison of the ram recoveries for the parallel- and divergent-walled intakes indicates that a considerable increase results from the use of divergent walls at the low mass flow ratios both at the entrance and at the compressor.

The principal cause of the lower ram recovery for an inlet with parallel walls, especially in the mass flow range less than 1.0, is the rapid growth of the boundary layer due to the adverse pressure gradient along the ramp. Such is not the case for the inlet with divergent walls. Even though the pressure gradient is no less adverse, surveys at the entrance show that the boundary layer on the floor of the divergent-walled inlet starts anew and remains relatively thin, despite the adverse gradient. This probably accounts for the difference in ram recovery at the low mass flow ratios between divergent and parallel-walled submerged inlets. The pressure losses with divergence have a different origin. The boundary layer on the fuselage skin, outside the ramp, is partially kept from flowing over the divergent ramp edges by two factors. The first of these is the pressure gradient over the rear 40 percent of the ramp, the pressures in this region being greater than those of the surface into which the inlet is placed. The second factor is that the outside boundary layer does not flow over the sharp edge of the ramp wall as easily as it does with the edge rounded. The cause for this is not fully understood.

The pressure losses at the entrance for an NACA submerged inlet are concentrated in two symmetrical regions, as shown in figure 3. A major part of these pressure losses appears to originate from a turbulent mixing process set up by a change in the flow direction as indicated in this same figure. It is probable that some of the outside boundary layer is emmeshed and becomes a part of this disturbance.

An extensive investigation has been made to determine the effect of modifications on submerged inlets. Variations in ramp angle, ramp-wall divergence, width-to-depth ratio, ramp-floor shape, and boundary-layer thickness have been tested. Results are given in reference 1. An evaluation of these data indicates that satisfactory duct characteristics may be obtained for a range of the test variables. It appears that an optimum design of these inlets should employ curved diverging ramp walls, a ramp angle between  $5^{\circ}$  and  $7^{\circ}$ , and a width-to-depth ratio of from 3 to 5. From measured lip and ramp pressures, high critical speeds were estimated.

The drag attributable to this type of inlet is shown in figure 4 as a function of mass flow ratio. These data were obtained on a  $\frac{1}{5}$ -scale typical duct installation on a fighter airplane. The drag coefficients

are based on wing area. For an airplane using a 24c jet engine and operating at a high-speed design mass flow ratio of 0.60, there is no incremental change in airplane  $C_d$ , due to the duct installation.

In order to check the validity of the small scale measurements, models identical except for scale were designed and tested in both the Ames 7- by 10-foot and the Ames 40- by 80-foot tunnels. The agreement between the  $\frac{1}{5}$ -scale and full-scale tests is shown in figure 5.

The duct location used in this investigation is noted in the figure. These data show excellent agreement between the two tests and indicate that with proper design high ram recoveries are attainable on full-scale installations. (Reynolds number based on duct depth.) It might be added further that the variation of ram recovery ratio with angle of attack was slight for these and other installations.

One especially important aspect of this study concerned the effects of high-speed flight on the operation of this type duct. Tests of a duct installation on a  $\frac{1}{4}$ -scale model of a fighter airplane have been made in the Ames 16-foot high-speed tunnel. The results of these tests illustrate the effect of Mach number and of the location of the inlet on the fuselage. The effect of Mach number is shown in figure 6, for constant mass flow ratios. The recovery remains essentially the same for the entire Mach number range of the tests (from 0.3 to a maximum of 0.875). It has not yet been determined how high a Mach number can be attained while still maintaining the high pressure recovery. In figure 7 it may be seen that at a Mach number of 0.875 the critical pressure coefficient was just reached along the front of the ramp floor. A shock disturbance would probably first occur in this high velocity region when the free-stream Mach number became somewhat greater than 0.875. It may be seen that this region extends only over a small portion of the duct width, the flow outside of the ramp on the fuselage skin being still subsonic. Because the disturbance takes place over a smaller duct width, it might then be indicated that the pressure recovery would decrease less severely for a divergent-walled entry than for a parallel-walled one, once the airplane speed was increased enough so that a shock wave formed along the ramp.

Given in figure 8 are the four inlet locations on the fuselage of the  $\frac{1}{4}$ -scale model, in percent of the root chord forward or rearward of the wing leading edge. It may be seen that the recovery decreases slightly as the inlet is moved rearward. This was expected since the boundary-layer thickness increases in this direction. Even though the decrease in ram recovery ratio may not be considered prohibitive, caution



should be exercised in moving the inlet rearward. Primary consideration should be given the flow field into which the inlet is placed. At the farthest rear position (58.4 percent root chord) the flow along the basic fuselage became sonic at about the same time as the flow on the wing. When the duct was located at this position, the pressure recovery began to decrease when the Mach number exceeded 0.80. This drop became much more marked at moderate angles of attack, the flow on the side of the fuselage abruptly separating due apparently to the position and intensity of the shock wave on the wing.

In conclusion, NACA submerged inlets may be designed to obtain high ram recovery at a low resultant drag. High-speed tests on a  $\frac{1}{4}$ -scale model showed that for this installation the ram recovery remained essentially constant up to a Mach number of 0.875.

#### REFERENCE

1. Mossman, Emmet A., and Randall, Lauros M.: An Experimental Investigation on the Design Variables for NACA Submerged Entrances. NACA RM No. A7I30, 1947.

Mossman

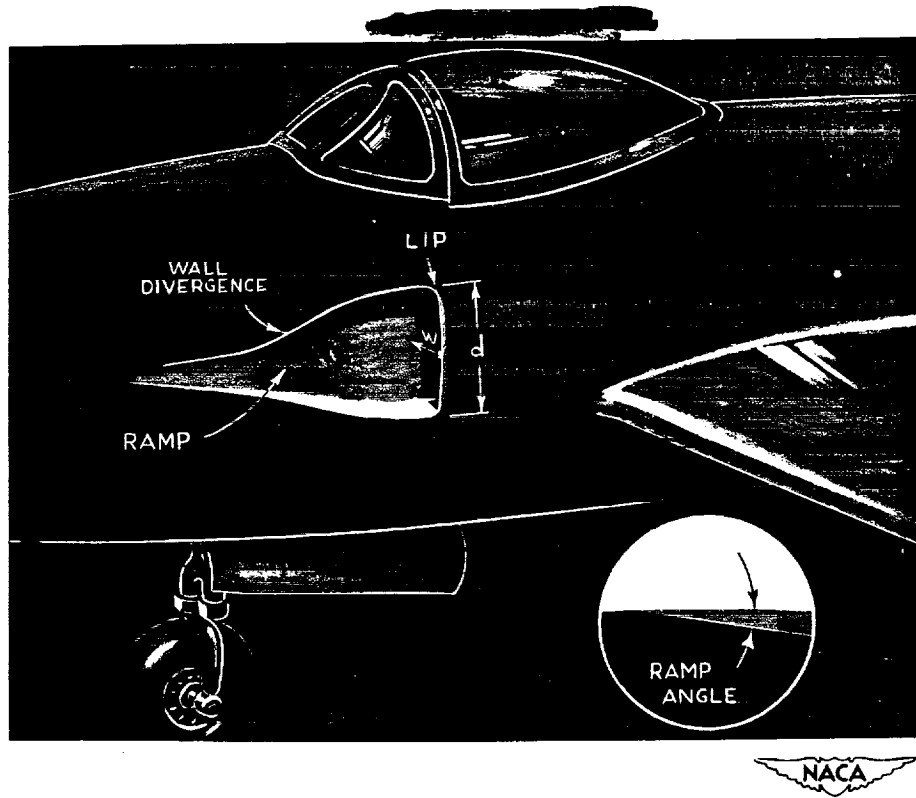


Figure 1.- Schematic view of a NACA submerged inlet installation.

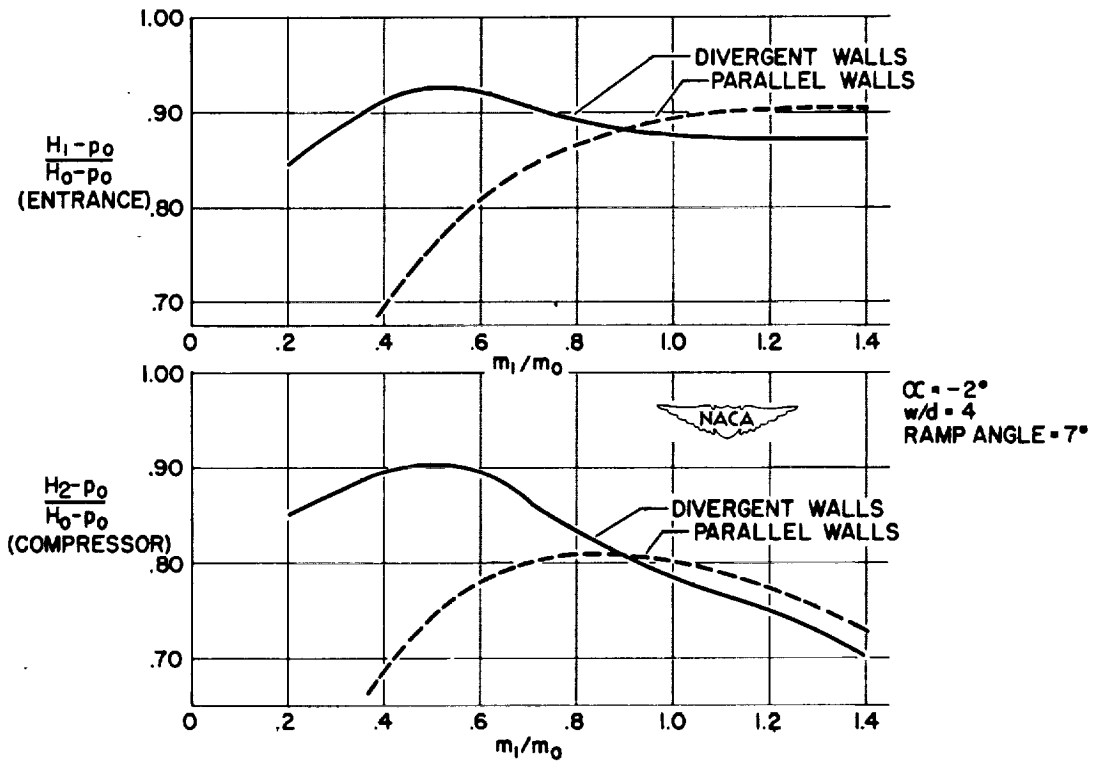


Figure 2.- Comparison of the ram recovery ratio for divergent- and parallel-walled submerged inlets. Full-scale duct installation.

Mossman

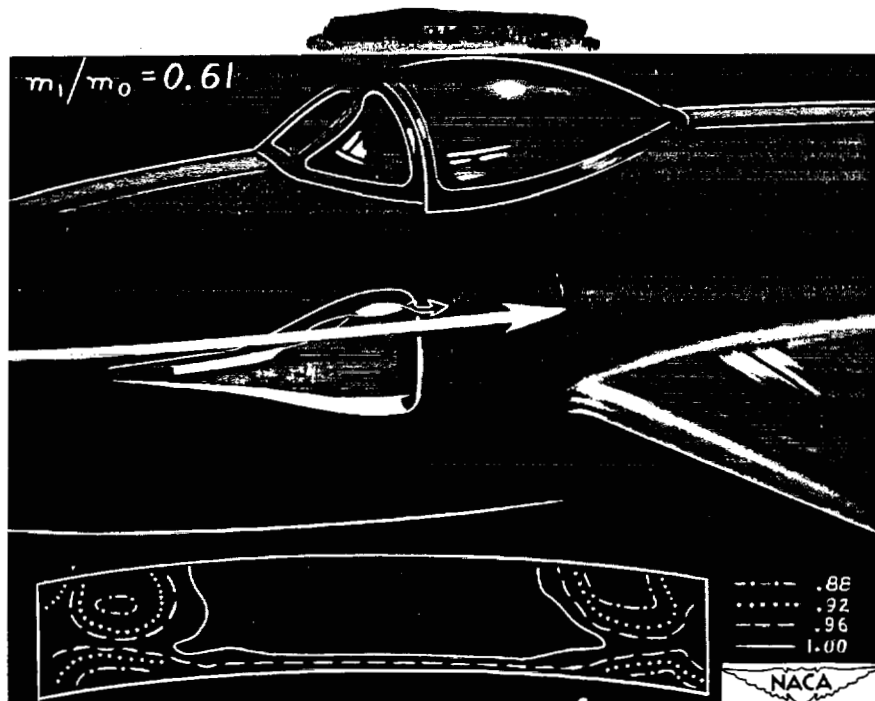


Figure 3.- Ram-recovery-ratio contours at the entrance of an NACA submerged duct installation.

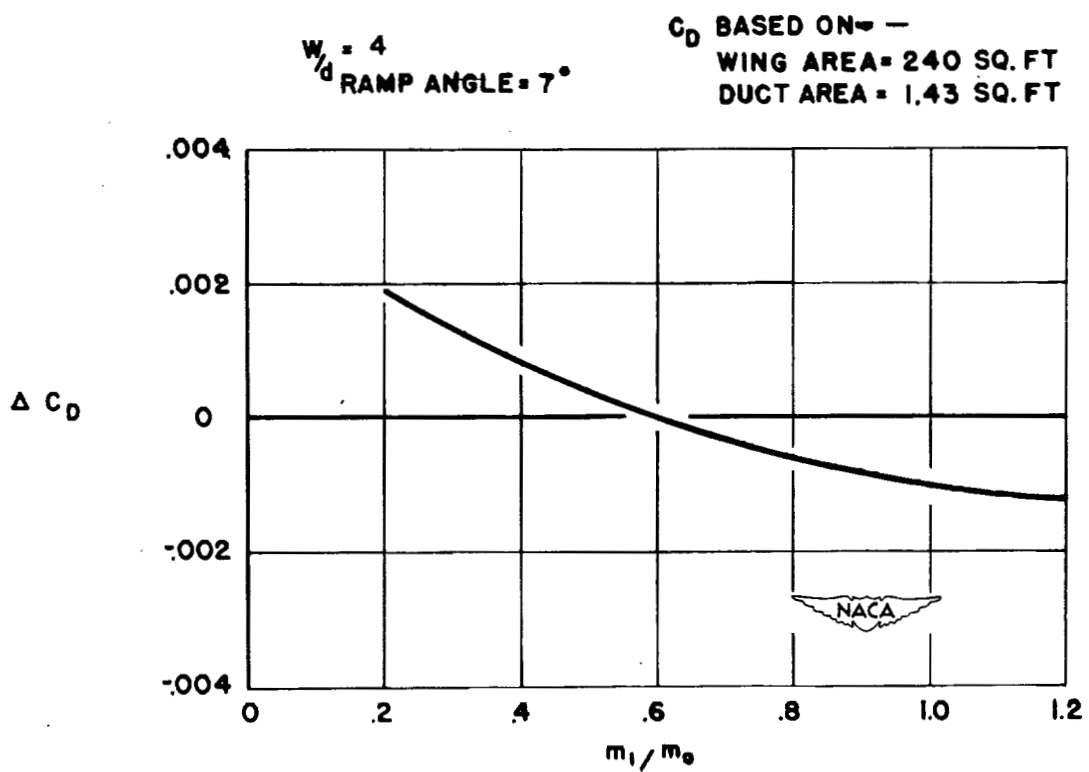


Figure 4.- Incremental change in airplane drag coefficient due to an NACA submerged duct installation.  $\frac{1}{5}$ -scale model of a fighter airplane.

Mosgman

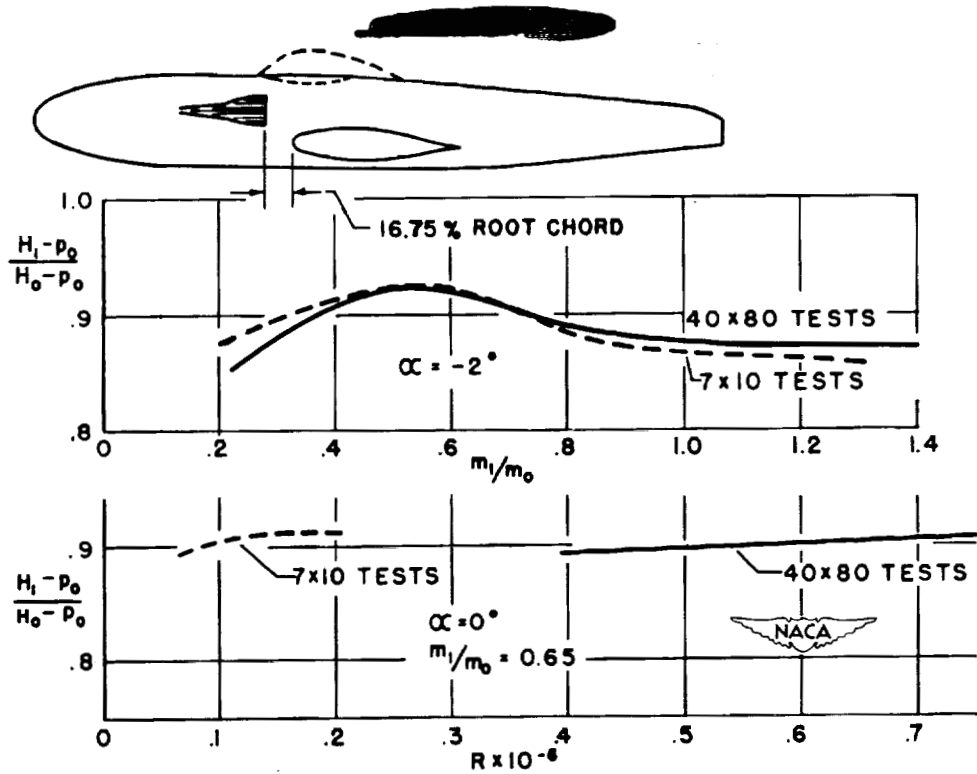


Figure 5.- Entrance ram recovery ratio for comparison of  $\frac{1}{5}$ -scale and full-scale NACA submerged duct installations.

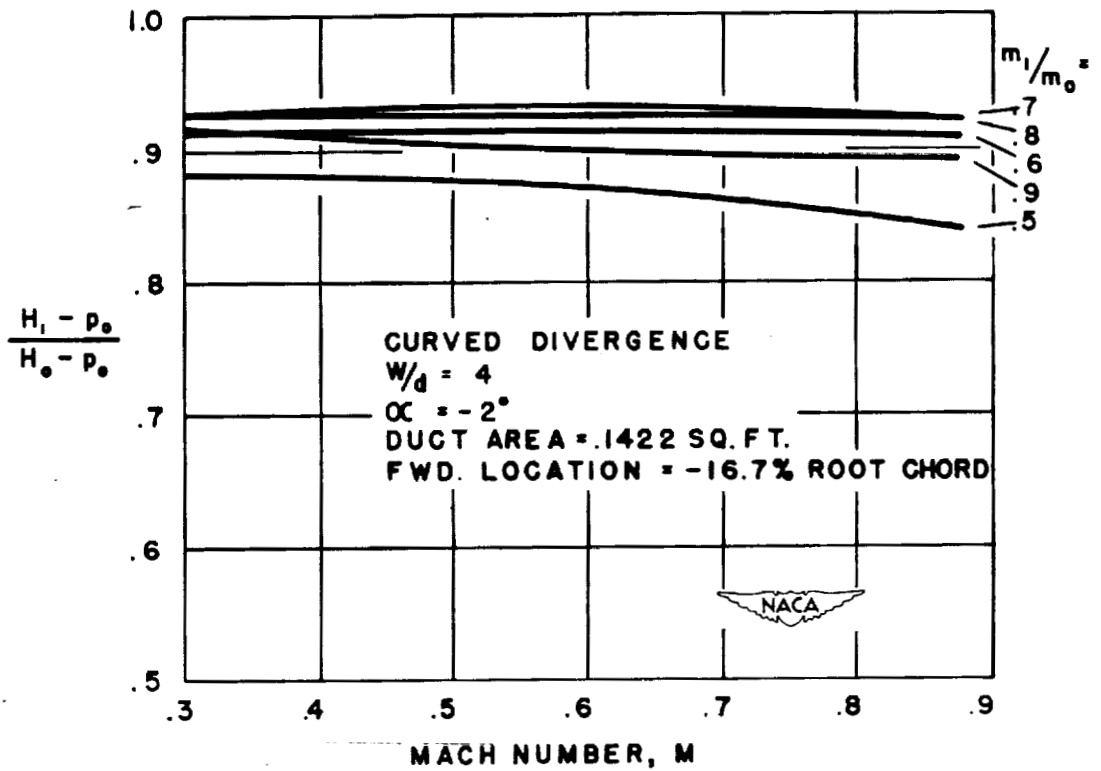


Figure 6.- Effect of Mach number on the ram recovery ratio at the entrance for a  $\frac{1}{4}$ -scale NACA submerged inlet installation.

$w/d = 4.0$   
 RAMP ANGLE =  $7^\circ$   
 $\alpha = -2^\circ$   
 $m_1/m_0 = 0.53$   
 $M = 0.875$

- - - - BASIC FUSELAGE  
 ——— DUCT INSTALLED

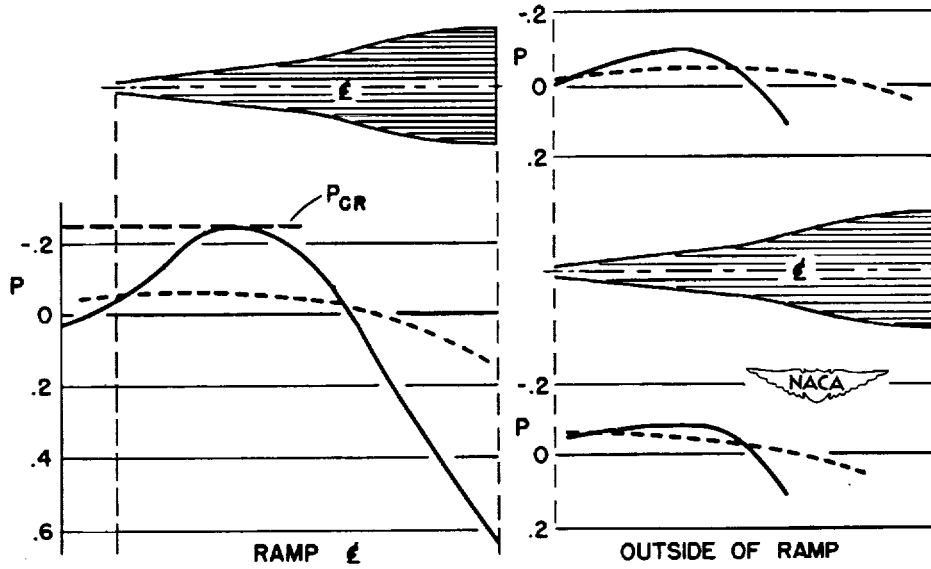


Figure 7.- Pressure distribution along the ramp of an NACA submerged inlet installation.  $\frac{1}{4}$ -scale typical fighter airplane.

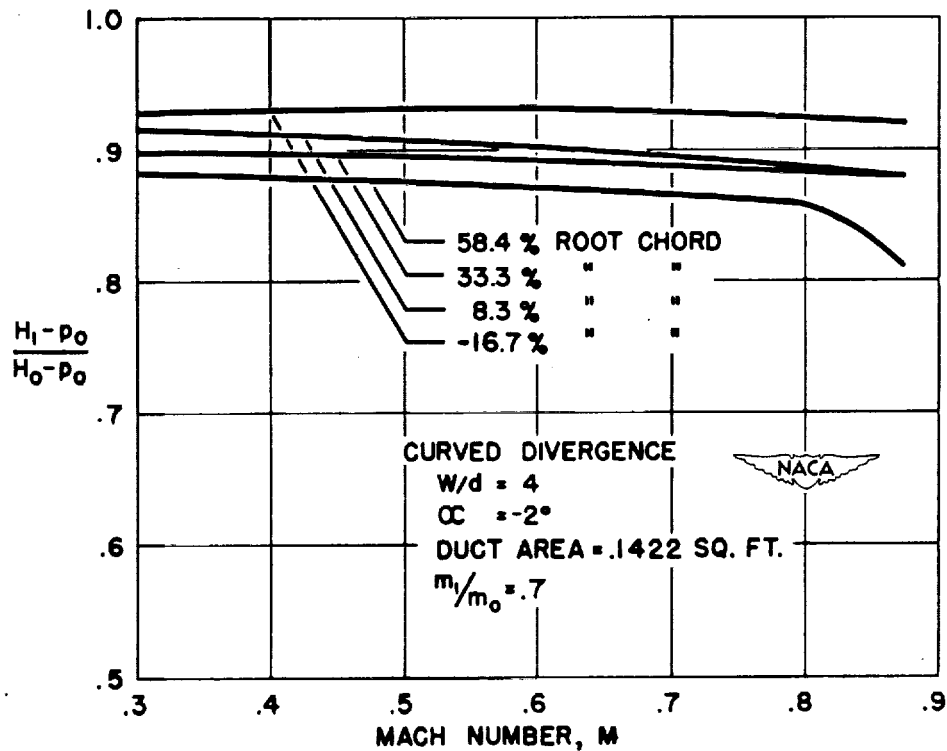


Figure 8.- Effect of an NACA submerged duct location on the fuselage of a  $\frac{1}{4}$ -scale typical fighter airplane.

## INVESTIGATION OF SIDE INLETS AT SUPERSONIC SPEEDS

By Wallace F. Davis

Ames Aeronautical Laboratory

Although a very high diffusion efficiency can be attained at supersonic speeds by nose inlets such as those discussed in reference 1, practical design considerations often make side inlets more desirable. For this reason, tests are being performed at supersonic speeds upon inlets that are situated in a region of appreciable boundary layer. Preliminary tests have shown that the presence of the boundary layer can cause a relatively poor recovery of total pressure because the severe adverse pressure gradient produced by a rapid deceleration of the flow at high speeds causes the boundary layer to thicken and separate. The results of the separation are a fluctuating flow through the intake and a maximum total-pressure ratio after diffusion that is limited to about two-thirds of that occurring across a normal shock wave at the same Mach number. (See reference 2.)

To improve the pressure recovery attainable through a side inlet, the severity of the compression inside the duct must be reduced, the amount of low-energy air of the boundary layer that enters the inlet must be diminished, or both factors must be reduced simultaneously. These considerations have been used in the design of side inlets for tests in the Ames 8- by 3-inch supersonic tunnel. Both annular and twin-scoop inlets are being investigated because applications for the two types may be found in the design of high-speed aircraft.

The tests are being performed at Mach numbers between 1.36 and 2.01 and at Reynolds numbers, based upon the length of the body ahead of the intake, of between 2.23 and 3.09 million. Only measurements of the pressure recovery attainable after diffusion with the various inlet designs at an angle of attack of  $0^\circ$  have been made at the present time. Angle-of-attack and comparative-drag studies together with tests at subsonic speeds are to be performed in the future.

## ANNULAR INLETS

Three methods for improving the total-pressure recovery attainable after diffusion through an annular inlet are being investigated. The first method is to reduce the inlet Mach number and thus the adverse pressure gradient that is imposed upon the boundary layer inside the duct by deflecting the stream ahead of the inlet to create an oblique shock wave. A photograph of a model is shown in figure 1. The outside diameter of the inlet is about one inch, and the inlet area

is about one-third of the frontal area at the station of the duct entrance. The length of the forebody is five times the diameter of the cylindrical section ahead of the ramp. The ramp angle that deflects the flow is increased to increase the intensity of the oblique shock wave by reducing the length of the ramp while the height remains the same.

The second and third methods for improving the recovery both reduce the amount of low-energy air that flows through the inlet. Drawings of the models that have been tested are shown in figure 2; these models are of the same general size and shape as the ramp model. With the model of figure 2(a), the boundary layer is drawn from the surface of the forebody through an auxiliary scoop at the station of the duct entrance by vacuum pumps located outside the wind tunnel. With the model of figure 2(b), energy is added to compensate for the energy decrement in the boundary layer by ejecting high-velocity air along the surface of the forebody upstream of the duct entrance. This jet is supplied by an air bottle from outside the wind tunnel, and the air is expelled through an annular nozzle that is designed to eject the air at a Mach number of 2.2. The width of the nozzle throat is 0.0045 inch and that of the outlet is 0.009 inch.

The results of tests upon these three models are shown in figure 3, in which the maximum total-pressure recovery after diffusion through the annular inlets is plotted against the Mach number of the free stream. The results are compared with the total-pressure ratio of a normal shock wave, with that of a model having no ramp or boundary-layer control, and also with that attainable with the nose inlets described in reference 1.

The model that utilizes an oblique shock wave to reduce the inlet Mach number was tested with ramp angles of  $5^\circ$ ,  $10^\circ$ ,  $15^\circ$ , and  $17.5^\circ$ . Throughout the Mach number range of the tests, the recovery of total pressure increases with ramp angle up to an angle of  $15^\circ$ , at which value the maximum total-pressure ratio is still relatively low, about three-quarters of the recovery through a normal shock wave.

With a suction slot through which 12 percent of the mass of air flowing through the inlet is drawn, the maximum total-pressure ratio attained at a Mach number of 1.36 is 81 percent and at a Mach number of 2.01, the recovery is 44 percent. Calculations based upon the available theory indicate that the amount of air in the boundary layer should be no more than 4 percent of that flowing through the inlet. The reason that the pressure recovery is not greater if more than this mass of air is removed is not understood and is being investigated at the present time.

When high-pressure air is ejected at a Mach number of 2.2 to compensate for the energy decrement in the boundary layer, the apparent recovery is relatively high at the low supersonic Mach numbers; but, as the Mach number of the free stream approaches that of the ejected air, the improvement in the total-pressure ratio decreases. The "apparent" recovery indicates the total pressure that would exist at the face of the compressor of a turbo-jet engine. However, since the engine would have to supply the high-pressure air to the nozzle, the effective recovery, as far as the overall propulsive system is concerned, is considerably less. If the total-pressure and mass-flow ratios attained during the tests are assumed to occur in a hypothetical engine operating in the isothermal atmosphere, the greatest effective pressure recovery occurs when 14 percent of the air flowing through the inlet is recirculated. The effective recovery would then be 74 percent at a Mach number of 1.36 and 44 percent at 2.01; in other words, it is about 15 percent less than the apparent recovery. It is to be expected that scale has an appreciable effect upon these results because the process is largely dependent upon viscous forces. Tests at a larger scale will probably show greater effective total-pressure ratios.

#### TWIN-SCOOP INLETS

An entry, such as a twin-scoop inlet, that does not completely encircle the fuselage does not receive all of the boundary layer resulting from the flow over the forebody and, therefore, has an initial advantage over an annular entrance. It is to be expected that greater effective total-pressure ratios can be attained than with an annular inlet and that, for the same entrance area, the greatest pressure recovery will be attained by the inlet that encloses the smallest portion of the circumference of the forebody.


Photographs of the two twin-scoop models that have been tested are shown in figure 4. The shape of the forebody, the entrance area, and the expansion ratio of the subsonic diffuser are the same as those of the models having annular entrances. The scoops of the model shown in figure 4(a) enclose 37.2 percent of the maximum circumference of the forebody, and the height of one scoop is 75 percent of the width. The inlet of figure 4(b) encloses 61.5 percent of the circumferential length, and the height is 28 percent of the width. In order to reduce the inlet Mach number, ramps were tested as with the models having annular entrances. A ramp may have an additional advantageous effect with a twin-scoop model because of the three-dimensional nature of the flow about the scoops. A compression over the surface of the ramp may cause a cross-flow that will tend to make the boundary layer flow around the inlet.



The only method for controlling the boundary layer flowing into the scoops that has as yet been tested is to pass the boundary layer out of the subsonic diffuser through slots cut along the sides of the duct next to the central body. A photograph of the arrangement is shown in figure 5. Slots of various widths and lengths have been tested with the models having the two different scoop shapes.

The results of the tests upon these twin-scoop models are summarized in figure 6 in which the maximum total-pressure ratio attained after diffusion is plotted against the free-stream Mach number. The reduction in the amount of boundary-layer air flowing through the inlet that results from the use of twin-scoops causes an improvement in the total-pressure ratio that is about the same as the improvement produced by the addition of a  $5^\circ$  ramp to the annular intake. The difference in the recovery attained by the inlet that encloses 61.5 percent of the circumferential length of the forebody and that attained by the model enclosing 37.2 percent of the circumference is less than 3 percent. The addition of a ramp improves the pressure recovery of both inlets. The maximum recovery with the 61.5-percent entry occurs with a ramp angle of about  $5^\circ$ ; with the 37.2-percent entry the optimum ramp angle is about  $10^\circ$ . If slots are cut along the sides of the duct, the optimum ramp angle increases. The effectiveness of the slot increases with ramp angle; at angles less than  $5^\circ$  the slots cause no improvement. With the 61.5 percent entry having a slot whose depth is 50 percent of the height of a scoop and whose length is 6 percent of the length of the subsonic diffuser, the optimum ramp angle is  $12^\circ$  and the total-pressure ratio is about 88 percent of that occurring across a normal shock wave. The 37.2-percent entry having the same ramp and slots of the same dimensions produces a total-pressure ratio that is about 8-percent greater at a Mach number of 1.36 and the same at a Mach number of 2.01. If the length of the slots of this model is increased to 9 percent of the length of the subsonic diffuser, the total-pressure ratio attained is practically equal to that of a normal shock wave at Mach numbers between 1.36 and 1.70. The recovery after diffusion is 96 percent at a Mach number of 1.36, or it is equal to that of the Ferri-type nose inlet. Although this high recovery is obtained at the expense of external drag, the increase in the drag force may be small in comparison to the improvement in the total-pressure recovery. If so, the inlet will be satisfactory for aircraft flying at low supersonic Mach numbers. The pressure recovery decreases a small amount in relation to that through a normal shock wave for Mach numbers above 1.70. At a Mach number of 2.01 the recovery attained by this model is 94 percent of normal-shock recovery.

  
REFERENCES

1. Ferri, Antonio, and Nucci, Louis M.: Preliminary Investigation of a New Type of Supersonic Inlet. NACA RM No. 16J31, 1946.
  2. Davis, Wallace F., Brajnikoff, George B., Goldstein, David L., and Spiegel, Joseph M.: An Experimental Investigation at Supersonic Speeds of Annular Duct Inlets Situated in a Region of Appreciable Boundary Layer. NACA RM No. A7G15, 1947.
- 

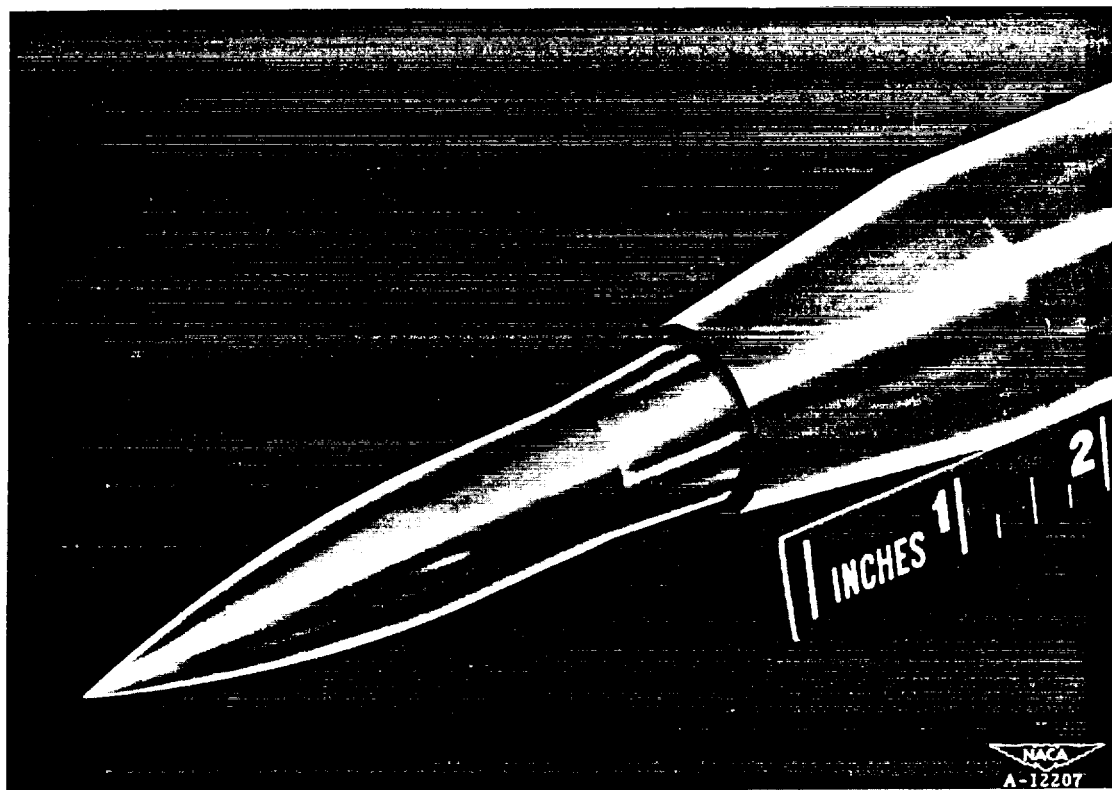
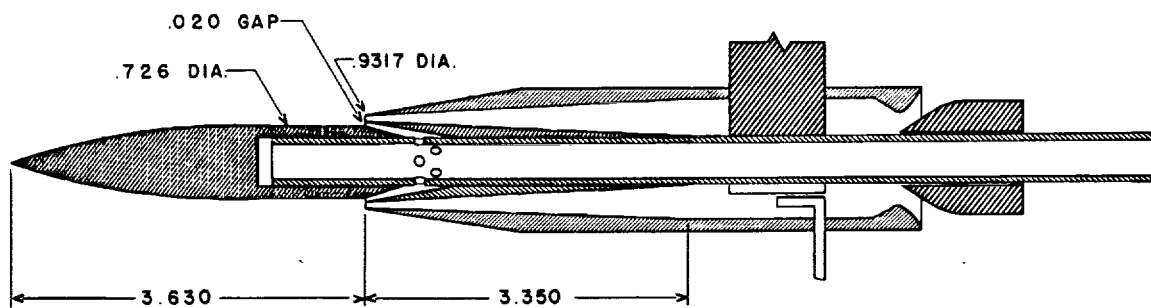
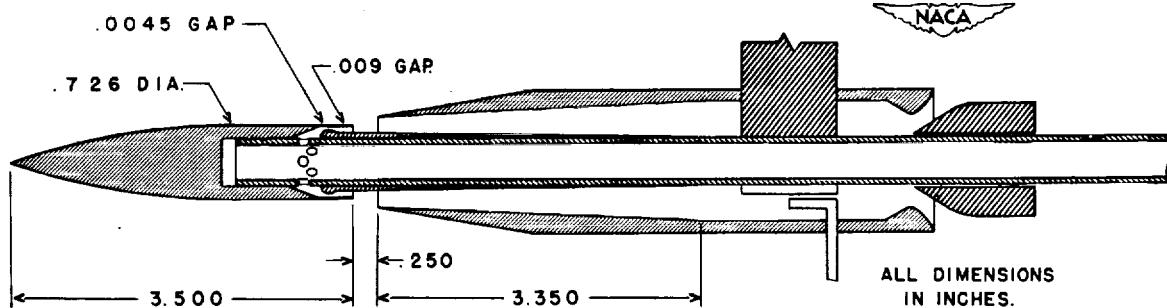


Figure 1.- Annular-entrance model with 5° ramp.



(a) Model with boundary-layer suction slot.



ALL DIMENSIONS  
IN INCHES.

(b) Model with nozzle to accelerate the boundary layer.

Figure 2.- Annular-entrance models with boundary-layer control.

Davis

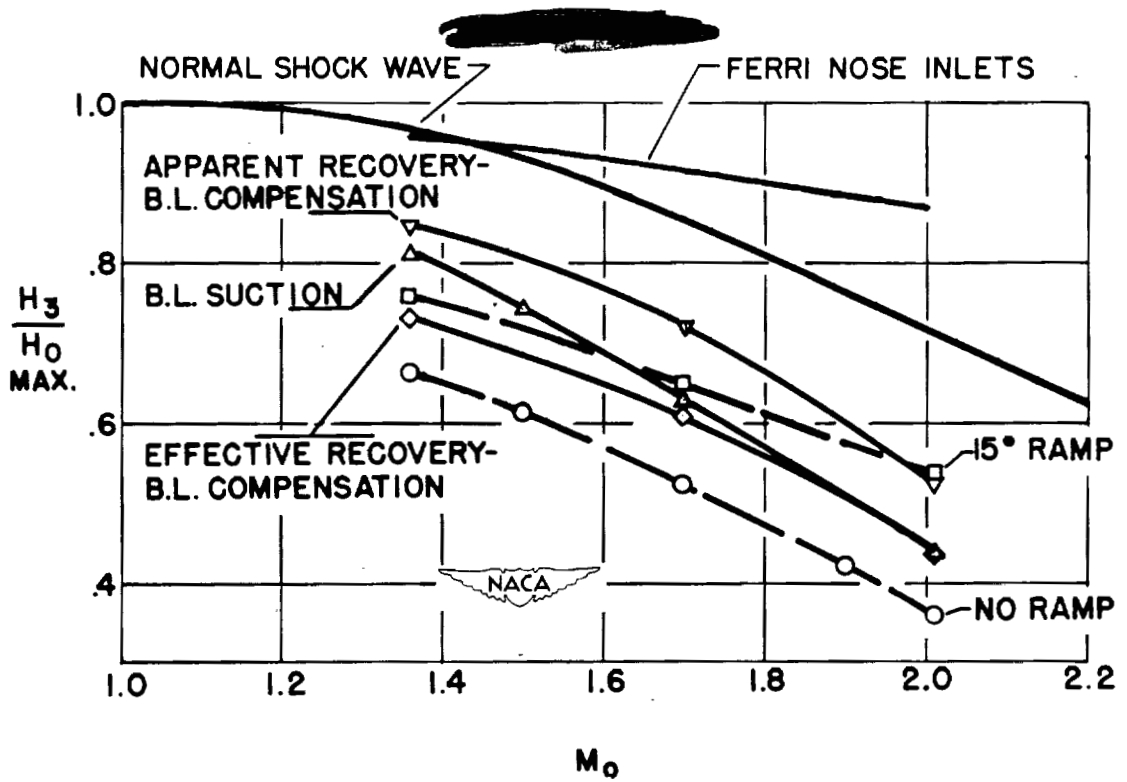
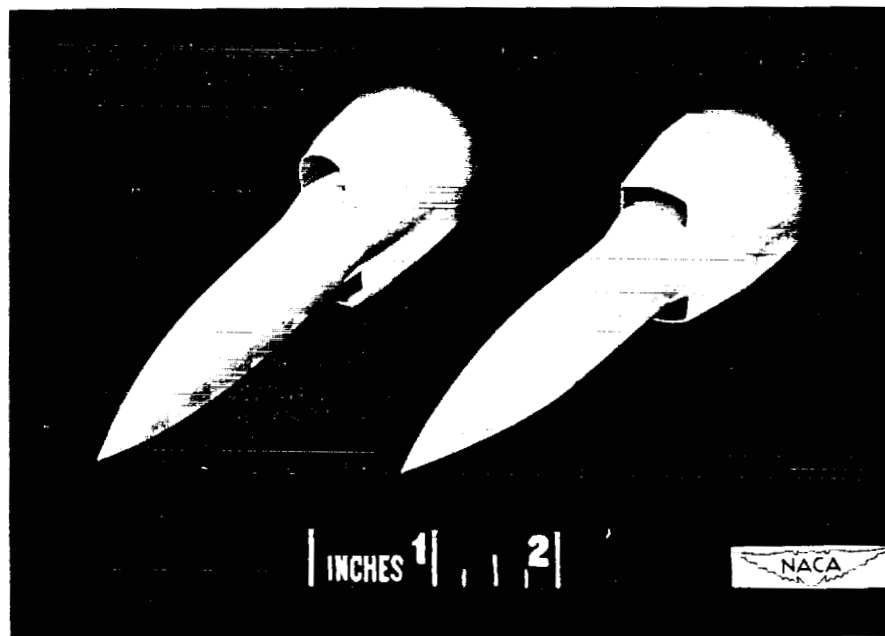


Figure 3.- Variation of maximum total-pressure ratio with Mach number for annular-entrance models.



(a) Inlet enclosing 37.2 percent of the circumference of the forebody.

(b) Inlet enclosing 61.5 percent of the circumference of the forebody.

Figure 4.- Twin-scoop models with 9° ramps.

58(a)

Davis

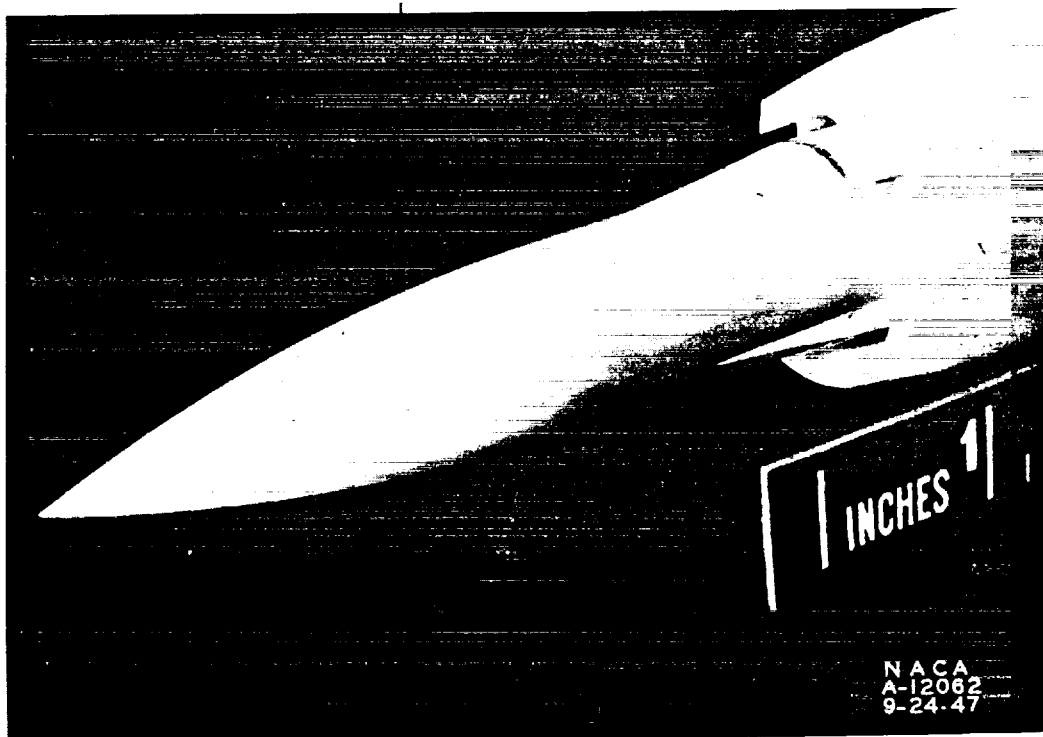


Figure 5.- Twin-scoop model with slots.

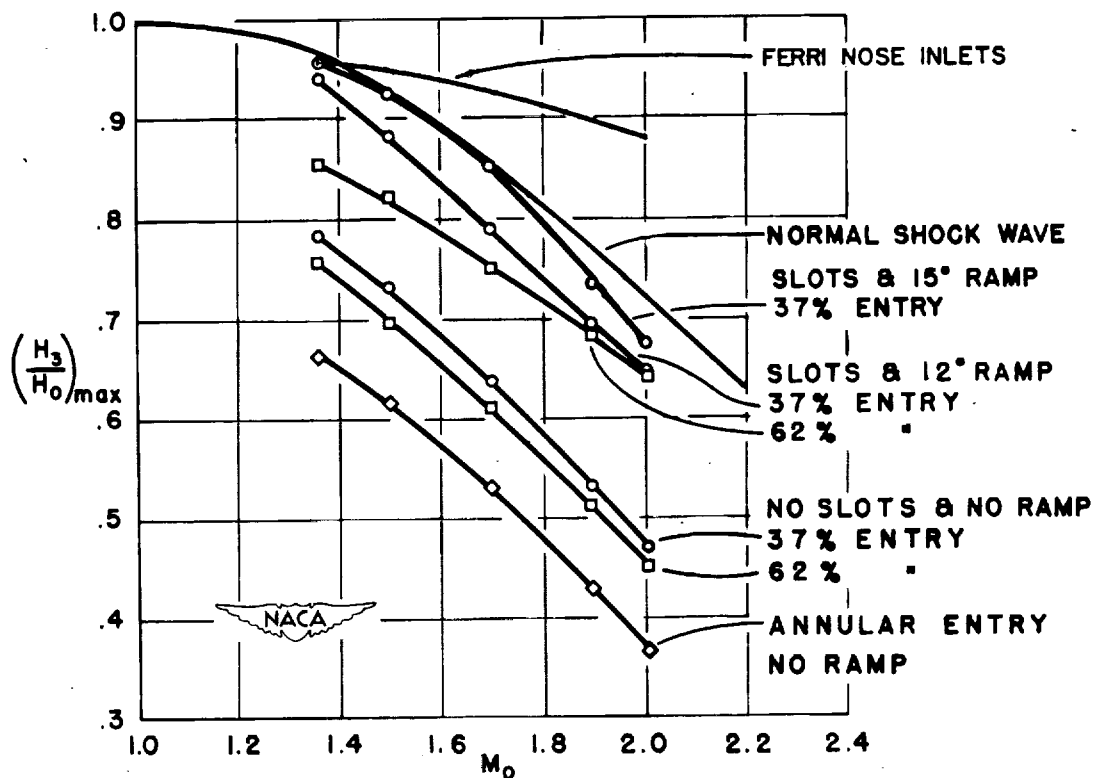


Figure 6.- Variation of maximum total-pressure ratio with Mach number for the twin-scoop models.

NACELLES FOR HIGH CRITICAL SPEEDS ON

STRAIGHT AND SWEEP WINGS

By Robert E. Dannenberg

Ames Aeronautical Laboratory

The development of a large high-speed airplane utilizing jet engines normally requires that the engines be enclosed in nacelles attached to the wing. In order to achieve high flight velocities, it is necessary to design the nacelle so that not only is the air ducted to the jet engine in an efficient manner but also so that the air flow over the nacelle does not detrimentally affect the high-speed drag characteristics of the airplane. The combination of the wing and nacelle give rise to interference effects (particularly on the drag and critical speed of the wing-nacelle combination) that are controlled through the design of the nacelle contour and its position on the wing.

The Langley Laboratory has recently made high-speed wind-tunnel measurements on the interference effects of nacelles on straight wings (reference 1). As shown in figure 1, the simulated nacelle for these tests, an NACA 111 body of fineness ratio 6, was mounted in various vertical positions on a two-dimensional straight wing having an NACA 65-210 section. This figure shows the effects of the vertical position of the nacelle located 66-percent-chord length ahead of the wing, as shown by the corresponding lines, on the nacelle drag coefficient based on the frontal area  $C_{DF}$  as a function of Mach number M.

In the underslung position (shown by the solid-line curves), the drag increment at the maximum available test Mach number of 0.7 indicated a smaller tendency to increase at an angle of attack  $\alpha$  of  $0^\circ$  than in the other positions. At an angle of attack of  $2.5^\circ$ , the underslung-nacelle drag variation was similar to that of the plain wing, whereas the positions above the wing showed large drag rises. The fact that these interference drags arise from the increased velocities provided by the nacelle over the midchord section of the wing is confirmed by the pressure-distribution studies.

At an angle of attack of  $0^\circ$ , the peak suction pressures of the nacelles are located near the midchord section of the wing. For the nacelle in the underslung position, these pressures combine with the lower surface pressures of the wing. The pressures over the upper surface remained essentially the same as over the undisturbed wing. Raising the nacelles from the low position increased the velocities over the wing adjacent to the nacelles and resulted in a decreased Mach number at which the severe drag rises occurred. This effect is even more pronounced at higher angles of attack.

Figure 2 shows the influence of horizontal position on the drag characteristics of the underslung nacelle. Although little drag variation was noted at an angle of attack of  $0^\circ$  up to the maximum test Mach number, the drag coefficients decreased with forward nacelle location at an angle of attack of  $2.5^\circ$ . Little change was noted on the wing pressures from varying the nacelle position horizontally; however, the forward position resulted in an appreciable loss in lift of the wing-nacelle combination. Giving the nacelle (shown by the solid-line curve) either positive or negative incidence reduced the Mach number at which the drag rise occurred.

The Ames Laboratory has made wind-tunnel studies of the interference effects of a nacelle with internal air flow as shown in figure 3. This research covered nacelle types for conventional-wing high-speed bombers, powered with four jet engines housed either in two dual-unit nacelles, which also enclose the landing wheel, or in four single-unit nacelles. Tests were made for the nacelles underslung beneath the wing and for nacelles centrally located on the wing. Figure 4 shows the internal arrangement of the dual-unit nacelles. The jet engines were placed well forward on the wing to aid in providing proper balance to the airplane. Retracting the landing wheel into a forward position of the nacelle allowed the cusp-type afterbody to taper more gradually and kept the frontal and surface areas as small as possible. The forebody shape ahead of the wing was designed to have no localized velocity peaks over the lips. The general body lines were selected to give constant cross-sectional area for the central portion of the nacelle to minimize the additional interference velocities produced by the nacelle in the region of the wing.

The dual-unit nacelles as shown in figure 4 and the single-unit nacelles were developed in a low-speed wind-tunnel investigation on a  $\frac{1}{4}$ -scale model (reference 2). The nacelles showed desirable aerodynamic characteristics. Satisfactory internal pressure recoveries were obtained. The drag of each nacelle based on the frontal area was approximately 0.05. Negligible adverse interference effects on the maximum lift and pitching-moment characteristics were experienced. Locating the nacelle underslung beneath the wing resulted in a slight increase of the angle of zero lift. The predicted critical compressibility speed for the combination of the wing and each nacelle above an inlet-velocity ratio of 0.5 was above that of the plain wing except in the wing-nacelle juncture.

The high-speed characteristics of the dual-unit nacelles were obtained with a  $\frac{9}{100}$ -scale model of the wing, fuselage, and two nacelles (references 3 and 4). The external-drag coefficient of

the underslung and central dual nacelles, based on the frontal area, were 0.06 and 0.044, respectively, at zero lift and at a Mach number of 0.74. The variation in pitching moment and angle of attack for zero lift with Mach number was slight up to drag divergence.

Pressure studies at high speeds showed satisfactory distribution over the nacelle except in the wing-nacelle juncture. This was similar to the results predicted from the low-speed tests. Normally, the critical Mach numbers are compared as an indication of whether the Mach number for drag divergence of the wing-nacelle combination is equal or below that of the plain wing. Figure 5 shows the predicted critical Mach number  $M_{cr}$  as a function of the angle of attack  $\alpha$  of the various sections of the dual underslung nacelle. The critical Mach number of the upper center line, the lip section, the half-breadth, as well as the upper and lower junctures, are presented inasmuch as they are representative of the type encountered with an underslung nacelle. The lower wing-nacelle juncture, although filleted, was critical over a small angle range (fig. 5). These predicted critical Mach numbers were based on the peak suction pressures occurring at the juncture leading edge. Basing the predicted Mach number on the juncture pressure at the midchord section would result in a value above that of the wing. Centrally located nacelles exhibit similar characteristics except that the critical pressures usually occur in the upper-surface juncture at the maximum thickness of the wing.

The high-speed drag characteristics of the dual nacelles are presented in figure 6. In this figure the drag coefficient  $C_D$  of the wing and fuselage with two nacelles are presented as a function of Mach number  $M$  and are shown by the corresponding lines for lift coefficient  $C_L$  of 0 and 0.2. The presence of either type nacelle had no appreciable effect on the Mach number of drag divergence compared to the basic wing-fuselage combination other than to steepen the rise of the drag curves after the divergence Mach number was reached. It is interesting to note that the predicted Mach number as set by the leading-edge-juncture pressures was well below that obtained by actual test. This would indicate that a predicted critical Mach number, based on the very localized suction pressure occurring in a wing-nacelle juncture, is evidently quite conservative. Extensive pressure surveys made in the wing-fuselage juncture revealed that the critical pressures were contained in a very small region adjacent to the nacelle that extended but  $\frac{1}{100}$ -chord length along the span. Outboard of this region the pressures were satisfactory.

When the problem of nacelle design on a sweptback wing is considered, it is desired that the interference effects resulting



from the addition of the nacelles on the swept wing will not reduce the divergence Mach number. Any reduction will tend to nullify the advantages gained through the use of sweepback.

Before proceeding with the problem of the design of an air-flow nacelle, it was necessary to obtain information relative to the interference effects of a jet nacelle body on a sweptback wing. For this purpose, a nacelle was mounted at various positions along the 31-percent semispan station of a sweptback wing as shown in figure 7. The nacelle was simulated by a prolate ellipsoid of fineness ratio 5 mounted on an NACA 64-212 wing swept  $35^\circ$ .

The nacelles were investigated at low speed at the central locations shown in figure 7: (1) a forward position 40-percent-chord length ahead of the wing leading edge, (2) a leading-edge position coincident with the wing leading edge, and (3) an aft position coincident with the 40-percent wing-chord line. The nacelle was also mounted in an underslung position 40-percent-chord length ahead of the wing leading edge and on a strut below the wing as it was believed that such a position may be necessary to reduce the interference effects. The nacelle was located ahead and coincident with the wing leading edge on different length struts.

The experimental results of the low-speed investigation (reference 5) showed that the nacelle in the above locations had negligible effect on the maximum lift and pitching-moment characteristics. Locating the nacelle beneath the wing and on the struts slightly increased the angle of zero lift. The external-drag coefficient based on the frontal area was approximately 0.05. Practically the only effect of the nacelle position was on the pressure distribution. All the wing-mounted nacelles produced a velocity distribution over the center lines which were less than the maximum velocities over the basic swept wing. The lowest velocity distribution was obtained over the center line of the nacelle having the minimum pressure point farthest aft of the minimum pressure point of the wing (that is, the nacelle in the aft position). The application of a wing-leading-edge entrance with such a nacelle position is indicated.

The pressure distribution along the inboard wing-nacelle juncture varied with nacelle location. With the nacelle in the forward position, the peak suction pressures at the juncture leading edge were well above those of the wing. In the leading-edge position, the pressures were generally of the same magnitude as the pressures along the midchord of the wing. Locating the nacelle in the aft position reduced the juncture pressures well below those of the wing.

The pressure distribution along the outboard junctures were satisfactory for all nacelle positions.

The pressure distribution over the nacelle mounted on the strut of lengths 20-percent and 30-percent chord below the wing were satisfactory; however, the strut junctures at the nacelle and particularly at the wing showed the formation of high localized velocities over the inboard surface. These high velocities were due in part to the suction pressures of the strut and lower wing surface being coincident at the same chordwise station. Undoubtedly these velocities could be reduced by changing the location of the strut peak pressure with respect to that of the wing.

The Langley Laboratory (reference 6) investigated the effect of a central nacelle located ahead of the leading edge of a sweptback wing where the angle of sweep  $\Lambda$  is equal to  $45^\circ$  as shown in figure 8. Up to the maximum available test Mach number of 0.61, the addition of the nacelle had but little effect on the lift, drag, and moment characteristics. The pressure-coefficient contours over the upper surface of the wing and nacelle are shown in figure 8 for a Mach number of 0.61 and a lift coefficient of 0.20. The pressures over the nacelle are less than those over the midchord section of the basic wing except for a very small region at the inboard-juncture leading edge. A possible detrimental interference effect due to the nacelle is the shifting of the constant pressure lines along the plain wing from a position parallel to the wing leading edge to one normal to the flight path. Further research at high speeds is necessary to evaluate this effect on the drag characteristics. Similar results were obtained with the same nacelle location but with the wing swept forward  $45^\circ$ , except that the leading-edge peak suction pressures shifted to the outboard juncture.

In summary, the design of a high-critical-speed wing-nacelle combination is primarily dependent on the location of the nacelle such that the peak suction pressures of the nacelle and wing do not coincide at the same chordwise position or unite in an area that is largely influenced by the lift additional of the wing. The low-speed or basic drag of the combination depends upon the contours of the nacelle and its location on the wing. It is greatest when the wing-nacelle components intersect in such a way that regions of adverse pressure gradients face each other upon their surfaces. Early drag rises resulted for a wing-nacelle combination on a straight wing in which the pressures coincide in the midchord section of the wing, particularly with the nacelle in a central position. Satisfactory drag characteristics were obtained for the nacelle design in which the peak suction pressures were located behind those of the wing. High-speed drag results showed that the localized peak suction

pressures at the leading edge of the wing-nacelle juncture on a conventional wing did not contribute to a reduction in the critical speed of the combination.

## REFERENCES

1. McLellan, Charles H., and Cangelosi, John I.: Effect of Nacelle Position on Wing Nacelle Interference. (Prospective NACA paper)
2. Dannenberg, Robert E.: The Development of Jet-Engine Nacelles for a High-Speed Bomber Design. NACA RM No. A7D10, 1947.
3. Pengal, Joseph R., and Butterworth, Keith L.: High-Speed Characteristics of Nacelles for Jet-Propelled Aircraft - An Underslung Nacelle Housing a Landing Wheel and Two Jet Engines. NACA MR No. A6A28, Army Air Forces, 1946.
4. Pengal, Joseph R., and Butterworth, Keith, L.: High-Speed Characteristics of Nacelles for Jet-Propelled Aircraft - A Centrally Located Nacelle Housing a Landing Wheel and Two Jet Engines. NACA MR No. A6D04, Army Air Forces, 1946.
5. Hanson, Frederick H., and Allison, George E.: Effect of Streamline Body Location on the Aerodynamic Characteristics of a Sweptback Wing. (Prospective NACA paper)
6. Heiser, Gerald, and Whitcomb, Charles F.: Investigation of the Effects of Sweep on a Wing and Wing-Nacelle Combination. (Prospective NACA paper)

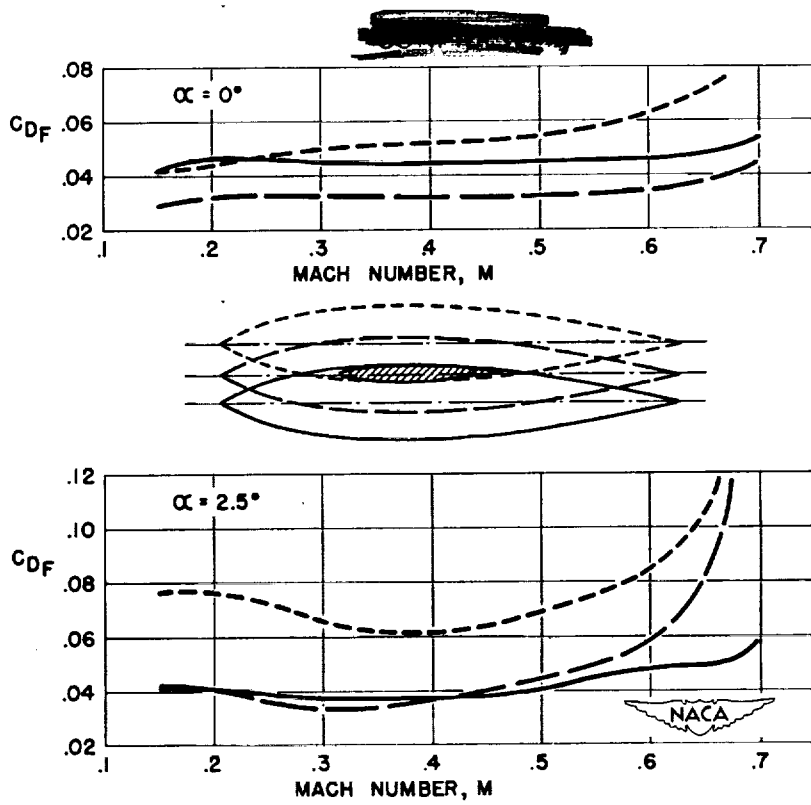


Figure 1.- The effect of vertical nacelle position on the drag coefficient.

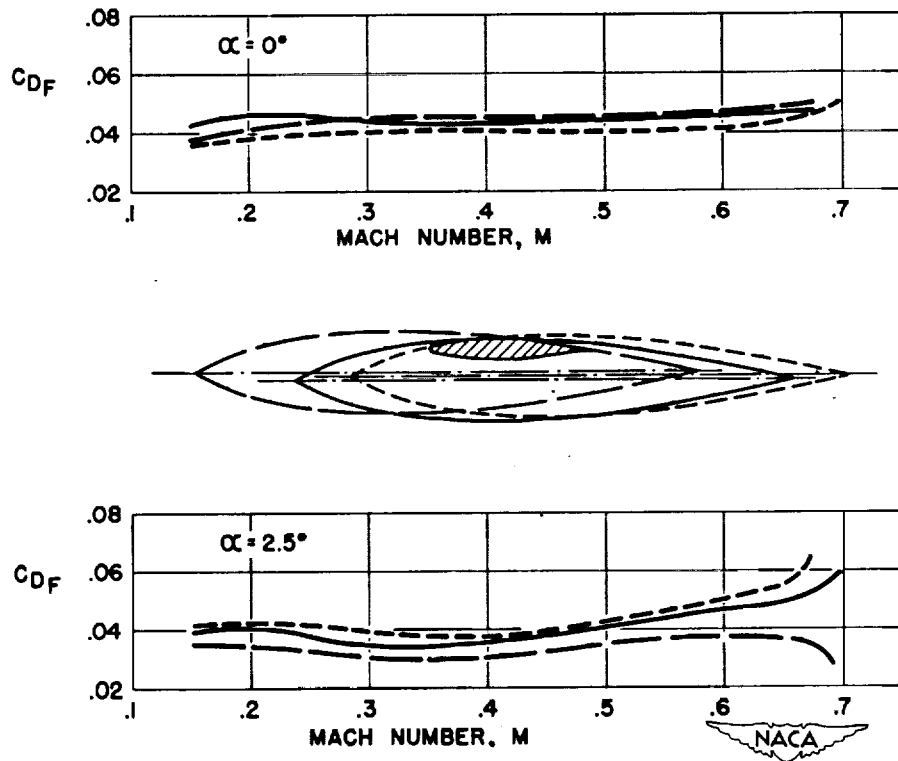


Figure 2.- The effect of horizontal nacelle position on the drag coefficient.

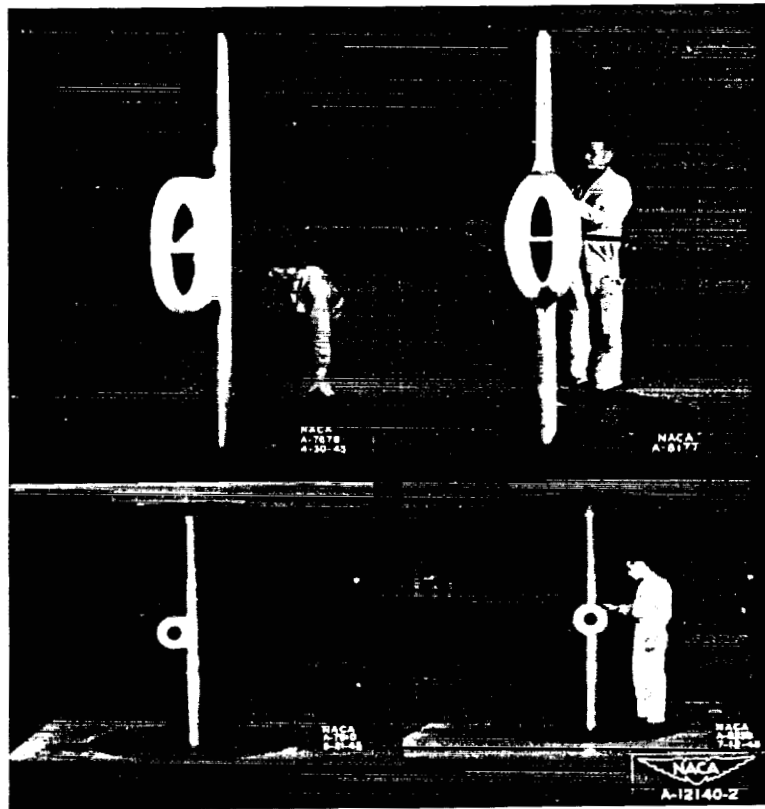


Figure 3.- Jet-engine nacelles mounted on the wing panel.

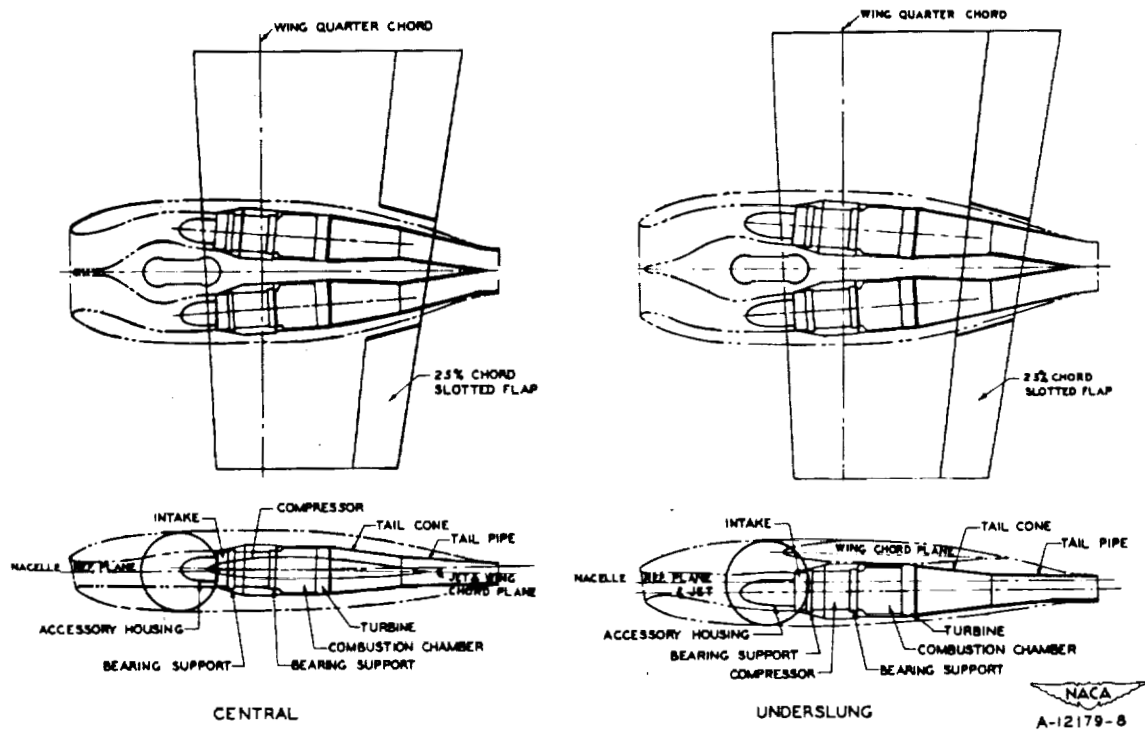


Figure 4.- Internal arrangement of the dual jet-engine nacelles.

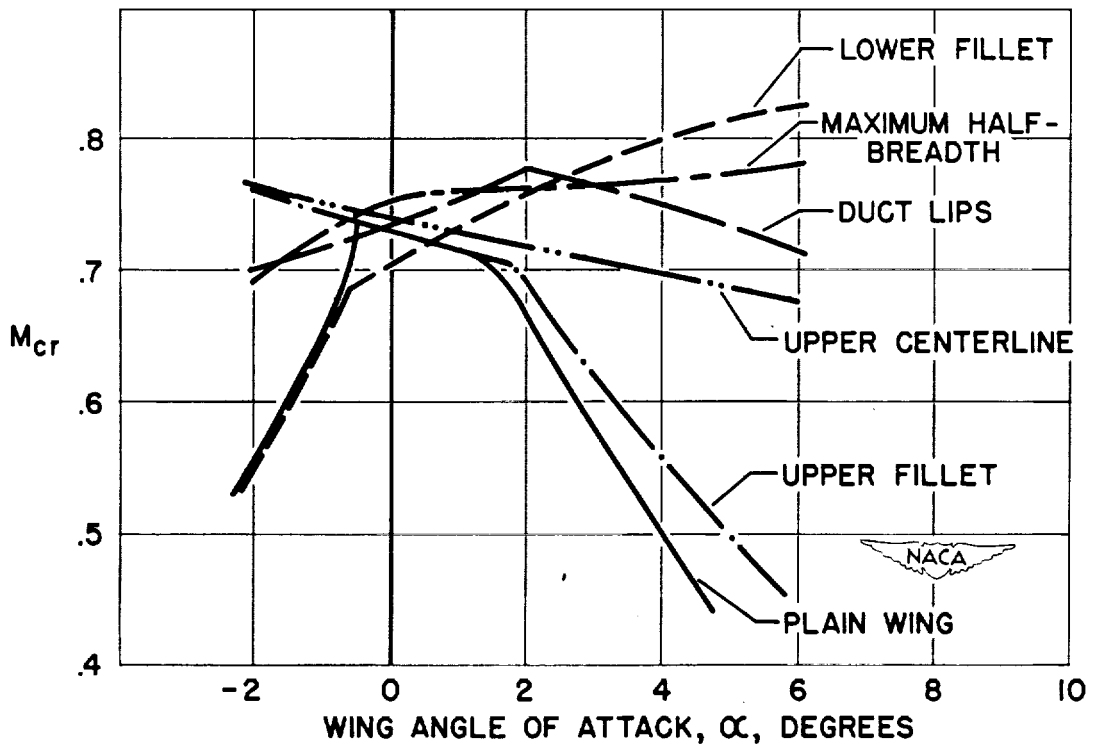


Figure 5.- Critical Mach number characteristics of the underslung nacelle at an inlet-velocity ratio of 0.8.

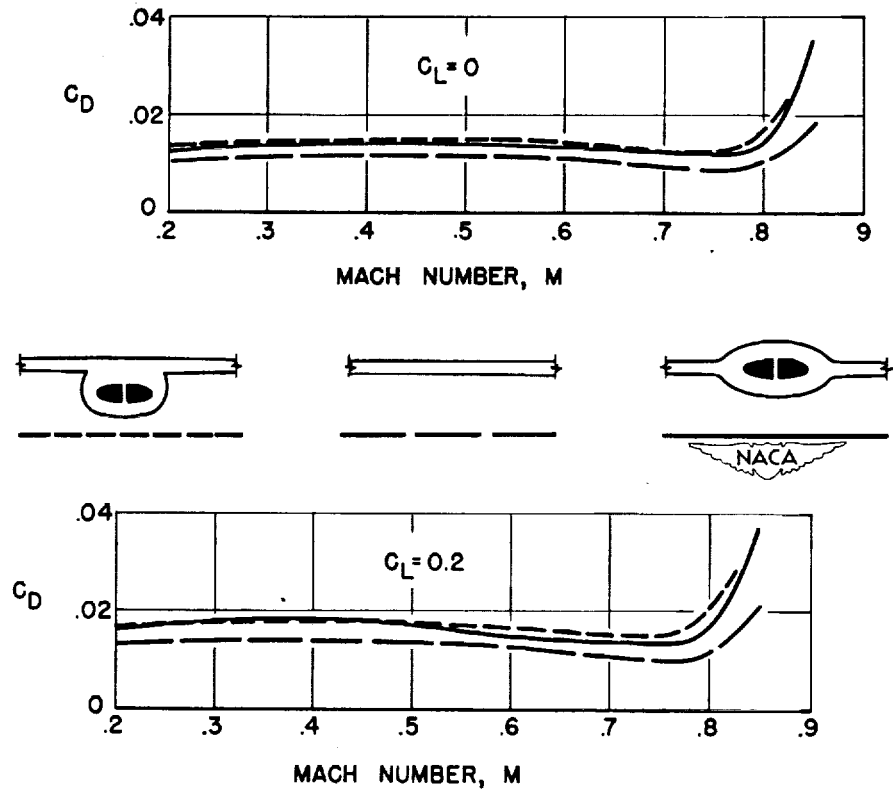


Figure 6.- High-speed drag characteristics of the wing and fuselage with two dual nacelles.

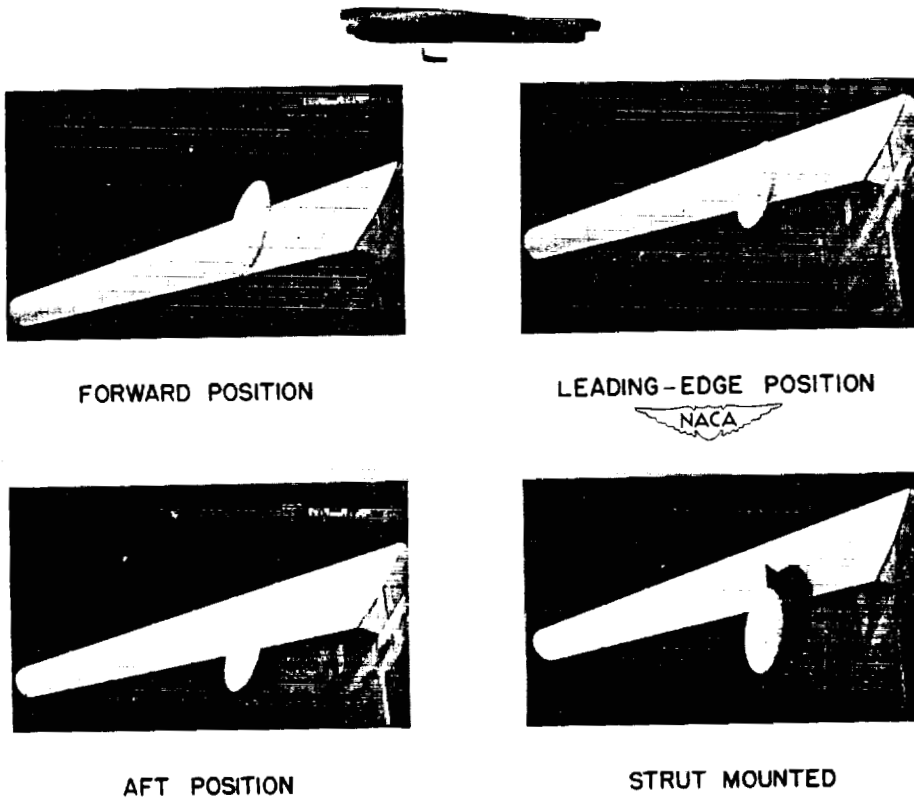


Figure 7.- Nacelle body locations on a 35° sweptback wing.

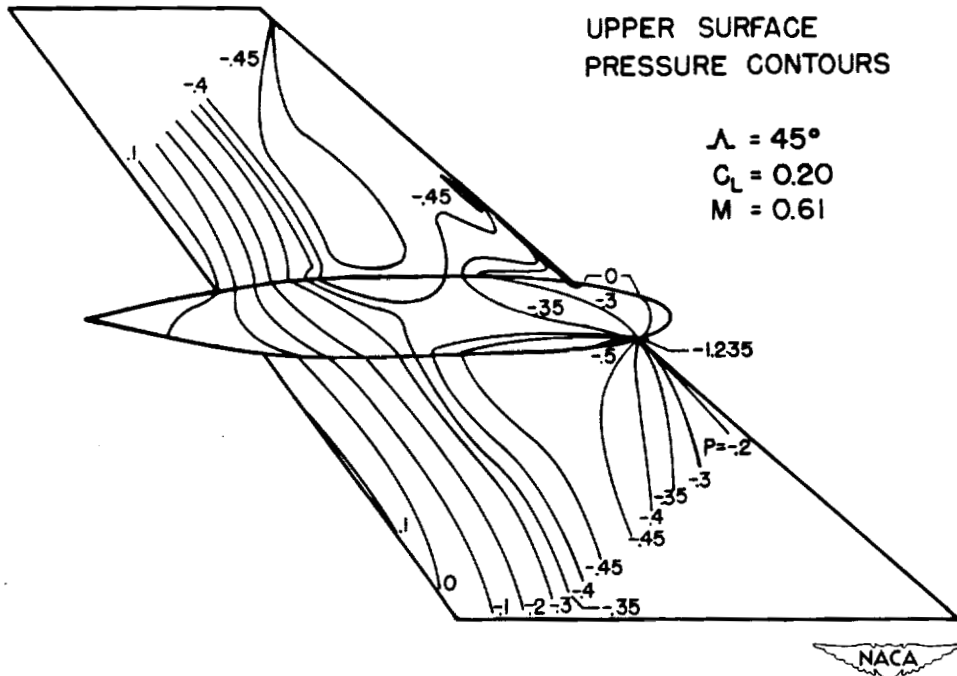


Figure 8.- Pressure-coefficient contours of a centrally located nacelle on a 45° sweptback wing.

PROPELLERS



## PROPELLERS AT HIGH SPEEDS

By Eugene C. Draley

Langley Memorial Aeronautical Laboratory

The first NACA high forward-speed propeller tests were conducted during the recent war period. The purpose of these high-speed propeller tests was to study the factors affecting the propeller performance at high speeds and to obtain information permitting the design of propellers having high performance at high forward speeds. The purpose of this paper is to present the more recent results obtained in this program. Studies have been made of air flow phenomena at low speeds, which are therefore not included in this paper, of some of the basic factors which affect high-speed propeller performance. These studies cover research on propeller pitch distribution (reference 1), propeller design and performance (references 2, 3, and 4), dual-rotation propellers (references 5 and 6), and the field of flow around air inlet cowlings and propeller spinners (reference 7).

The results of the tests of the NACA 4-508-03 propeller in the Langley 8-foot high-speed tunnel are presented in figure 1 which shows the status of the high-speed research program on propellers. In the upper part of this figure is a plot of maximum efficiency against forward Mach number. The design numerals represent, in order of presentation, the propeller diameter, the design camber in terms of design lift coefficient at the 0.7 blade-radius station, the thickness ratio at the 0.7 blade-radius station, and the solidity per blade. These test results were obtained for a blade-angle setting of  $60^\circ$ . For purposes of comparison there are included in this figure the efficiency characteristics of propellers currently in use at the time the high-speed propeller program was initiated. Also included, for purposes of comparison, is the variation in ideal jet-propulsion efficiency based upon typical values of the thrust per unit area currently used in jet engines. Comparison between the previous propeller efficiency and the NACA high-speed propeller efficiency indicates the gains made in the early phase of the research program. It should be noted that the levels of efficiency for the NACA propeller at low speeds is unusually high, well in excess of 90 percent. The results indicate that propellers with relatively high levels of efficiency could be designed for speeds as high as 500 miles per hour. These high levels are the result of using optimum NACA 16-series propeller airfoils with very thin sections, of eliminating the thick shank sections of propellers, and of designing the propeller to operate with ideal Betz loadings by methods outlined in references 8 and 9. Comparison of this efficiency with the efficiency of typical previous propellers indicates the gains in propeller performance thus obtained by improved

Preceding page blank

design. The onset of compressibility effects was delayed by about 100 miles per hour in forward speed.

The early phase of this research program was limited in forward Mach number to approximately 0.7 (approximately 500 miles per hour) and this limit is indicated by the cross-hatched region in figure 1.

A recent phase of this work has included the extension in the Langley 8-foot high-speed tunnel of this study to higher forward speeds in excess of 90 percent of the speed of sound. The part of the curve to the right of the cross-hatched region represents the results of these tests (reference 10). The purpose of the tests was to obtain data at extremely high forward speeds and increased power loadings for a study of the phenomena in this speed range and thus to define for modern propellers the maximum efficiency characteristics and to obtain indications of possible further improvement in propeller performance.

The test results show that, at forward Mach numbers in the order of 70 percent of the speed of sound, very large serious adverse effects of compressibility occur so that efficiency levels of the order of 50 percent to 55 percent are reached at forward Mach numbers of 85 percent of the speed of sound. Thus, for the first time, a comparison is obtained which defines the range of forward speeds in which propellers are more efficient than jet engines and the range of speeds in which jet engines are more efficient than propellers. It should be noted, however, that this comparison between the ideal jet efficiency and the propeller efficiency is subject to changes, as illustrated by the fact that large improvement over the previous propeller characteristics has already been obtained.

The second part of figure 1 is a plot of the power coefficient corresponding to the maximum efficiency curve for the two-blade NACA propeller shown in the upper part of the figure. Of interest here is the fact that the effects of compressibility on the power coefficient corresponding to maximum efficiency does not lead to very serious and abrupt reductions in the value of this power coefficient, which reduction will be shown later to occur at lower settings of the blade angle. As a matter of fact, at the maximum speed shown there is a tendency toward further increases in this power coefficient. Tests made at higher speeds where maximum efficiency was not obtained indicated moreover that at these higher speeds further rapid increases in the power coefficient can be expected. Predictions based on low-speed information of the power coefficient for maximum efficiency for the high advance-diameter

ratios (approximately 4) associated with blade angles of  $60^\circ$  are thus indicated to underestimate the high-speed value of the power coefficient.

The lower part of figure 1 illustrates some of the reasons for the aforementioned changes. It is a plot of the radial distribution of thrust along the blade radius measured by momentum surveys. At low speeds the distribution of thrust very closely approaches the ideal loading for which the propeller was designed. As the forward speed is increased, however, effects of compressibility lead to loss in thrust, first at the tip, and, with further increases in speed, these losses progressively move toward the root section of the propeller. This type of phenomenon has been illustrated before at lower advance-diameter ratios (references 11 and 12). As this loss progressively moves inboard, however, another phenomenon begins to occur at the tip at these high blade angles and results in increased tip loads. This increase of load at the tip compensates for the loss in load at the inboard sections. Indications of this effect have also been found in flight (reference 13).

The increased load at the tip sections of the propeller is believed to be associated with the second force-break characteristic shown to occur for wings and airfoils in the transonic-speed range where, in plots of wing lift coefficient for constant angles of attack against Mach number, there is an abrupt rise in the lift values following the well-known loss in lift characteristics (reference 14).

The resultant section Mach number has been calculated for a large number of these measured thrust distributions for the points along the blade radius where the loss in thrust between the low-speed thrust value and the value at any high speed is the maximum. The resultant Mach number for all cases tends to scatter closely around a value of the resultant section Mach number of 0.9.

It is believed that, with such thrust distributions as were measured for forward Mach numbers of 0.85, the aforementioned losses in efficiency for these speeds may include a large component of induced loss because of the departure from the ideal loading (as indicated by a comparison of the low-speed and the high-speed thrust distributions). Modification of pitch distribution, for example, to provide a closer approach to the ideal type of load distribution may offer considerable improvement in the efficiencies shown.

Calculations have further indicated that a large part of the induced losses which may occur at these high forward speeds and high advance-diameter ratios can be expected to be associated with induced

rotational losses. Thus the use of dual-rotational propellers which theoretically at least eliminate the rotational losses are indicated to offer improvements in propeller efficiency.

The use of sweep to delay the onset of compressibility effects to even higher forward speeds is also currently being studied. Preliminary tests with sweep incorporated in just the tip section of propeller blades has indicated that the use of sweep will permit a significant delay in the onset of compressibility effects (reference 15). More recently the NACA found that there were propeller blades incorporating sweep which had been built for flight tests by a manufacturer. It appeared that these blades would be available sooner than existing NACA designs which are currently being built. Steps were taken to procure these blades for testing in the Langley 16-foot high-speed tunnel.

Figure 2 describes the propellers and the test results obtained. Two propellers were tested, one straight and one with sweep as indicated by the plan-form lines. The part below the propellers is a plot of the variation of sweep angle along the radius of the swept propeller. The results of the tests are shown in the lower part of this figure in the form of maximum efficiency plotted against resultant tip Mach number which is chosen rather than forward Mach number since the resultant tip Mach number is a more exact indication of the onset of compressibility effects. The differences in maximum efficiency between the straight and swept propellers shown are within the experimental accuracy of the tests. The results show that sweep can be incorporated throughout the blade radius without serious adverse effects on low-speed efficiencies. Even at the maximum tip speed attained, which was a limitation imposed by the larger diameter (13 ft) of this propeller as compared to the standard size (10 ft) for which the dynamometer equipment was designed, there were no essential differences in the propeller efficiencies. Presumably, delays in the onset of compressibility effects might be indicated at higher tip Mach numbers. Because no effects of compressibility are shown, the magnitude of the delay from the amount of sweep used has not been defined.

Included in the part just under the blade plan-form curves for the two propellers to indicate the amount of sweep required for a given delay of compressibility effects is the variation in sweep indicated by analytical studies to be required to delay compressibility effects by approximately 100 miles per hour. These values indicate that large amounts of sweep are necessary before significant delays in the onset of compressibility effects can be realized. This same characteristic has already been shown for wings where

sweep angles of less than  $30^\circ$  are not effective in delaying compressibility effects.

In addition to the recent work performed to study the phenomena on propellers at speeds in excess of 500 miles per hour, there has been made concurrently with the work just discussed a study at speeds up to 500 miles per hour in the Langley 16-foot high-speed tunnel of the effects of various design parameters on propeller performance (references 16, 17, 18, and 19).

Included in this work is the effect of solidity. These results are shown in figure 3 for studies of three propeller configurations. Tests were made of a two-blade narrow propeller, a two-blade wide propeller having increase in solidity of 50 percent over the narrow blade propeller, and a three-blade propeller utilizing the same narrow propeller blade, thus providing again a 50-percent increase in propeller solidity. The results are presented in the upper part in the form of a plot of maximum efficiency against resultant tip Mach number for a blade angle of  $45^\circ$ . It is indicated that little or no changes in efficiency occur in increasing the solidity by increasing the number of blades or the blade width. As a matter of fact, the changes in efficiency shown correspond in magnitude to the calculated changes in efficiency due to the increased induced losses occurring for the higher solidity propellers.

The lower part is a plot of the power coefficient corresponding to the maximum efficiency curves presented above. At low tip speeds the three-blade propeller absorbs considerably much more power at maximum efficiency than does the two-blade wide propeller. Thus an increase in solidity by the use of an increased number of blades is indicated to be more effective in increasing the power capacity of the propeller than is an increase in solidity by increasing the blade width. *for full blade angle!*

At high tip Mach numbers where the effects of compressibility are shown to be severe, very large reductions in the power coefficient for maximum efficiency for all three propellers tested was observed.

These curves, which are presented for blade angles of  $45^\circ$  (advance-diameter ratio of approximately 2), are in marked contrast to the power coefficient curves for maximum efficiency shown in figure 1 where for blade angles of  $60^\circ$  (advance-diameter ratio approximately 4) no such large losses were shown.

The large variation in these power-coefficient characteristics at the high tip Mach numbers together with the differences at different advance-diameter ratios indicates that predictions of these

characteristics based on low-speed data could be expected to be inaccurate. However, in order to attain even the maximum efficiency shown at the higher tip Mach numbers, it is necessary to operate at or very near these power coefficients because the results indicate that departure from these power coefficients would lead to efficiency values considerably less than the maximum values shown.

*Possible  
to  
use  
the  
same  
blade  
width  
as  
the  
three-blade  
propeller  
but  
with  
a  
different  
aspect  
ratio.*

The onset of compressibility effects for the wide-blade propeller occurs at a higher tip Mach number than it does for the three-blade propeller. This difference is believed to be a result of the effects of aspect ratio, the wider blade having the lower aspect ratio. Reductions in aspect ratio have been shown in studies of wings by Stack and Lindsey to lead to delays in the onset of compressibility effects (reference 20). Increase in solidity by use of wide propeller blades has been studied through a range of solidities approximately twice that presented in figure 3 (reference 21). The results of these tests have given similar indication that wide propeller blades tend to delay the onset of compressibility effects.

Airfoil and wing studies at high speeds have long indicated that reductions in airfoil thickness ratio provides delays in the onset of compressibility effects. Studies of propeller airfoil sections (reference 22) have indicated that increased values of efficiency even at low speeds can be obtained through the use of thinner propeller sections. Tests of propellers having different thickness ratios have been studied to evaluate these effects in terms of propeller performance.

Figure 4 includes test results of two sets of propellers having different thickness ratios. A pair of propellers having the plan form shown on the left of the figure and having identical camber ( $C_{LD} = 0.3$ ), but with sectional thickness ratios of 12 and 8 percent, respectively, were tested. The distribution of the thickness ratio along the propeller-blade radius is shown. The maximum efficiency for these two propellers is plotted against a tip Mach number. The results indicate that even at low speeds, as was indicated by the airfoil studies, the thinner propeller has the higher efficiency and this incremental efficiency becomes considerably larger above tip Mach numbers of 0.92. Moreover, the point at which the effects of compressibility begin to occur are shown to be delayed by the thinner propeller.

On the right-hand side of the figure, test results are shown for another pair of propellers having identical characteristics but with thickness ratios of 5 and 6 percent, respectively, at the 0.7 blade-radius station. The variation in the thickness ratio

along the blade radius is shown. In the plot of maximum efficiency characteristics, the thinner blade is the more efficient which, at the highest tip Mach number presented, amounts to an improvement in efficiency of approximately 2 percent and, at the same time, indicates further delays in the compressibility effects. For example, up to tip Mach numbers of 0.97, the 5-percent-thick propeller shows no adverse effects of compressibility; whereas the 8-percent-thick propeller in the left-hand part has shown effects of compressibility at tip Mach numbers in the order of 0.94. Thus, reductions in propeller thickness ratio to as low as 5 percent are shown to offer improvements in propeller efficiency.

Recent high-speed research on propeller airfoils in the Langley 24-inch high-speed tunnel has included studies of the effect of camber as well as effects of thickness ratio (reference 22). The effects of camber at high speeds, as indicated from this airfoil data, is shown in figure 5 in which is plotted the section efficiency of two propeller airfoils having the thickness, differing only in design camber (NACA 16-506 and NACA 16-106). The section efficiency is calculated from the equation shown in the figure and is a function only of the L/D characteristics of the section. The values of L/D for the two airfoils were chosen at a lift coefficient of 0.5 which is the design operating condition for the higher cambered airfoil. The results have been plotted against section Mach number.

At low speeds, as would be expected, the higher cambered airfoil when operating at its design lift coefficient of 0.5 is approximately 2 percent more efficient than the lower cambered airfoil. However, at high speeds the comparison is reversed, the lower cambered airfoil being 2 percent more efficient than the higher cambered airfoil even though the lift coefficient is considerably in excess of the design value for the low cambered airfoil. Data for other thickness ratios and for other airfoils have also indicated the same trend, and the results indicate that at supercritical speeds the most efficient airfoil sections are those which have very small amounts of camber or no camber. Thus, improvements in propeller performance is indicated through the use of reduced camber, particularly in the tip section of propellers where the sections are often designed to operate at supercritical speed conditions.

High-speed propeller tests of propellers having variations in camber have substantiated this conclusion in general, and figure 6 shows the results of a series of tests on three propellers differing only in camber. The propeller-blade form is shown in the figure, and the variation in the design lift coefficient along the blade radius is also shown for the three propellers. The test results are

plotted in the form of maximum efficiency against tip Mach number. The highest values of efficiency at low Mach numbers are shown for the propeller having camber corresponding to design lift coefficient of 0.5. The propeller blade having a design lift coefficient of 0.3 is, at low tip speeds, only a few percent less efficient than the propeller blade having a design lift coefficient of 0.5. The propeller blade having a design lift coefficient of 1.0 shows the poorest efficiency throughout the range. At supercritical tip speeds, however, there is a tendency toward reversal of the comparison between the propellers having 0.5 and 0.3 design cambers, the lowest cambered blade having slightly the best efficiency. The effect is not as strong as was indicated by the study of propeller airfoils.

The results of the propeller airfoil study are somewhat masked by the fact that there exists a Mach number gradient all along the propeller-blade radius so that the effect of supercritical-speed operation is confined to the tip portions of the propeller, and thus the full effect of the improvement in efficiency through reduction in camber at supercritical section speeds is confined to a small portion of the propeller. At higher advance-diameter ratios where the Mach number gradient along the blade is more uniform, this effect would be expected to be larger.

High-speed propeller research has thus indicated that propellers having high levels of efficiency up to forward speeds in the order of 500 miles per hour are possible; that improvements in propeller efficiencies at speeds in excess of 500 miles per hour are indicated through the use of pitch distribution modifications and dual-rotation propellers; and that more extensive increases are possible through the use of sweepback and perhaps low aspect ratio in propeller blades. However, experimental studies to define the magnitude of these effects have not been made. The proper selection of camber, solidity, and propeller-section thickness ratio has also been shown to effect significant improvement in propeller performance.

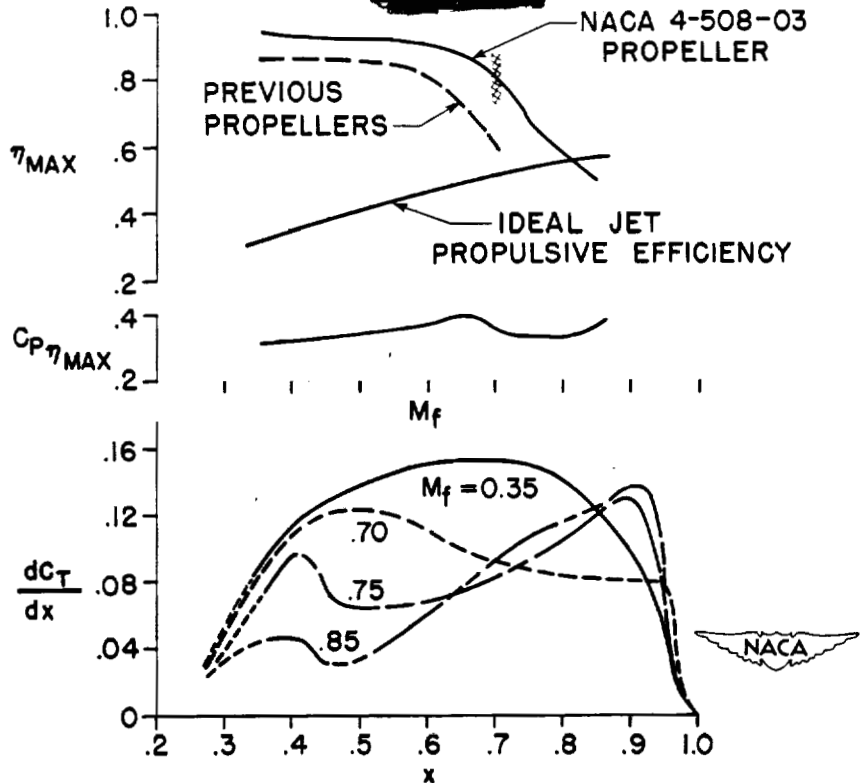


## REFERENCES

1. Gilman, Jean, Jr.: Wind-Tunnel Tests and Analysis of Three 10-Foot-Diameter Three-Blade Tractor Propellers Differing in Pitch Distribution. NACA ARR No. L6E22, 1946.
2. Crigler, John L., and Talkin, Herbert W.: Propeller Selection from Aerodynamic Considerations. NACA ACR, July 1942.
3. Crigler, John L., and Talkin, Herbert W.: Charts for Determining Propeller Efficiency. NACA ACR No. L4I29, 1944.
4. Crigler, John L.: Comparison of Calculated and Experimental Propeller Characteristics for Four-, Six-, and Eight-Blade Single-Rotating Propellers. NACA ACR No. 4B04, 1944.
5. Crigler, John L.: Application of Theodorsen's Theory to Propeller Design. (Prospective NACA paper)
6. Gilman, Jean, Jr.: Wind-Tunnel Tests and Analysis of Two 10-Foot-Diameter Six-Blade Dual-Rotating Tractor Propellers Differing in Pitch Distribution. (Prospective NACA paper)
7. Boswinkle, Robert W., Jr.: Air-Flow Surveys in the Vicinity of Representative NACA 1-Series Cowlings. (Prospective NACA paper)
8. Hartman, Edwin P., and Feldman, Lewis: Aerodynamic Problems in the Design of Efficient Propellers. NACA ACR, Aug. 1942.
9. Lock, C. N. H., and Yeatman, D.: Tables for Use in an Improved Method of Airscrew Strip Theory Calculation. R. & M. No. 1674, British A.R.C., 1935.
10. Carmel, Melvin M., and Robinson, Harold L.: Further Investigation of NACA 4-(5)(08)-03 Two-Blade Propeller at High Forward Speeds. NACA RM No. L7E12, 1947.
11. Delano, James B., and Carmel, Melvin M.: Effect of Shank Design on Propeller Performance at High Speeds. NACA ARR No. L6D23, 1946.
12. Vogeloy, A. W.: Climb and High-Speed Tests of a Curtiss No. 714-102-12 Four-Blade Propeller on the Republic P-47C Airplane. NACA ACR No. L4L07, 1944.

13. Gardner, J. J.: Effect of Blade Loading on the Climb and High-Speed Performance of a Three-Blade Hamilton Standard No. 6507A-2 Propeller on a Republic P-47D Airplane. NACA MR No. L5G09a, 1945.
14. Whitcomb, Richard T.: Investigation of the Characteristics of a High-Aspect-Ratio Wing in the Langley 8-Foot High-Speed Tunnel. NACA RM No. L6H28a, 1946.
15. Evans, Albert J., and Klunker, E. Bernard: Preliminary Investigation of Two Full-Scale Propellers to Determine the Effect of Swept-Back Blade Tips on Propeller Aerodynamic Characteristics. NACA RM No. L6J21, 1946.
16. Corson, Blake W., Jr., and Maynard, Julian D.: The NACA 2000-Horsepower Propeller Dynamometer and Tests at High Speed of an NACA 10-(3)(08)-03 Two-Blade Propeller. (Prospective NACA paper)
17. Maynard, Julian D., and Davidson, Robert E.: Aerodynamic Characteristics at High Speeds of Related Full-Scale Propellers having Different Solidities. (Prospective NACA paper)
18. Gray, W. H., and Solomon, William: Aerodynamic Characteristics at High Speeds of Related Full-Scale Propellers having Different Blade Section Thickness Ratios. (Prospective NACA paper)
19. Maynard, Julian D., and Salters, Leland B.: Aerodynamic Characteristics at High Speeds of Related Full-Scale Propellers Having Different Blade Section Cambers. (Prospective NACA paper)
20. Stack, John, and Lindsey, W. F.: Characteristics of Low-Aspect-Ratio Wings at Supercritical Mach Numbers. NACA ACR No. L5J16, 1945.
21. Delano, James B.: The Effect of High Solidity on Propeller Characteristics at High Forward Speeds from Wind-Tunnel Tests of the NACA 4-(3)(06.3)-06 and NACA 4-(3)(06.4)-09. NACA RM No. L6L19, 1946.
22. Lindsey, W. F., Daley, Bernard N., and Stevenson, D. B.: The Aerodynamic Characteristics of 24 NACA 16-Series Airfoils at Mach Numbers between 0.3 and 0.8. (Prospective NACA paper)

Drakeley



COMPRESSIBILITY EFFECTS ON PROPELLER CHARACTERISTICS OF NACA 4-508-03 PROPELLER  $\beta = 60^\circ$

Figure 1.

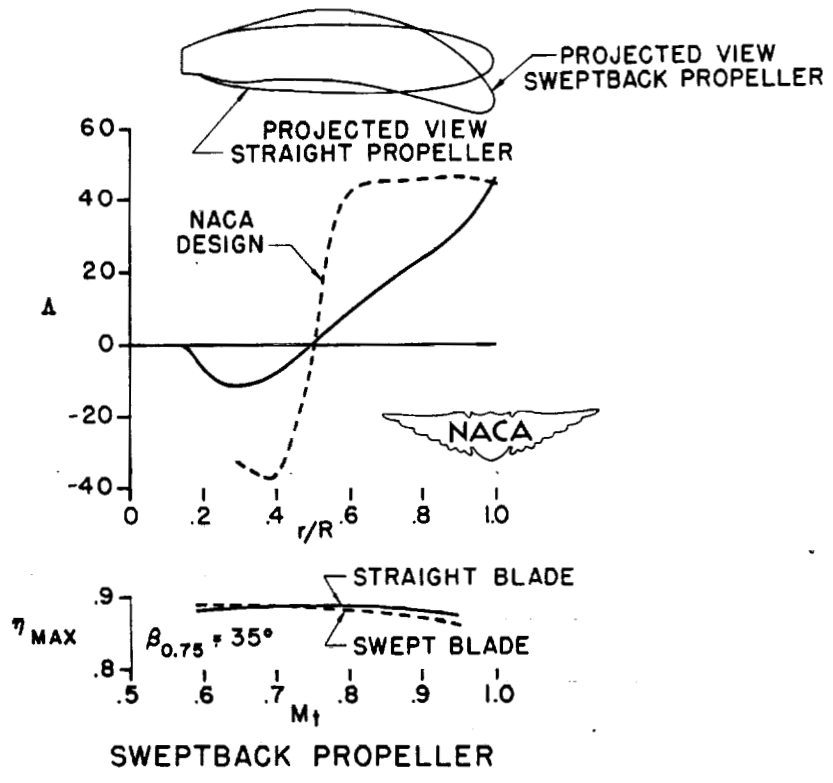
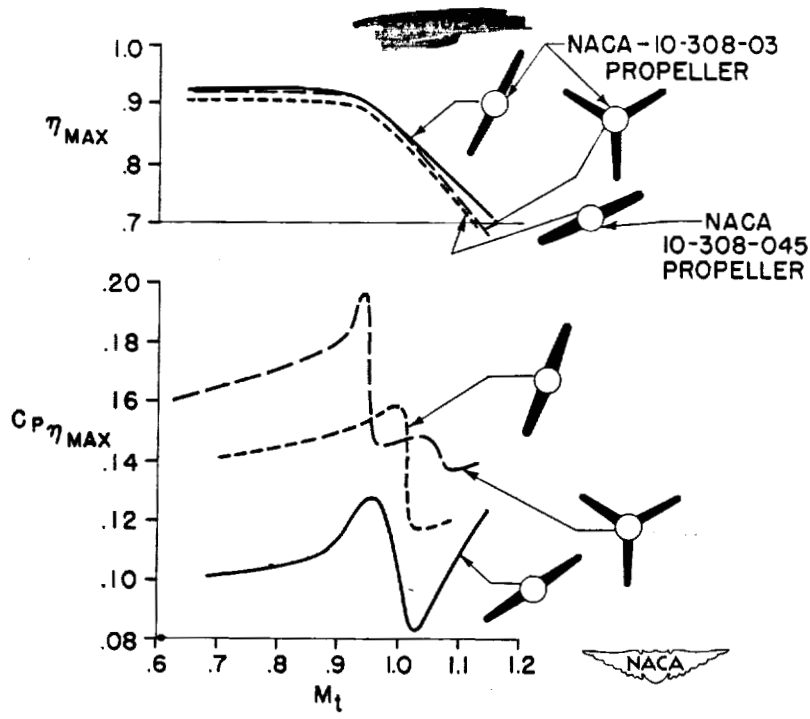
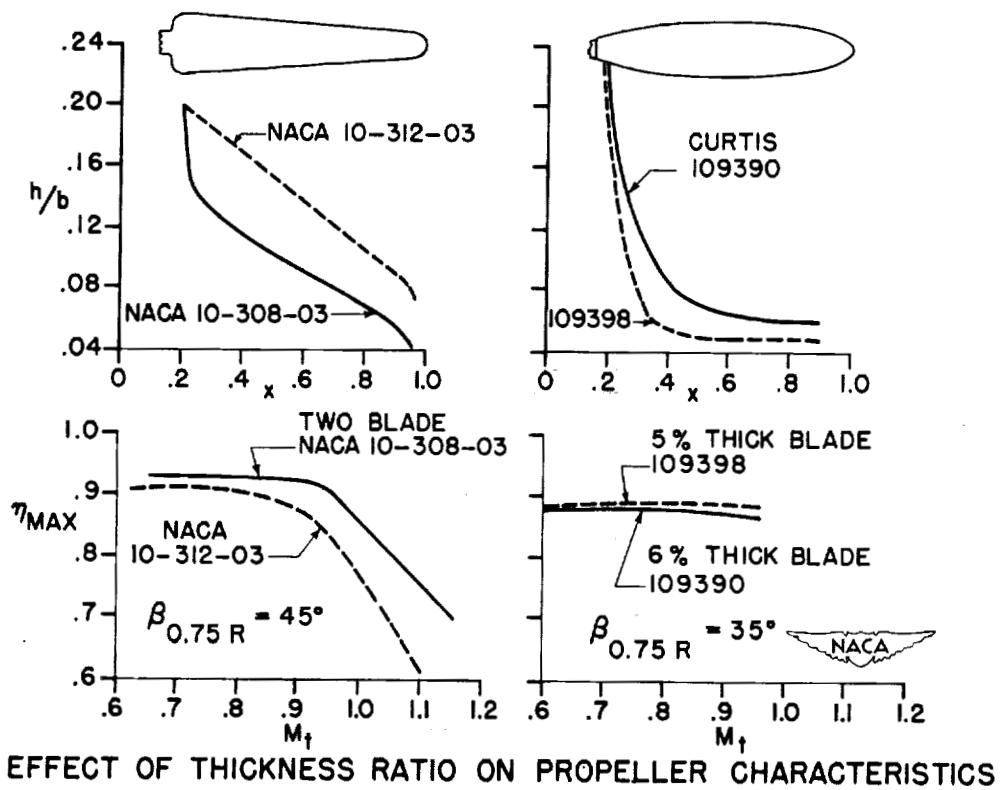


Figure 2.



EFFECT OF SOLIDITY ON PROPELLER CHARACTERISTICS  
 $\beta_{0.75R} = 45^\circ$

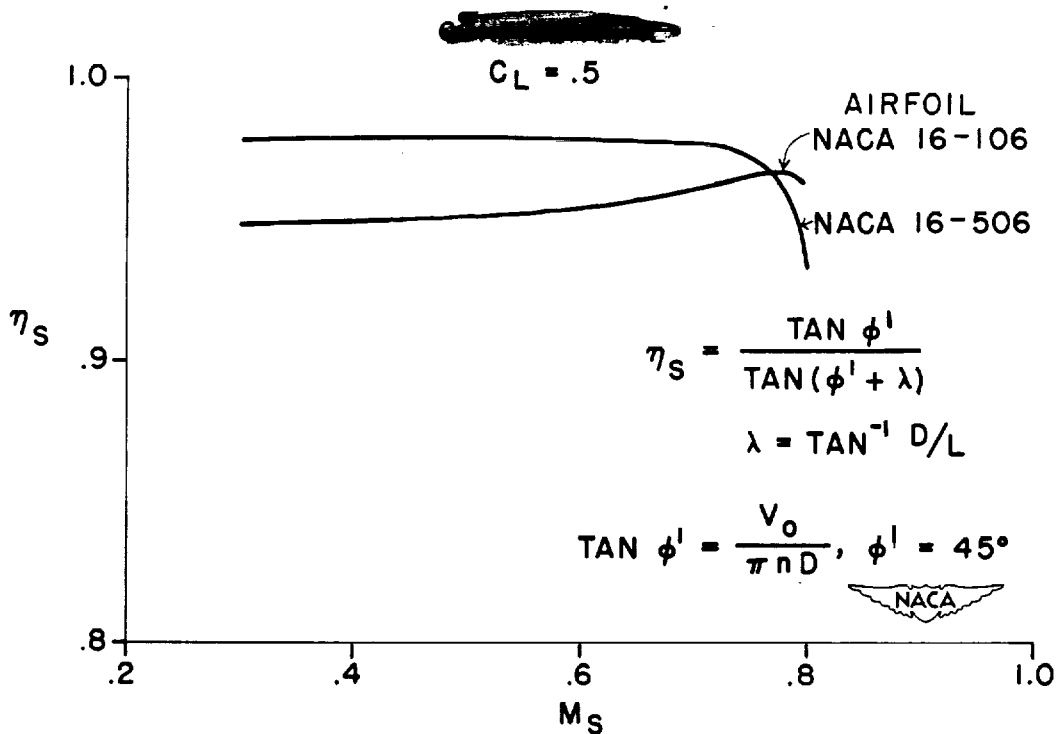
Figure 3.



EFFECT OF THICKNESS RATIO ON PROPELLER CHARACTERISTICS

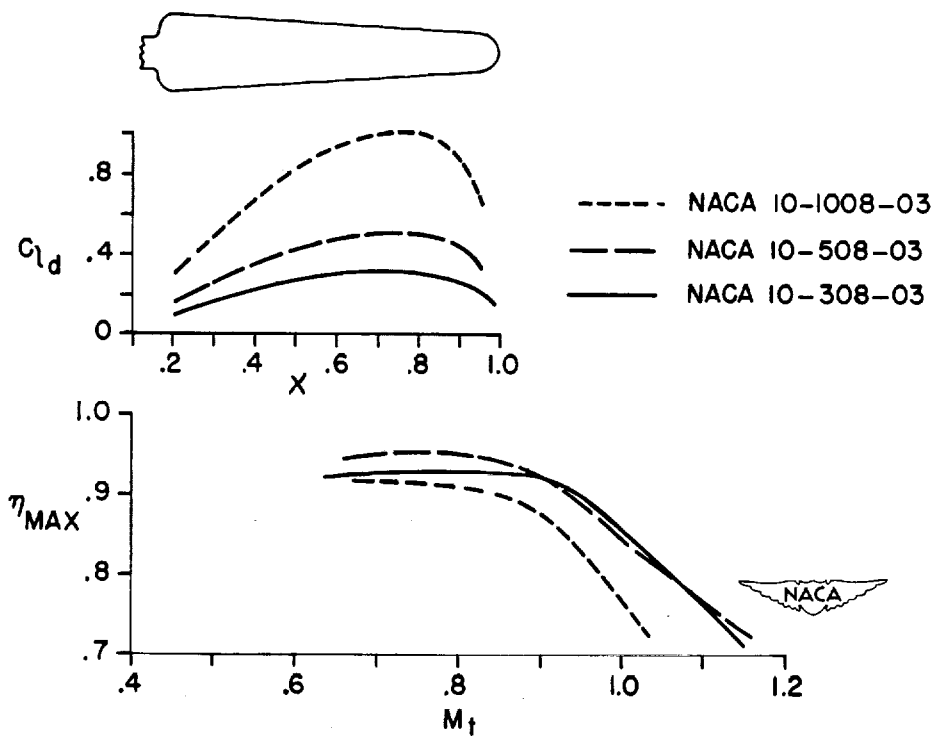
Figure 4.

Draley



SECTION EFFICIENCY OF TWO PROPELLER AIRFOILS

Figure 5.



EFFECT OF CAMBER ON PROPELLER CHARACTERISTICS

Figure 6.

FLUTTER



SOME HIGH-SPEED FLUTTER STUDIES

By I. E. Garrick

Langley Memorial Aeronautical Laboratory

It is intended to present a brief review and progress report of some of our recent studies on flutter at high speeds. In order to present this work with a degree of continuity, it is perhaps desirable to make a few observations of general interest on the past stream of flutter work.

The field of flutter is concerned essentially with a study of the circumstances whereby a complicated elastic structure such as an aircraft or aircraft component can spontaneously become a "flutter" machine and absorb energy from the airstream to the extent of damaging or destroying itself. Hence it would appear that knowledge of nonstationary aerodynamic phenomena is a basic requirement to our understanding of flutter. Yet in the old days (some twenty years ago) flutter was discussed without this knowledge of even the low-speed air forces, and analysis employed either statically determined aerodynamic coefficients or, as continues even to the present day, a set or matrix of numbers arrived at by some combination of reason, guess, and hope.

Although these older investigations sometimes led to some misleading specific rules, nevertheless they also led to certain basic principles for flutter prevention. Thus, the basic safeguards of (a) increased stiffness, (b) avoidance of coupling (implying, for example) proper mass balance, and (c) sufficient damping - followed without specific knowledge of the air forces.

The detailed questions of what kind of stiffness, how much stiffness, how to attain it; how much mass balance, where to put it, what modes to balance against; how much damping is needed, how reliable is the damping available, how "irreversible" is irreversible when applied to control surfaces such as tabs. These and similar questions are not yet answered in general but only in special circumstances, for these questions are tied up with elastic problems which are too complex to be anything but approximately handled, even without consideration of air forces, and with aerodynamic problems which are complicated enough even in the steady case and for rigid structures.

Yet the accumulated experience in flutter is of formidable quantity (as anyone who has struggled with the flutter field can attest) and represents information obtained by combinations of statistical studies, analysis, theory, and testing.



An example of a distillate of this experience in the form of recommended procedures in design is the Army, Navy, Commerce bulletin, soon to be made available: ANC-12 (1) "Procedure for Aircraft Structural Vibration Survey" and ANC-12 (2) "Methods of Flutter Prevention" Another example is the torsional stiffness criterion of reference 1.

Although stiffness criteria and similar procedural rules of thumb can be of great practical help they should not serve as a substitute for thought or camouflage the need for understanding.

Before discussing the experimental studies I would like to give a thumb-nail sketch of the theoretical basis for study of the aerodynamic forces and some of the implications. I intend to present only the governing field equations and their significance without going into any mathematical details.

The general nonstationary flow equations for irrotational potential flow of a compressible fluid can be expressed in an invariant form:

$$\frac{1}{c^2} \left( \frac{\partial}{\partial t} + \bar{v} \cdot \nabla \right)^2 \phi = \nabla^2 \phi \quad (1)$$

where the differential symbols  $\frac{\partial}{\partial t}$  and  $\bar{v} \cdot \nabla \left( = v_x \frac{\partial}{\partial x} + v_y \frac{\partial}{\partial y} + v_z \frac{\partial}{\partial z} \right)$  operate only on the velocity potential  $\phi$  (not on  $v$ ) and where, for the adiabatic pressure-density relation, the local (variable) speed of sound is

$$c^2 = c_0^2 - \frac{\gamma - 1}{2} v^2$$

The compressible-flow equations have not, so far as I am aware, been given this wave-equation form before and perhaps that is a valid reason for showing it here. The potential is propagated in the manner of a wave disturbance of finite amplitude throughout a medium in which the velocity of sound is variable.

The invariant form serves to unify the general compressible potential-flow picture, at least for purposes of discussion. For example when  $\frac{\partial}{\partial t}$  is absent and the disturbance not necessarily small the equation becomes the one treated by Raleigh, Janzen, and



Poggi. In a space of one dimension, for example, it reduces to the equation of Riemann for aerial plane waves of finite amplitudes. (For  $c = \infty$ , it reduces to the incompressible case.)

For small disturbances from a main stream  $V$  in the  $x$ -direction the original nonlinear equation becomes a linear one and  $c$  is now treated as a constant

$$\frac{1}{c^2} \left( \frac{\partial}{\partial t} + V \frac{\partial}{\partial x} \right)^2 \phi = \nabla^2 \phi \quad (2)$$

This equation contains the equation for the propagation of sound ( $V = 0$ ), the equation leading to thin-airfoil theory and the Prandtl-Glauert and Ackeret rules in steady flow, and the equation treated by Possio and others for subsonic and supersonic non-stationary flow. The treatment of flow in a plane on the basis of this equation is in pretty fair shape and a number of theoretical papers and applications exist but much remains to be done on the handling of finite-span problems. (See references 2 and 3.)

In the near sonic region the linearized theoretical basis clearly requires modification as indicated by the Prandtl-Glauert and Ackeret rules leading to infinite slopes of the lift curve at  $M = 1$ . It is likely that in this region it is necessary to employ iterative methods and to take into account second-order and other effects (including viscosity and shape factors) but even the small-disturbance equation appears differently. Thus, if all velocities are only slightly different from the velocity of sound  $c^*$ , and the main stream is in the  $x$ -direction, there is obtained for the equation satisfied by the velocity potential

$$\frac{1}{c^{*2}} \left( \frac{\partial}{\partial t} + c^* \frac{\partial}{\partial x} \right)^2 \phi = \nabla^2 \phi + (\gamma + 1) \phi_{xx} \left( 1 - \frac{\phi_x}{c^*} \right) \quad (3)$$

or

$$(\gamma + 1) \phi_{xx} \left( 1 - \frac{\phi_x}{c^*} \right) + \phi_{yy} + \phi_{zz} - \frac{1}{c^{*2}} \left( \phi_{tt} + 2c^* \phi_{xt} \right) = 0$$

This equation reduces in the steady case to a nonlinear equation leading to the transonic similarity rules discussed by von Karman in his Wright lecture. With this small background of theoretical considerations it is apparent that the detailed flow

picture in the nonstationary case, particularly at near sonic speeds, can become very complicated. But in this subject we often have to postpone our understanding of details in order to obtain knowledge, in reasonable time, of integrated effects. Information on some of these integrated effects was the objective of the first phase of our experimental work.

Study of torsion-bending wing flutter at high speeds has been made by means of wind-tunnel testing and also with the aid of recently pioneered techniques employing bomb drops and rockets.

The scope of the wind-tunnel investigation which was made in the Langley 4.5-foot flutter-research tunnel, is indicated in figure 1. The models were cantilever wings which were simply built since flutter fatalities were many. They were mainly of wood construction, many with suitable metal inserts, a few had ribs and spars covered with fabric. A range of semispan-chord ratios is covered, a range of sweep including some types of built-in sweep and rotated models and some tapered wings.

Figure 2 shows a particular swept wing mounted as a cantilever in the Langley 4.5-foot flutter-research tunnel. Two noteworthy features of this wind tunnel are the 30 to 1 possible density change in the medium and the relatively high Mach numbers attained at different density conditions with low power by the use of mixtures of air and Freon-12. Some erratic results have been obtained near top tunnel speeds corresponding to choking conditions but in general the tunnel data taken at Mach numbers below 0.8 are considered reliable.

Figure 3 shows a high-speed-rocket flutter vehicle. It has a top speed corresponding to about  $M = 1.5$ , an acceleration of about 50 g. Its weight is about 100 pounds. It is the high acceleration type of rocket which experienced a large number of failures when originally used for aerodynamic tests and which led to the empirical torsional-stiffness criterion given in reference 1.

This test vehicle is at present used for exploratory flutter testing and employs a break-wire to determine time of wing failure (reference 4). Telemeter equipment for it is also being planned. Because of its high acceleration, when wing failure occurs, it takes place within about a second from the time of launching. The few cases tested to date have shown fairly consistent results with duplicate firings and also in comparison with the low-acceleration bomb drop tests; however it is planned to test further for effects of acceleration.

Figure 4 is a photograph of the larger low-acceleration rocket (designated FR-1) shown with  $45^\circ$  sweptback test wings. Its weight is about 250 pounds, its acceleration from 2 to 4g and its top speed corresponds to a Mach number about 1.2. This rocket is equipped with a telemeter to transmit strain gage, breakwire, and acceleration records of the wings. A sample record (reference 5) will be shown subsequently.

Figure 5 shows a free-fall-bomb flutter vehicle. First successful telemetered flutter records were obtained with this type of vehicle. The bombs have been released at various altitudes up to 35,000 feet, and are accelerated by gravity to attain a Mach number from about 1.0 to 1.3. A sample record is given in another figure.

Figure 6 shows the first telemetered record obtained from a low-acceleration rocket test. This particular rocket carried two  $45^\circ$  sweptback wings as shown in figure 4. Flutter occurred at a Mach number of 0.67 in a symmetrical mode. In spite of large flutter amplitudes, however, one wing apparently did not break off. It may be of interest to mention that the ratio of flutter frequency to the wing torsional frequency was 0.55.

Figure 7 shows a telemetered record from a free-fall bomb vehicle carrying two  $45^\circ$  sweptback wings. (See reference 6.) Bending and torsion strain on one wing and torsion on the other are recorded. (Four channels were used in this case; it is expected to employ additional channels in some later tests.) This flutter occurred at  $M = 0.92$ , one wing failed at once, the other fluttered for another second or so subsequent to the first wing failure before it too failed. The flutter frequency was 0.38 that of wing torsion.

A composite plot is shown in figure 8 of some of the wind-tunnel, bomb, and rocket data for unswept uniform rectangular wings of various aspect ratios or rather semispan-chord ratios  $l/c$ . The abscissa is the Mach number and the ordinate is the ratio of flutter speed measured to flutter speed calculated on the basis of two-dimensional incompressible-flow considerations. The data shown are for wings of several different mass ratios, elastic axes, and center-of-gravity locations. The full curve represents theoretical (two-dimensional) calculations for mass ratio  $\frac{I}{K} = 50$  and center of gravity and elastic axes at 45 percent chord. The effect of Mach number and of variation of the semispan-chord ratio  $l/c$  is indicated by the data. For  $l/c$  from 3 to 6 there is only a small effect, while for  $\frac{l}{c} = 1$  there is a fairly significant rise.

It will be recalled that extrapolations from theoretical considerations based on subsonic and supersonic linearized theory indicated that, for center-of-gravity locations forward of the midchord, the design critical range is the near sonic speed range. (It was also shown that the particular quantity  $\frac{bc_0}{c}$  (half chord times torsional frequency divided by sound speed) plays an interesting role as a basic nondimensional parameter, around which it appears that convenient empirical rules can be developed.)

In general the data of figure 8 indicate that the transonic range may be the determining factor in deciding the stiffness as far as wing flutter is concerned. Other data will be published in various NACA papers.

Figure 9 is a plot against Mach number of the effect on the flutter speed of rotating a uniform (4 inch x 4 inch) cantilever wing in the wind tunnel, the sweepback being changed by rotating the model mount. The problem of sweep brings into the flutter analysis several new problems which have thus far been only lightly touched upon by several workers. Thus, there is the problem of the modes of vibration, in particular for a curved or bent back elastic axis, involving a greater degree of coupling between bending and torsion, and there is the aerodynamic coupling in the finite-span problem.

It perhaps should be mentioned that for an infinite uniform yawed wing (yawed at an angle not near 90°) two-dimensional low-speed considerations indicate that the flutter speed increases as one over the cosine of the angle of sweep. However, the combined effects of the elastic and aerodynamic coupling, together with the finite-span problem, apparently result in no such favorable increase. In general it appears that up to 30° sweep there is only a very small increase in the flutter speed.

The rocket-data points (fig. 9) are for built-in 45° swept wings (of length 27 inches along the leading edge and chord 12 inches normal to the leading edge). The free-fall-bomb-data points are for a wing of dimensions 28 inches along the leading edge and 8 inches normal to leading edge. It may be seen that for 45° angle of sweep the wind-tunnel, rocket, and bomb data are in fair agreement.

Some effects have been found to be due to the manner in which the root was built in or the tip cut off; also models with large length to chord ratio tend to introduce higher mode effects leading to erratic sweep effects for low angles of sweep as in this figure.

Figure 10 shows some effects of sweep for models which had the same section parallel to the airstream (sheared back) and the same span normal to the airstream; that is the aspect ratio was kept constant. The lower curve gives the measured torsional frequency as a function of the sweep angle. Dimensional considerations indicate that this frequency should be constant (except for tip and root effects) for the sheared-back uniform wing and the data bear this out.

The flutter speed also appears to be relatively constant, though there is appreciable scatter. The data thus indicate that the flutter speed of a sweptback homogeneous wing (sheared back in the manner described) is about the same as the wing without sweep. The Mach number at flutter and the flutter frequency for the test points are also shown in the figure.

Figure 11 gives some results of an investigation on the effect of concentrated weights on the flutter of a cantilever wing. The investigation includes single and multiple weights, and the mass and its moments of inertia are varied, as well as the spanwise and chordwise positions in conjunction with uniform, tapered and swept-back wings. The figure is, however, for a uniform unswept cantilever ( $\frac{l}{c} = 6$ ) and for a single weight 93 percent of wing weight (reference 7). (The mass of the weight was constant for these tests but the polar moment of inertia about the elastic axis of the wing varied with the chordwise location.) The abscissa of the chart is the location of the weight along the span. The ordinate is the flutter speed measured with the weight on divided by the flutter speed without the weight (wing alone). Each curve is drawn for a single chordwise location of the weight; the center of gravity location of the weight is sketched in the figure.

It is noted that the rearward location of the weight lowered the flutter speed while the forward location raised the flutter speed. (There is a small decrease for the near inboard positions in all cases.) For the most forward chordwise location there was a range of span positions at which no flutter occurred below the divergence speed of the wing. However, with the weight at a tip location in this case a higher-frequency type flutter did occur. This effect probably depends on the zero airspeed frequency spectrum and hence is probably different as the aspect ratio of a given wing is changed.

The test data in this single chart corresponds to well over 100 flutter tests taken at Mach numbers around 0.3 to 0.4. A similar series of tests for the weight location near the wing

center of gravity has been run for Mach numbers up to 0.7 and showed the same trends as indicated in the figure.

Theoretical calculations for the flutter speed have been made for the case in which the chordwise location of the weight is near the elastic axis. The uncoupled modes were used in these calculations, and theory compared well with the experimental results. For weight locations far from the elastic axis, however, higher modes or coupled modes are probably required. An extension of the treatment of Goland and Luke (reference 8) for the work is being examined. Results of these calculations are not yet available.

The quantitative correlation of theory and experiment is the goal of this study. These data provide an opportunity for such a quantitative check and should prove useful in evaluating the degree of refinements necessary in both the elastic and aerodynamic parts of the theory in order to keep each in step with the other.

A selection of results obtained at the Langley Laboratory are presented here. Many things have been left unsaid and many more things have been left undone. Various recent aircraft company reports on aeroelastic problems exist to which specific reference here is not feasible. It is hoped that information may be obtained at high-speed conditions for the mixed subsonic-supersonic types of flow (for instance, on the effects of thick and thin sections, of rounded and sharp leading edges) to examine possible nonstationary effects of detached and attached strong shocks. Also measurements of aerodynamic derivatives in the near sonic and supersonic speed ranges require exacting experimental techniques and critical tests.

This talk has been only of potential flow or classical flutter. It is also desirable to examine the separated flow types of instability which particularly at high speeds may be due to a variety of causes. These instabilities may be associated with wide movements of the center of pressure and with regular breakaway and reattachment of the flow. In addition there is the interaction of the aerodynamic and elastic forces in the class of stability problems involving control effectiveness and control reversal. The whole field of aeroelasticity is pretty wide open and remains a challenging field of inquiry.

## REFERENCES

1. Budiansky, Bernard, Kotanchik, Joseph N., and Chiarito, Patrick T.: A Torsional Stiffness Criterion for Preventing Flutter of Wings of Supersonic Missiles. NACA RM No. L7G02, 1947.
2. Garrick, I. E., and Rubinow, S. I.: Flutter and Oscillating Air-Force Calculations for an Airfoil in a Two-Dimensional Supersonic Flow. NACA TN No. 1158, 1946.
3. Garrick, I. E., and Rubinow, S. I.: Theoretical Study of Air Forces on an Oscillating or Steady Thin Wing in a Supersonic Main Stream. NACA TN No. 1383, 1947.
4. Barmby, J. G., and Teitelbaum, J. M.: Initial Flight Tests of the NACA FR-2, a High-Velocity Rocket-Propelled Vehicle for Transonic Flutter Research. NACA RM No. L7J20, 1947.
5. Angle, E. E.: Initial Flight Test of the NACA FR-1-A, a Low Acceleration Rocket-Propelled Vehicle for Transonic Flutter Research. NACA RM No. L7J08, 1947.
6. Clevenson, S. A., and Lauten, William T., Jr.: Flutter Investigation in the Transonic Range of Six Airfoils Attached to Three Freely Falling Bodies. NACA RM No. L7K17, 1947.
7. Runyan, Harry L., and Sewall, John L.: Experimental Investigation of the Effects of Concentrated Weights on Flutter Characteristics of a Straight Cantilever Wing. (Prospective NACA paper)
8. Goland, M., and Luke, Y. L.: The Flutter of a Uniform Wing with Tip Weights. Rep. No. 1-536-E-4, Midwest Res. Inst., Kansas City, Mo., Jan. 2, 1947.

Garrick

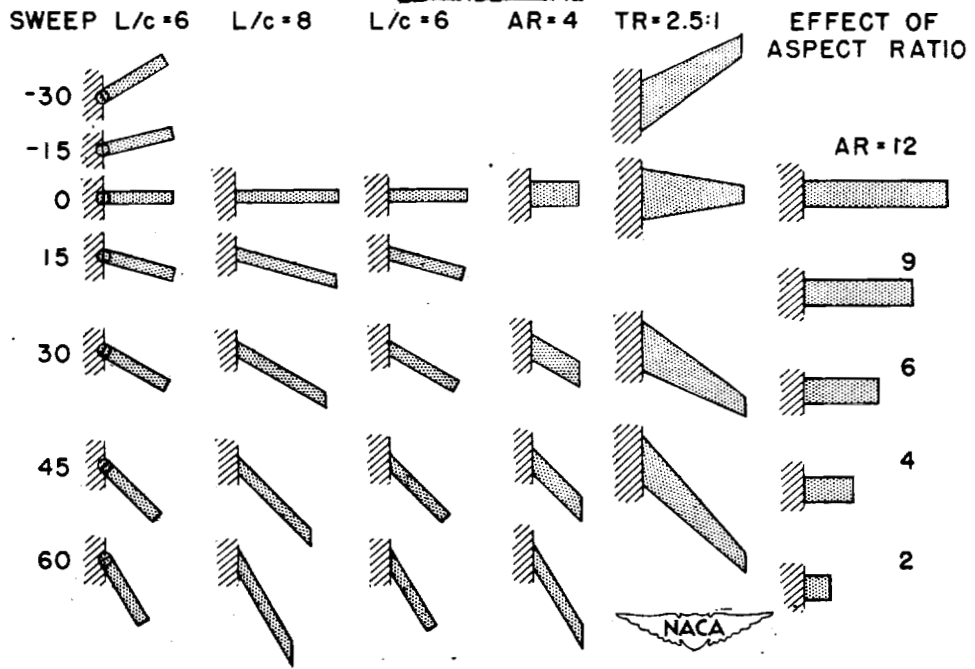


Figure 1.- Flutter-tunnel models.



Figure 2.- Swept wing mounted as cantilever in flutter tunnel.



Garrick

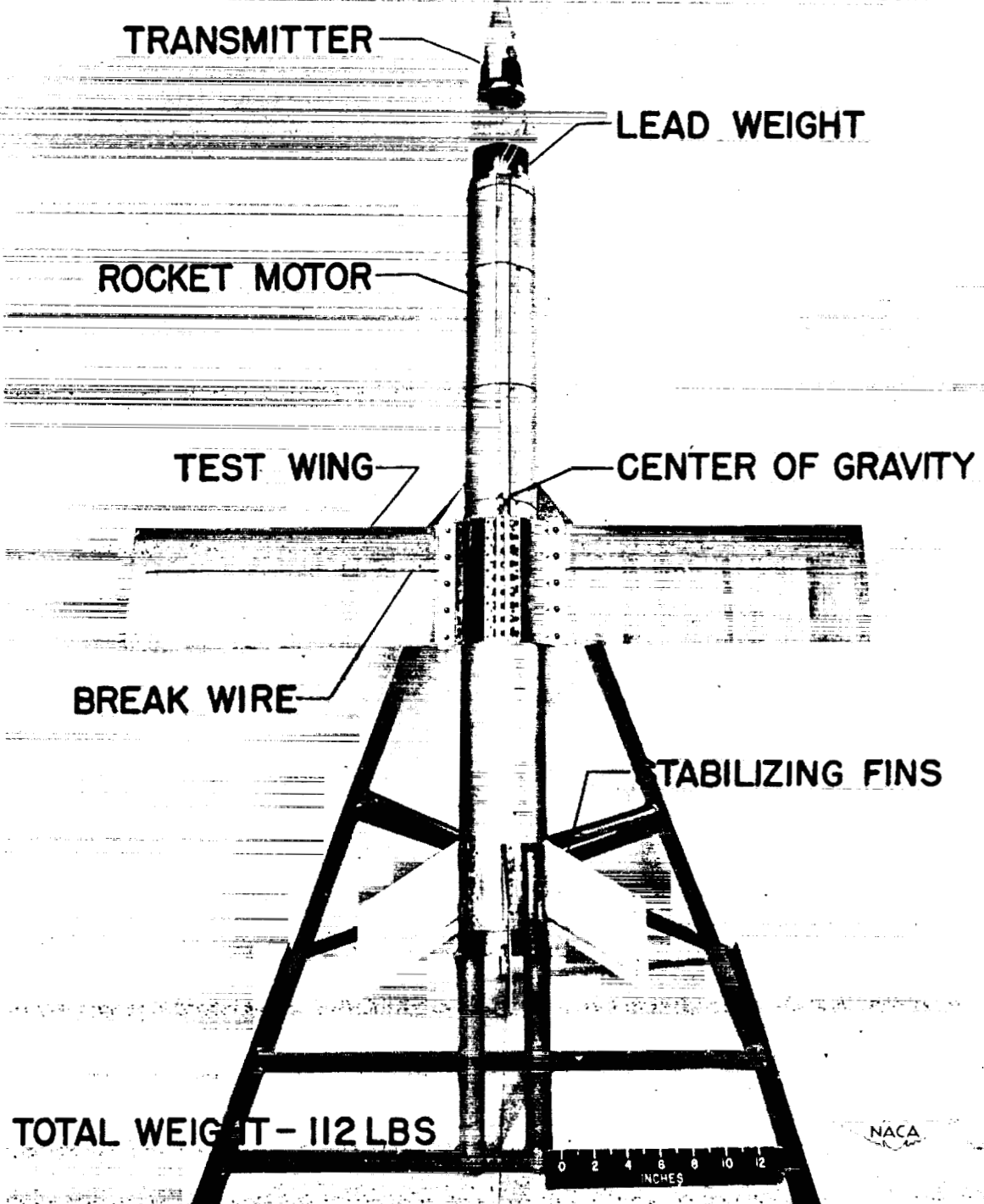


Figure 3.- High-speed-rocket flutter vehicle.

35(a)

Garrick

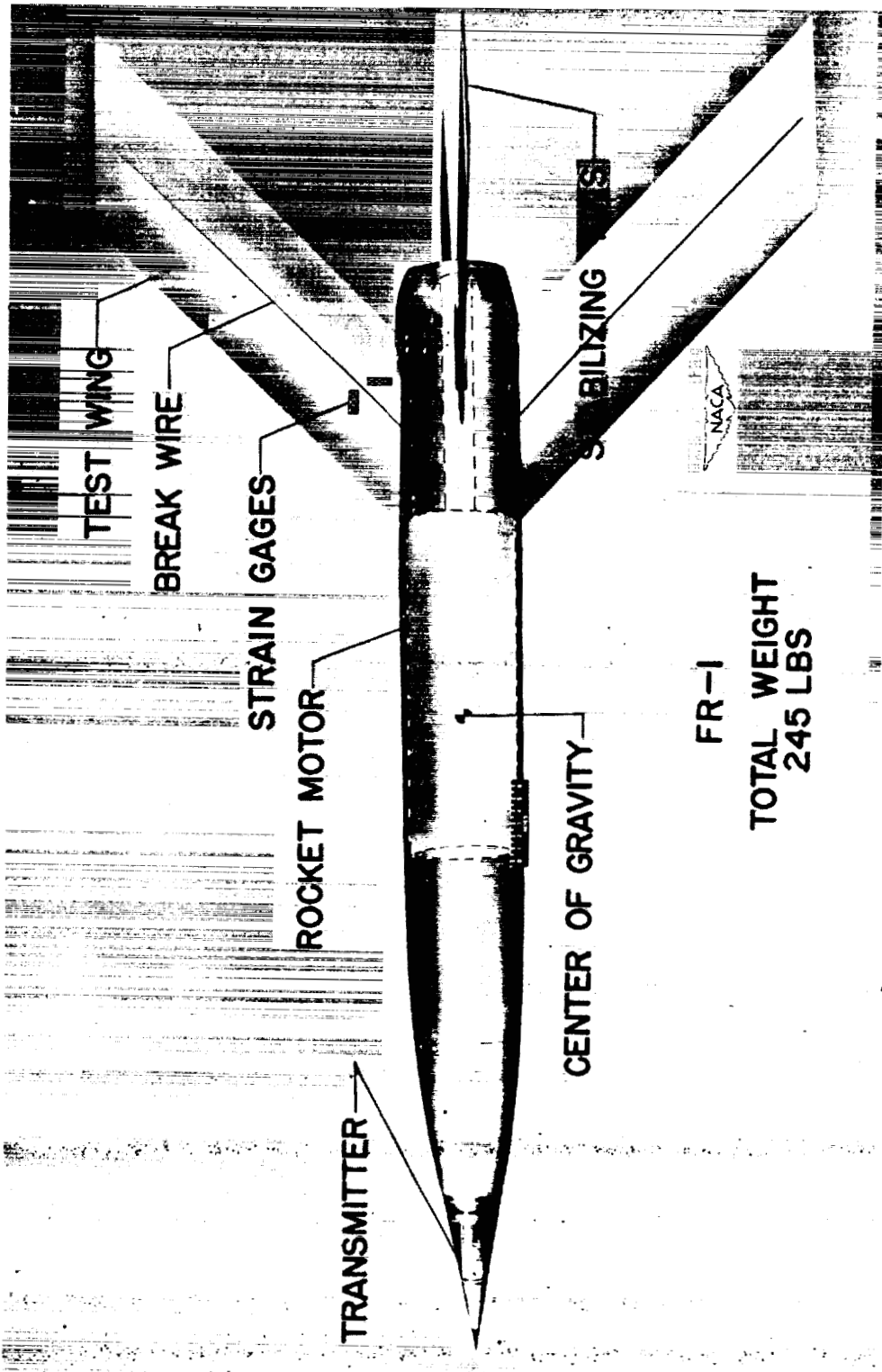


Figure 4.- Low-acceleration rocket (FR-1).

Garrick

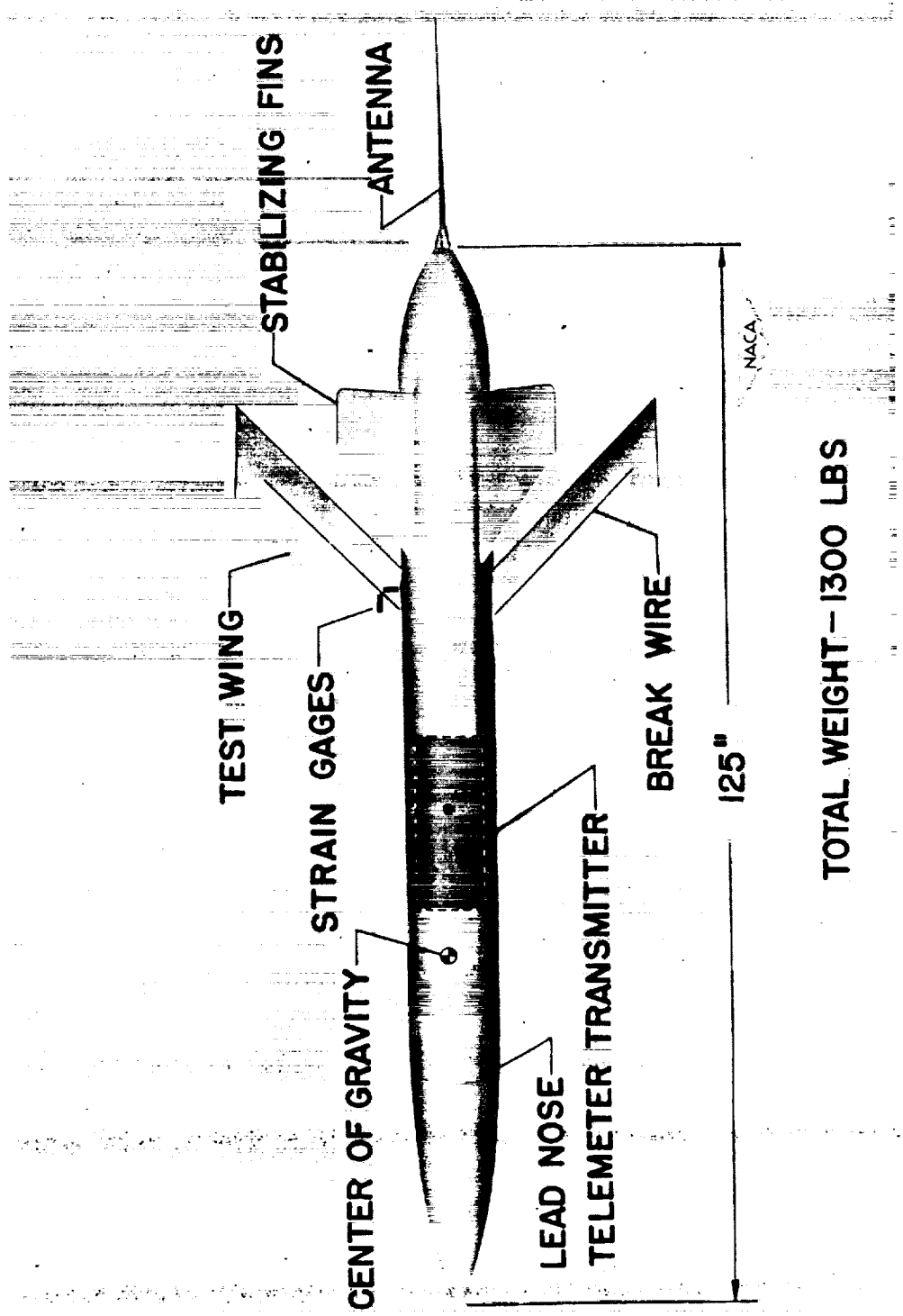


Figure 5.- Free-fall-bomb flutter vehicle.

Garrick

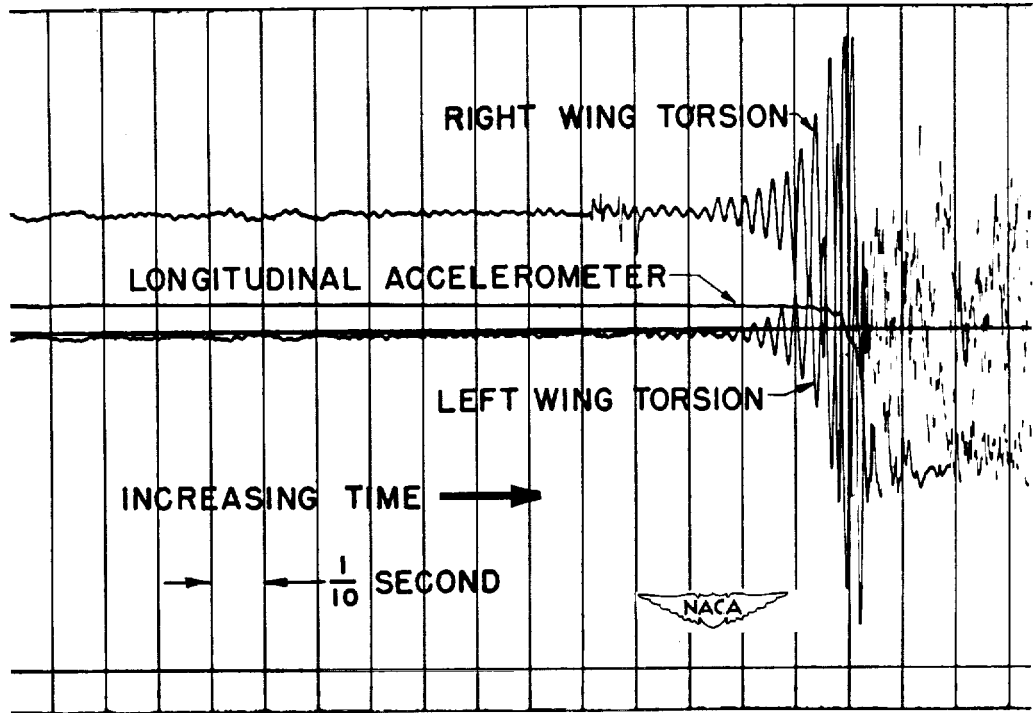


Figure 6.- Rocket telemeter record.

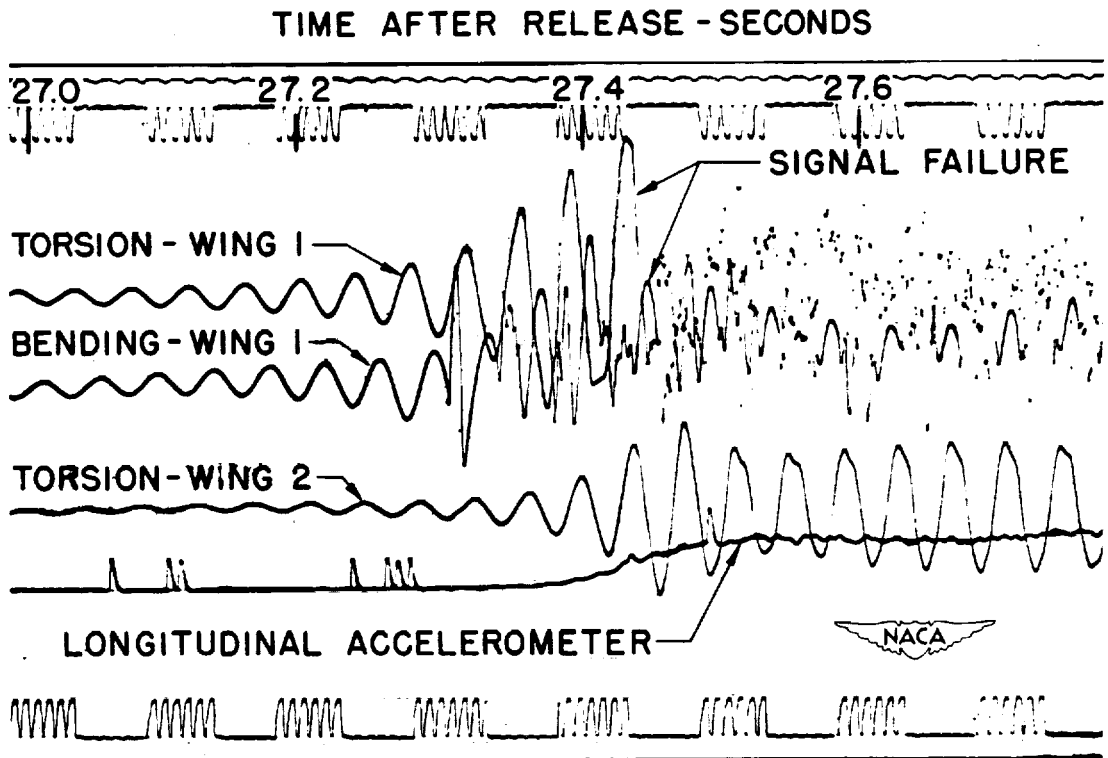


Figure 7.- Bomb telemeter record.

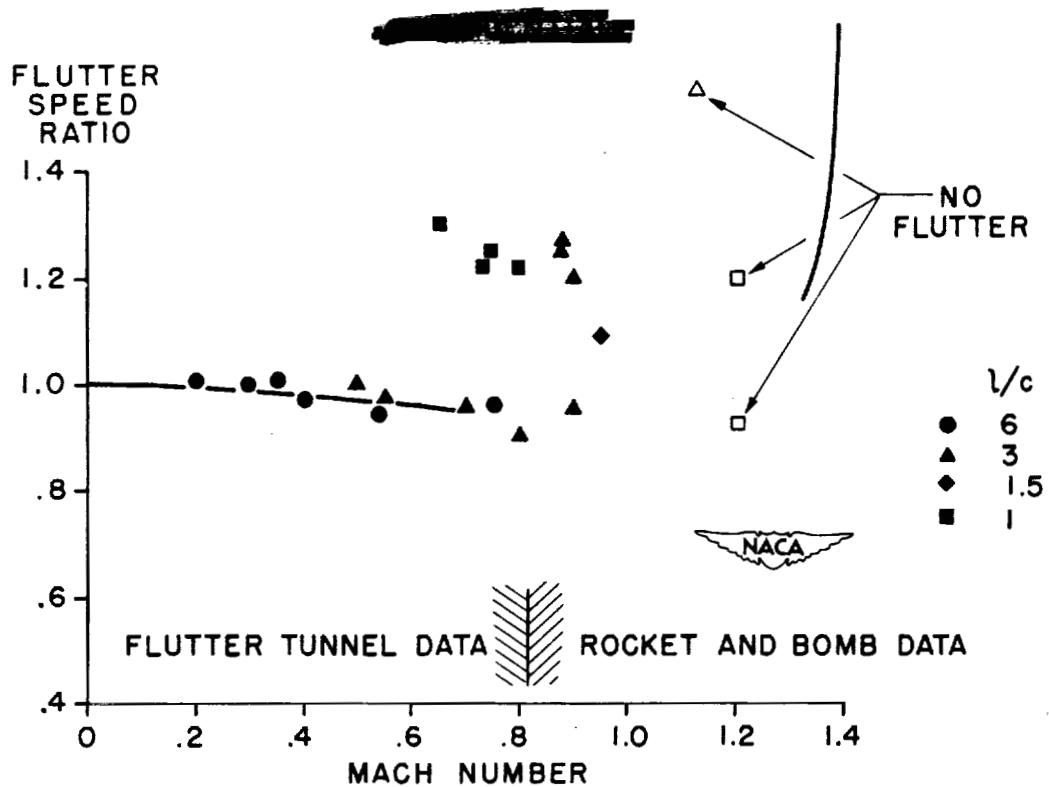


Figure 8.- Wing bending-torsion flutter.

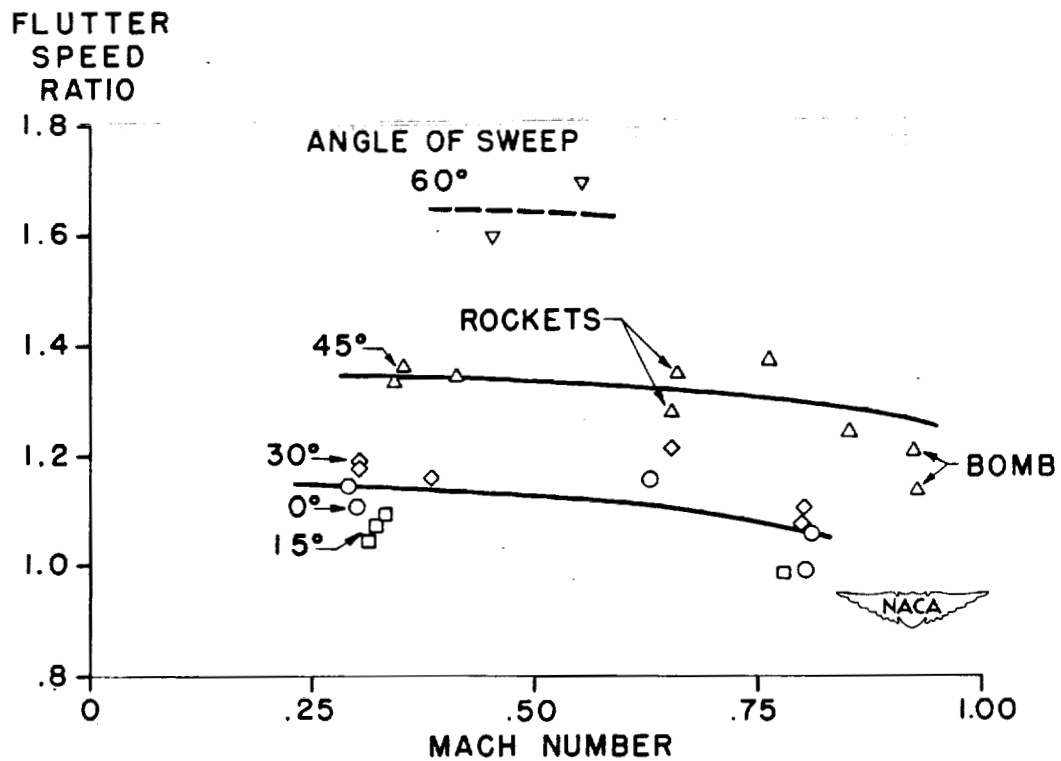


Figure 9.- Effect of sweep for rotated cantilever wing.

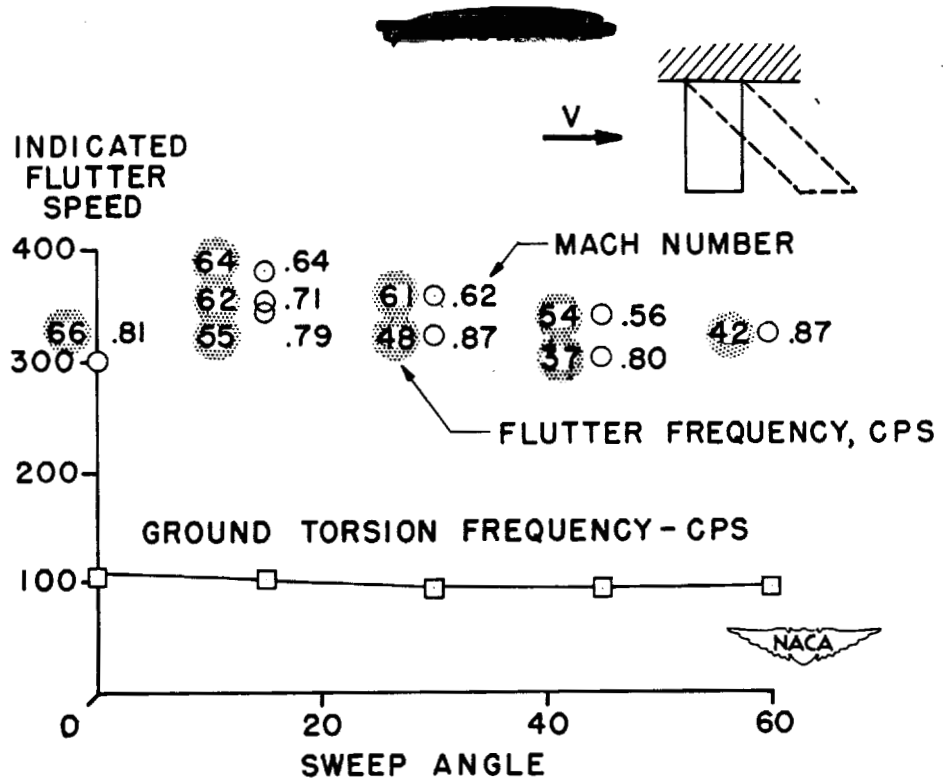


Figure 10.- Effect of sweep for sheared-back models.

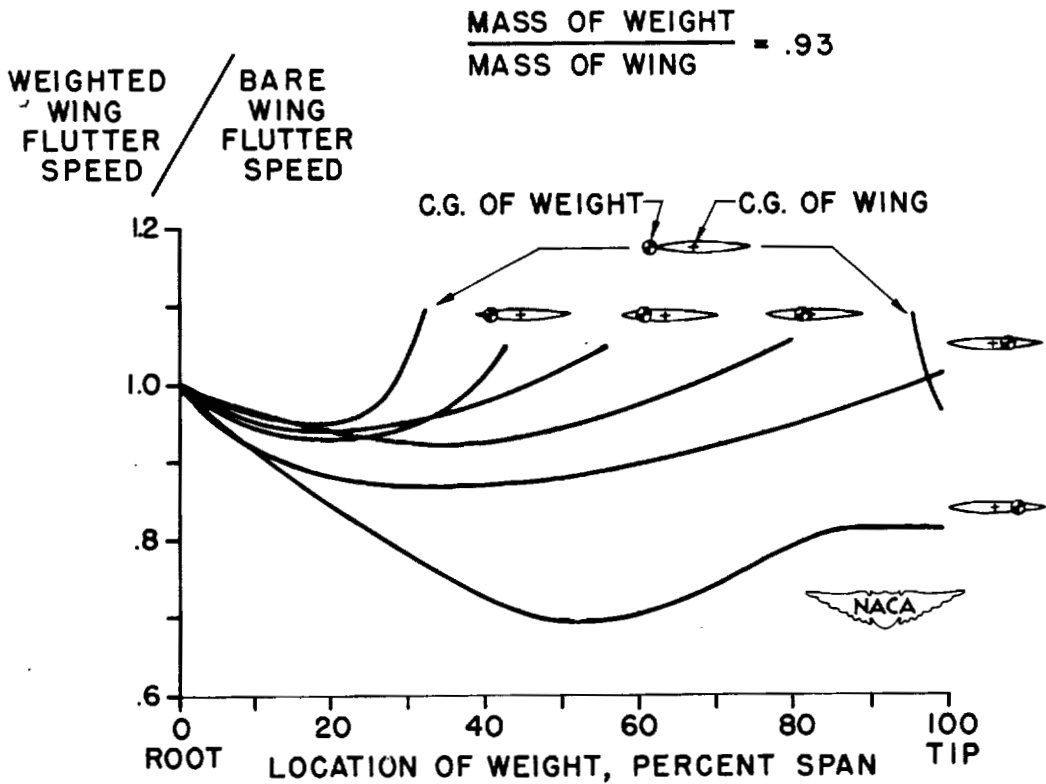


Figure 11.- Concentrated weights.

## TRANSONIC FLUTTER OF CONTROL SURFACES

By Albert L. Erickson

Ames Aeronautical Laboratory

The one-degree-of-freedom type of transonic flutter is a new flutter problem encountered in the transonic range in addition to the classical or two-or-more-degrees-of-freedom problem. It is intended in this paper to discuss only the one-degree-of-freedom case. This type of flutter results from some form of time delay. This time delay has been explained as being caused by separation resulting from the shock front across the wing. In the case of separation, flutter can be explained as being due to the periodic breakaway and reattachment of the flow about the airfoil, an effect similar to that which can be obtained at low speed on stalled airfoils due to high angle of attack or excessive thickness. It has also been considered, however, that due to the high velocities over the airfoil, changes in the hinge moment could be retarded during flutter so that an unstable condition might exist even without separated flow. Of course, in the actual case separation generally does occur; and it has been found that as separation becomes more severe the flutter becomes less violent in that the amplitude decreases. It should be noted that the one-degree-of-freedom type of flutter cannot be prevented by any of the standard flutter prevention methods which involve the uncoupling of mechanical movements. If the flutter is due to a time delay which does not necessarily involve separations, elimination of the aerodynamic force does not appear to be very feasible. Therefore, the solution of first importance involves the determining of the flutter frequency to be expected with any given system.

By use of the available experimental data, an empirical solution has been developed which appears to have sufficient merit to be of practical use. The problem involved has been set up in its simplest form and is shown in these first equations (fig. 1). The first equation is the simple one-degree-of-freedom equation with all the mechanical forces on the left side and the aerodynamic force shown as a single resultant on the right side. The solution of the equation used makes it necessary to determine the flutter frequency, a phase angle, and the magnitude of the hinge moment. With this equation the conditions for instability can be easily shown. In order to determine the flutter frequency some measure of the time lag is necessary. The basic parameter selected for indicating the time lag has been called the aerodynamic frequency and is based on the distance from the wing trailing edge to the minimum pressure point and on an assumed average velocity distribution after the shock which goes from slightly below a Mach number of 1 to free-stream velocity at the trailing edge. The equation then takes this form (fig. 1) with the constant K experimentally determined. The parameter was selected on the basis that impulses or changes

at the trailing edge could not get through the shock front outside of the boundary layer; this assumption is substantiated by steady-state results which show that deflections of a control have little effect on the flow in front of a shock wave. Therefore, the parameter appears to be a reasonable one in determining time lags. The type of analysis used assumes that the actual phase angle would be a direct function of the difference between the aerodynamic period and the flutter period which is the basis of this approximate phase-angle equation. The constant in the aerodynamic frequency parameter was determined for the most part from the results of one test and then checked against all other available data. In the basic test the phase angle for several conditions of flutter was determined by use of a shadowgraph system of visualizing shock and aileron motion. Figure 2 shows the type of shock pictures obtained. It was possible by analyzing a large number of these pictures to obtain the phase relationships as shown in figure 3. It was then assumed that, inasmuch as the time delays of pressure propagations would be greatest in moving from the trailing edge to the shock and much less when moving from the shock to the trailing edge, the phase relationship of the shock motion as shown must be an indication of the phase relationship of the hinge moment on the aileron. It was this type of information, obtained from a series of tests (table I), that was used actually to check the phase-angle equation. By use of the computed phase angle and the known mechanical parameters it was found that the dynamic resultant hinge-moment slope was the same as the static hinge-moment slope. Therefore, the magnitude of the dynamic hinge moment can be estimated from static data until more exact solutions are obtained. These results also show that increasing the separation causes a decreased flutter amplitude as was previously mentioned.

The equations developed have been checked for general correctness as to predicting flutter frequencies on six different models as shown in table II. It is believed that the wide range of frequencies involved makes the check quite reliable. It is interesting to note that the wing with the NACA 0012-64 section had internal aerodynamic balance and this balance was very effective in helping to prevent flutter, it being necessary to go to a Mach number of 0.875 to get any indication of flutter at all; and even then the flutter was not of a dangerous nature since a very small amount of damping such as might be in an ordinary control system would have stopped the flutter. (See table II.) The Langley Laboratory obtained the flutter of the control-surface type on the sweptback wing during rocket-propelled tests. Figure 4 shows the type wing and airfoil sections involved. The aerodynamic frequency was computed by use of the airfoil normal to the leading edge. The flutter range to be expected, as shown in table II, was found to be from 73 to 109 cycles per second. The actual test results shown in figure 5 show that the flutter range was from about 90 to 115 cycles per second. It is not believed that this one test is sufficient evidence to warrant the general use of the equations for sweptback-wing analysis, although it



is important to note that the sweepback merely delays the onset of flutter to Mach numbers above 1 in this case.

In order to explore and to understand further the one-degree-of-freedom transonic flutter, instantaneous pressure cells were installed on a test wing and the pressures were measured at several flutter frequencies. Figure 6 shows the type of pressure record obtained. The notations on the records indicate the position of the cell in percent chord and whether it is top or bottom surface. An oil damper was inserted in the system to control the amplitude, the damping force being measured by a strain gage. One cell shows a square-wave effect. It was found upon investigation that the shock wave passes over this cell and results in the very sharp changes. From these records, pressure-distribution changes at various points through the cycle were plotted as shown in figure 7. By following these records through a cycle it is possible to see the propagation of the pressure waves with time. The dotted lines indicate the lower surface and the solid lines, the upper. By use of the part of these plots over the aileron it was possible to integrate and to determine the instantaneous hinge moments due to the upper surface and the lower surface independently along with the resultant hinge moment as is shown in figure 8. This figure shows the instantaneous aileron angle plotted against the instantaneous hinge moment, the time lag causing the hysteresis effect. The area of this figure is a measure of the energy expended in overcoming the mechanical forces. The greater the time lag, the more open the figure becomes. It may be seen that subsonic flow is probably induced on the lower surface as the aileron goes down, that the lag effect disappears, and that no work is done. The upper surface shows a similar effect in that the energy loop becomes less open when the aileron is in the upper position. Other curves of this same nature have actually shown that at the lower Mach numbers or at lower angles of attack a certain amount of damping due to the lower surface occurs in this region. By using the maximum amplitudes measured and by setting the areas of these loops equal to the area of the ellipse that would do the same amount of work, the phase angles noted are determined. It is interesting to note that when the upper and lower surfaces are combined into the total hinge moment the result is a fairly uniform figure approaching closely the pure elliptic form. In the final plot the aileron motion and total hinge moment are plotted as a function of time to show the relative purity of the wave shapes. Generally speaking, it has been found that the relationships suggested by the empirical solution are in reasonable agreement with the results of the pressure tests. It has been indicated, however, that the actual lower-flutter frequency may be slightly less than that predicted by the present solution, although the exact lower limit is difficult to determine.

In conclusion it can be said that an empirical method has been developed that can be used to predict the flutter-frequency range, and

by knowing the mechanical characteristics of the control and the static hinge-moments the possibility of flutter occurring can be computed. Furthermore, there is as yet no indication that airfoil section can in itself have any effect in preventing flutter except that it should control the possible flutter-frequency range. It is also evident that inasmuch as static hinge moments are a measure of the dynamic hinge moments, internal aerodynamic balance can be sufficient to prevent a serious one-degree-of-freedom flutter problem.

#### BIBLIOGRAPHY

- Brown, Harvey H., Rathert, George A., Jr., and Clousing, Lawrence A. : Flight-Test Measurements of Aileron Control Surface Behaviour at Supercritical Mach Numbers. NACA RM No. A7A15, 1947.
- Spreiter, John R., Galster, George M., and Cooper, George E. : Flight Observations of Aileron Flutter at High Mach Numbers as Affected by Several Modifications. NACA RM No. A7B03, 1947.
- Barmby, J. G., and Clevenson, S. A. : Initial Test in the Transonic Range of Four Flutter Airfoils Attached to a Freely Falling Body. NACA RM No. L7B27, 1947.
- Erickson, Albert L., and Stephenson, Jack D. : Transonic Flutter of Control Surfaces. NACA RM No. A7F30, 1947.

TABLE I.

SUMMARY OF SHADOWGRAPH RESULTS

CONFIGURATION	AILERON MOTION, TOTAL (DEG.)	PHASE DIFF, $\phi$ (DEG.)	FREQUENCY $f$ (cps)	MAX HINGE MOMENT $H_0$ (FT. - LBS.)
STANDARD	18.4	67	21.2	1500
SPOILERS AT 0.50c	6.6	17	19.5	360
BUMPS AT 0.50c	18.6	51	21.2	1362
BUMPS AT 0.70c	9	54	19.4	570
TAPERED BUMP	16.0	25	20.8	1030



Erickson

TABLE II

SUMMARY OF FLUTTER RESULTS

AIRFOIL SECTION	RELATIVE RESTRAINT CONDITION	CHORD INCHES	COMPUTED FLUTTER FREQUENCY	ACTUAL FLUTTER FREQUENCY
65, - 213 a = 0.5	FIXED	56	24 TO 32	28, 32
65, - 213 a = 0.5	FREE	56	15 TO 24	15 TO 25
4412	FIXED	6	240	250
SYMMETRICAL DOUBLE WEDGE	RESONANT	8	102	100
0012 - 64 EXTENDED TRAILING EDGE, 10.7% THICK	FREE	55	12 TO 18	15.6 TO 17.3
0012 - 64 EXTENDED TRAILING EDGE, 10.7% THICK	FIXED	55	18 TO 24	23
66 - 2X - 216 a + 0.6	FREE	65	18 TO 27	20
65 - 010 45° SWEEP WING	FREE	10	72 TO 109	90 TO 120




$$I \ddot{\delta}_a + C \dot{\delta}_a + K_m \delta_a = H_0 \sin \omega t$$

$$\delta_a = \delta_{a_0} \sin (\omega t - \phi)$$

$$\tan \phi = \frac{C\omega}{K_m - I\omega^2}$$

$$f_a = \frac{a(1-M)}{2Kd}$$

$$\phi = \left(1 - \frac{f}{f_a}\right) 360^\circ$$



Figure 1.- Equations used in the empirical solution of transonic control surface flutter

Erickson

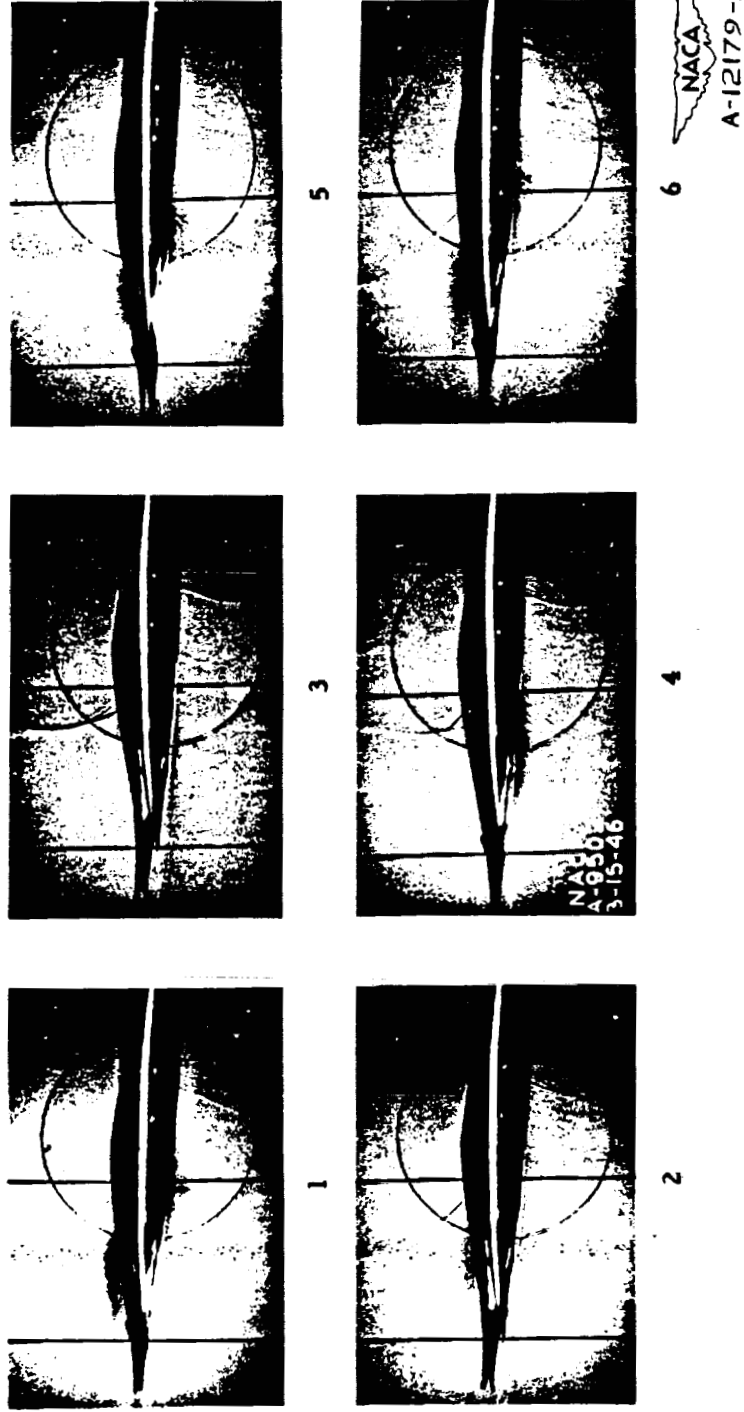


Figure 2.- Shadowgraphs of wing with alleron free.

Erickson

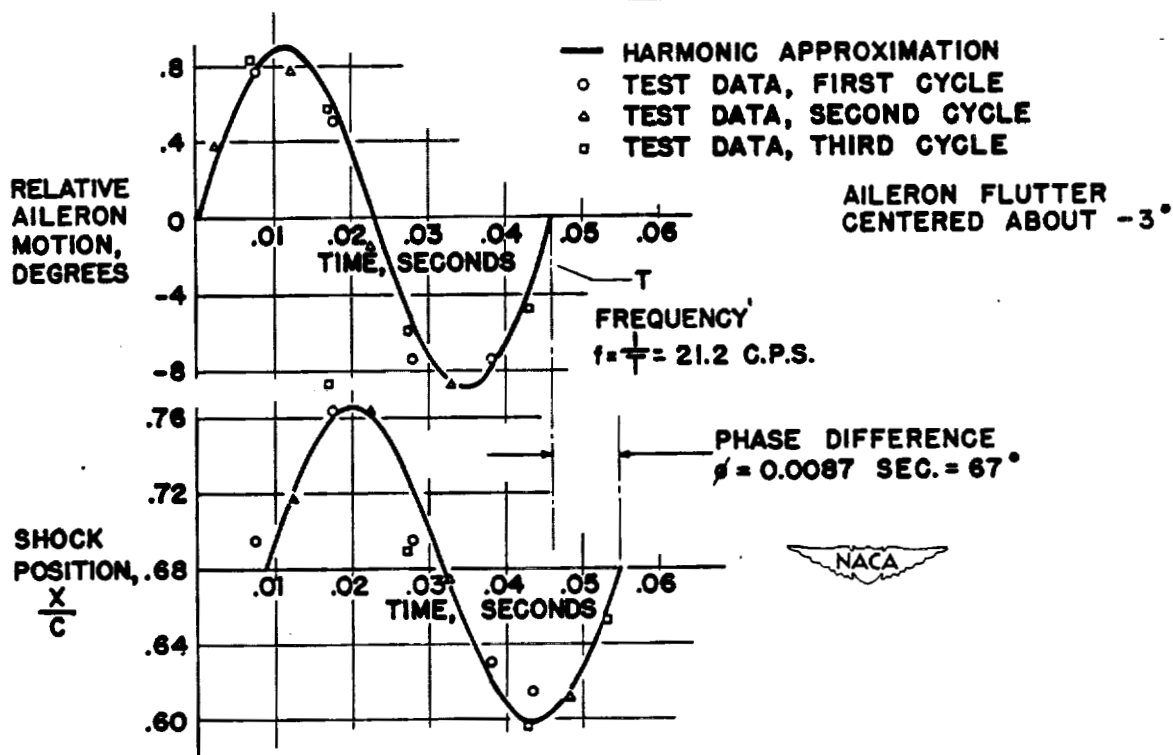


Figure 3.- Relative shock and aileron motion as a function of time.

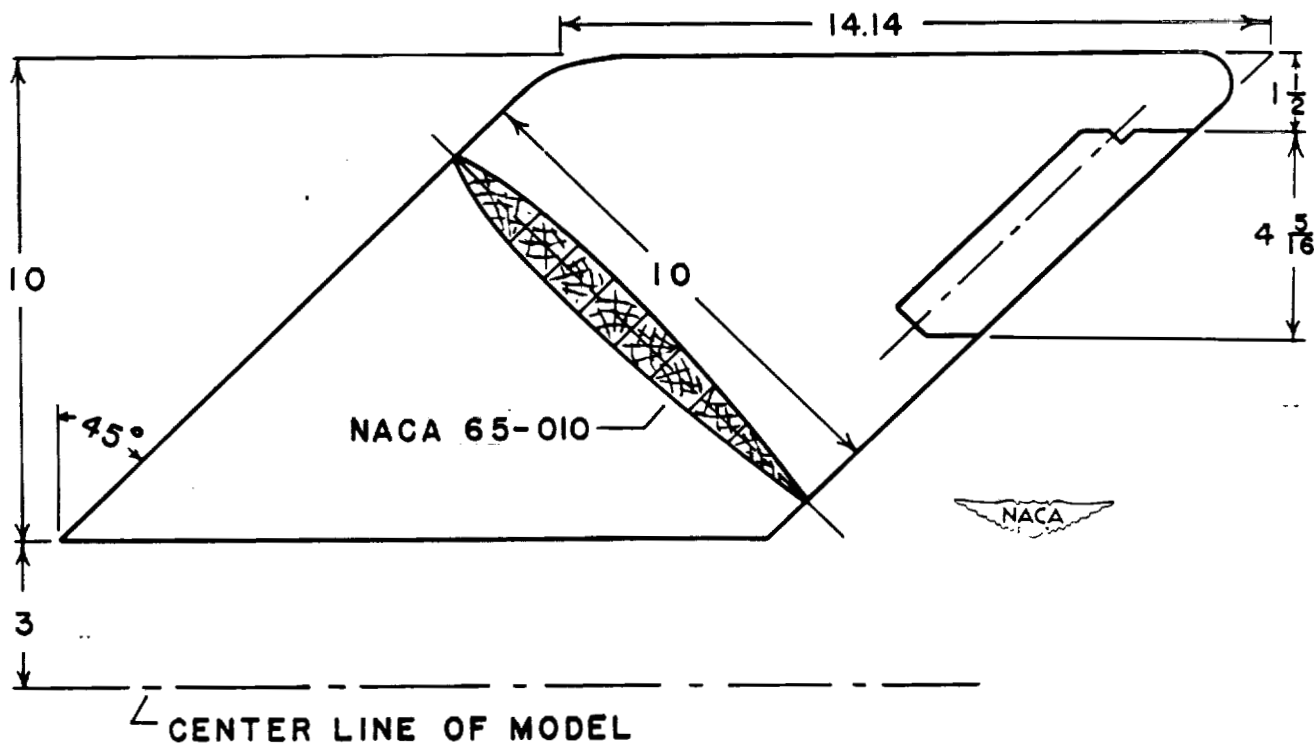


Figure 4.- Plan form of sweptback flutter model.

72(d)

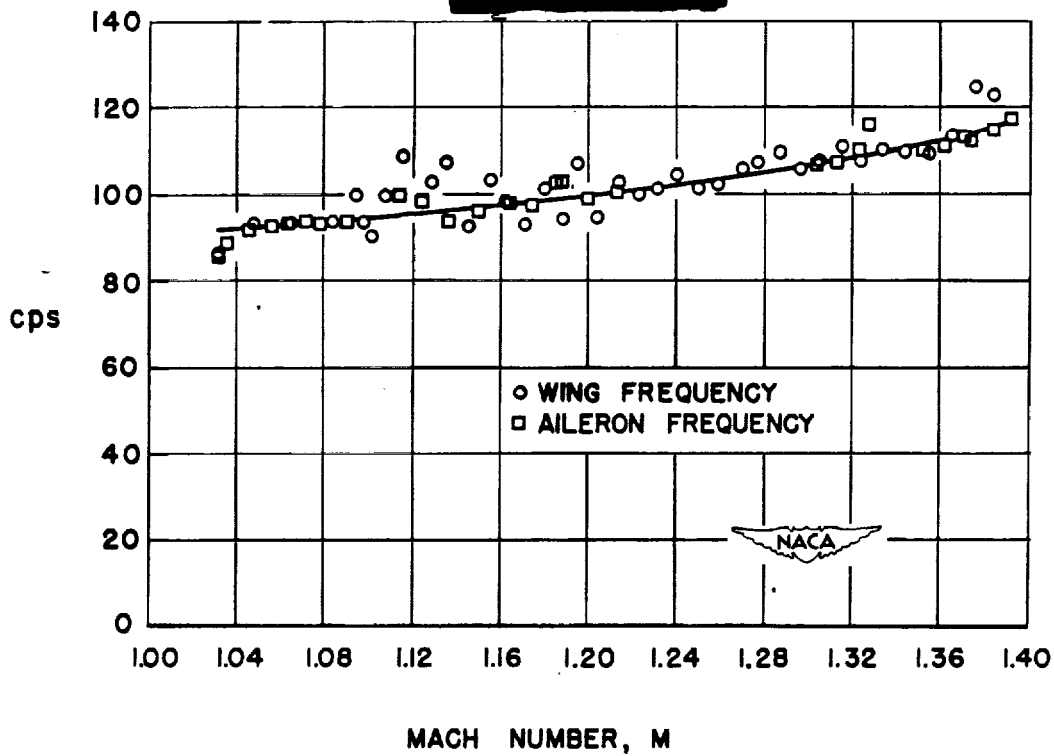


Figure 5.- Flutter results obtained with a sweptback wing.

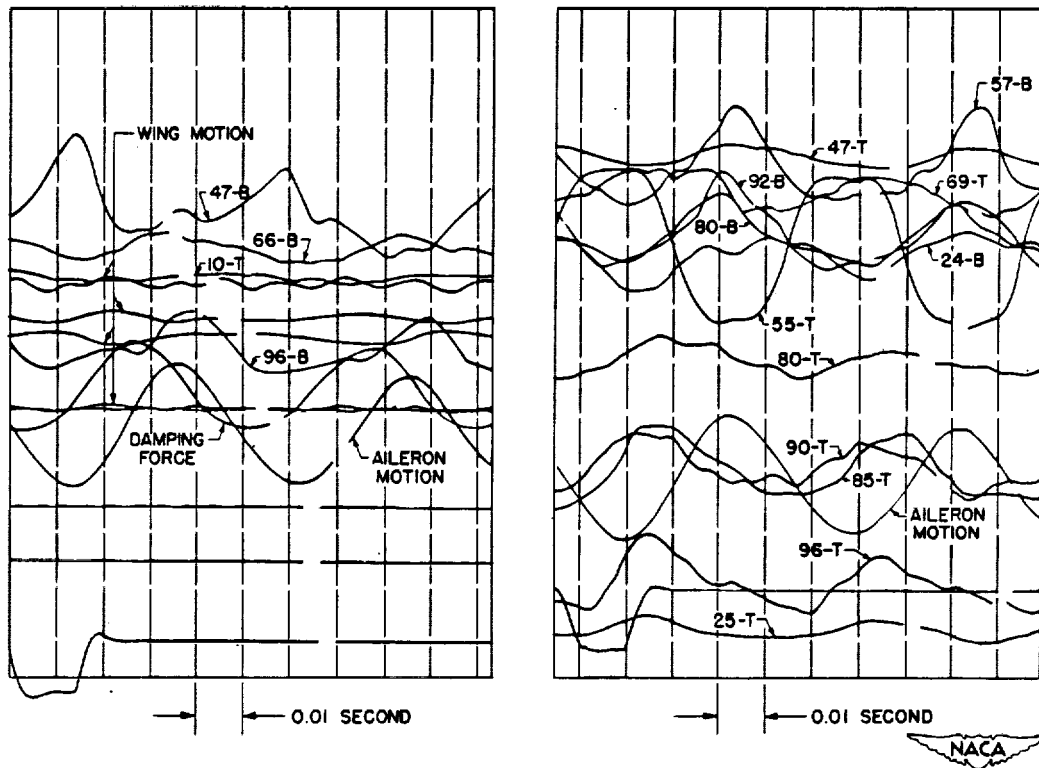


Figure 6.- Typical records obtained with instantaneous pressure recorders.

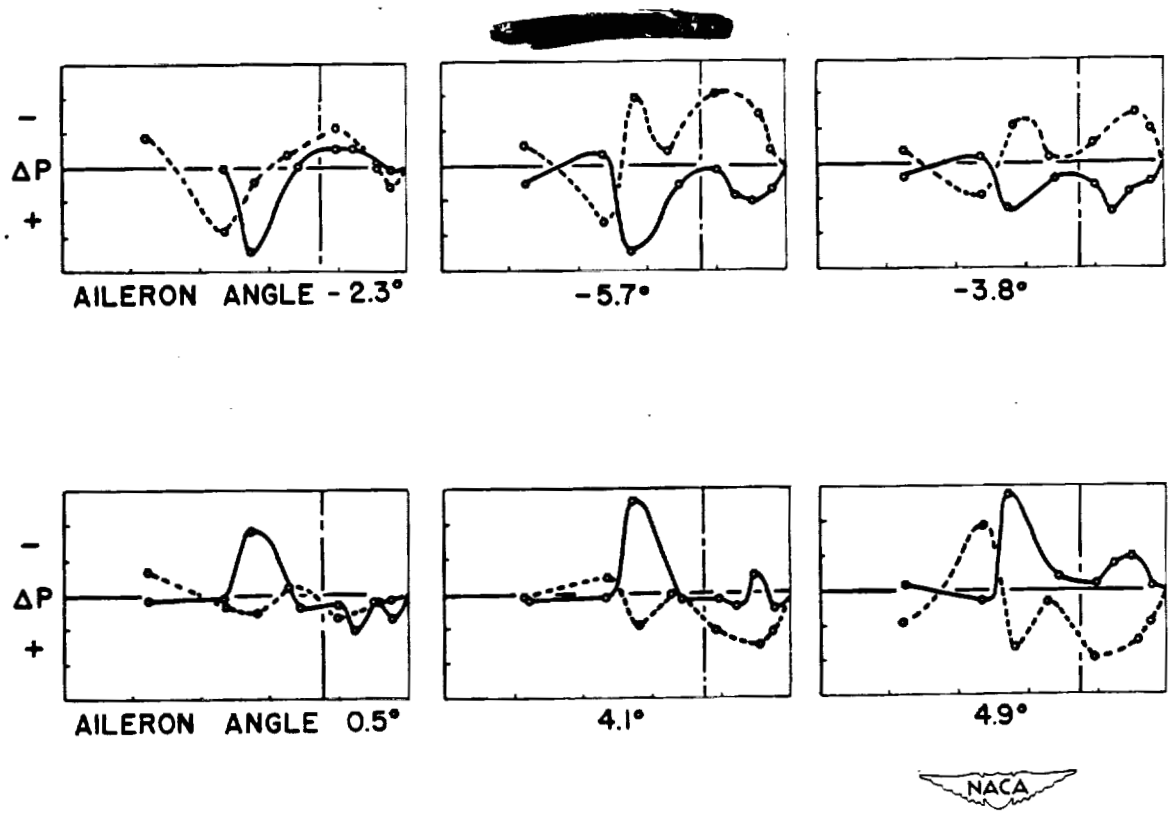


Figure 7.- Pressure-distribution changes at various points through a cycle.

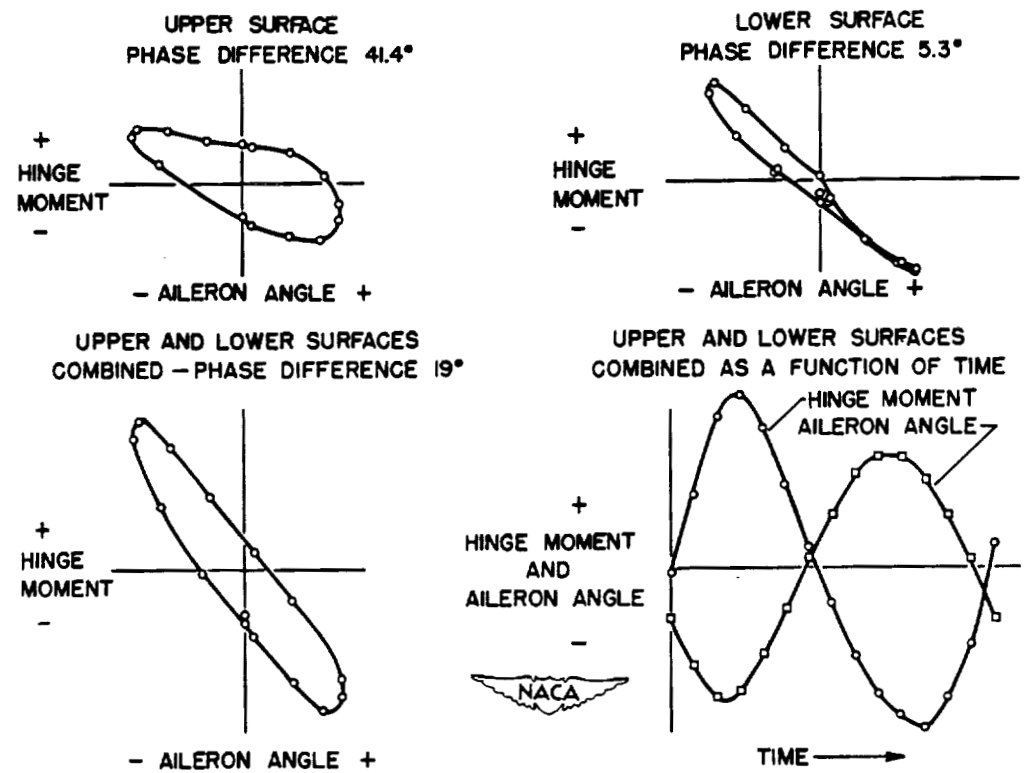


Figure 8.- Hinge-moment results obtained by the use of instantaneous pressure cells.

Erickson



STABILITY AND CONTROL

PREDICTION OF THE AERODYNAMIC CHARACTERISTICS  
OF WINGS OF ARBITRARY PLAN FORM

By Victor I. Stevens

Ames Aeronautical Laboratory

In our present effort to fly in and through the transonic-speed range we have resorted to widely diversified plan forms. Ranges of sweep, aspect ratio, and taper ratio are being considered which extend far beyond those considered practical several years ago, and the effect of wide variations in these parameters on the subsonic aerodynamic characteristics of wings is as yet largely unknown. The multiplicity of possible plan forms precludes an investigation of each experimentally. As a result, considerable effort has been directed towards developing a theoretical method of predicting the loading over the wing since, once this loading has been determined, not only can structural loads be estimated but values of the various aerodynamic characteristics such as lift-curve slope, aerodynamic-center location, and induced drag can also be found. The investigation of several theoretical methods for the prediction of loading and the application of one of these methods to a wide range of plan forms is the subject of this paper.

The theoretical methods studied were those developed by Falkner, by Mutterperl, and by Weissinger. In each of these methods the wing is replaced by a distribution of vortices. The strength distribution of these vortices is fixed by the boundary condition which requires that the induced velocities of these vortices produce no flow through the plane of the wing. The difference among the methods lies in differences in physical location of the vortices, in the disposition of the control points where the boundary condition is applied, and in the mathematical manipulation. Figure 1 compares the layout of vortices and control points for the methods. Falkner replaced the wing with a distribution of finite horseshoe vortices, both spanwise and chordwise. He likewise distributed the control points both spanwise and chordwise, hence his method is classified as a lifting-surface method. As a result of his work Falkner has recommended a particular vortex and control point distribution which was followed in our studies. In contrast to the Falkner lifting-surface method, both the Weissinger and the Mutterperl methods are lifting-line methods; that is, the loading is concentrated on the quarter-chord line, and the control points are distributed along the three-quarter-chord line. The Weissinger and Mutterperl methods differ in the spanwise location of the control points and in the mathematical development.

Van Dorn and DeYoung have examined each of these methods for accuracy and ease of application (reference 1). The accuracy was evaluated by comparing the predicted and the experimentally determined aerodynamic characteristics of five wings having sweep angles ranging from  $-45^{\circ}$  to  $45^{\circ}$ . By keeping an account of the time required, each method was also evaluated with regard to ease of application. The results of this study are shown in figure 1. From a comparison of the predicted and experimental values of spanwise loading, lift-curve slope, and spanwise center of pressure, the Falkner method was judged to be very accurate and the Weissinger method only slightly less accurate. The Mutterperl method, while predicting with moderate accuracy the characteristics of the sweptback wings, did not give accuracy comparable to other methods in the case of the sweptforward wings. The time required per solution was least for the Weissinger method (3 hr). In contrast 28 hours was required per solution for the Mutterperl method and 30 hours for the Falkner method.

On the basis of these results it was concluded that for a detailed study of a given plan form, where a high degree of accuracy was desired and where ease of application assumed lesser importance, the Falkner method was best. However, for a general study of a variety of plan forms the Weissinger method appeared best suited since good accuracy could be had at a 90 percent saving in computing time.

Accordingly we have utilized the Weissinger method to investigate the loading and associated aerodynamic characteristics of a wide range of plan forms. Figure 2 pictures the range covered but does not indicate the number of plan forms considered. Actually the characteristics of about 200 wings were calculated. The general range of variables included sweep from  $45^{\circ}$  forward to  $60^{\circ}$  back, aspect ratios from 1.5 to 8.0, and taper ratios from 0 to 1.5. The structural feasibility of the various shapes was used as a rough guide in selecting the limiting values of the geometric parameters.

The results of this investigation are found in reference 2. Charts presented in this reference allow a rapid and simple determination of the most important aerodynamic characteristics of any wing having a plan form falling within the range of this study. Aerodynamic characteristics which can be read directly from these charts include the span-loading coefficients, spanwise center of pressure, lift-curve slope, and aerodynamic center. These parameters are given as a function of sweep for families of aspect ratio and for various taper ratios. Sufficient values of aspect ratio and taper ratio were chosen to allow rapid and accurate interpolation.

Sample charts taken from reference 2 are shown in figure 3. For the sake of clarity in this presentation, the data shown have been limited to one taper ratio, to a few aspect ratios, and, in the case of spanwise loading, to one spanwise station. In the reference paper, of course, data are given for a complete range of these geometric parameters. The simplicity of obtaining the desired characteristics is obvious. The chart showing the characteristics is entered at the proper value of sweep of the quarter-chord line and the desired value of the characteristics obtained directly. In this manner it is possible to obtain the wing-loading coefficient at four spanwise stations, the lift-curve slope, the spanwise center of pressure, and the aerodynamic center. Aerodynamic characteristics obtained from these charts have been correlated with experimental results, and in general the agreement is good. Strictly speaking, the method applies only at zero lift. However since the aerodynamic characteristics are in general linear up to angles of attack where separation occurs, the theoretically predicted characteristics can be used with good accuracy up to this point. Specific correlations of lift-curve slope and aerodynamic center measured at zero lift will be discussed later.

Most of the qualitative effects of sweep and taper ratio on span loading are not new and hence will not be discussed in this paper. However, one of the most interesting results of this investigation showed that, for each angle of sweep there is a taper ratio for which aspect ratio has little effect on the span loading and for which the span loading is practically elliptical. This relationship is shown in figure 4. As the wing is swept forward more inverse taper is required, and as the wing is swept back more of the usual type of taper is required. Because of the elliptic loading, minimum induced drag and maximum lift-curve slope are obtained for wings on this line. For plan forms falling on this line, aspect ratio had no effect on the loading. For plan forms above the line, loading moves outboard with increasing aspect ratio, and, conversely, for plan forms below the line, loading moves inboard with increasing aspect ratio.

Two of the characteristics found directly from the Weissinger method, lift-curve slope and aerodynamic center, are of particular value because of their importance in longitudinal stability analysis and design. Since they are so important the accuracy with which the Weissinger method predicts these characteristics and the effects of plan form on these characteristics as predicted by the Weissinger method should be examined.

In figure 5 the theoretical and experimental values of lift-curve slope are correlated for a number of random plan forms. Where sufficient clearance between points existed, the wing plan forms have been superimposed. Included in this correlation are triangular wings, highly sweptback wings, sweptforward wings, and wings with inverse taper. Most of the experimental data were taken from reference 3 and the remainder from other American papers. Deviation from the  $45^\circ$  line indicates the error of correlation. On the average, this deviation is less than 3 percent. Although not shown herein, we have also compared the lift-curve slopes of unswept wings as estimated by the Weissinger method and by the method employing the modified Jones' edge-velocity correction, and the agreement is nearly perfect.

A similar correlation for aerodynamic center is given in figure 6. Experiment and theory do not show as good agreement for this parameter as for the lift-curve slope. There is no clear systematic variation in the correlation with plan form, and most of the discrepancies in correlation are of the order of the accuracy with which the aerodynamic center usually can be determined by experiment. In any event, for 75 percent of the plan forms the discrepancy is less than 2 percent of the M.A.C., which discrepancy is small compared to the effects of plan form. It is our belief that the Weissinger method gives both lift-curve slope and aerodynamic center with sufficient accuracy for use in preliminary design studies.

Sample charts of lift-curve slope are shown in figure 7. Lift-curve slope is given as a function of sweep for taper ratios of 0, 0.5, and 1.5 and for aspect ratios of 1.5, 3.5, 8, and  $\infty$ . Many of the curves have again been omitted for clarity. The curve for infinite aspect ratio in each case is obtained from simple sweep theory and hence is a cosine curve. Note that in each case the effect of aspect ratio falls off with increase in sweep. Also note that for low aspect ratios, small angles of sweep have little effect on lift-curve slope. As the wing approaches a more pointed plan form, the lift-curve slope increases on sweptback wings and decreases on sweptforward wings, while inverse taper reduces lift-curve slope on sweptback wings and increases it on sweptforward wings. On highly swept wings this effect is of such magnitude that taper ratio exerts as great an influence on lift-curve slope as does aspect ratio. Thus in any theoretical approach the importance of including the effects of taper ratio is obvious.

Figure 8 presents sample charts of the aerodynamic center which is also plotted as a function of sweep for taper ratios of 0, 0.5, and 1.5 and for aspect ratios of 1.5, 3.5, and 8.0. For the plan forms investigated, the aerodynamic-center location ranged from as

far forward as 15 percent of the M.A.C. to as far back as 40 percent of the M.A.C. In contrast, the aerodynamic center on unswept wings is seldom more than 2 or 3 percent of the M.A.C. from the 25 percent M.A.C. point. On highly tapered wings sweepback moves the aerodynamic center rearward and sweepforward moves it forward. As taper is decreased, the trend is reversed so that, on wings having inverse taper, sweepback moves the aerodynamic center forward while sweepforward moves the aerodynamic center back. The magnitude of this movement in each case is generally increased by increase in aspect ratio.

As stated earlier, lift-curve slope and aerodynamic-center location are important in longitudinal stability analysis. That the Weissinger method can predict values of these characteristics with sufficient accuracy for preliminary design has been shown. One other parameter must however be evaluated to complete the longitudinal stability analysis, and that parameter is the downwash in the location of the tail. The Weissinger method can readily be extended to compute downwash in the plane of the vortex sheet. We are at present evaluating the accuracy of the downwash results obtained in this manner by checking them with experimental data. Preliminary results of such an evaluation are given in figure 9. The maximum downwash angles as predicted and measured in a vertical plane approximately 30 percent of wing semispan out from the plan of symmetry are shown as a function of angle of attack for five swept wings tested in the Ames 40- by 80-foot tunnel. For these wings, theory predicts the variation of downwash with angle of attack within 20 percent of the measured value. Insufficient comparisons have been made to date, however, to warrant generalizations as to the accuracy of this method for a wide range of plan forms. In our present investigation we plan to establish this accuracy, improve the method where possible, and then extend the method so that downwash may be determined at points above and below the vortex sheet.

All the results obtained through use of the Weissinger method apply only to incompressible flow. However, through an application of the Prandtl-Glauert rule, it is possible to account for the effects of compressibility on span-loading characteristics for speeds below the critical speed. The method, which has been summarized in some detail in reference 4, translates the effect of compressibility into an effective change in plan form in addition to the well-known increase in section pressures.

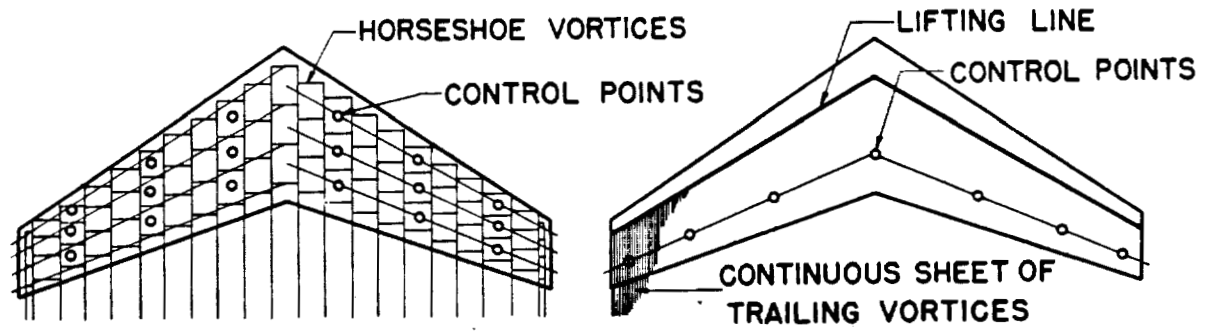
It is apparent that, if such an approach serves to predict accurately the effects of compressibility, it can be used in conjunction with the subject paper to give a rapid estimation of the characteristics of wings throughout the Mach number range below the

critical speed. At each Mach number the geometry of the wing would simply be distorted in the proper manner and new characteristics obtained from the charts. Only a few random experimental checks of this procedure have been made, but these comparisons have indicated moderately good agreement between theory and experiment. It is our plan to continue this study to establish the accuracy of the method, and, if necessary, search for means of improving the accuracy.

#### REFERENCES

1. Van Dorn, Nicholas H., and DeYoung, John: A Comparison of Three Theoretical Methods of Calculating Span Load Distribution on Swept Wings. NACA TN No. 1476, 1947.
2. DeYoung, John: Theoretical Additional Span Loading Characteristics of Wings with Arbitrary Sweep, Aspect Ratio and Taper Ratio. NACA TN No. 1491, 1947.
3. Shortal, Joseph A., and Maggin, Bernard: Effect of Sweepback and Aspect Ratio on Longitudinal Stability Characteristics of Wings at Low Speed. NACA TN No. 1093, 1946.
4. Dickson, R.: Comparison of Two Methods of Calculating Aerodynamic Loading on an Aerofoil with Large Sweepback and Small Aspect Ratio. TN No. Aero 1700, British R.A.E., June 1946.

Stevens



	FALKNER	MUTTERPERL	WEISSINGER
ACCURACY	VERY GOOD	VARIABLE	GOOD
TIME	30 HR	28 HR	3 HR



Figure 1.- Comparison of theoretical methods for determining loading.

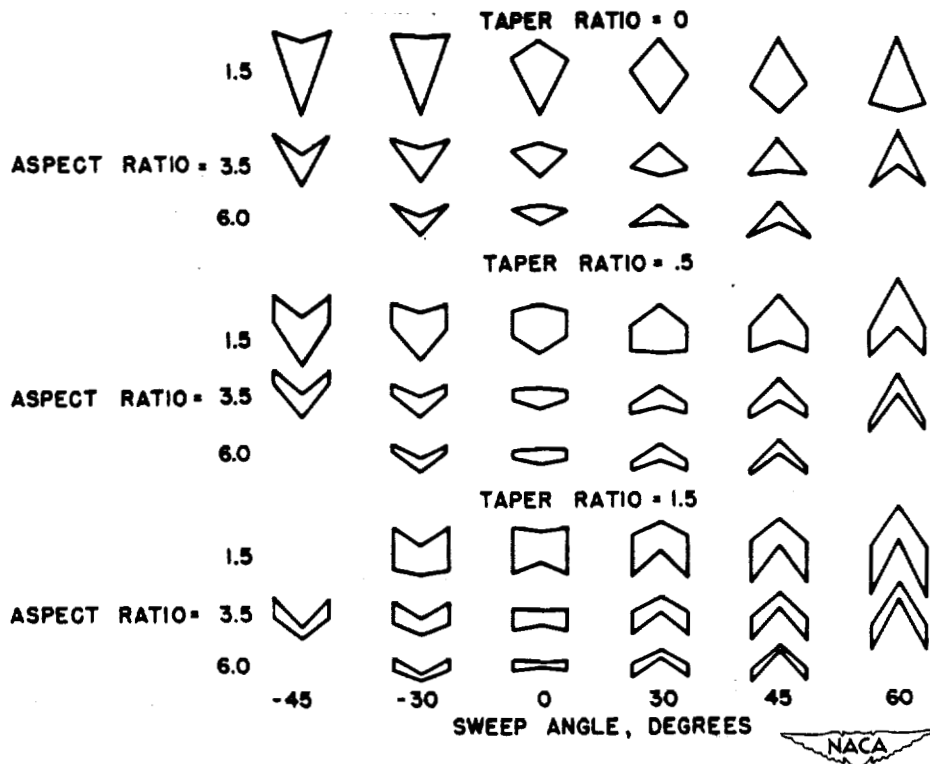


Figure 2.- Range of plan forms investigated by Weissinger method.



TAPER RATIO = .5

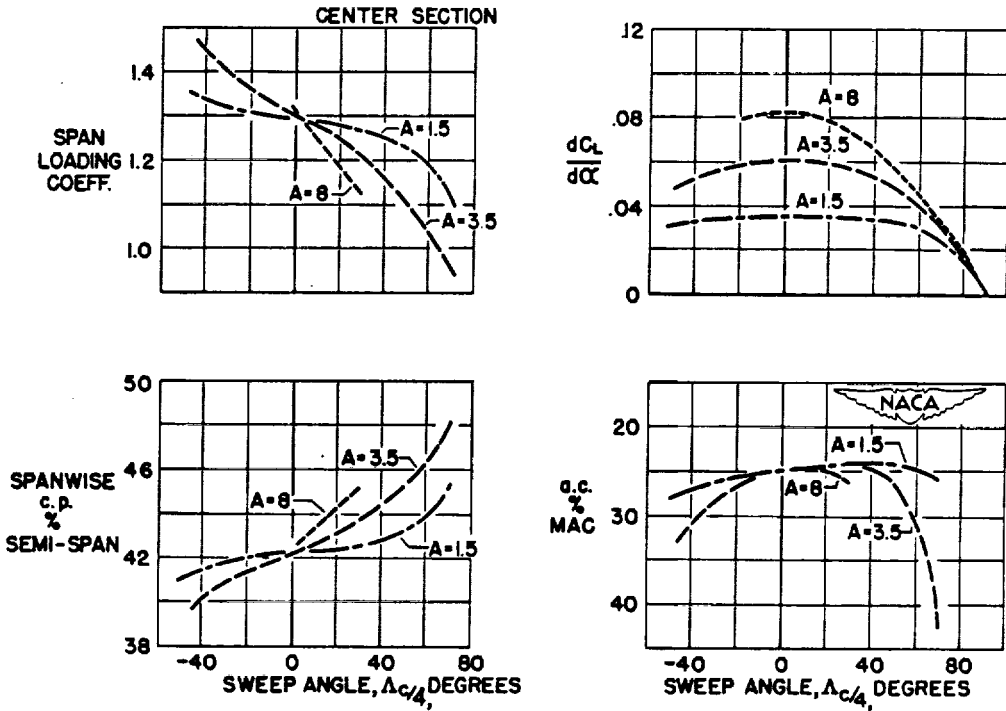


Figure 3.- Sample charts of data obtained by Weissinger method.

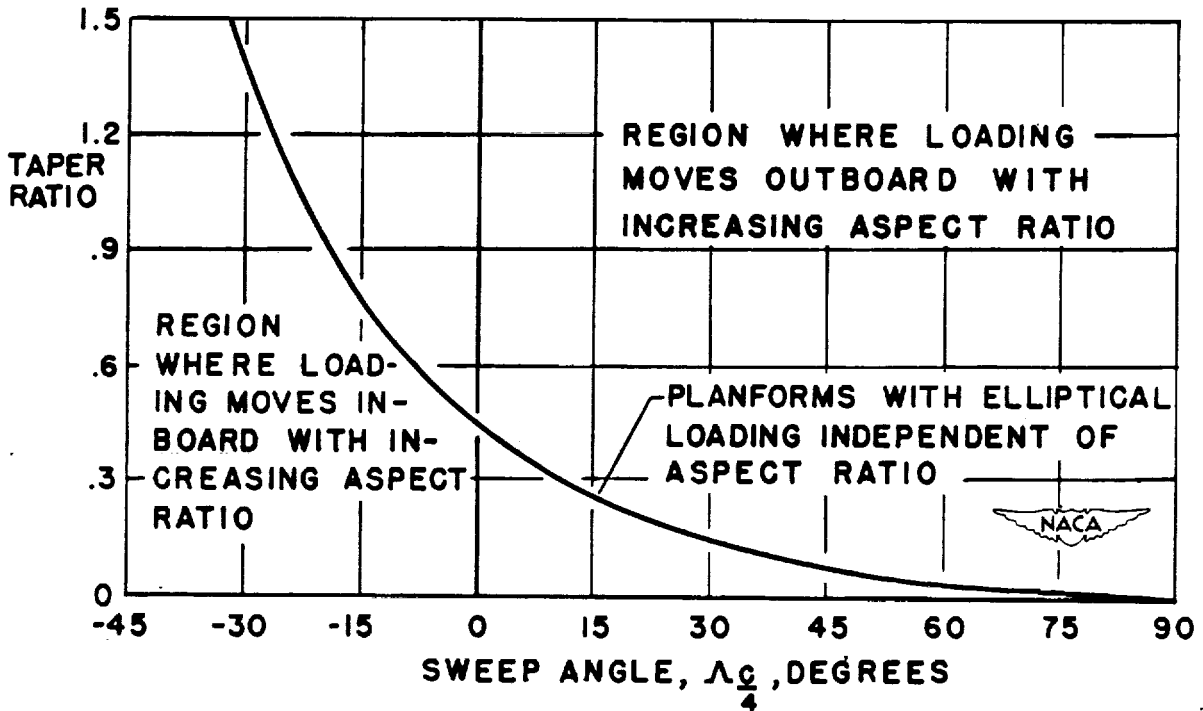


Figure 4.- Taper ratio - sweep angle relationship giving elliptic loading.

Stevens

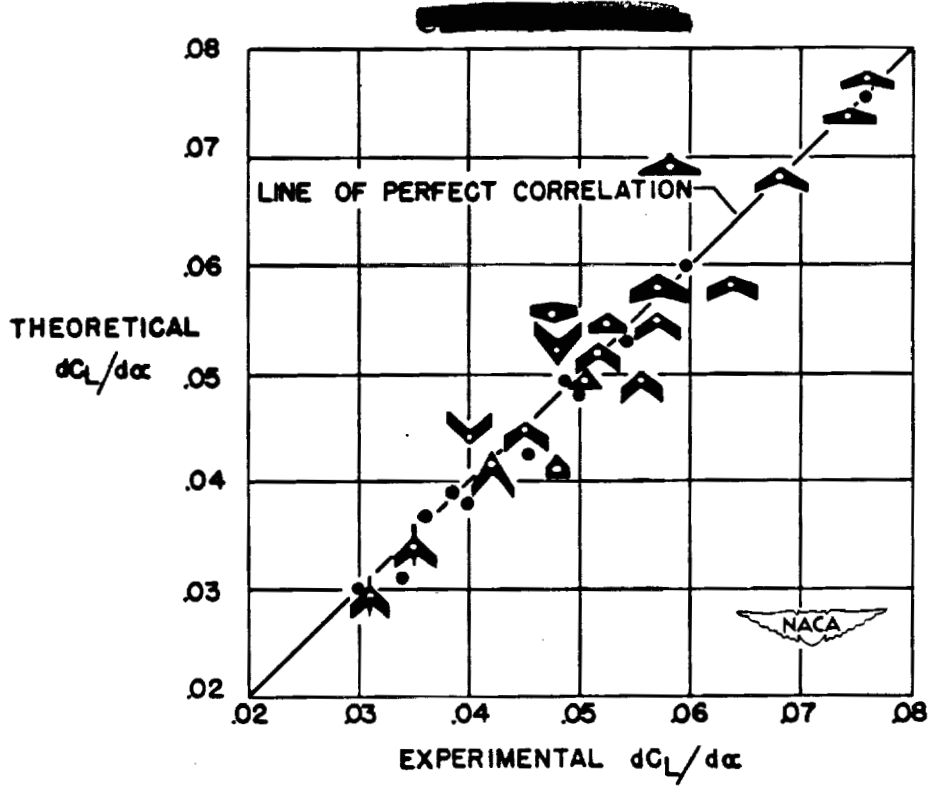


Figure 5.- Correlation of theoretical and experimental values of lift-curve slope.

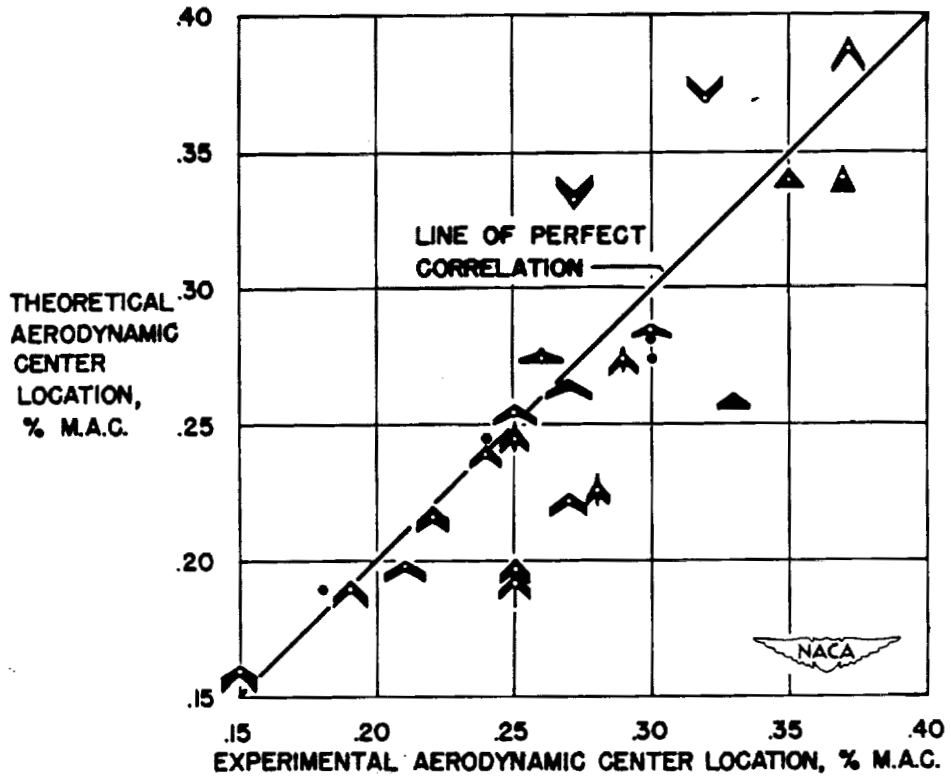


Figure 6.- Correlation of theoretical and experimental locations of the aerodynamic center.

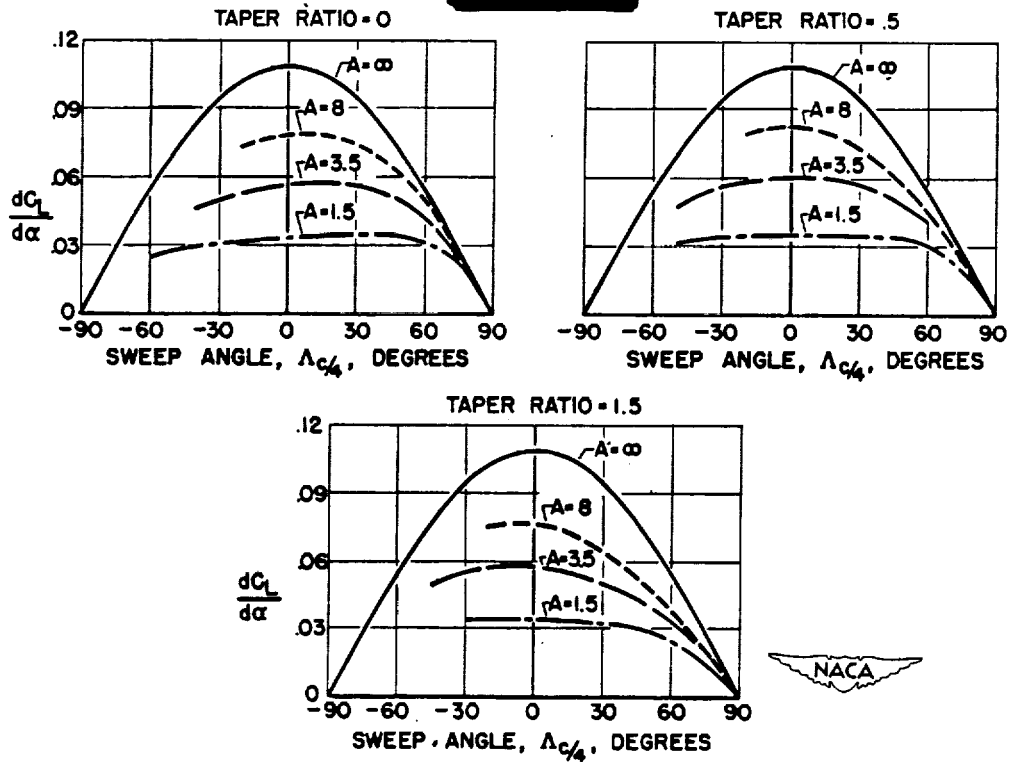


Figure 7.- Effect of sweep, taper ratio, and aspect ratio on lift-curve slope.

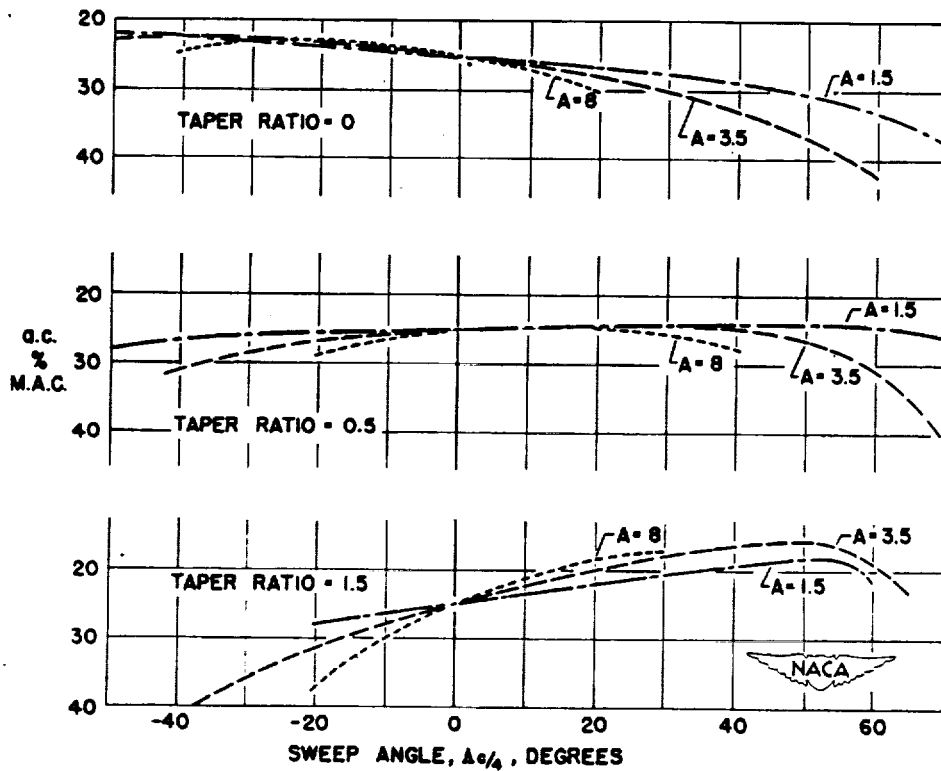


Figure 8.- Effect of sweep, taper ratio, and aspect ratio on aerodynamic-center location.

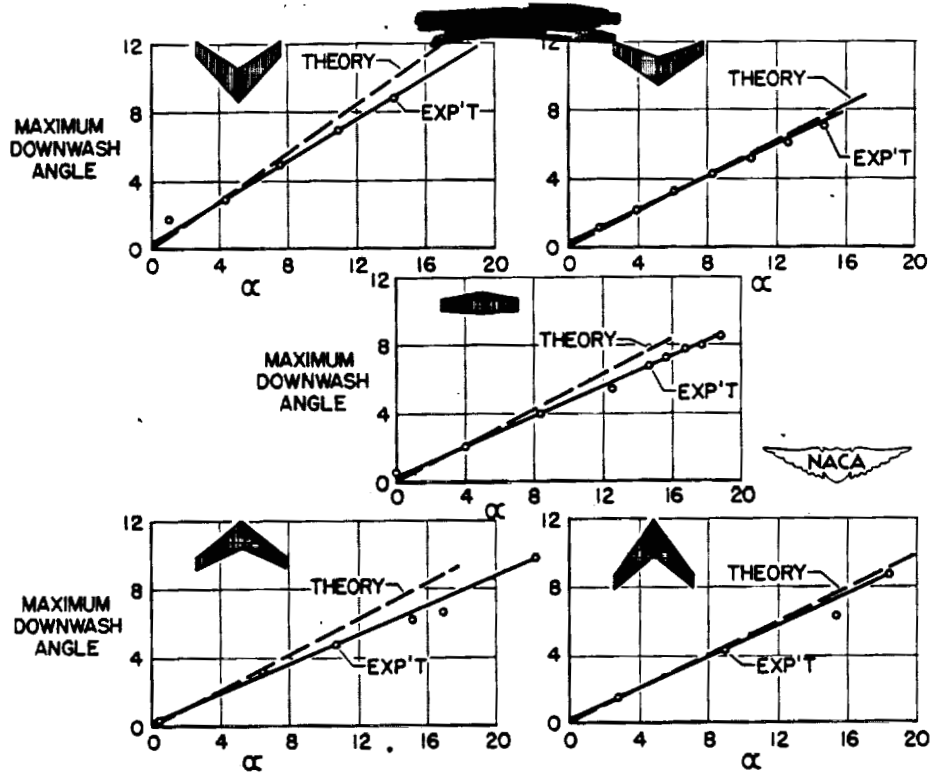


Figure 9.- Comparison of theoretical and experimental values of downwash.

## CURRENT STATUS OF LONGITUDINAL STABILITY

By Charles J. Donlan

Langley Memorial Aeronautical Laboratory

## INTRODUCTION

The purpose of this paper is to focus attention on some recent investigations that have been concerned with longitudinal stability problems both at high speeds and at low speeds and to summarize briefly the current state of affairs in regard to these problems.

## HIGH-SPEED PROBLEMS

## Static Stability and Control

Recent investigations.— A number of longitudinal stability investigations of various airplane configurations have been conducted at high subsonic Mach numbers in the Committee's high-speed wind tunnels and at transonic Mach numbers up to 1.2 utilizing the NACA wing-flow method and the associated wind-tunnel transonic-bump technique. These investigations are contained in references 1 to 15, and some of the configurations investigated together with the Mach number range for which data are available are summarized in figure 1.

For the tailless configuration (a), Langley high-speed 7- by 10-foot tunnel data for a sting supported model and for a semispan model exist up to a Mach number of 0.95, and wing-flow data are available up to a Mach number of 1.20. The three sets of data are in general qualitative agreement, although the increase in the lift-curve slope with Mach number was somewhat more rapid for the sting-supported tunnel model than for the semispan tunnel model and semispan wing-flow model.

Configuration (b) was investigated as a semispan wing-flow model and was also tested on a transonic bump in the Langley high-speed 7- by 10-foot tunnel. This model is similar to the XS-1 model for which Langley 8-foot high-speed tunnel data are available to a Mach number of 0.92. The agreement between the data obtained by the wing-flow method and the transonic-bump method was satisfactory throughout most of the Mach number range.

Model (d) was similar to model (b) except for the swept tail. It also was tested as a wing-flow model.

Model (c) was investigated on the transonic bump, model (e) as a semispan model in the Ames 16-foot tunnel, and model (f) was investigated as a sting-supported model in the Langley 8-foot high-speed tunnel.

Despite the fact that most of the results available thus far are limited to relatively few configurations, it is interesting to observe in the data certain trends in regard to the manner in which stability and trim changes with Mach number are manifested.

Characteristic data.— Data representative of the variation of pitching-moment coefficient with lift coefficient for several Mach numbers for a straight-wing design are shown in figure 2. Although these data apply to the design indicated, similar trends in the data for other straight-wing designs have been observed. The data at  $M = 0.6$  are typical of the behavior before force break, and some comments regarding the predicability of the characteristics in this range is probably pertinent at this point.

The important changes in longitudinal stability for straight-wing designs at high Mach numbers are, of course, not indicated by formulas based on linear-perturbation theory. Such formulas, however, are useful in interpreting experimental trends at subcritical Mach numbers. In consideration of the Mach number effects on a wing and tail combination, the trends indicated by the theory may be divided into three categories: (1) direct changes in the position of the wing aerodynamic center, (2) changes in the downwash at the tail, and (3) disproportionate changes in the lift-curve slopes of the wing and tail resulting from the differences in aspect ratio. For a flat elliptic wing of aspect ratio 4, theory indicates a forward shift of the aerodynamic center of only about 1.4 percent at a Mach number of 0.8 (reference 16). However, forward shifts of the aerodynamic center of 5 percent or more have been obtained experimentally on straight wings at high Mach numbers particularly for those employing sections having large trailing-edge angles. At the present time, therefore, it appears that the changes in wing aerodynamic-center position with Mach number must be determined experimentally even at subcritical speeds. A limited amount of German data has indicated that this effect is minimized for small trailing-edge angles.

The theories regarding the change in downwash characteristics at the tail and the change in the lift-curve slopes of the wing and tail with Mach number, however, appear to agree fairly well with experiment at subcritical Mach numbers (references 17 and 18). These two effects have indicated forward shifts in the neutral point of the order of 5 percent in some cases. At Mach numbers approaching that of force break and at supercritical Mach numbers, recourse must be made to experiment.

Marked changes in the variation of the basic wing-fuselage pitching moment with lift coefficient is apparent at a Mach number of 0.905 and 0.933, and the appearance of flat spots in the resultant pitching-moment curve in the lower lift range is somewhat characteristic for this type of design at supercritical speeds. In many instances local reversals in slope have been encountered, particularly for different stabilizer and elevator settings. The nonparallelism of the pitching-moment curves in this range for the different stabilizer settings is significant and evidences the nonlinear contribution of the tail to stability. Consequently, in evaluating the stability characteristics of a design possessing nonlinearities of this kind, it is essential, of course, to consider conditions at tail settings in the vicinity of trim at the particular lift coefficient in question and also the lift-coefficient range over which the nonlinearities extend.

Similar data for a sweptback tailless configuration are shown in figure 3. The data for  $M = 0.7$  and  $0.95$  were obtained from Langley high-speed 7- by 10-foot tunnel tests of a semispan model. The data for  $M = 1.00$  were obtained from wing-flow tests of a smaller model. The increased slope of the pitching-moment curves at the higher Mach numbers is again evident. At  $M = 0.95$  the control effectiveness has been considerably reduced and appreciable trim changes occur, but the vicious changes in stability that are frequently manifested by straight-wing designs at supercritical speeds are absent.

The effect that sweepback can have on delaying the Mach number at which significant trim changes and stability changes are manifested is further illustrated in figure 4. The straight-wing design and the tailless design are the configurations for which typical data have been presented (figs. 2 and 3). The model with a  $45^\circ$  swept wing and tail was an arbitrary configuration investigated on the transonic bump. In evaluating the control settings required for trim at the various Mach numbers, appropriate flight plans at altitude were assumed for each configuration. It is interesting to note the manner in which the initial trim changes have been postponed to higher Mach numbers for the swept configurations and in particular the extremely small trim changes associated with the  $45^\circ$  configuration. Above their respective critical speeds, both the straight-wing design and the tailless configuration manifested irregular trim changes. It is desirable to keep trim changes as small as possible, although the amount of trim change that can safely be tolerated depends to a considerable extent on the type of stability associated with  $\left(\frac{\partial c_m}{\partial C_L}\right)_M$ . For the straight-wing configuration two boundaries are presented for the parameter  $\left(\frac{\partial c_m}{\partial C_L}\right)_M$  at supercritical speeds. The lower boundary is associated with the local flat spots in the pitching-

moment data previously discussed (fig. 2). These flat spots extended over a lift-coefficient range of less than 0.1 and are relatively unimportant for the particular flight plan employed for this example, inasmuch as the minimum lift coefficient attained is about 0.2. The response of the airplane to disturbances necessary to effect accelerations of the order of 2 or 3 g's is probably more nearly associated with some value between the two boundaries.

For the 35° swept design, this parameter is more precisely determinable and does not change appreciably up to a Mach number of 0.88, although it also increases rather rapidly at the higher supercritical Mach numbers.

For the 45° swept configuration, changes in the parameter have been delayed until a Mach number of about 0.95 has been reached and then  $-\left(\frac{\partial C_m}{\partial C_L}\right)_M$  increases rather gradually. This comparison illustrates the need for employing a large degree of sweepback if trim and stability changes in the transonic region are to be minimized.

Two factors greatly affecting the value of  $\left(\frac{\partial C_m}{\partial C_L}\right)_M$  are the wing-fuselage-aerodynamic-center position and the downwash at the tail. The manner in which these factors changed with Mach number for the straight-wing design and the 45° swept design are shown in figure 5.

The large variations in the local position of the wing-fuselage-aerodynamic-center position (denoted by  $-\left(\frac{\partial C_m}{\partial C_L}\right)_M$  tail off) for the straight-wing design is immediately apparent, and this variation is reflected in the behavior of the tail-on results, although the magnitude of the fluctuations has been decreased because of the increased tail effectiveness effected by the reduction in  $\frac{d\epsilon}{dC_L}$  at the tail at the supercritical Mach numbers.

For the 45° swept configuration, the wing-fuselage-aerodynamic-center position varied only a small amount, and the increase in  $\left(\frac{\partial C_m}{\partial C_L}\right)_M$  (tail on) at the higher Mach number was largely due to the increased tail effectiveness caused by the reduction in downwash slope at the tail.



The parameter  $\left(\frac{\partial c_m}{\partial C_L}\right)_M$  also influences to some extent the frequency of the short-period longitudinal oscillation. Some computations for a few characteristic designs were made in order to observe the manner in which this quantity affected the dynamic stability characteristics, and the results of the computations for a tailless design investigated are presented in figure 6. It is immediately apparent that altitude has a pronounced effect on the period of the oscillation and that the period becomes shorter as the speed is increased. The period varies in a somewhat hyperbolic manner with  $\left(\frac{\partial c_m}{\partial C_L}\right)_M$  so that for the values  $-\left(\frac{\partial c_m}{\partial C_L}\right)_M$  less than 0.05 the period will increase very rapidly, whereas for values of  $-\left(\frac{\partial c_m}{\partial C_L}\right)_M$  greater than 0.15 the period will change only slightly. The importance of the frequency of the short-period oscillation will probably have to await flight experience, inasmuch as it will depend to some extent on the damping characteristics. It will be noted that while the damping, as evaluated by the number of seconds to damp to 1/2 amplitude, depends to a considerable extent on altitude and speed it is independent of the parameter  $\left(\frac{\partial c_m}{\partial C_L}\right)_M$ . It is influenced significantly, however, by the damping in pitch, and for airplanes with a tail the damping will be more rapid than that indicated here. For a particular design the characteristics of the short-period oscillation can be rapidly evaluated inasmuch as one needs only to determine the roots of the second-degree equation usually associated with this mode of the longitudinal motion.

#### LOW-SPEED PROBLEMS

##### Static Stability in High Lift Range

One of the factors that has limited the amount of sweepback that can be beneficially employed on transonic designs has been the difficulty of providing satisfactory stability and control characteristics in the landing condition.

Basic wing characteristics.— At lift coefficients prior to that at which separated flow ensues on the wing, the position of the aerodynamic center of the wing can be estimated fairly reliably, and a paper entitled "Prediction of the Aerodynamic Characteristics of Wings of Arbitrary Plan Form" by Victor I. Stevens dealing with this subject

has already been presented. The shift in the aerodynamic-center position that occurs at high lift coefficients is less amenable to theoretical computations, and numerous experimental investigations have been concerned with this effect. From the data examined thus far it appears that aspect ratio and sweep angle are still the two most important factors that influence the type of pitching-moment variation to be expected at the stall. The familiar manner in which sweep angle and aspect ratio affect the character of the pitching-moment variation at the stall is illustrated in figure 7, which is taken from reference 19. Combinations of sweep and aspect ratio that fall above the line on the figure have been found to yield the characteristically unstable pitching-moment variation indicated. Other factors such as airfoil section, wing taper, Reynolds number, and surface roughness have been found to influence the lift coefficient at which instability is first manifested, but the ultimate variation at that stall has still been found to be consistent with that indicated on the figure.

While figure 7 reflects the behavior of plain wings it has been found that the addition of trailing-edge flaps has resulted in an unstable pitching-moment variation even for wings falling in the stable region on figure 7. A considerable number of investigations have therefore been concerned with the development of devices designed to alleviate the tip stalling that is responsible for this behavior (references 20 to 24).

Stall control devices.— At the present time stall control devices have been successfully applied to wings with leading-edge sweep angles up to  $42^\circ$ . Some of the results of an investigation (references 20 and 21) covering the effect of stall control devices on the pitching-moment characteristics of a  $42^\circ$  sweptback wing equipped with a split flap are shown in figure 8. This wing has an NACA  $6_4-112$  section and an aspect ratio of 4. This investigation was conducted in the Langley 19-foot pressure tunnel at a Reynolds number of about 6,840,000. The basic wing-fuselage combination exhibited an unstable pitching-moment variation at the stall. The addition of leading-edge flaps of the type indicated covering about 60 percent of the span resulted in a stable break of the pitching-moment curve at the stall, and this type of leading-edge device was the most satisfactory tested. Similar effects were also obtained with a leading-edge slat arrangement which covered 60 percent of the span except for a small region of instability just before  $C_{L_{max}}$ . This unstable region was removed by the addition of a fence located at the inboard end of the slot. This effect is somewhat typical of fence behavior. If located properly, fences, in general, have been found helpful in minimizing local unstable variations in the pitching-moment curve up to the maximum lift coefficient but do not appreciably affect the ultimate character of the pitching-moment variation at the stall.

Effect of fuselage.— The percent span of leading-edge flap or slat required to effect satisfactory pitching-moment behavior at the stall depends somewhat on the size of the fuselage to which the wing is attached and, to a lesser extent, on the position of the wing on the fuselage. The effect is illustrated in figure 9 (reference 21). The configuration represented by  $0.575 \frac{b}{2}$  leading-edge slots is the same wing configuration discussed in figure 8 and the fuselage is seen to have little effect on the character of pitching-moment variation at the stall. When the leading-edge flap span was increased to  $0.725 \frac{b}{2}$ , however, the wing-fuselage combination was unstable at the stall, whereas the wing alone still exhibited favorable characteristics. Similar results were obtained for a high- and low-wing arrangement. It appears from tuft studies of these configurations that the flow over the fuselage delays the stalling of the center section to such an extent that initial separation again began over the flapped portion of the wing.

Effect of tail location.— Thus far we have discussed only the characteristics of the basic wing-fuselage combination. The addition of a tail adds further complications but, in general, it has been found that stable behavior of the resultant pitching-moment at the stall is most likely to be achieved when the basic wing-fuselage pitching moment exhibits a stable variation. The location of the tail, however, is an important consideration and the effect of adding a tail to the wing-fuselage configuration with  $0.575 \frac{b}{2}$  leading-edge flaps and  $0.50 \frac{b}{2}$  trailing-edge flaps is shown in figure 10 (reference 22).

A study of these data indicate that the most satisfactory pitching-moment behavior at the stall was actually achieved with the low tail position by virtue of the decreased rate of change of downwash associated with this tail location. This low position was close to the edge of the wing wake, however, and may be objectionable from other considerations. The more desirable midtail location possessed a local region of instability just before  $C_{L_{max}}$  which was removed by the addition of a fence.

## CONCLUSIONS

In recapitulation, the following generalizations can be made:

1. The incorporation of large amounts of sweepback on both the wing and the horizontal tail has been found to increase the Mach number at which trim changes and stability changes are first manifested and to greatly reduce the trim changes and stability changes encountered at supercritical speeds.

2. Longitudinal stability in the landing condition has been attained for configurations with sweep angles of the order of  $45^\circ$  utilizing various stall-control devices, but at the present time optimum arrangements for these devices must be determined experimentally.

## REFERENCES

## Complete Model Investigations

1. Mattson, Axel T.: Force and Longitudinal Control Characteristics of a 1/16-Scale Model of the Bell XS-1 Transonic Research Airplane at High Mach Numbers. NACA RM No. L7A03, 1947.
2. Mattson, Axel T., and Loving, Donald L.: Force, Static Longitudinal Stability, and Control Characteristics of a 1/16-Scale Model of the Bell XS-1 Transonic Research Airplane at High Mach Numbers. (Prospective NACA paper)
3. Wright, John B., and Loving, Donald L.: High-Speed Wind-Tunnel Tests of a 1/16-Scale Model of the D-558 Research Airplane. Lift and Drag Characteristics of the D-558-1 and Various Wing and Tail Configurations. NACA RM No. L6J09, 1946.
4. Wright, John B.: High-Speed Wind-Tunnel Tests of a 1/16-Scale Model of the D-558 Research Airplane. Basic Longitudinal Stability of the D-558-1. (Prospective NACA paper)
5. Wright, John B.: High-Speed Wind-Tunnel Tests of a 1/16-Scale Model of the D-558 Research Airplane. Longitudinal Stability and Control of the D-558-1. (Prospective NACA paper)
6. Goodson, Kenneth W., and Myers, Boyd C., II: An Investigation of the Aerodynamic Characteristics of an 0.08-Scale Model of the Chance Vought XF7U-1 Airplane in the Langley High-Speed 7- by 10-Foot Tunnel. Part IV - Aileron Characteristics - TED No. NACA DE308. NACA RM No. L7E22, Bur. Aero., 1947.
7. Kuhn, Richard E., and Myers, Boyd C., II: An Investigation of the Aerodynamic Characteristics of an 0.08-Scale Model of the Chance Vought XF7U-1 Airplane in the Langley High-Speed 7- by 10-Foot Tunnel. Part V - Wing-Alone Tests and Effect of Modifications to the Vertical Fins, Speed Brakes, and Fuselage. TED No. NACA DE308. NACA RM No. L7J09, Bur. Aero., 1947.
8. Sawyer, Richard H., and Trant, James P., Jr.: Longitudinal Stability and Control Characteristics of a Semispan Model of the XF7U-1 Tailless Airplane at Transonic Speeds by the NACA Wing-Flow Method. NACA RM No. L7I08, Bur. Aero., 1947.
9. Goodson, Kenneth W.: An Investigation of an 0.08-Scale Semispan Model of the Chance Vought XF7U-1 Airplane in the Langley 7- by 10-Foot Wind Tunnel. (Prospective NACA paper)

10. Spearman, M. Leroy: Longitudinal Stability and Control Characteristics at Transonic Speeds of a Model Equipped with a  $45^\circ$  Swept Wing and Tail by the Transonic-Bump Method. (Prospective NACA paper.)
11. Zalovcik, John A., and Sawyer, Richard H.: Longitudinal Stability and Control Characteristics of a Semispan Airplane Model at Transonic Speeds from Tests by the NACA Wing-Flow Method. NACA ACR No. L6E15, 1946.
12. Weil, Joseph, and Spearman, M. Leroy: Longitudinal Stability and Control Characteristics of a Semispan Airplane Model at Transonic Speeds as Obtained by the Transonic-Bump Method and a Correlation with Results Obtained by the NACA Wing-Flow Method. (Prospective NACA paper)
13. Zalovcik, John A., and Sawyer, Richard H.: Longitudinal Stability and Control Characteristics of a Semispan Airplane Model with a Swept-Back Tail From Tests at Transonic Speeds by the NACA Wing-Flow Method. NACA MR No. L6G09, 1946.
14. Boddy, Lee E., and Morrill, Charles P., Jr.: The Aerodynamic Effects of Modifications to the Wing and Wing-Fuselage Intersection of an Airplane Model with the Wing Swept Back  $35^\circ$ . NACA RM No. A7J02, 1947.
15. Morrill, Charles P., Jr., and Boddy, Lee E.: Stability and Control Characteristics of a Fighter Airplane Model with a Sweptback Wing and Tail. (Prospective NACA paper)

#### Theoretical Investigations.

16. Jones, Robert T.: Properties of Low-Aspect-Ratio Pointed Wings at Speeds below and above the Speed of Sound. NACA TN No. 1032, 1946.
17. Owen, P. R.: The Effect of Compressibility on Longitudinal Stability below the Shock Stall. Rep. No. Aero 1829, British R.A.E., March 1944.
18. Nielsen, Jack N., and Sweberg, Harold, H.: Note on Compressibility Effects on Downwash at the Tail at Subcritical Speeds. NACA CB No. L5C09, 1945.

## Low-Speed Investigations

19. Shortal, Joseph A., and Maggin, Bernard: Effect of Sweepback and Aspect Ratio on Longitudinal Stability Characteristics of Wings at Low Speeds. NACA TN No. 1093, 1946.
20. Neely, Robert H., and Conner, D. William: Aerodynamic Characteristics of a  $42^\circ$  Sweptback Wing with Aspect Ratio 4 and NACA 64<sub>1</sub>-112 Airfoil Sections at Reynolds Numbers from 1,700,000 to 9,500,000. NACA RM No. L7D14, 1947.
21. Conner, D. William, and Neely, Robert H.: Effects of a Fuselage and Various High-Lift and Stall-Control Flaps on Aerodynamic Characteristics in Pitch of an NACA 64-Series  $40^\circ$  Swept-Back Wing. NACA RM No. L6L27, 1947.
22. Spooner, Stanley H.: Longitudinal Stability Characteristics of a  $42^\circ$  Sweptback Wing and Tail Combination. (Prospective NACA paper)
23. Weil, Joseph, Comisarow, Paul, and Goodson, Kenneth W.: Longitudinal Stability and Control Characteristics of an Airplane Model Having a  $42.8^\circ$  Sweptback Circular-Arc Wing with Aspect Ratio 4.00, Taper Ratio 0.50, and Sweptback Tail Surfaces. NACA RM No. L7G28, 1947.
24. Schuldenfrei, Marvin, Comisarow, Paul, and Goodson, Kenneth W.: Stability and Control Characteristics of an Airplane Model Having a  $45.1^\circ$  Swept-Back Wing with Aspect Ratio 2.50 and Taper Ratio 0.42 and  $42.8^\circ$  Swept-Back Horizontal Tail with Aspect Ratio 3.87 and Taper Ratio 0.49. NACA RM No. L7B25, 1947.

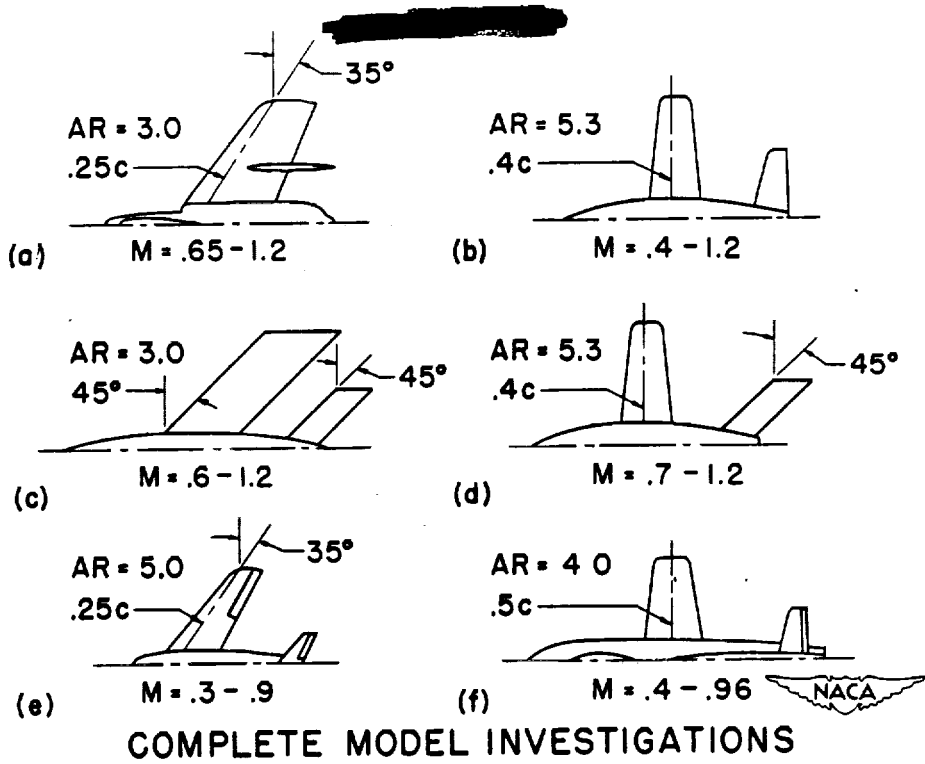
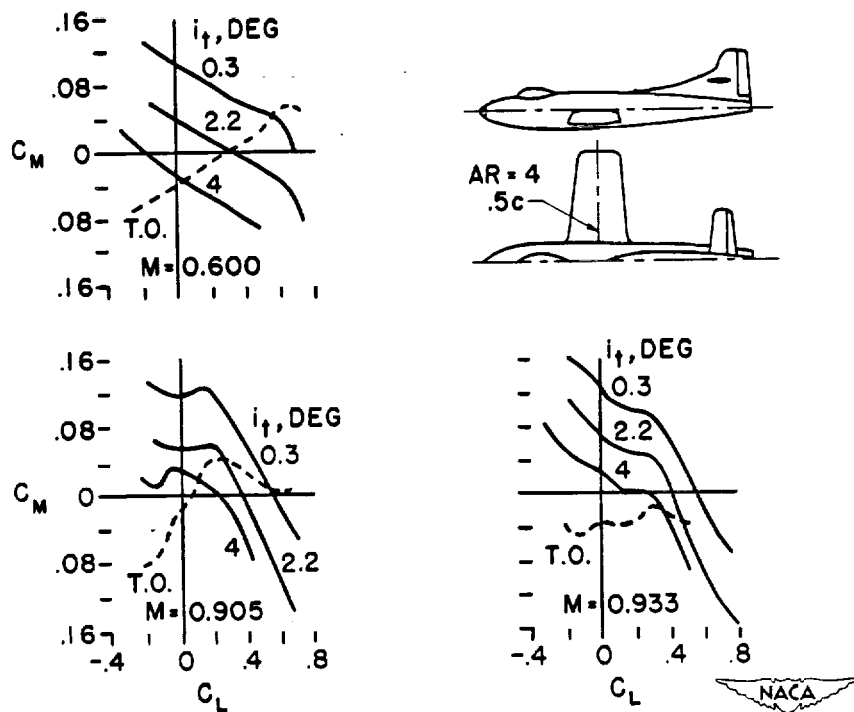


Figure 1.



PITCHING CHARACTERISTICS OF A STRAIGHT-WING DESIGN

Figure 2.



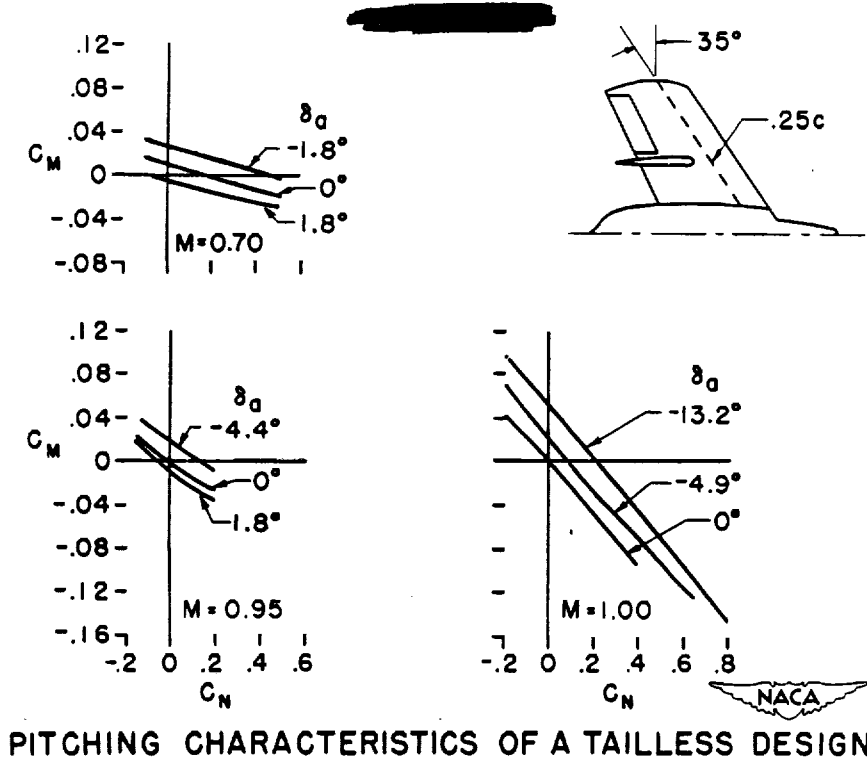


Figure 3.

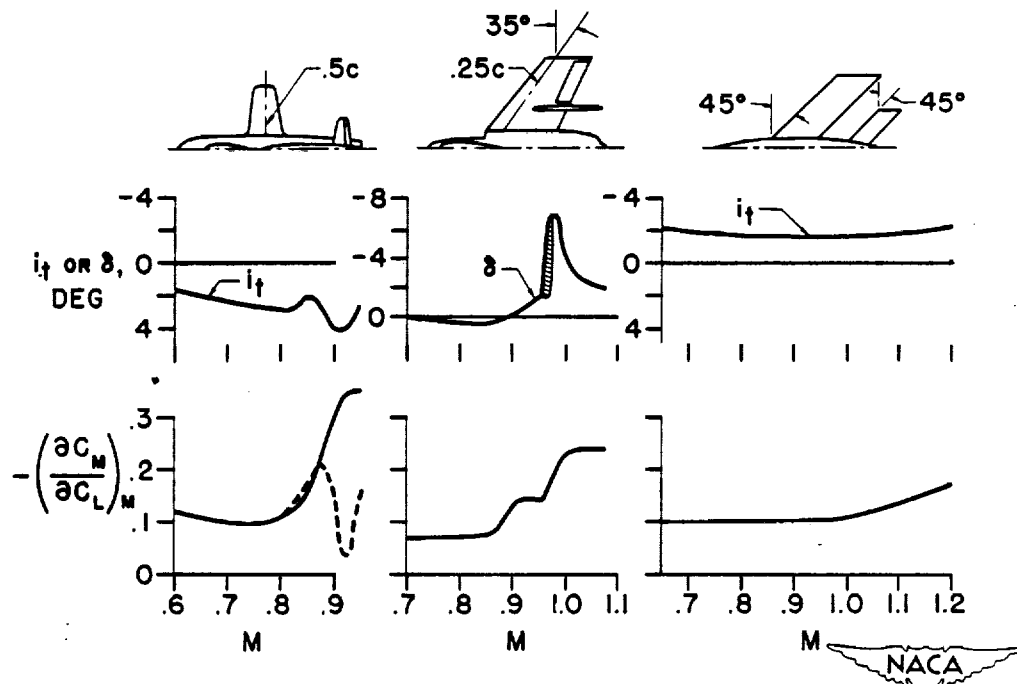
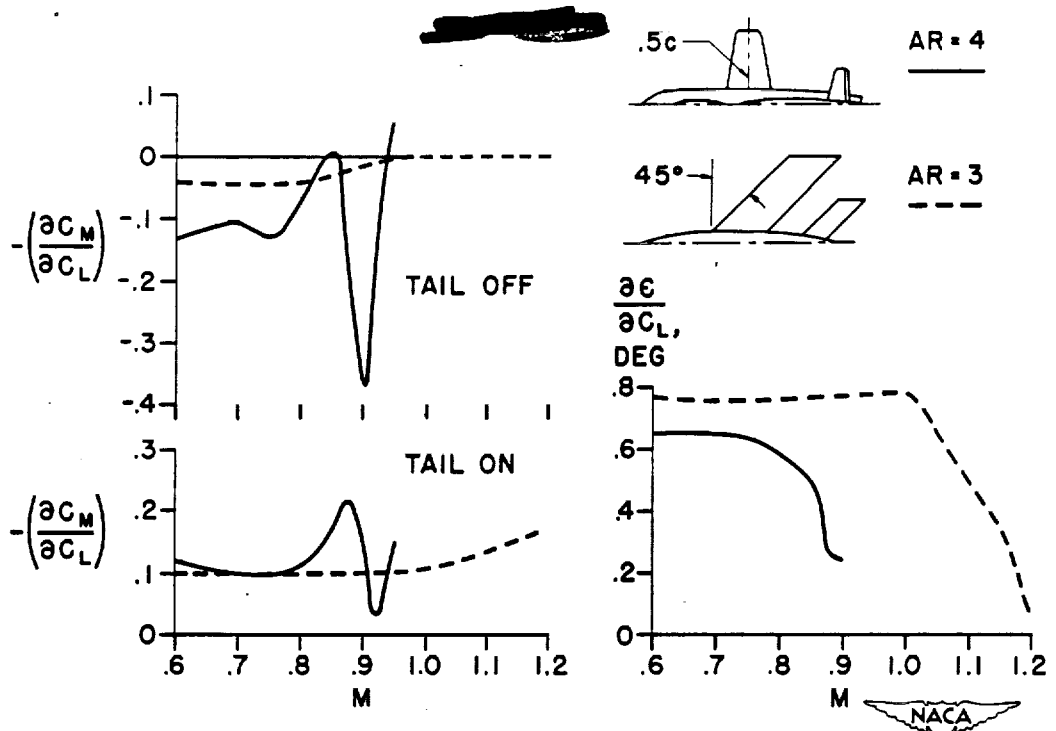


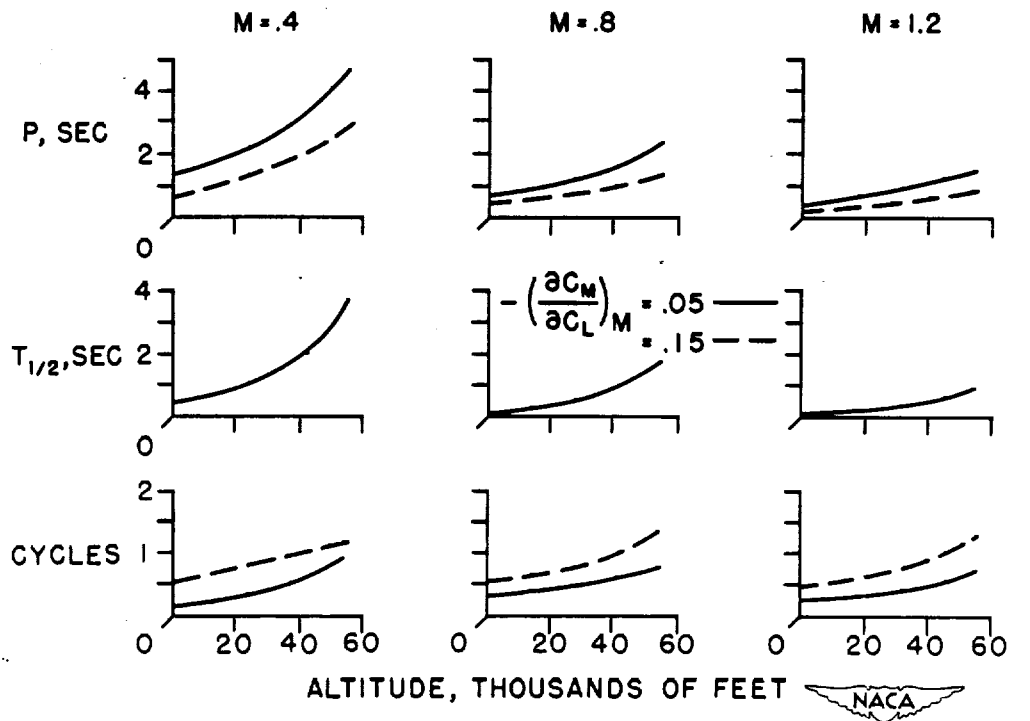
Figure 4.

Donlan



EFFECT OF SWEEP ON STABILITY COMPONENTS

Figure 5.



DYNAMIC STABILITY OF A TAILLESS DESIGN W/S=28.0

Figure 6.

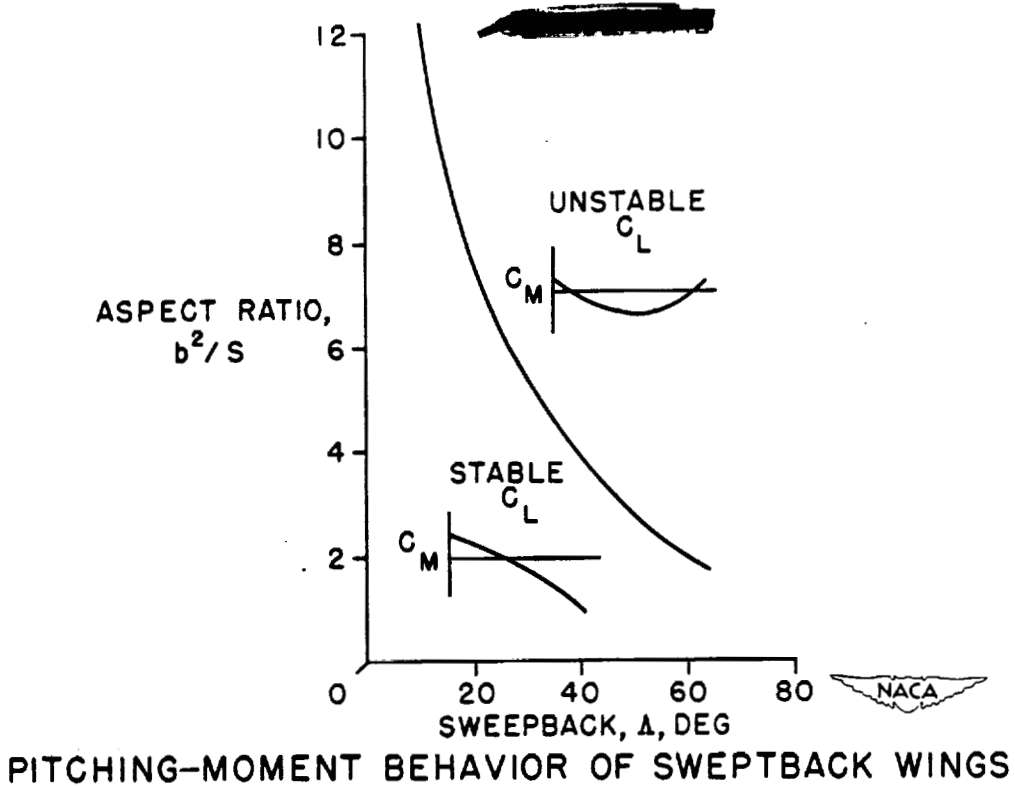


Figure 7.

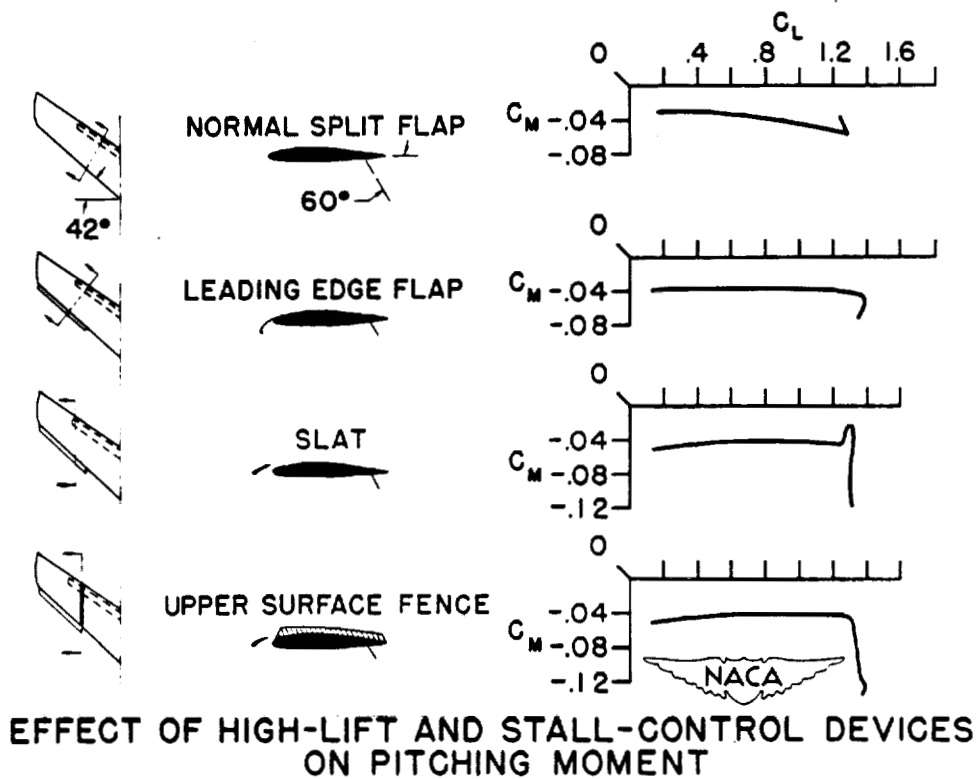
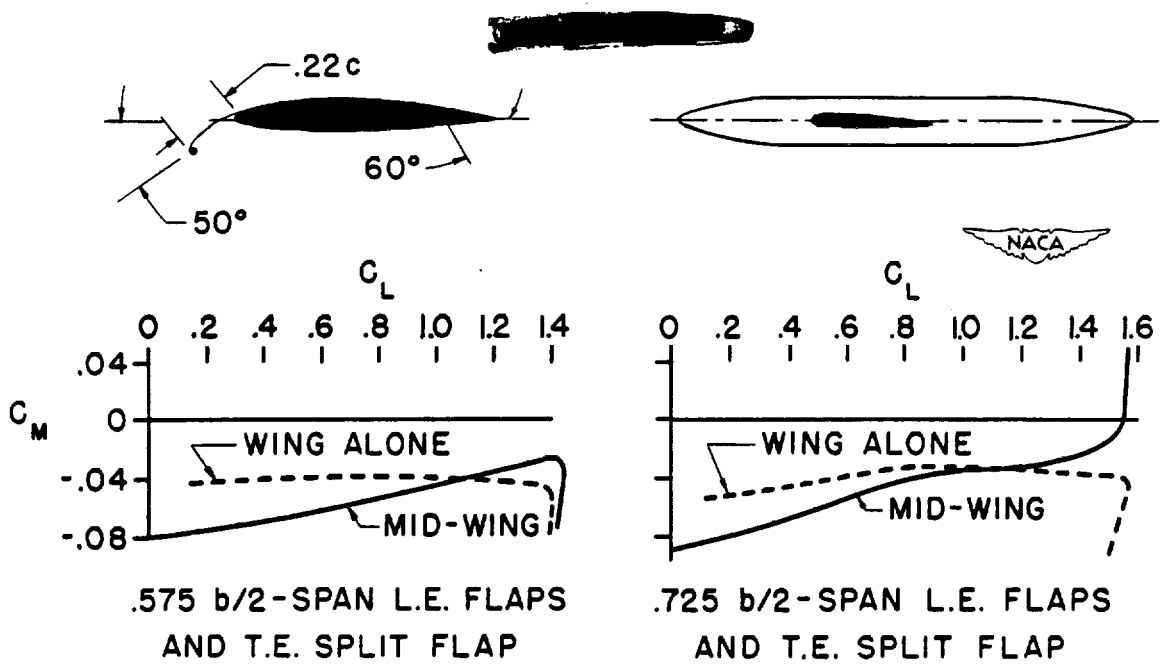
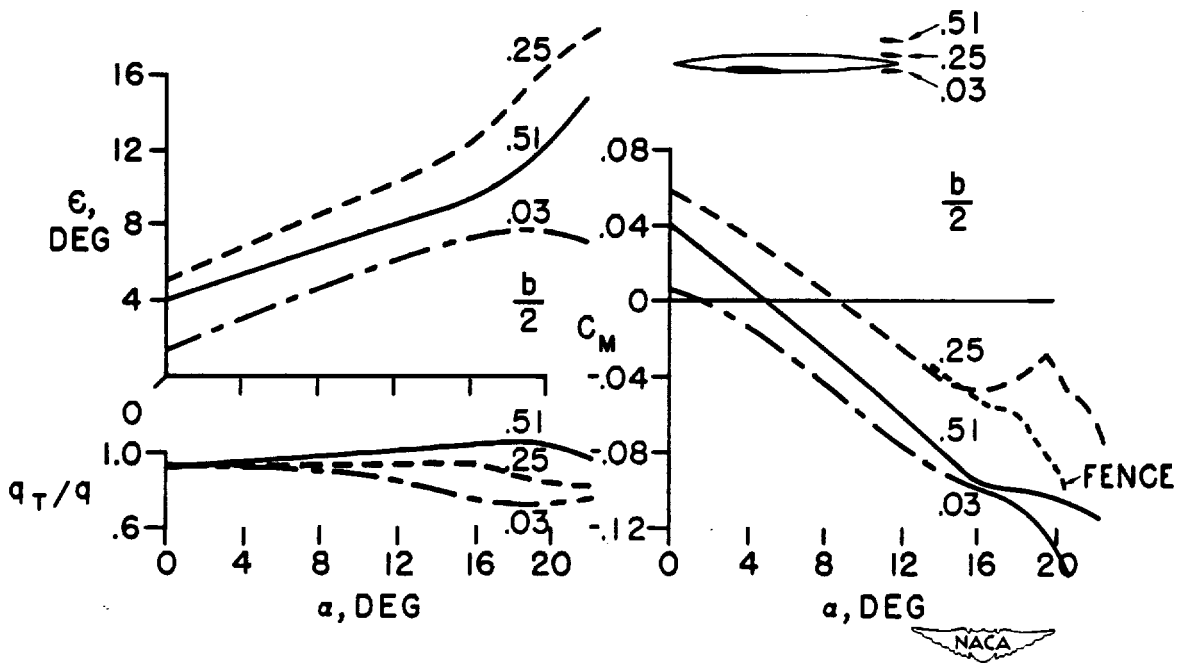


Figure 8.



EFFECT OF FUSELAGE ON PITCHING MOMENT

Figure 9.



EFFECT OF TAIL LOCATION

Figure 10.

## EFFECTS OF SWEEP ON CONTROLS

## I - EFFECTIVENESS

By John G. Lowry and Harold I. Johnson

Langley Memorial Aeronautical Laboratory

## INTRODUCTION

The design of controls for unswept wings that fly at low speed has been discussed in several papers (references 1 to 7). The design procedures set forth in these papers are adequate to allow for the prediction of control characteristics within small limits. However, with airplane speeds approaching and sometimes exceeding the critical speed of the wing surface, these low-speed characteristics are drastically changed. This paper will use the results of about 25 investigations (references 8 to 28) to indicate the nature of these changes and to discuss the design of controls on swept wing.

At the present time, information on the behavior of controls in the transonic speed range is too meager to permit the development of a rational design procedure that applies at transonic speeds. Because of this situation, the design of control surfaces for transonic airplanes must still be based primarily on low-speed considerations. At the same time, however, the experimental results that are available for transonic speeds indicate certain trends which should be kept in mind in order to reduce the unfavorable effects of compressibility at high speeds. With this thought in mind, therefore, some of the important experimental data at transonic speeds will be discussed and a design procedure based on low-speed data will be presented. For convenience, the discussion will be divided into aileron effectiveness, lift effectiveness, and pitching-moment effectiveness. However, it should be realized that the parameters are closely interdependent and hence, if a certain geometric design feature causes a particular change in one of the parameters, it will usually cause a corresponding change in the others.

## AILERON EFFECTIVENESS

## Effects of Compressibility

Effects of sweep.— Information on the effect of sweep on aileron effectiveness at high subsonic speeds was obtained recently from tests in the Langley 8-foot high-speed tunnel (references 8 and 9). These tests were run on a wing of NACA 65-210 section which for the unswept case had an aspect ratio of 9.0, a taper ratio of 0.4, and a 20-percent-chord plain aileron covering 37.5 percent of the wing semispan near the

tip. In order to obtain the swept-wing configurations, the straight wing was rotated about the 40-percent-root-chord point and the tips extended so that they were parallel to the airstream. This procedure changed somewhat the aspect ratio, taper ratio, and wing section parallel to the stream direction but retained the advantages inherent in testing the same model at different angles of sweep. Some typical results from the investigation are shown in figure 1.

Here we have the change in rolling-moment coefficient produced by 20° change in total aileron angle plotted against Mach number for the straight wing and for the two wings sweptback 32.6° and 47.6°. It is noted that the ailerons on the straight wing remained fully effective up to the critical Mach number of the wing which was 0.73 at design lift coefficient. Beyond the critical Mach number the ailerons continued to lose effectiveness up to the highest test Mach number of 0.925. This large loss in rolling-moment effectiveness at supercritical Mach numbers is apparently a direct reflection of the generally large loss in lift effectiveness of trailing-edge control surfaces on straight airfoils at supercritical Mach numbers. The effects of sweepback are seen to be twofold. First, the aileron effectiveness, before compressibility effects appear, is reduced approximately by the factor  $\cos^2 \Lambda$  in accordance with the simple theory of the effect of sweepback on flap effectiveness. Second, the Mach number at which compressibility effects first appear is raised by sweeping the wing back. For example, the aileron on the straight wing began to lose effectiveness at a Mach number of about 0.7, that on the 32.6° sweptback wing at a Mach number of 0.8, and that on the 47.6° sweptback wing at a Mach number of 0.9. It might be noted also that the drop-off in effectiveness due to compressibility effects becomes less abrupt as the sweepback angle is increased. These data show the desirability of resorting to sweepback in order to delay the loss in aileron control effectiveness that occurs at high subsonic speeds.

Some qualitative data on the effectiveness of ailerons at Mach numbers between the critical and 1.3 have been obtained by the Langley Pilotless Aircraft Research Division (reference 10) and are shown in figure 2. In these tests rocket-propelled test vehicles were fitted with low-aspect-ratio wing of NACA 65-series section having 20-percent-chord sealed ailerons deflected about 5° parallel to the relative wind. From continuous measurements of the rolling velocity and speed of the missiles the rolling-effectiveness parameter  $\frac{pb}{2V}$  was determined as a function of Mach number. It should be noted that this parameter  $\frac{pb}{2V}$  depends on the wing damping moment due to rolling as well as the aileron effectiveness so that some of the results are only qualitative with regard to aileron effectiveness. However, the results probably indicate correctly the effects of the various major design parameters on aileron effectiveness at transonic speeds. In figure 2 we have plotted the

$\frac{pb}{2V}$  per degree of aileron deflection against the flight Mach number.

It is seen that for these wings of 9-percent thickness and aspect ratio of 3 the unswept configuration experiences a sudden serious loss in aileron effectiveness at Mach numbers around 0.925. Because of the effects of rotational inertia of the rocket-propelled body and the longitudinal deceleration during these tests, the actual loss in effectiveness was somewhat greater than is shown by the data. As the sweepback angle is increased, the abrupt loss in effectiveness grows smaller until at a sweepback angle of  $45^\circ$  there appear to be no sudden changes in effectiveness through the transonic range. The aileron effectiveness at supersonic speeds is much less than at subsonic speeds for all sweepback angles, the difference being greatest for the unswept wing and least for the most highly swept wing.

Effect of thickness.— Other rocket tests (reference 10) have shown that airfoil section thickness appears to have a major effect on the loss in effectiveness of controls in the transonic range. Figure 3 illustrates this point. Here we have tests of two NACA 65-series symmetrical airfoils of different thickness ratios at an aspect ratio of 3.0. The 9-percent-thick section exhibited an abrupt loss in effectiveness at a Mach number of 0.925, but the 6-percent-thick section, although showing an equal loss in effectiveness from Mach number of 0.9 to 1.3, does not show the discontinuity at Mach numbers of about 0.9. Data for sweptback wings similar to that shown here indicated that for  $45^\circ$  sweepback, sudden changes in control effectiveness in the transonic speed range will be avoided if the thickness ratio is less than 10 or 12 percent. These data apply for deflections of  $5^\circ$  and therefore may not represent the variations for smaller deflections.

Effect of aspect ratio.— The effect of aspect ratio at  $45^\circ$  sweepback as determined from rocket tests (reference 10) is shown in figure 4. The control on the airfoil of aspect ratio 1.75 was considerably more effective than that of the airfoil of aspect ratio 3.0. This may very well be largely an effect of change in the damping moment due to rolling of the airfoils. The same trend in control effectiveness with aspect ratio was observed also on unswept airfoils of aspect ratio 1.75 and 3.0.

Effect of trailing-edge angle.— The trailing-edge angle of controls also appears to determine to a large extent the behavior of ailerons at transonic speeds. Some results from the Langley 8-foot high-speed tunnel (reference 8) and from the Ames 16-foot high-speed tunnel are shown in figure 5. This figure shows the rolling moment produced by aileron deflection for several wings at  $2^\circ$  angle of attack and at Mach numbers of about 0.85. We see that the aileron with a  $20^\circ$  trailing-edge angle on the unswept 12-percent-thick wing showed a reversal in effectiveness for the up-going aileron. This reversal of effectiveness extended to deflections of  $10^\circ$ , the largest tested. The aileron with the  $11^\circ$  trailing-edge angle on the unswept 10-percent-thick wing did not however show any

reversal even at slightly higher Mach numbers. Sweeping the wing with the large trailing-edge angle back  $47^\circ$ , as shown in this figure, also eliminated the reversal in effectiveness over the complete deflection range. Other Ames 16-foot high-speed-tunnel data (reference 16) indicate, however, that the trailing-edge angle of controls on swept wings is also critical. For example, ailerons with  $16.4^\circ$  trailing-edge angle on a  $37^\circ$  sweptback wing showed serious decreases in effectiveness with Mach number, whereas reducing the trailing-edge to  $11.2^\circ$  alleviated the large decrease in effectiveness. These results indicate two things: first, that the trailing-edge angle is important and should be kept as small as possible, and second, that sweeping the wing will reduce but will not necessarily eliminate the adverse effects of large trailing-edge angles on aileron effectiveness.

#### Aileron Design

Experimental results.— From the discussion thus far we see that the main effects of sweep are to delay the adverse effects of compressibility to higher Mach numbers and to reduce the magnitude of these effects when, and if, they do occur. In order to determine to what extent the design procedure for controls on unswept wings would have to be modified for swept wings, a semispan wing with an aspect ratio of 6 and taper ratio of  $1/2$  was tested in the Langley 300 MPH 7- by 10-foot tunnel, unswept and with three sweep angles (reference 11). The wing was equipped with a variable-span, plain-sealed, 20-percent-chord aileron.

The variation of the rate of change of rolling-moment coefficient with deflection  $C_{l\delta}$  with span of aileron for the various angles of sweep is shown in figure 6. The aileron for this investigation extended inboard from the tip but the data are applicable for other aileron locations. The variation of  $C_{l\delta}$  with sweep shown here also includes the effect of aspect ratio which varied from 6 for the straight wing to 3.43 for the  $51.3^\circ$  swept wing. It will be noted that as the sweep is increased and the aspect ratio decreases, the values of  $C_{l\delta}$  decrease considerably and that this decrease is even greater for ailerons located near the wing tip. It should be remembered, however, that these data are for low Mach numbers and Reynolds number of about  $2 \times 10^6$ . In order to make this chart of a more general nature, the data were reduced to the form more generally used — that is, the change in rolling moment for unit change in angle of attack over the aileron span  $\frac{C_l}{\Delta\alpha}$ . In making this reduction it was necessary to establish a nomenclature for swept wings. In order to be consistent with established procedures, the chords and spans of the swept wings are measured parallel and perpendicular to the plane of symmetry and the sweep angle is that of the wing leading edge (see fig. 7). The control surface deflections are measured in a plane perpendicular to the control hinge line. When the "unswept" wing



panel is referred to, it will represent the wing that would be obtained if the swept wing were rotated about the midpoint of the root chord until the 50-percent-chord line is perpendicular to the plane of symmetry. The tip is cut off parallel to the plane of symmetry. The chords in this case are measured perpendicular to the 50-percent-chord line. (The unswept spans and chords are primed in fig. 7.)

Design procedure.— In reducing the data of figure 6 from  $C_{l\delta}$  to  $\frac{C_l}{\Delta\alpha}$  as shown in figure 8, the values of  $C_{l\delta}$  at each spanwise station were divided by  $\cos^2\Lambda$  and the value of flap effectiveness parameter  $\alpha_\delta$  for the "unswept" wing panel. It will be noted that this method brought the curves together for large-span ailerons and for ailerons on wings swept less than  $30^\circ$ . The curve for  $\Lambda = 0^\circ$  to  $30^\circ$  agrees with the theoretical curve (reference 2) for the same aspect ratio and taper ratio as the unswept wing. Short-span tip ailerons show, however, a loss in effectiveness for the higher sweep angles and indicate that on highly swept wings a partial-span aileron located slightly inboard will give more rolling moment than the same aileron located at the wing tip.

In using this chart for design purposes, it is necessary to correct the values of  $\frac{C_l}{\Delta\alpha}$  for aspect ratio, taper, and flap chord. Aileron effectiveness  $C_{l\delta}$  is obtained by using the formula at the top of the figure where  $\frac{C_l}{\Delta\alpha}$  is obtained from the appropriate curve on this chart. The aspect-ratio correction  $K_1$  is the ratio of  $\frac{C_l}{\Delta\alpha}$  for the aspect ratio of the "unswept" wing to the value of  $\frac{C_l}{\Delta\alpha}$  for aspect ratio 6 (obtained from reference 2) and for taper ratio of 1/2. The taper-ratio correction  $K_2$  is the ratio of the value of  $\frac{C_l}{\Delta\alpha}$  for the taper ratio of the "unswept" wing to the value of  $\frac{C_l}{\Delta\alpha}$  for taper ratio of 1/2; both values (obtained from reference 2) are for aspect ratio 6. The flap effectiveness parameter  $\alpha_\delta$  is based on the unswept-aileron-chord ratio (see reference 1) and  $\Lambda$  is the sweep of the wing leading edge. The values of  $C_{l\delta}$  thus obtained are for low lift coefficients and for small deflections, and some changes will occur if either is varied considerably.

Effect of deflection.— Figure 9 shows the ratio of  $C_{l\delta}$  obtained at large aileron deflections to the values of  $C_{l\delta}$  obtained from the previous figures. It will be noted that the loss in  $C_{l\delta}$  for larger deflections is less for the swept wing than for the straight wing. The difference appears to be about the same as the difference in deflections

of the ailerons on the two wings measured in the stream direction. Thus, it would appear that larger deflections can be used on swept wings which would tend to alleviate the low effectiveness of the ailerons. The results of swept-wing-aileron investigations indicate that the effectiveness, as with straight wings, is relatively constant with lift coefficient so long as no unusual or sudden changes in flow occur over the wing.

Comparison of estimated and test results.— In order to determine the reliability of this method in predicting  $C_{l8}$  for wings of other sweeps, aspect ratios, and taper ratios, values of  $C_{l8}$  were estimated for 14 wings and are compared in figure 10 with the measured values.

Figure 10 is a plot of  $C_{l8_{est}}$  against  $C_{l8_{test}}$ ; the solid line is the line of agreement. The scatter of points around the line of agreement indicates that the method gives good agreement for these rather conventional sweptback wings, that is, wings of aspect ratio between 2.5 to 6 and taper ratios between 0.4 to 1. This method, however, cannot be expected to give as good results for all cases of swept wings, particularly for those of extremely low aspect ratio and/or with extreme taper.

## LIFT EFFECTIVENESS

### Effects of Compressibility

Effects of sweep.— The problem of control lift effectiveness is closely related to the problem of aileron rolling effectiveness. In the case of ailerons, we are interested in the rolling moment caused by the lift effectiveness of a control located some distance outboard on a wing. In the case of an elevator or a rudder, we are interested directly in the lift effectiveness of the control, inasmuch as this lift effectiveness determines how much elevator control will be required to pitch the airplane through its angle-of-attack range or how much rudder control will be required to offset yawing moments due to the use of ailerons, asymmetric power, and so forth. Because of the close functional relationship between all the primary controls, therefore, one might expect to find that the effects of compressibility on the lift effectiveness of elevators and rudders will be largely the same as the effects of compressibility on the rolling-moment effectiveness of ailerons and vice versa. This expectation is borne out by an analysis of the available experimental data pertaining to full-span controls that would likely be used as elevators and rudders. Some effects of compressibility on the lift effectiveness of such controls will be considered now.

An examination of the data for full-span control surfaces on unswept airfoils, tested recently in the Langley 3-foot high-speed tunnel, the Langley 16-foot high-speed tunnel, and the Langley 24-inch high-speed tunnel (references 15 and 25 to 28), permit two conclusions to be made regarding lift effectiveness at high subsonic speeds. First, below the critical speed of the airfoil the control lift effectiveness is essentially unaffected by compressibility effects. Second, at speeds slightly above the critical speed the controls tested always experienced an abrupt loss in effectiveness which continued up to the highest speed tested. The data suggest that the control effectiveness for small deflections for these unswept configurations of conventional thickness would probably reverse at Mach numbers in the neighborhood of 0.9.

Further light is shed on this phenomenon by results obtained from wing-flow tests (references 12 and 13), which are shown in figure 11. This plot shows the control-effectiveness parameter  $C_{L\delta}$ , measured over  $\pm 4^\circ$  control deflection, plotted against Mach number. Data are shown for an unswept configuration of 10-percent thickness, the actual sweep of leading edge being  $13^\circ$ , and for a  $35^\circ$  sweptback configuration of 9-percent thickness. It is noted that the control effectiveness for the unswept tail surface actually did reverse for small deflections at a Mach number of approximately 0.95. At higher Mach numbers the control regained effectiveness for small deflections. It may be noted also that the sweptback configuration did not lose completely its control effectiveness at any speed up to a Mach number of 1.10. Actually, the control effectiveness of the sweptback configuration fell off by about 40 percent from its low-speed value. Although these data were obtained at very low Reynolds number, that is, approximately one million, there is no proof that the phenomenon of control reversal shown by the unswept configuration will not occur also at higher Reynolds numbers, perhaps to a different degree. From figure 11 it should not be assumed that the unswept control had reversed effectiveness at all deflections.

Effect of deflection.— Figure 12 will show how the lift produced by the control varies with deflection at different Mach numbers for the straight tail surface. One curve is for a Mach number of 0.35 where the force break occurred, one is for a Mach number of 0.96 where the control effectiveness was reversed, and one is for a Mach number of 1.04 where the control had regained effectiveness at all deflections.

It should be noted that, although the flap gave a net loss in lift between deflections of  $-4^\circ$  and  $4^\circ$  at a Mach number of 0.96, as was shown in figure 11 by the negative value for  $C_{L\delta}$  at higher deflections, the flap produced lift in the proper direction. Hence, it would probably be possible to use such a control for trimming in combination with an adjustable stabilizer or an adjustable fin at transonic speeds,

but it is believed everyone would object to such a control because of the illogical type of control motion it would introduce. In this connection, however, floating-model tests of very thin unswept airfoils have not shown reversed control effectiveness at transonic speeds for the moderately small deflections that were tested. Hence, it seems premature to condemn completely the use of unswept configurations at transonic speeds. Much more data is needed to determine the effects of airfoil thickness, of flap trailing-edge angle, and of possibly other geometric parameters on the flap effectiveness of unswept tail surfaces. For the present time, however, we know that the flap on the 9-percent-thick,  $35^\circ$  sweptback tail surface showed no signs of complete loss of effectiveness even for small deflection at any speed up to a Mach number of 1.10, the highest Mach number reached.

#### Design Procedure

Since the control lift effectiveness is so closely related to the aileron rolling effectiveness, the design of controls such as elevators on tailless aircraft will not be discussed in detail. The lift effectiveness parameter  $C_{L\delta}$  however showed about the same variation with sweep as did the aileron effectiveness; that is, there was a decrease in  $C_{L\delta}$  with increase in sweep and decrease in aspect ratio (see fig. 13). Reducing these data to eliminate the sweep angle and flap chord by dividing the values of  $C_{L\delta}$  at each spanwise station by  $\cos^2\Lambda$  and  $c\delta$  of the "unswept" control brought the curves together except for the small-span controls on highly swept wings which again showed a loss in effectiveness (see fig. 14). The values of  $C_{L\delta}$  for other wings equipped with tip controls may be obtained in a manner similar to the aileron effectiveness, except that the aspect-ratio correction is the ratio of the lift-curve slope for the "unswept" wing to the lift-curve slope for aspect ratio 6 ( $K_3$ ) (see fig. 14). As with aileron effectiveness, the reliability of this method was checked by estimating  $C_{L\delta}$  for nine wings and comparing with the measured value of  $C_{L\delta}$ . Good agreement was obtained for all wings except two for which the control was located other than at the tip. Since unswept lift data indicate the lift effectiveness is different for controls starting at the tip than for those starting at the root, this disagreement would probably be expected. Thus, in addition to the restriction placed on the method of prediction of aileron effectiveness, that is, aspect ratio and taper ratio, we must also limit this method to controls starting at the wing tip.

## PITCH EFFECTIVENESS

### Effects of Compressibility

Reproduced from  
best available copy.

In addition to a knowledge of the effects of compressibility on aileron characteristics and lift effectiveness, the designer of a high-speed flying-wing-type airplane needs to know what the effects of compressibility will be on the pitching moment produced by trailing-edge flaps. Here, the emphasis is on sweptback configurations almost entirely because of the necessity for providing a reasonably large, allowable, center-of-gravity range together with a reasonably high, trimmed, maximum lift coefficient. Some data showing the effects of compressibility on the pitching-moment effectiveness of longitudinal controls on sweptback wings are shown in figure 15.

This figure shows the pitching-moment parameter  $C_{m\delta}$  plotted against Mach number for various sweptback wing-flap combinations (references 12 and 14). The pitching-moment slopes shown here are with reference to a point at 17 percent of the mean aerodynamic chord of each of the wings. This point was found to be the low-speed aerodynamic-center location for the isolated wings, having  $35^\circ$  and  $45^\circ$  of sweepback and an aspect ratio of 3, which are shown in this figure. It is seen that the effects of compressibility on pitching-moment control are relatively small at all speeds tested which are up to a Mach number of 1.1. The maximum loss in effectiveness of the  $\frac{1}{4}$ -chord plain flap on the  $35^\circ$  sweptback NACA 65-009 airfoil, which was the only configuration tested through the speed of sound, was about 30 percent. Partial-span flaps on the tapered  $35^\circ$  sweptback wing show a similar tendency to lose pitching-moment effectiveness as the speed of sound is approached. With  $45^\circ$  of sweepback, the longitudinal control effectiveness of the full-span 25-percent-chord flap on a 12-percent-thick wing was completely unaffected by compressibility up to a Mach number of 0.89. These data indicate that trailing-edge-type longitudinal controls will retain considerable pitching-moment effectiveness at transonic speeds if as much as  $35^\circ$  sweepback is used and if the wing thickness is not too great; for the cases under consideration the maximum thickness was about 12 percent.

### Effects of Sweep

The limited amount of low-speed data for the effects of sweep and spanwise location on the pitch effectiveness does not permit the construction of design charts. The pitching-moment data for one series of swept wings do, however, show consistent variations with sweep for sweep angles greater than  $30^\circ$  (fig. 16) but are not complete enough to account for all the variables.

CONFIDENTIAL

~~SECRET~~

CONFIDENTIAL

### CONCLUSIONS

It appears from the data presented that no serious problems resulting from compressibility effects will be encountered so long as the speeds are kept below the critical speed of the wing or tail surface and the trailing-edge angle is kept small, that is, less than about  $14^\circ$ . Above critical speeds, however, the behavior of the control depends to a large extent on the wing sweep angle. The main effects of sweeping the wing or tail are to postpone to higher Mach numbers the adverse effects of compressibility and to decrease these adverse effects when they occur. The design procedures presented, although of a preliminary nature, appear to offer a method of estimating the effectiveness of flap-type controls on swept wings of normal aspect ratio and taper ratio.

~~SECRET~~

## REFERENCES

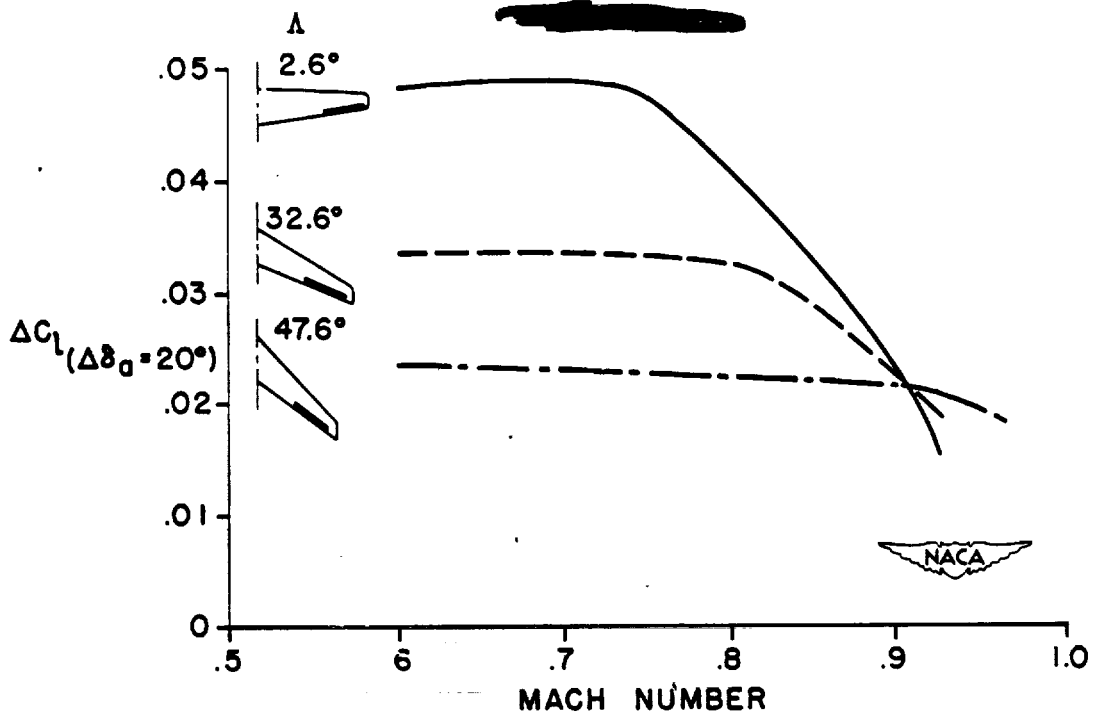
1. Langley Research Department: Summary of Lateral-Control Research (Compiled by Thomas A. Toll.) NACA TN No. 1245, 1947.
2. Weick, Fred E., and Jones, Robert T.: Résumé and Analysis of N.A.C.A. Lateral Control Research. NACA Rep. No. 605, 1937.
3. Ames, Milton B., Jr., and Sears, Richard I.: Determination of Control-Surface Characteristics from NACA Plain-Flap and Tab Data. NACA Rep. No. 721, 1941.
4. Crane, Robert M.: Computation of Hinge-Moment Characteristics of Horizontal Tails from Section Data. NACA CB No. 5B05, 1945.
5. Swanson, Robert S., and Crandall, Stewart M.: Lifting-Surface-Theory Aspect-Ratio Corrections to the Lift and Hinge-Moment Parameters for Full-Span Elevators on Horizontal Tail Surfaces. NACA TN No. 1175, 1947.
6. Fischel, Jack, and Ivey, Margaret F.: Collection of Test Data for Lateral Control with Full-Span Flaps. NACA TN No. 1404, 1947.
7. Pitkin, Marvin, and Maggin, Bernard: Analysis of Factors Affecting Net Lift Increment Attainable with Trailing-Edge Split Flaps on Tailless Airplanes. NACA ARR No. L4I13, 1944.
8. Luoma, Arvo A.: An Investigation of a High-Aspect-Ratio Wing Having 0.20-Chord Plain Ailerons in the Langley 3-Foot High-Speed Tunnel. NACA RM No. L6H28d, 1946.
9. Luoma, Arvo A., Bielat, Ralph P., and Whitcomb, Richard T.: A Wind-Tunnel Investigation of the Lateral Control Characteristics of Plain Ailerons on a Wing with Various Amounts of Sweep. NACA RM No. L7I15, 1947.
10. Sandahl, Carl A., and Strass, H. Kurt: Additional Results in a Free-Flight Investigation of Control Effectiveness of Full-Span, 0.2-Chord Plain Ailerons at High Subsonic, Transonic, and Supersonic Speeds to Determine Some Effects of Wing Sweepback, Aspect Ratio, Taper, and Section Thickness Ratio. (Prospective NACA paper)
11. Fischel, Jack, and Schneider, Leslie E.: Low-Speed Wind-Tunnel Investigation of a  $51^\circ$  Sweptback Semispan Wing Equipped with Ailerons Having Three Spans and Three Trailing-Edge Angles. (Prospective NACA paper)

12. Johnson, Harold I.: Measurements of the Aerodynamic Characteristics of a  $35^\circ$  Sweptback NACA 65-009 Airfoil Model with  $\frac{1}{4}$ -Chord Plain Flap by the NACA Wing-Flow Method. NACA RM No. L7F13, 1947.
13. Adams, Richard E., and Silsby, Norman S.: Tests of a Horizontal-Tail Model through the Transonic Speed Range by the NACA Wing-Flow Method. NACA RM No. L7C25a, 1947.
14. Kuhn, Richard E., and King, Thomas J., Jr.: An Investigation of the Aerodynamic Characteristics of an 0.08-Scale Model of the Chance Vought XF7U-1 Airplane in the Langley High-Speed 7- by 10-Foot Tunnel. Part III - Longitudinal Control Characteristics. TED No. NACA DE308. NACA RM No. L7E01, Bur. Aero., 1947.
15. Bielat, Ralph P.: Investigation at High Speeds of a Horizontal-Tail Model in the Langley 8-Foot High-Speed Tunnel. NACA RM No. L6L10b, 1947.
16. Boddy, Lee E., and Morrill, Charles P., Jr.: The Aerodynamic Effects of Modifications to the Wing and Wing-Fuselage Intersection of an Airplane Model with the Wing Swept Back  $35^\circ$ . NACA RM No. A7J02, 1947.
17. Schuldenfrei, Marvin, Comisarow, Paul, and Goodson, Kenneth W.: Stability and Control Characteristics of an Airplane Model Having a  $45.1^\circ$  Swept-Back Wing with Aspect Ratio 2.50 and Taper Ratio 0.42 and  $42.8^\circ$  Swept-Back Horizontal Tail with Aspect Ratio 3.87 and Taper Ratio 0.49. NACA RM No. L7B25, 1947.
18. Goodson, Kenneth W., and Comisarow, Paul: Lateral Stability and Control Characteristics of an Airplane Model Having a  $42.8^\circ$  Sweptback Circular-Arc Wing with Aspect Ratio 4.00, Taper Ratio 0.50, and Sweptback Tail Surfaces. NACA RM No. L7G31, 1947.
19. Gilruth, R. R., and Wetmore, J. W.: Preliminary Tests of Several Airfoil Models in the Transonic Speed Range. NACA ACR No. L5E08, 1945.
20. Daum, Fred L., and Sawyer, Richard H.: Tests at Transonic Speeds of the Effectiveness of a Swept-Back Trailing-Edge Flap on an Airfoil Having Parallel Flat Surfaces, Extreme Sweepback, and Low Aspect Ratio. NACA CB No. L5H01, 1945.



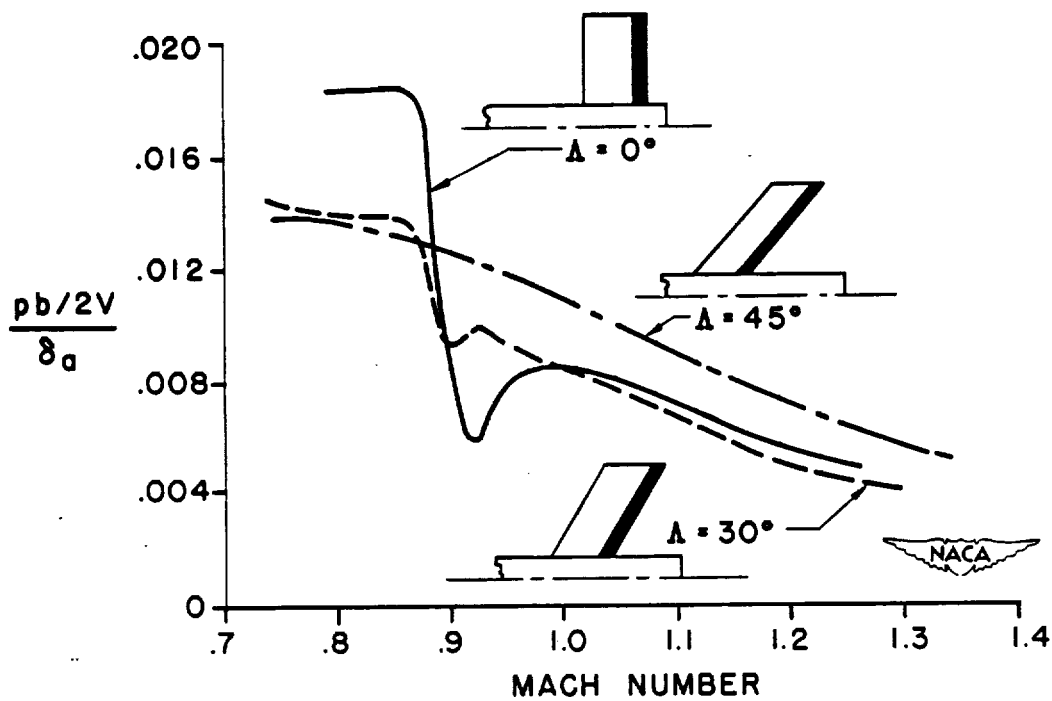
21. Bennett, Charles V., and Johnson, Joseph L.: Experimental Determination of the Damping in Roll and Aileron Rolling Effectiveness of Three Wings Having  $2^\circ$ ,  $42^\circ$ , and  $62^\circ$  Sweep-back. NACA TN No. 1278, 1947.
22. Goodson, Kenneth W., and Myers, Boyd C., II: An Investigation of the Aerodynamic Characteristics of an 0.08-Scale Model of the Chance Vought XF7U-1 Airplane in the Langley High-Speed 7- by 10-Foot Tunnel. Part IV - Aileron Characteristics. TED No. NACA DE308. NACA RM No. L7H22, Bur. Aero., 1947.
23. Letko, William, and Goodman, Alex: Preliminary Wind-Tunnel Investigation at Low Speed of Stability and Control Characteristics of Swept-Back Wings. NACA TN No. 1046, 1946.
24. Feigenbaum, David, and Goodman, Alex: Preliminary Investigation at Low Speeds of Swept Wings in Rolling Flow. NACA RM No. L7E09, 1947.
25. Schueller, Carl F., Korycinski, Peter F., and Strass, H. Kurt: Tests of a Full-Scale Horizontal Tail Surface in the Langley 16-Foot High-Speed Tunnel. NACA TN No. 1074, 1946.
26. Schueller, Carl F., Hieser, Gerald, and Cooper, Morton: Aerodynamic Force Characteristics at High Speeds of a Full-Scale Horizontal Tail Surface Tested in the Langley 16-Foot High-Speed Tunnel. NACA RM No. L7D08a, 1947.
27. Lindsey, W. F.: Effect of Compressibility on the Pressures and Forces Acting on a Modified NACA 65,3-019 Airfoil Having a 0.20-Chord Flap. NACA ACR No. L5G31a, 1946.
28. Ilk, Richard J.: Characteristics of a 15-Percent-Chord and a 35-Percent-Chord Plain Flap on the NACA 0006 Airfoil Section at High Subsonic Speeds. NACA RM No. A7H19, 1947.

Lowry



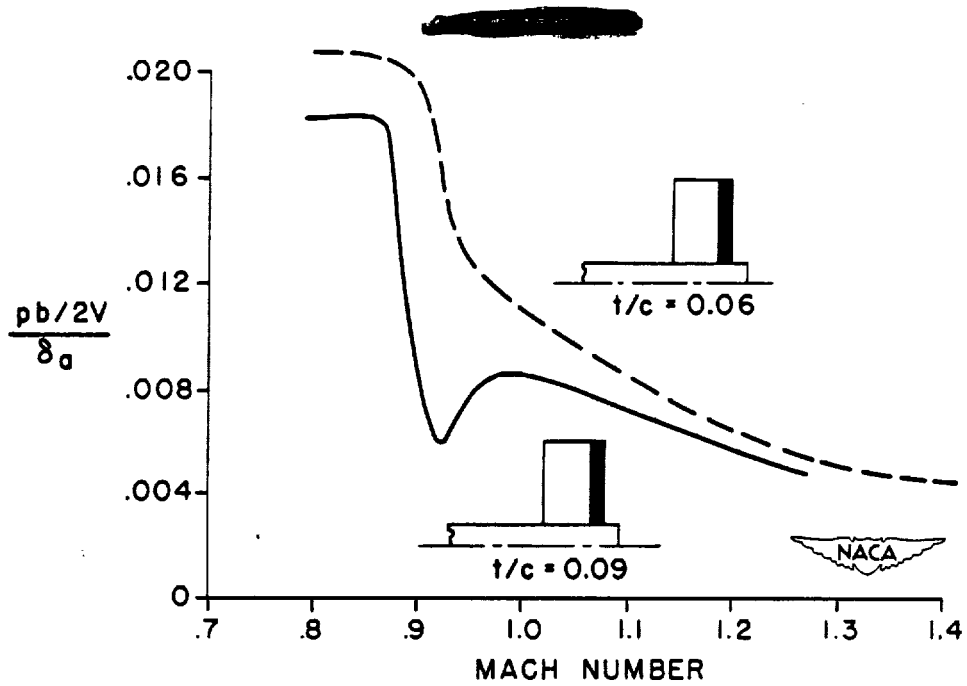
### AILERON EFFECTIVENESS AT HIGH SUBSONIC SPEEDS

Figure 1.



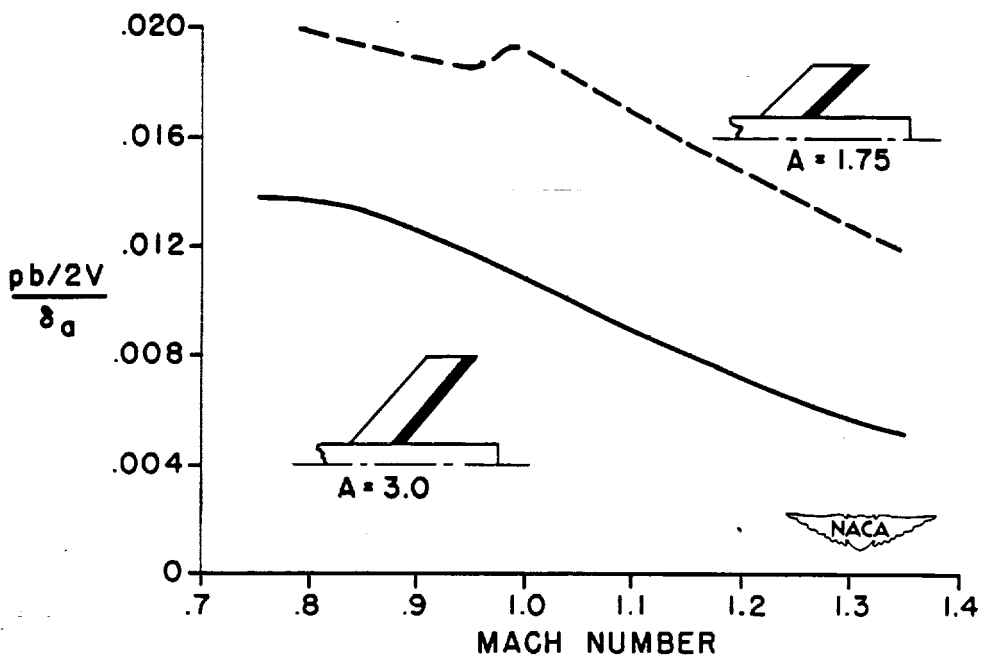
### ROLLING EFFECTIVENESS AT TRANSONIC SPEEDS

Figure 2.



EFFECT OF THICKNESS ON ROLLING EFFECTIVENESS AT TRANSONIC SPEEDS

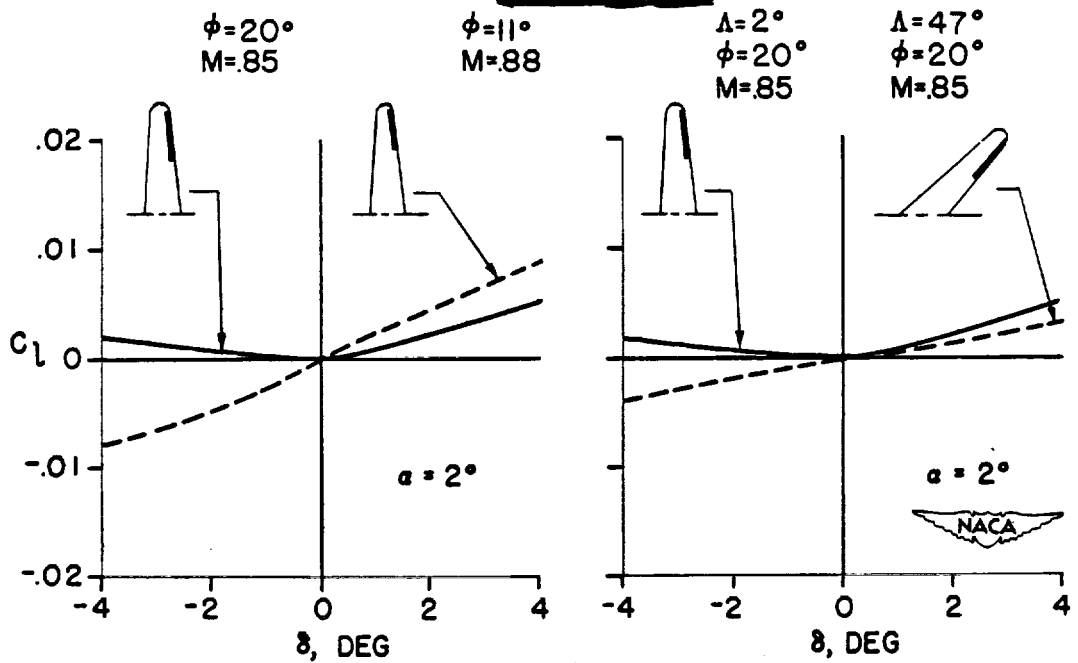
Figure 3.



EFFECT OF ASPECT RATIO ON ROLLING EFFECTIVENESS AT TRANSONIC SPEEDS

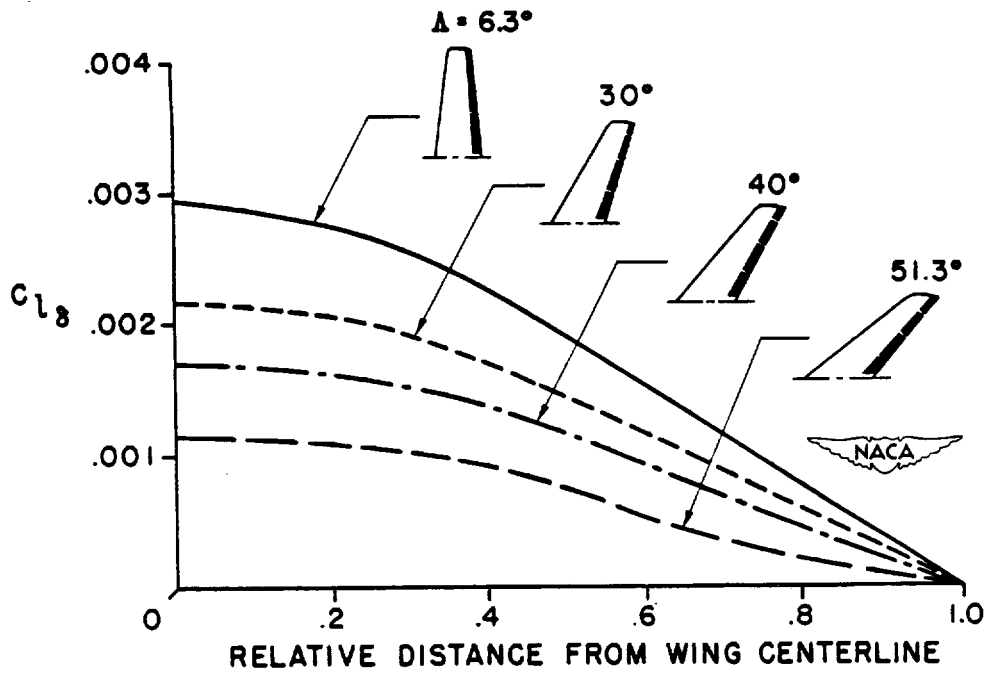
Figure 4.

Lowry



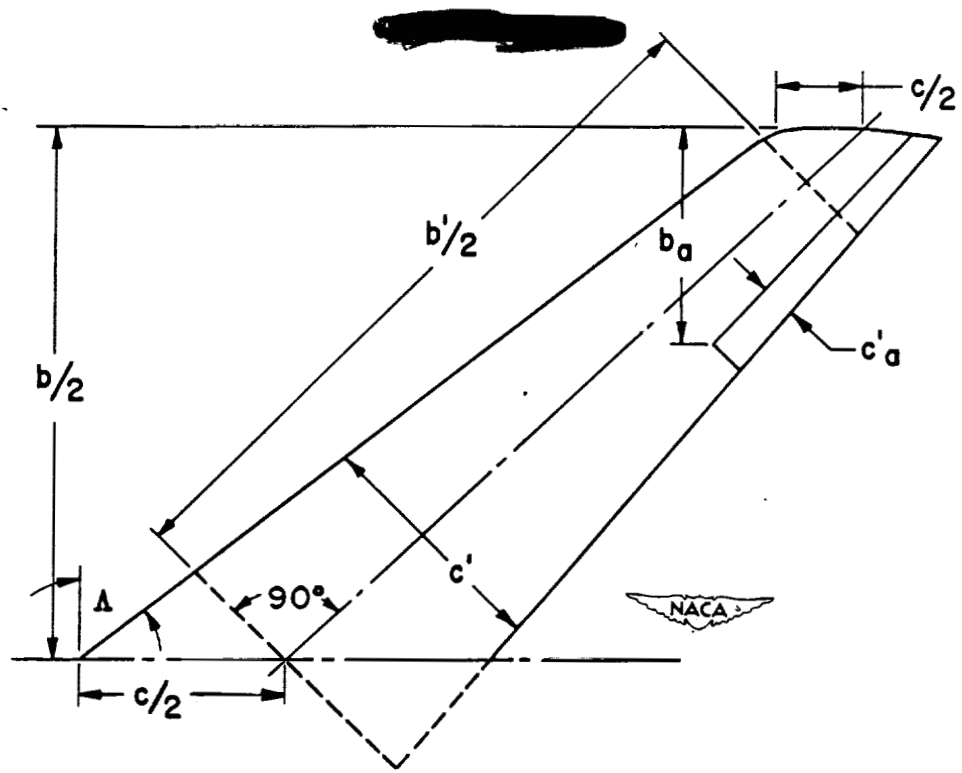
EFFECTS OF TRAILING-EDGE ANGLE AND SWEEP ON AILERON EFFECTIVENESS

Figure 5.



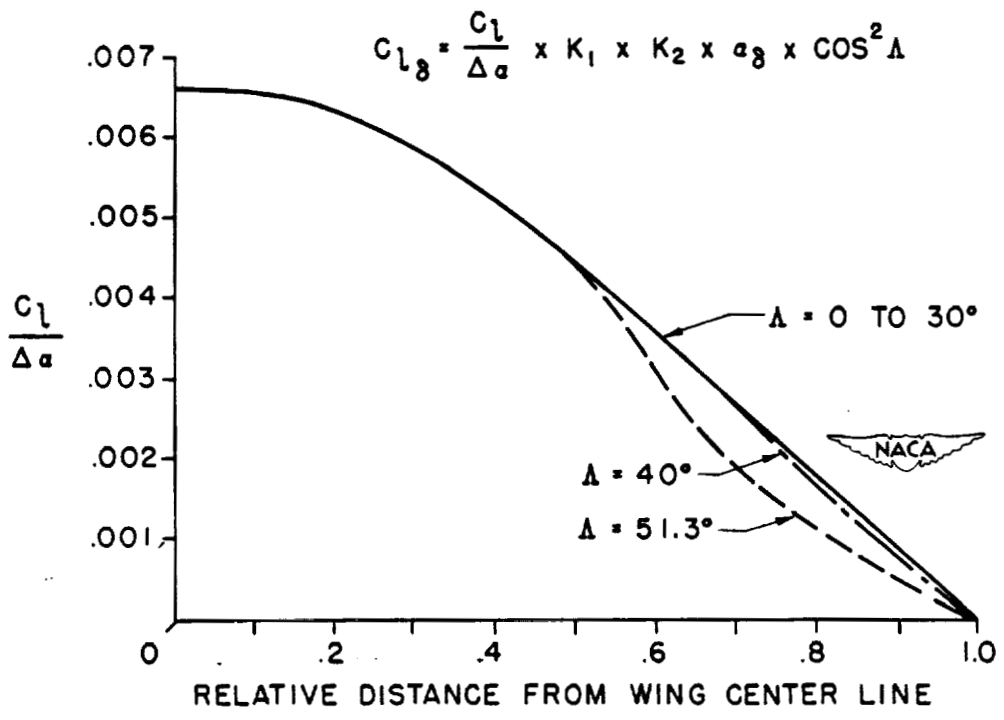
EFFECT OF SWEEP AND SPANWISE LOCATION ON AILERON EFFECTIVENESS

Figure 6.



Swept-wing nomenclature.

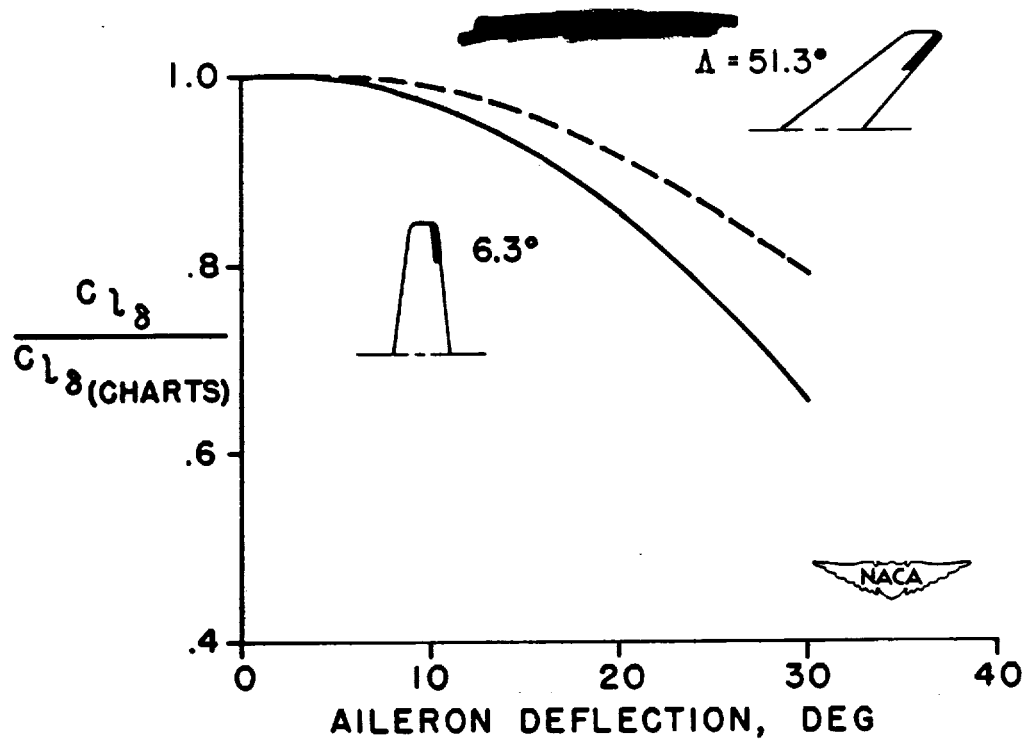
Figure 7.



DESIGN CHART FOR AILERONS ON SWEEP WINGS

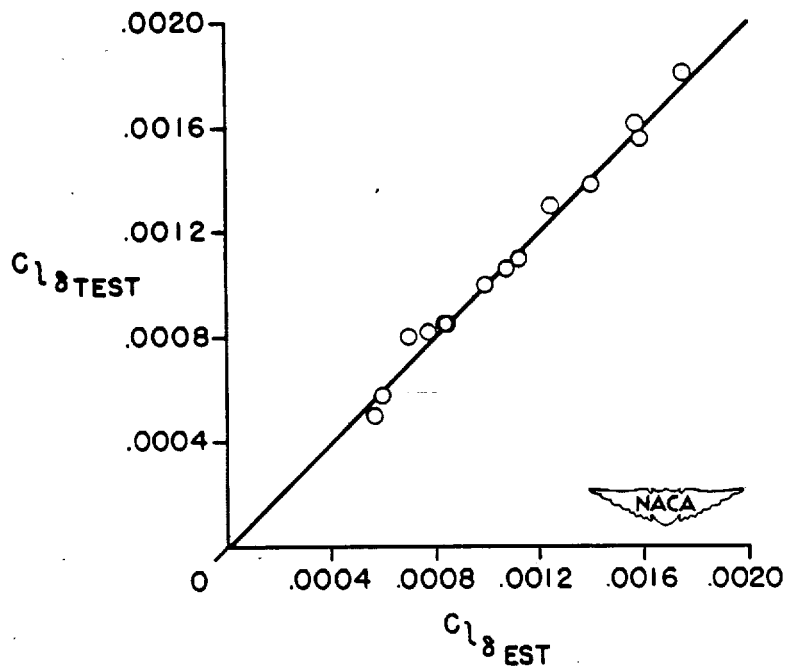
Figure 8.

Lowry



### LOSS IN EFFECTIVENESS AT LARGE DEFLECTIONS

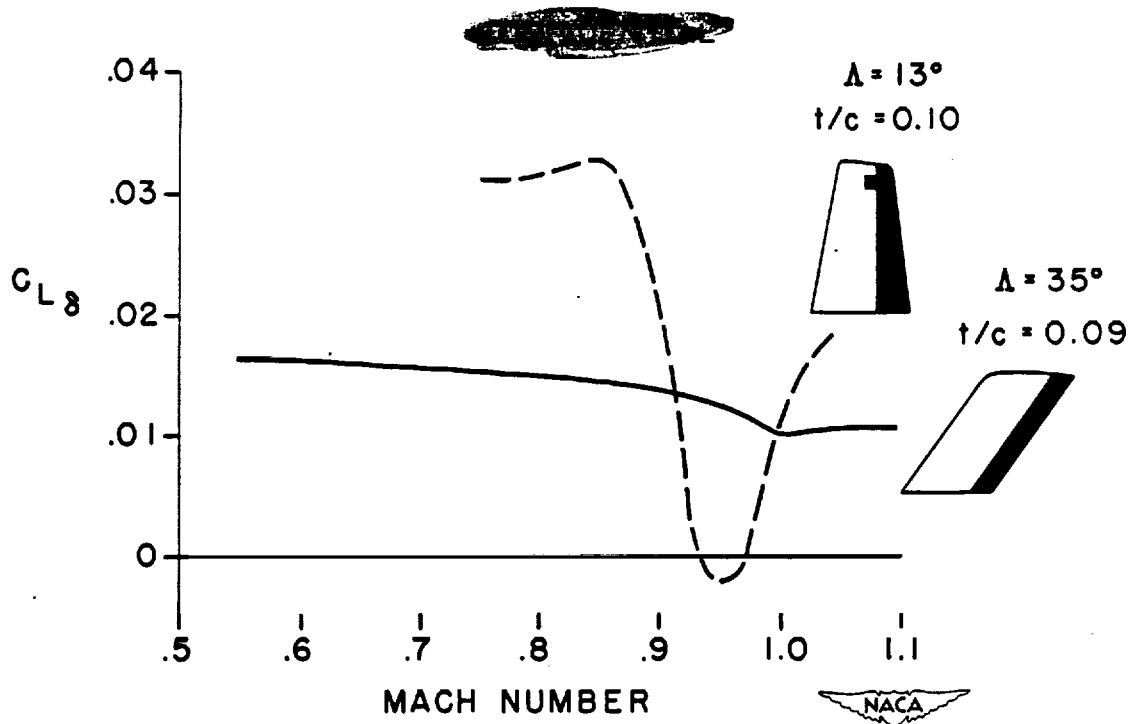
Figure 9.



### COMPARISON OF ESTIMATED AND EXPERIMENTAL AILERON EFFECTIVENESS

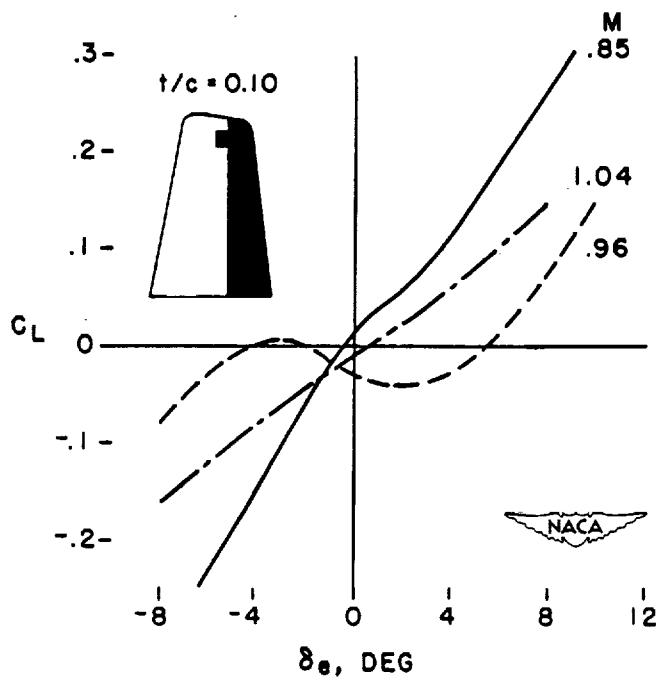
Figure 10.

126 d 7



CONTROL EFFECTIVENESS AT TRANSONIC SPEEDS

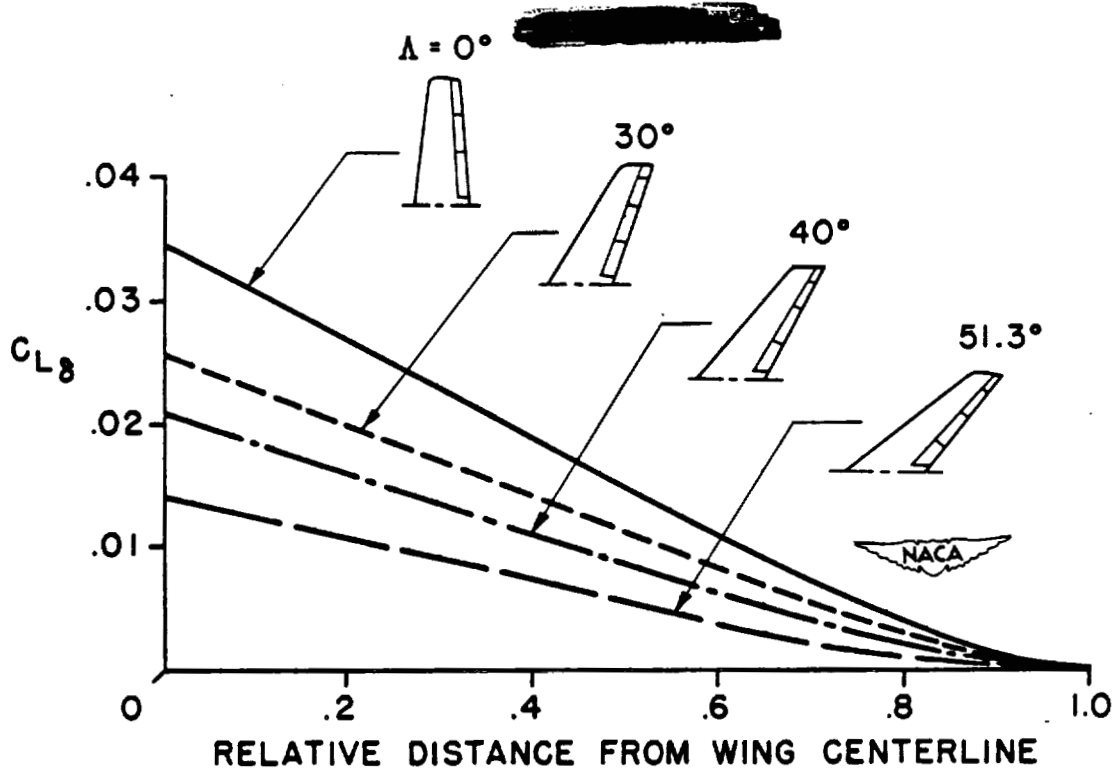
Figure 11.



VARIATION OF CONTROL EFFECTIVENESS WITH DEFLECTION

Figure 12.

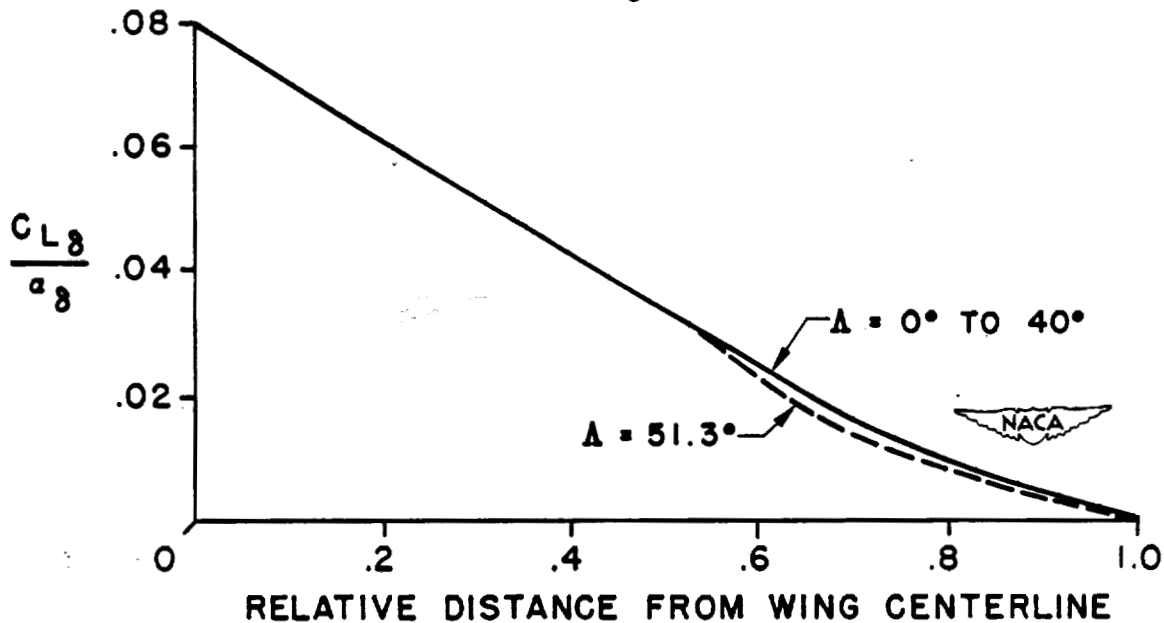
Lowry



Effect of sweep and spanwise location on control effectiveness.

Figure 13.

$$C_{L\delta} = \frac{C_{L\delta}}{a_\delta} \times K_3 \times a_\delta \times \cos^2 \Lambda$$

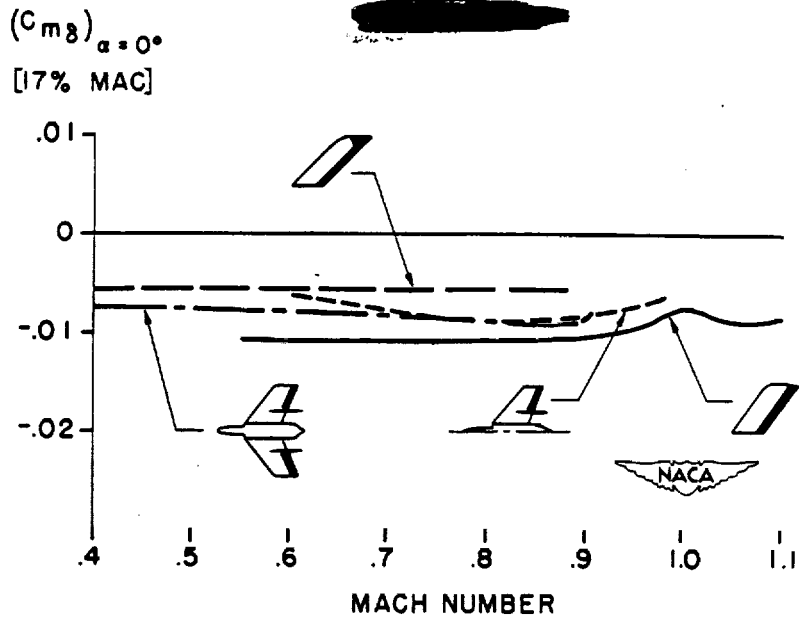


Design chart for  $C_{L\delta}$  on swept wing.

Figure 14.

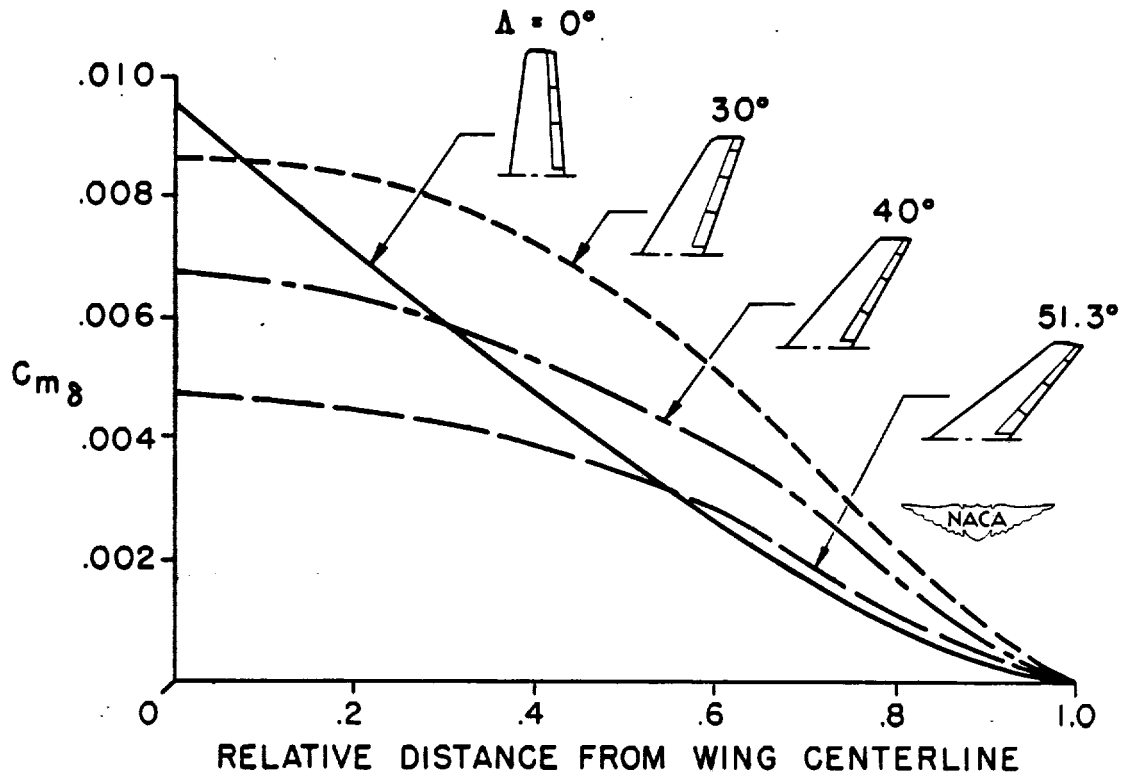
~~SECRET~~  
126(f)





PITCH CONTROL AT TRANSONIC SPEEDS

Figure 15.



Effect of sweep and span on  $C_{m\delta}$

Figure 16.

D/5

EFFECTS OF SWEEP ON CONTROLS

II - HINGE MOMENTS

By John A. Axelson

Ames Aeronautical Laboratory

INTRODUCTION

In the discussion by Lowry, an empirical method for predicting the effectiveness of swept control surfaces has been presented. There is not sufficient high-speed data available as yet for developing a reliable method of predicting hinge moments of control surfaces in the transonic-speed region. Efforts to approach the problem theoretically have not yielded satisfactory results because of the lack of a suitable approach which accounts for the many variables, such as effects of the viscosity of the air, boundary layer, and separation. High-speed data furnish the best guide for use in control surface design and for estimating the high-speed characteristics of surfaces. Although there has only been a limited amount of hinge-moment data thus far obtained in the transonic-speed range, the existing data have given several definite results, the more significant of which will be discussed, first with respect to unbalanced control surfaces, and then with respect to aerodynamically balanced surfaces.

UNBALANCED CONTROL SURFACES

Sweep.- Sweep has been shown to be very useful in delaying the effects of compressibility on the effectiveness of control surfaces and in decreasing the magnitude of the changes when they occur. The same general trends exist in the hinge-moment characteristics

In figure 1 are presented the variations of the aileron hinge-moment parameters  $C_{h\alpha}$  and  $C_{h\delta}$  with Mach number for three wings having varying degrees of sweep. (See reference 1.)  $C_{h\alpha}$  and  $C_{h\delta}$  are the variations of hinge-moment coefficient with angle of attack and control-surface deflection, respectively. It will be noted, as it was in the case with effectiveness, that the main effects of sweep on hinge moments are to delay the effects of compressibility to a higher Mach number and to decrease the magnitude of the changes when they occur. In the results shown here,  $C_{h\alpha}$  and  $C_{h\delta}$  are both negative, and the effect of sweep is to reduce the absolute value of the hinge-moment parameters with increasing sweep. In other tests in the Ames 16-foot high-speed tunnel of a model having a large

trailing-edge angle,  $C_{h\alpha}$  and  $C_{h\delta}$  were positive for the unswept configurations, and sweeping the wing back tended to reduce the positive values of the parameters. Thus, in these and other investigations, sweeping the model tended to reduce the magnitude of  $C_{h\alpha}$  and  $C_{h\delta}$ , whether the parameters were positive or negative for the unswept configuration. Such an effect is to be expected because the magnitudes of the hinge-moment parameters are directly related to the lift or loading parameter  $C_{L\delta}$ , which has been shown to decrease roughly as the cosine of the angle of sweep.

Trailing-edge angle.- The importance of control-surface profile aft of the hinge line on the high-speed control-surface characteristics has been fully realized only relatively recently (reference 2). In many high-speed wind-tunnel and flight investigations, drastic changes in control-surface characteristics were unexpectedly encountered at high Mach numbers. In some cases, the unusual characteristics were found to be associated with bulges and in others with the trailing-edge angle of the control surface. Analysis of the results indicated that adverse effects generally came with the larger trailing-edge angles (which for bulged and cusped surfaces are best measured between the maximum tangents to the surface.) The larger the trailing-edge angle, the more positive became  $C_{h\alpha}$  and  $C_{h\delta}$  and the greater the increase of these parameters with increasing Mach number. This trend occurs for both unswept and swept control-surface combinations.

In figure 2 are presented the variations of  $C_{h\alpha}$  and  $C_{h\delta}$  with Mach number for three swept models having different trailing-edge angles. The trailing-edge angles indicated in the figure are those measured parallel to the wind stream. It can be seen that increasing the trailing-edge angle increases  $C_{h\alpha}$  and  $C_{h\delta}$  and leads to adverse changes with increasing Mach number. The large positive  $C_{h\delta}$  above .6 Mach number of the control surface having the greatest trailing-edge angle did not extend over the entire control-surface-deflection range but did cover the useful operating range as shown in figure 3. (See reference 3.) Although the aileron had a radius nose, considerable balancing effect was produced by the large trailing-edge angle at all Mach numbers, the degree of balance increasing rapidly at the higher Mach numbers, the ailerons then becoming overbalanced. At the same time the control effectiveness changed in a similar manner, reversed effectiveness occurring in the same general range as the positive  $C_{h\delta}$ . The airfoil section perpendicular to the quarter-chord line was the NACA 0011-64 section. Extension of the

chord and reduction of the trailing-edge angle as indicated in figure 3 materially improved the hinge-moment characteristics as well as causing a similar improvement in the effectiveness of the control surface and in the stability characteristics of the wing.

These results indicate that the trailing-edge angle should be kept to a minimum, preferably below  $14^\circ$ . In doing so, flat-sided control surfaces may be generally preferable to cusped surfaces both from a structural standpoint and because a cusp tends to heavy the hinge moments by negatively increasing  $C_{h\delta}$ . Bulges and bevels are definitely not suitable for high-speed use because of the accompanying large trailing-edge angles. Special care should be taken when using elliptical plan forms or curved trailing edges in order that the trailing-edge angles be kept uniformly small along the entire span of the control surface.

#### AERODYNAMICALLY BALANCED CONTROL SURFACES

Overhang.- Aerodynamic balancing of control surfaces is often desirable even where boosts are employed in the system (reference 2). The most common type of balance is the nose overhang, shown on three models in figure 4. The variations of  $C_{h\alpha}$  and  $C_{h\delta}$  with Mach number are presented for each of the three models, all of which had trailing-edge angles of  $14^\circ$  or less. Only the first model displayed an objectionable increase in  $C_{h\alpha}$  and  $C_{h\delta}$  with increasing Mach number over the test range. This was caused by the larger thickness of the overhang forward of the hinge line. These results and other similar data indicate that overhang balances can be used up to a Mach number of at least .85 and probably higher, provided the nose shape is properly formed and the thickness-to-chord ratio and trailing-edge angles are kept small. There is very little data on internal nose balances above .8 Mach number, but the same general remarks apply.

Tabs.- In figure 5 is shown the effect of sweep on tab effectiveness. Existing data on tabs indicate that the tab effectiveness generally decreases at high Mach numbers in a manner similar to that of the flap-effectiveness parameter  $C_{L\delta}$ , since the same factors, such as separation, influence both. The results show that sweeping the hinge line back  $45^\circ$  reduced the tab effectiveness at lower Mach numbers as might be expected but also resulted in a more favorable variation with Mach number. These effects of sweep on tab effectiveness are very similar to the effects of sweep on  $C_{L\delta}$ , which have already been discussed.

Horn balance.- In figure 6 is shown a collection of hinge-moment data (reference 4 and unpublished data) for horn balances on swept tail surfaces. Results are shown for a  $35^\circ$  swept-back model with and without the horn obtained from wing-flow tests and for a  $45^\circ$  swept model with a horn from wind-tunnel tests. It can be seen that the values of  $C_{h\delta}$  for the  $35^\circ$  and  $45^\circ$  swept tails having horn balances are very nearly constant with Mach number below a Mach number of .9.

At the low Reynolds number of about  $.8 \times 10^6$ , the horn on the  $35^\circ$  swept model loses effectiveness rather rapidly above a Mach number of .9; but at a higher Reynolds number, the effectiveness appears to hold at least to the speed of sound. The results for the horn on the  $45^\circ$  swept model at the left of figure 6, which was at a Reynolds number of about  $6 \times 10^6$ , shows the same trend as the high Reynolds number data on the  $35^\circ$  swept wings. The large Reynolds number effects, such as shown here, make it difficult to predict the characteristics at full-scale Reynolds number from tests of relatively small models because of the large influence of separation and boundary layer on trailing-edge type of controls.

The values of  $C_{h\alpha}$  for the horn balance on both the  $35^\circ$  and  $45^\circ$  swept tails are positive. It should be noted, however, that the unbalanced flap on the  $35^\circ$  swept wing gave almost zero  $C_{h\alpha}$  and most types of aerodynamic balance, with some exceptions, would be expected to give some positive increments of  $C_{h\alpha}$ .

The data presented indicate that the horn-type of balance apparently balances  $C_{h\delta}$  through Mach numbers of 1 but that the increasingly positive values of  $C_{h\alpha}$  with increasing Mach number might prohibit its use except for truly irreversible control systems where, for example, oscillations such as snaking offer no problem. In any case, the balancing power of the horn would be reduced by the positive  $C_{h\alpha}$ , which tends to heavy the controls during maneuvers because the combination of  $C_{h\alpha}$  and  $C_{h\delta}$  determined the resulting hinge moments and control forces in flight.

The results which have been presented indicate that favorable balancing characteristics can be obtained up to a Mach number of .9 and probably higher. The pronounced effects of sweep and trailing-edge angle on hinge moments in the transonic-speed range have also been demonstrated. The general remarks may be interpreted as applying to horizontal and vertical tails and to trailing-edge control surfaces on wings.

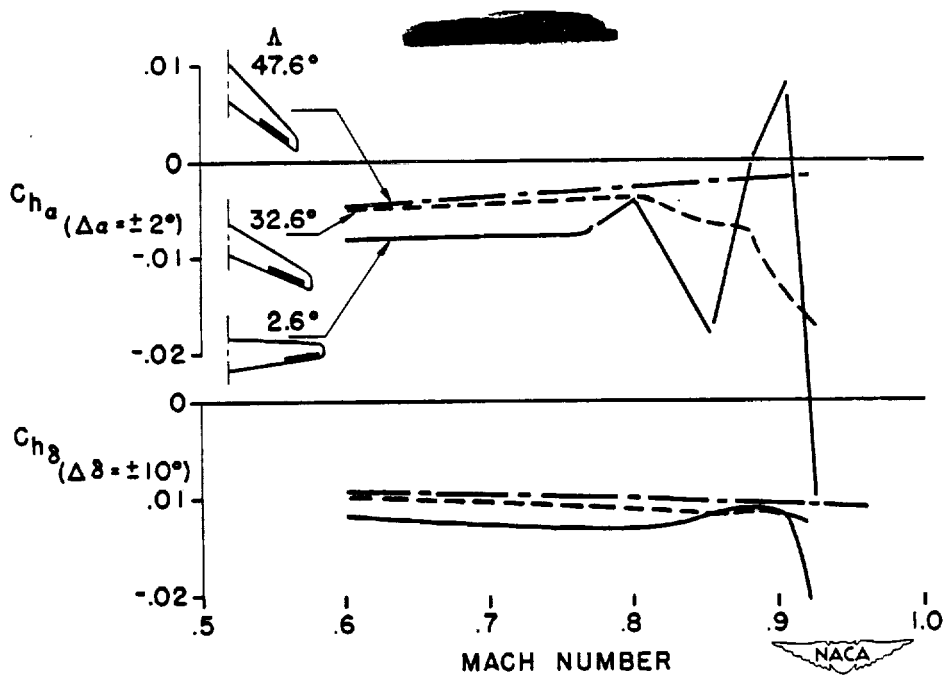
## REFERENCES

Reproduced from  
best available copy.



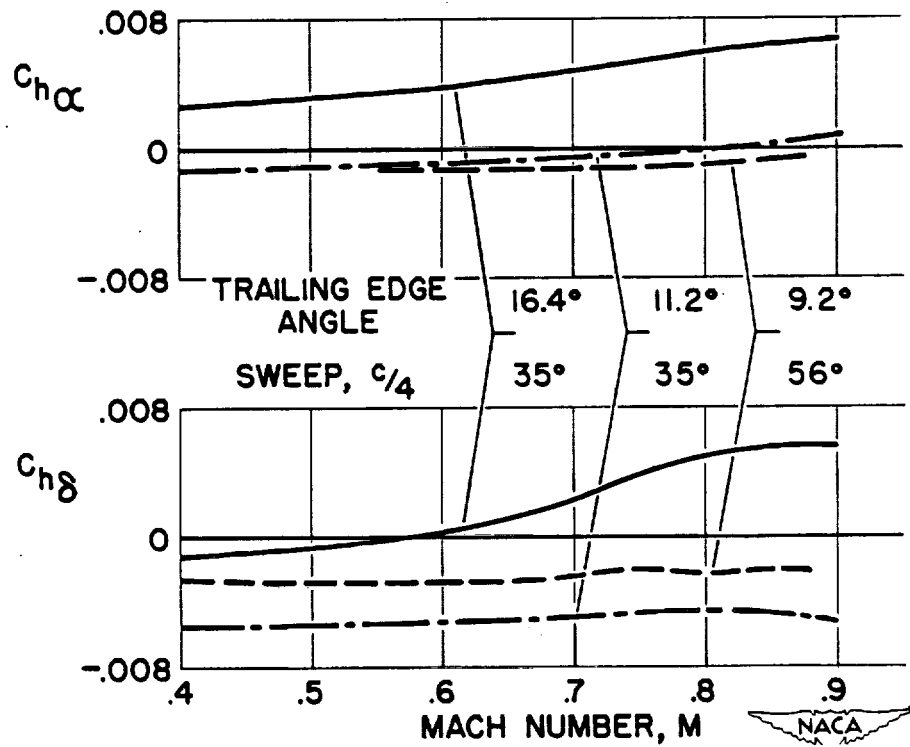
1. Luoma, Arvo A., Bielat, Ralph P., and Whitcomb, Richard T.: A Wind-Tunnel Investigation of the Lateral Control Characteristics of Plain Ailerons on a Wing with Various Amounts of Sweep. NACA RM No. L7I15, 1947.
2. Axelson, John A.: A Summary and Analysis of Wind Tunnel Data on the Lift and Hinge-Moment Characteristics of Control Surfaces up to a Mach Number of 0.9. (Prospective NACA paper)
3. Boddy, Lee E., and Morrill, Charles P., Jr.: The Aerodynamic Effects of Modifications to the Wing and Wing-Fuselage Intersection of an Airplane Model with the Wing Swept Back  $35^{\circ}$ . NACA RM No. A7J02, 1947.
4. Johnson, Harold I.: Measurements of Aerodynamic Characteristics of a  $35^{\circ}$  Sweptback NACA 65-009 Airfoil Model with a  $3/4$ -Chord Plain Flap by the NACA Wing-Flow Method. NACA RM L7F.3, 1947.

Axelson



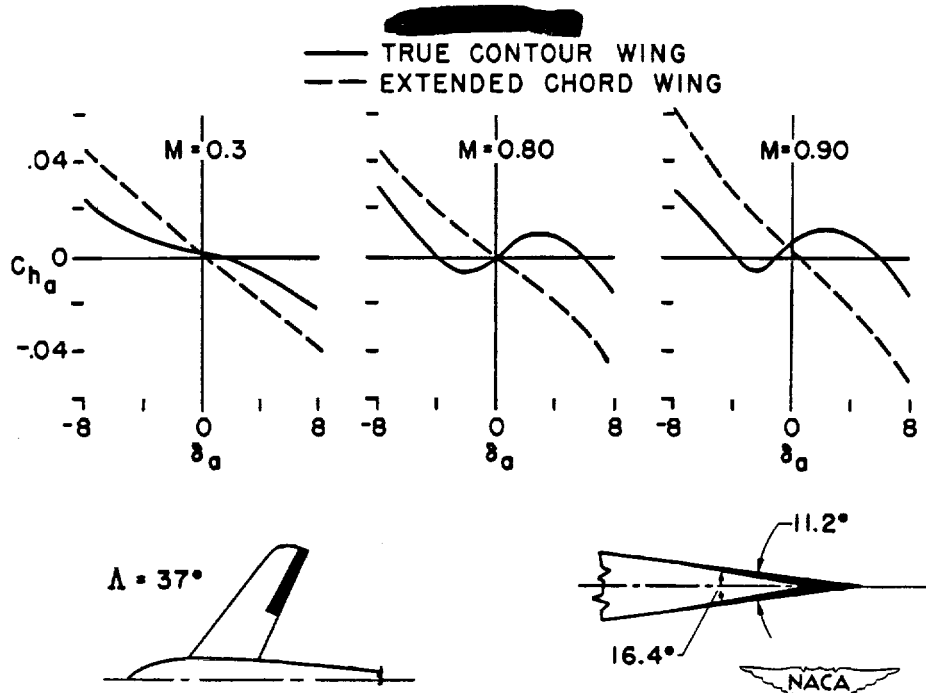
AILERON HINGE-MOMENT PARAMETERS AT HIGH SUBSONIC SPEEDS

Figure 1.



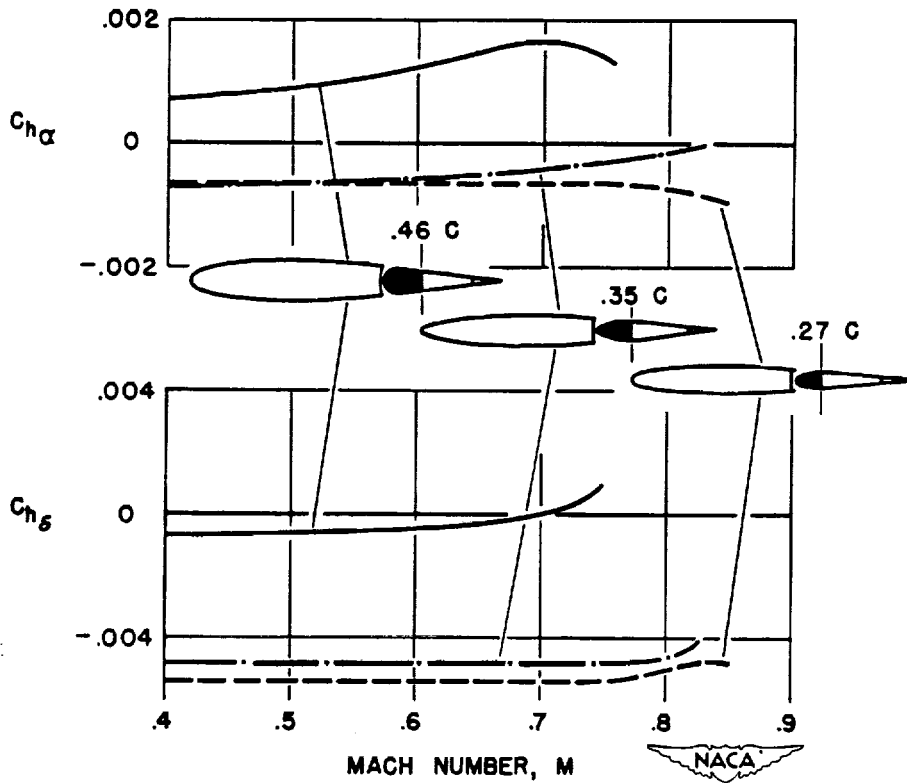
Effect of Trailing-Edge Angle on Hinge-Moment Parameters.

Figure 2.



EFFECT OF TRAILING-EDGE ANGLE AT HIGH SUBSONIC SPEEDS

Figure 3.

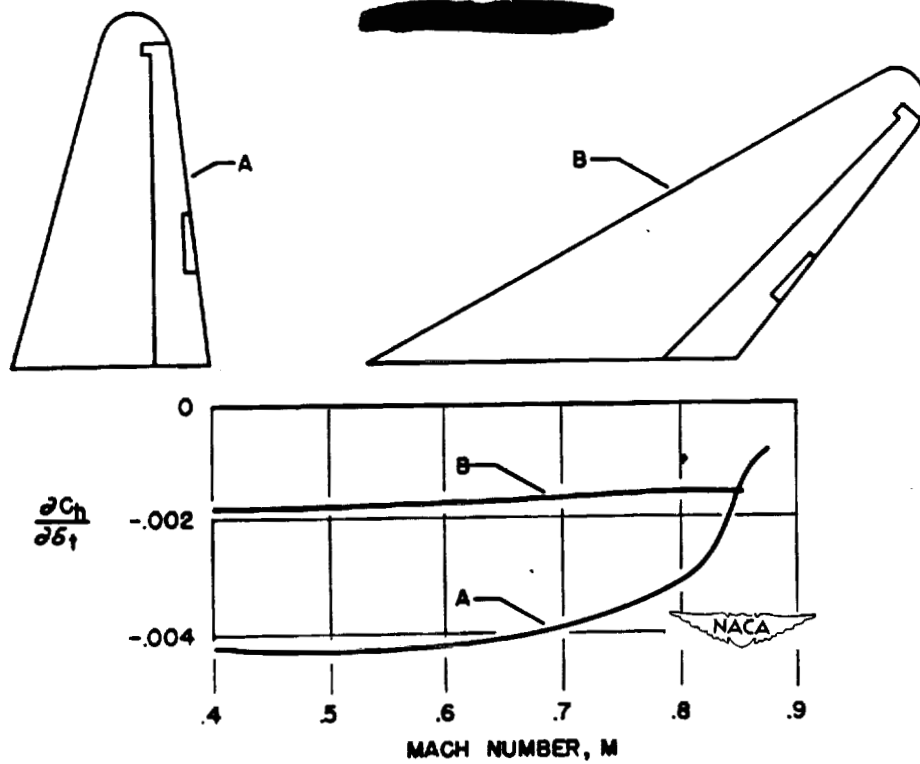


Effect of Nose Balance on Hinge-Moment Parameters.

Figure 4.

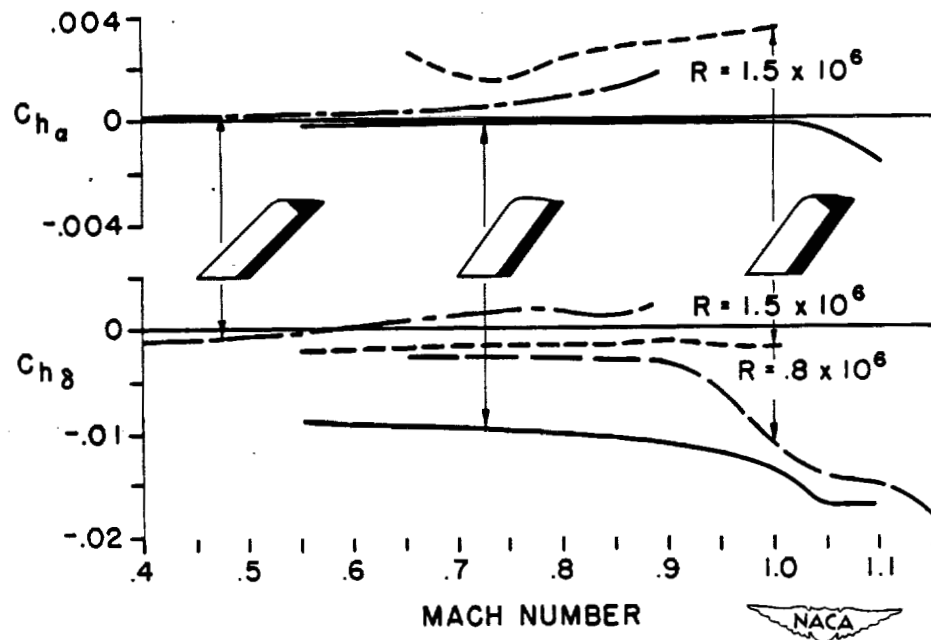


Axelsson



Effect of Sweep on Tab Effectiveness.

Figure 5.



HINGE-MOMENT PARAMETERS AT TRANSONIC SPEEDS

Figure 6.

132(A)

[REDACTED]

## FACTORS AFFECTING LATERAL STABILITY AND CONTROLLABILITY

By John P. Campbell and Thomas A. Toll

Langley Memorial Aeronautical Laboratory

The problem of obtaining satisfactory lateral stability has become increasingly difficult as airspeeds have increased and as designers have resorted to the use of extreme sweepback and low aspect ratio. At high speeds, many of our military airplanes have exhibited a lightly damped yawing oscillation - the so-called "snaking" oscillation. At low speeds, lateral-stability troubles are anticipated with sweptback and low-aspect-ratio designs, partly because of their relatively high effective dihedral and low damping in roll. In general, the problem of oscillatory, or Dutch-roll, stability does not now appear to be as serious for swept airplanes as originally anticipated, but in many cases it is important. In some cases, lateral controllability is a more important factor than Dutch-roll stability in determining the configuration of the airplane.

This paper will deal first with the effect on stability of some of the more important aerodynamic and mass characteristics and will then present methods for estimating the various stability parameters to be used in stability calculations for high-speed airplanes.

Two of the most important factors affecting lateral stability and controllability are the directional-stability parameter  $C_{n\beta}$  (or  $C_{n\psi}$ ) and the effective-dihedral parameter  $C_{l\beta}$  (or  $C_{l\psi}$ ). (See references 1 to 3.) These two factors are used as the basis for the conventional stability chart shown in figure 1. The ordinate is  $C_{n\beta}$  and the abscissa is  $-C_{l\beta}$  which is positive effective dihedral. The boundary shown is for neutral oscillatory or Dutch-roll stability calculated for a general research model tested in the Langley free-flight tunnel. In the figure are two points which represent two models or airplanes with different combinations of  $C_{n\beta}$  and  $C_{l\beta}$ . The first point at high  $C_{n\beta}$  and low  $C_{l\beta}$  is for a good flying condition. The oscillatory stability is very good and the controllability is also good because the large value of  $C_{n\beta}$  keeps adverse yawing to a minimum. The second point which has large  $C_{l\beta}$  and low  $C_{n\beta}$  represents a poor flying condition.

It can be seen that since this point is below the stability boundary, Dutch-roll instability is indicated. Even if the boundary were below this point (which is quite likely in many cases) the controllability for this condition would be poor because the low directional stability would permit excessive adverse yawing, which in combination with the high effective dihedral will cause a serious reduction in aileron rolling

[REDACTED]

effectiveness. (See reference 4.) This happened in the case of the L-39 sweptback research airplane.

Another important factor affecting lateral stability is the damping in roll which becomes smaller as the sweepback is increased and as the aspect ratio is decreased. The effect on lateral stability of reducing the damping in roll is shown in figure 2 which is a stability chart similar to that already presented. The oscillatory-stability boundaries have been plotted for values of the damping-in-roll parameter  $C_{l_p}$  of 0, -0.1, and -0.2. The value of  $C_{l_p}$  for a straight wing conventional airplane is about -0.4 or -0.5. These boundaries which were taken from reference 5 were calculated for a hypothetical transonic airplane and are intended only to indicate the trends obtained as  $C_{l_p}$  is varied. It is evident from the boundaries that reducing  $C_{l_p}$  reduces lateral stability.

Several airplanes now in the design stage have provisions for variable wing incidence to permit the fuselage to remain at a low angle of attack while the wing goes up to the high angles of attack required because of the high sweep and low aspect ratio. Recent theoretical work (reference 6) which has been checked by tests in the Langley free-flight tunnel (reference 4) has indicated that increasing the wing incidence might have a detrimental effect on lateral stability. This effect is illustrated in figure 3, which is a stability chart for a free-flight-tunnel sweptback-wing model with  $0^\circ$  and  $10^\circ$  wing incidence.

Changing the wing incidence in effect changes the inclination of the principal axes of inertia of the airplane which is the factor that produces the change in stability. For example, in the case of the airplane with  $0^\circ$  wing incidence the fuselage is at the same angle of attack as the wing; and, because the principal longitudinal axis of inertia is usually approximately in line with the fuselage, it also has the same positive angle of attack. In the case of the wing with  $10^\circ$  wing incidence, however, it can be seen that the fuselage and, hence, the principal axes of inertia will have very little angle of attack. A comparison of the two boundaries shows that the effect of using positive wing incidence is to decrease the oscillatory stability. It therefore appears desirable to avoid the use of large positive wing incidence if possible. Some calculations have shown that even a small change in wing incidence (as small as  $2^\circ$ ) can give large changes in stability.

The effects of mass distribution and relative density on lateral stability have been investigated both theoretically and by tests in the Langley free-flight tunnel (references 5, 7, and 8.) In general, the results have indicated that usually no pronounced effects on stability occur when the relative density is increased by increasing either the

wing loading or the altitude. Similarly, increasing the moment of inertia in yaw by increasing the weight in the fuselage does not usually appear to affect stability greatly. Increasing the moment of inertia in roll by increasing the weight carried in the wing, however, does have a pronounced effect on the stability as illustrated by figure 4, which is a stability chart for a typical sweptback fighter model tested in the Langley free-flight tunnel with and without wing tip tanks. A comparison of the two points on the chart shows that adding the tanks caused some slight changes in aerodynamic characteristics, but the main effect of the tanks was to increase the moment of inertia in roll which resulted in the large shift shown in the oscillatory-stability boundary. A pronounced reduction in the stability of the model is indicated when the wing tanks are installed. Since the period of the oscillation in this case is fairly long, however, it is possible that the airplane pilot would have less difficulty in flying with this unstable condition than he would in other cases where the oscillation is of shorter period and lightly damped.

Examples of lightly-damped short-period oscillations which are difficult to control have been encountered recently on a number of military airplanes. These airplanes exhibited poor lateral-oscillation characteristics or "snaking" in high-speed flight. A study of this snaking oscillation was recently conducted with a conventional single-engine low-wing attack airplane for which poor lateral-oscillation characteristics had been reported. The results of this investigation are summarized on figures 5 and 6. Figure 5 shows a time history of the rudder motion and yawing velocity after a disturbance in yaw for various rudder conditions for an indicated airspeed of about 350 miles per hour. With the rudder free, the snaking oscillation was very lightly damped even though the actual rudder deflections were less than half a degree. With the rudder locked the damping was much better and was considered satisfactory. The middle record shows that with just the rudder pedals fixed a true rudder-fixed condition was not obtained and the damping was not much better than with rudder free.

The variation of the damping with airspeed is shown in the first part of figure 6. The cycles required to damp to one-half amplitude and period of the oscillation are plotted as a function of indicated airspeed. With rudder locked, the damping in cycles remained constant over the speed range; while with rudder free with the original horn balance the damping was not as good as with rudder fixed at low speed and became progressively worse with increasing airspeed. When the horn balance was removed, the damping was essentially the same as with rudder locked.

An explanation for these changes in damping is given on the rudder-free stability chart on the right of this figure. On this plot of  $C_{H\dot{\psi}}$  against  $C_{H\delta}$  the calculated rudder-free stability boundaries for this

airplane with the effects of friction in the control system are taken into account. The boundaries, which were calculated by methods that were developed in references 9 and 10 and checked in reference 11, indicate the combinations of  $C_{h\psi}$  and  $C_{h\delta}$  which produce stability, divergence, constant-amplitude oscillations, or increasing oscillations. With the horn balance the measured hinge-moment factors were as indicated by the point on the chart. The fact that this point is not far from the constant-amplitude oscillation boundary explains why at low speeds the damping was less with rudder free than with rudder fixed.

The decrease in damping with increase in airspeed for the rudder-free condition is attributed to the effects of Mach number on the hinge-moment parameters  $C_{h\psi}$  and  $C_{h\delta}$ . Tests have shown that as Mach number is increased, both  $C_{h\psi}$  and  $C_{h\delta}$  might become more positive which would shift the point on the chart towards a region of worse damping. Removing the horn balance makes both  $C_{h\psi}$  and  $C_{h\delta}$  more negative and, therefore, shifts the point on the chart to a region of greater damping of the oscillation. This explains the improvement noted in the flight tests when the horn balance was removed. The current trend of airplane design which leads to intentional selection of a low  $C_{h\delta}$  and a positive  $C_{h\psi}$  is such as to invite snaking or poorly damped oscillations. It is therefore important that the damping characteristics be checked by calculations and that due allowance be made for the effect of Mach number on the hinge-moment parameters.

Although the rudder hinge-moment characteristics appear to have a very important effect on snaking oscillations, other factors are undoubtedly involved in many cases. For example, fuel sloshing has in some cases appeared to make the snaking motion worse, and such factors as the air flow at the tail-fuselage juncture and the arrangement of the tail pipe in the fuselage have been shown to affect snaking. Even when none of these factors are involved, an airplane might exhibit snaking in the rudder-fixed condition just because the damping of the Dutch-roll oscillation is weak. This might be the reason for the snaking experienced with the XS-1. The fact that in high-speed flight, the fuselage (and thus the principal longitudinal axis of inertia) is more nearly aligned with the relative wind will tend to make the Dutch-roll oscillation damping worse than at low speeds.

The discussion presented so far has indicated some of the design conditions that must be avoided if satisfactory lateral stability characteristics are to be obtained. In general, it has been found through experience with models in the Langley free-flight tunnel that flight characteristics can be predicted through solutions of the equations of motion, provided sufficient information is at hand regarding

the mass characteristics of the models and the values of the stability derivatives.

The theoretical stability derivatives given for unswept wings in reference 12 have generally been found to be adequate. The use of sweep may affect the values of some of the derivatives appreciably however; and, in general, the available rigorous theories applicable to swept wings are too cumbersome to be used for the preparation of charts similar to those given for unswept wings in reference 12. Analyses of swept-wing data, such as those given in reference 13, have indicated that through simple geometric considerations, correction factors may be derived to account for the effects of sweep. When these factors are applied to rigorous theoretical values of the derivatives of unswept wings, reasonably reliable derivatives for swept wings may be obtained. Such factors have been derived for the various derivatives and are given in reference 14. Some sample charts based on the method of reference 14 are shown in figure 7. These charts illustrate trends resulting from the effects of sweep on some of the important stability derivatives of wings having a taper ratio of 0.5 and no dihedral.

Perhaps the greatest effect of sweep is on the effective-dihedral derivative  $-C_{l\beta}$ . It should be noted that for small aspect ratios, a given angle of sweepback may result in high positive effective dihedral; whereas, the same angle of sweepforward may result in little or no negative effective dihedral. This is caused by the fact that, although the increment of  $C_{l\beta}$  resulting from sweep does not vary to any large extent with aspect ratio, the value of  $-C_{l\beta}$  for unswept wings increases rapidly as the aspect ratio decreases.

The approximate method of calculation indicates that the damping in roll  $C_{lp}$  is reduced by sweep, but this effect generally is not large except for relatively high aspect ratios. In this connection, it might be mentioned that the effectiveness of ailerons, which occupy a given portion of the wing surface, is found to decrease with sweep more rapidly than the damping in roll. If it is desired, therefore, to meet the usual rolling criterion of a specified value of the wing-tip helix angle  $\frac{db}{dy}$ , either larger ailerons or greater deflections must be provided as the sweep angle is increased.

Sweep causes appreciable increases in the magnitudes of the derivatives of yawing moment due to rolling  $C_{np}$  and rolling moment due to yawing  $C_{lr}$ . This is in contrast to the reductions noted for the value of  $C_{lp}$  and usually found for the lift-curve slope  $C_{L\alpha}$ .

Experimental determinations of the various stability derivatives have been made for a large number of wings through the use of the rolling- and curved-flow equipment of the Langley stability tunnel. In general, the test results have substantiated the trends shown by the charts. The data have indicated, however, that under some conditions, the calculated values of the derivatives may apply to only a limited lift-coefficient range. This fact is illustrated by figure 8 which shows comparisons of experimental and calculated values of the derivatives  $-C_{l\beta}$ ,  $C_{lr}$ , and  $C_{np}$  for an untapered  $45^\circ$  sweptback wing of aspect ratio 2.6. The tests, which were made at a Reynolds number of about 1,400,000, are reported in references 15 and 16.

For this case, the initial slopes of the derivatives against lift coefficient are in fairly good agreement with the slopes indicated by the calculations. The data begin to deviate from the initial slopes, however, at a lift coefficient of about 0.5, and the deviations become very important at high lift coefficients. Under these test conditions, the rolling moment due to sideslip and the rolling moment due to yawing decreased to about zero at maximum lift. The yawing moment due to rolling reversed its sign at a lift coefficient of about 0.7, so that at high lift coefficients the derivative  $C_{np}$  might be regarded as favorable rather than unfavorable as is normally expected. This can have an important effect on controllability at high lift coefficients. Free-flight-tunnel tests of models with positive values of  $C_{np}$  have indicated that the favorable yaw makes it possible to obtain good lateral flying characteristics without the necessity of coordinating the rudder with aileron control.

The deviations of the experimental data from the initial slopes probably result from tip stalling since rolling- and yawing-moment derivatives are affected primarily by flow conditions at the tips. An indication of partial stalling is given by the rise in the quantity  $C_D - \frac{C_l^2}{\pi A}$  which represents that part of the wing drag which is not ideally associated with lift. For convenience, this quantity will be referred to as the "drag index." For the case of a sweptback wing without devices which tend to delay stalling at the wing tips, such as vanes, leading-edge flaps, or slots, the drag index is found to rise at about the lift coefficient at which the derivatives  $C_{l\beta}$ ,  $C_{lr}$ , and  $C_{np}$  begin to deviate from the trends established at low lift coefficients. When devices which delay tip stalling are used, the drag index may not be a true indication of variations in derivatives, however, for it may rise because of separation of flow from inboard parts of the wing which would not greatly affect the rolling- and yawing-moment derivatives. For plain sweptback wings, however, it appears that the drag index might serve as a basis for predicting the lift-coefficient range over which the calculated characteristics might be expected to apply under specific conditions. An

important application of the drag-index concept is in the prediction of Reynolds number effects on derivatives such as  $C_{n_p}$  and  $C_{l_r}$  which can be determined only with special equipment which normally is not available in wind tunnels capable of making tests at high Reynolds numbers.

Figure 9 shows the effects of Reynolds number and of wing roughness on the effective-dihedral derivative  $-C_{l_\beta}$  and on the drag index for a  $40^\circ$  sweptback wing with an NACA 64<sub>1</sub>-112 airfoil section. These results, taken from reference 17, are from tests made in the Langley 19-foot pressure tunnel. Large effects of Reynolds number were noted when the wing surface was smooth; for example, at a Reynolds number of 5,300,000, the derivative  $-C_{l_\beta}$  increased linearly with lift coefficient almost until maximum lift was attained, and the drag index showed very little change with lift coefficient. At a Reynolds number of 1,720,000, however, the derivative  $-C_{l_\beta}$  began to deviate from its initial trend at a lift coefficient of about 0.5, and the drag index showed an abrupt rise at the same lift coefficient. Results obtained at a high Reynolds number, for the wing with roughness at the leading edge, were very similar to results obtained at a low Reynolds number for the wing with a smooth surface. The drag index again indicates the presence of tip stalling for the latter two cases but little or no stalling for the smooth wing at a high Reynolds number. It might be expected therefore that initial trends of the derivatives  $C_{n_p}$  and  $C_{l_r}$  also would persist to a high lift coefficient for the case of the smooth wing at a high Reynolds number.

The shape of the wing profile may, under some conditions, have large effects on lateral stability characteristics. Figure 10 shows comparisons of results obtained on the effective dihedral derivative  $-C_{l_\beta}$  for smooth wings having NACA 64<sub>1</sub>-112 and circular-arc airfoil sections. The tests (reference 18) were made at a Reynolds number of 5,300,000, which is the higher of the two values referred to in the preceding figure. With flaps off, the curve for the NACA 64<sub>1</sub>-112 airfoil is the same as given before. The values of  $-C_{l_\beta}$  for the circular-arc airfoil begin to deviate from their initial trend at a very low lift coefficient, probably because the tendency of sweptback wings to stall at the tips is aggravated through the use of an airfoil with a sharp leading edge. With leading-edge and trailing-edge flaps deflected, the derivative  $-C_{l_\beta}$  continued to increase almost linearly with lift coefficient until maximum lift was approached, regardless of the airfoil section. It appears that the wing characteristics are determined largely by the contour of the leading-edge flap and that the basic airfoil section has very little influence when the leading-edge flap is deflected. Since the leading-edge flap tends to delay tip stalling, it is probable that the



derivatives  $C_{n_p}$  and  $C_{l_r}$  also would show trends similar to that indicated for  $-C_{l_\beta}$ .

The discussion given so far has dealt largely with the more important effects of sweep on characteristics that are of particular interest at low speeds. In the design of a complete airplane, additional factors, such as the effects of the fuselage, or the size and location of the tail surfaces, must be considered. Experience has indicated that the effects of these additional factors on the various rotary-stability derivatives and on the effective-dihedral derivative  $-C_{l_\beta}$  can be accounted for in much the same manner that has been used for conventional-aircraft designs. Particular attention should be paid, however, to the possible adverse effect of swept wings on directional stability near maximum lift. It is not yet possible to select with any degree of certainty a configuration that will have satisfactory directional stability characteristics at all lift coefficients, but it generally has been possible to correct an undesirable condition in the course of wind-tunnel development tests.

Very little theoretical or experimental information regarding subsonic compressibility effects on the lateral-stability derivatives is available at the present time. Results of tests made on one model in the Langley high-speed 7- by 10-foot tunnel are shown in figure 11. The tests included determinations of the derivatives  $C_{n_\beta}$ ,  $-C_{l_\beta}$ , and  $C_{l_p}$  through a range of Mach number. The model configuration used in the determination of  $C_{l_p}$  was slightly different from that used in the determinations of  $C_{n_\beta}$  and  $-C_{l_\beta}$ . The compressibility effects on these derivatives were found to be very small for Mach numbers below 0.82. At higher Mach numbers, the directional-stability derivative  $C_{n_\beta}$  increased, probably because, with the model in sideslip, the critical Mach number of the leading-wing panel was exceeded and, consequently, the drag of the leading-wing panel increased. At an angle of attack of  $6^\circ$  the effective-dihedral derivative  $-C_{l_\beta}$  decreased as the Mach number exceeded 0.82. This probably results from a loss in lift on the leading-wing panel as its critical Mach number is exceeded. The damping-in-roll derivative  $C_{l_p}$  showed no abrupt change through the test range of Mach number.

The problem of lateral behavior at transonic speeds, extending through a Mach number of 1.0, is now being investigated by means of free-flight rocket models, but results are not yet available. Several theoretical investigations which apply to Mach numbers of about 1.2 and above have been completed or are in progress. The case of the supersonic derivatives of triangular wings already has been covered rather completely in reference 19. The methods used in reference 19 are now

being extended to "notched" triangles, or swept wings with zero taper ratio. Investigations of unswept rectangular wings also are underway.

In summarizing, it might be said that progress is being made in the determination of the stability derivatives for swept and low-aspect-ratio airplane configurations; and it appears that by using the proper stability derivatives with existing theoretical methods, the lateral stability characteristics of high-speed airplanes can, at least qualitatively, be predicted.

## REFERENCES

1. McKinney, Marion O., Jr. : Experimental Determination of the Effects of Dihedral, Vertical-Tail Area, and Lift Coefficient on Lateral Stability and Control Characteristics. NACA TN No. 1094, 1946.
2. Drake, Hubert M. : The Effect of Lateral Area on the Lateral Stability and Control Characteristics of an Airplane as Determined by Tests of a Model in the Langley Free-Flight Tunnel. NACA ARR No. L5L05, 1946.
3. Drake, Hubert M. : Experimental Determination of the Effects of Directional Stability and Rotary Damping in Yaw on Lateral Stability and Control Characteristics. NACA TN No. 1104, 1946.
4. McKinney, Marion O., Jr. and Drake, Hubert M. : Correlation of Experimental and Calculated Effects of Product of Inertia on Lateral Stability. NACA TN No. 1370, 1947.
5. Sternfield, Leonard : Some Considerations of the Lateral Stability of High-Speed Aircraft. NACA TN No. 1282, 1947.
6. Sternfield, Leonard : Effect of Product of Inertia on Lateral Stability. NACA TN No. 1193, 1947.
7. Campbell, John P., and Seacord, Charles L., Jr. : The Effect of Mass Distribution on the Lateral Stability and Control Characteristics of an Airplane as Determined by Tests of a Model in the Free-Flight Tunnel. NACA Rep. No. 769, 1943.
8. Campbell, John P., and Seacord, Charles L., Jr. : Effect of Wing Loading and Altitude on Lateral Stability and Control Characteristics of an Airplane as Determined by Tests of a Model in the Free-Flight Tunnel. NACA ARR No. 3F25, 1943.
9. Greenberg, Harry, and Sternfield, Leonard : A Theoretical Investigation of the Lateral Oscillations of an Airplane with Free Rudder with Special Reference to the Effect of Friction. NACA Rep. No. 762, 1943.
10. Neumark, S. : A Simplified Theory of the Lateral Oscillations of an Aeroplane with Rudder Free, Including the Effect of Friction in the Control System. Rep. No. Aero 2049, British R.A.E., May 1945.
11. Maggin, Bernard : Experimental Verification of the Rudder-Free Stability Theory for an Airplane Model Equipped with a Rudder Having Positive Floating Tendencies and Various Amounts of Friction. NACA TN No. 1359, 1947.

12. Pearson, Henry A., and Jones, Robert T. : Theoretical Stability and Control Characteristics of Wings with Various Amounts of Taper and Twist. NACA Rep. No. 635, 1938.
13. Letko, William, and Goodman, Alex : Preliminary Wind-Tunnel Investigation at Low Speed of Stability and Control Characteristics of Swept-Back Wings. NACA TN No. 1046, 1946.
14. Toll, Thomas A., and Queijo, M. J. : Approximate Relations and Charts for the Low-Speed Stability Derivatives of Swept Wings. (Prospective NACA paper)
15. Feigenbaum, David, and Goodman, Alex: Preliminary Investigation at Low Speeds of Swept Wings in Rolling Flow. NACA RM No. L7E09, 1947.
16. Goodman, Alex, and Feigenbaum, David: Preliminary Investigation at Low Speeds of Swept Wings in Yawing Flow. NACA RM No. L7I09, 1947.
17. Neeley, Robert H., and Conner, D. William: Aerodynamic Characteristics of a  $42^\circ$  Swept-Back Wing with Aspect Ratio 4 and NACA 64<sub>1</sub>-112 Airfoil Sections at Reynolds Numbers from 1,700,000 to 9,500,000. NACA RM No. L7D14, 1947.
18. Salmi, Reino J., and Fitzpatrick, James E.: Yaw Characteristics and Sidewash Angles of a  $42^\circ$  Sweptback Circular-Arc Wing with a Fuselage and with Leading-Edge and Split Flaps at a Reynolds Number of 5,300,000. NACA RM No. L7I30, 1947.
19. Ribner, Herbert S., and Malvestuto, Frank S., Jr. : Stability Derivatives of Triangular Wings at Supersonic Speeds. (Prospective NACA paper)

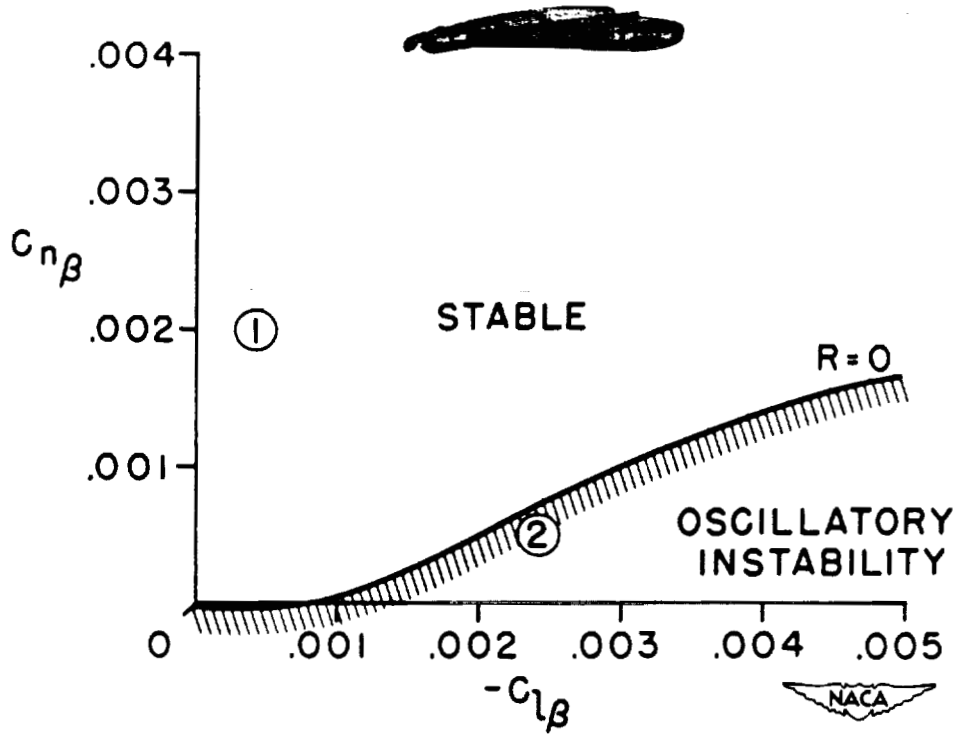


Figure 1.- Stability chart for a general research model tested in the Langley free-flight tunnel ( $C_L = 1.0$ ).

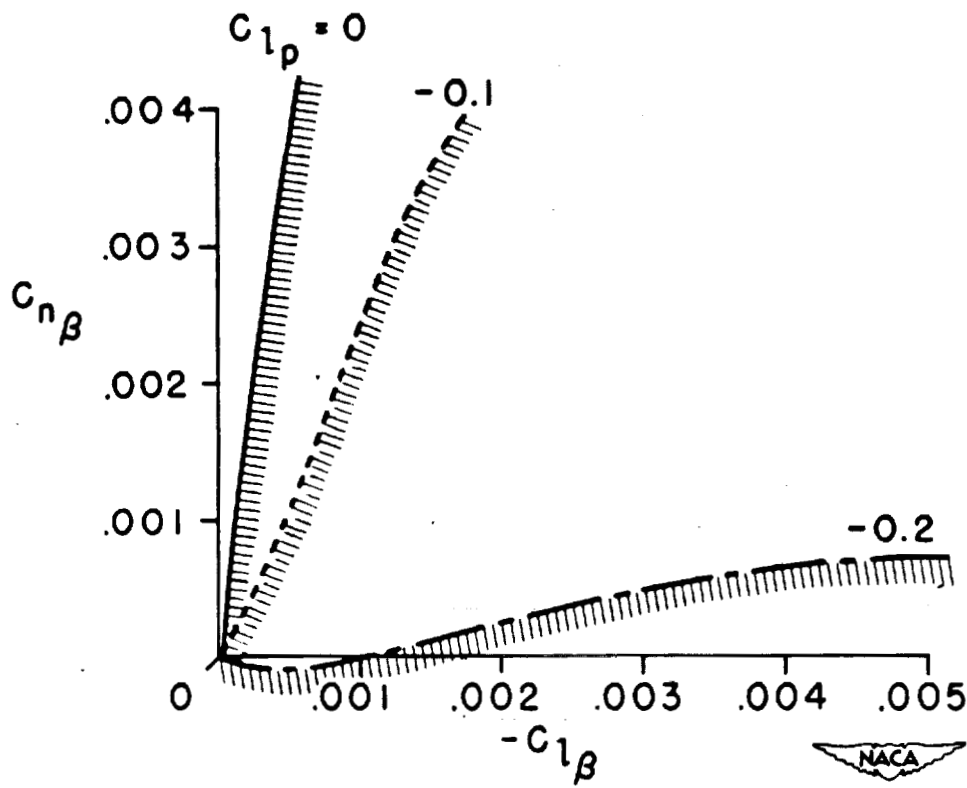


Figure 2.- Effect of damping in roll on the lateral stability of a high-speed airplane ( $C_L = 1.0$ ).

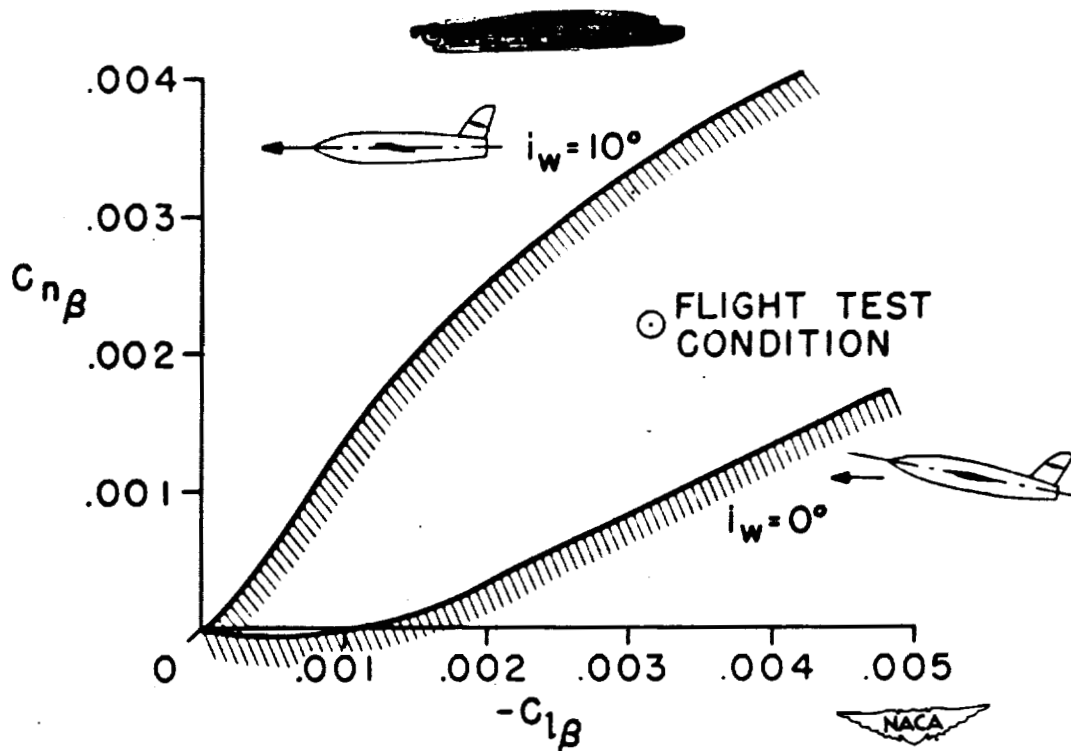


Figure 3.- Effect of wing incidence on the lateral stability of a free-flight-tunnel research model ( $C_L = 0.6$ ).

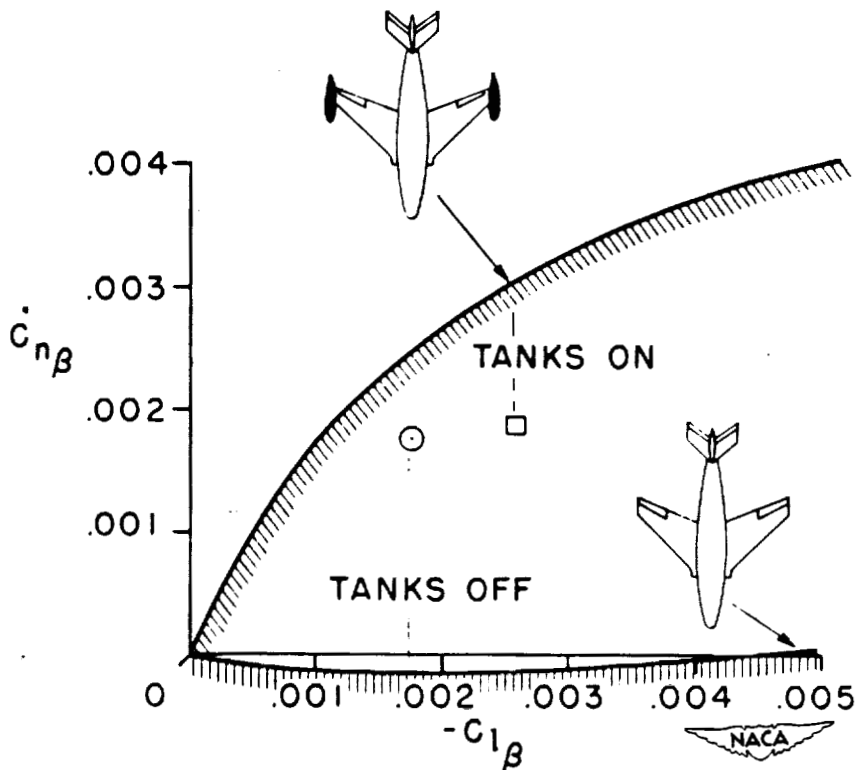


Figure 4.- Effect on the lateral stability of the change in mass distribution caused by adding wing-tip tanks ( $C_L = 0.7$ ).

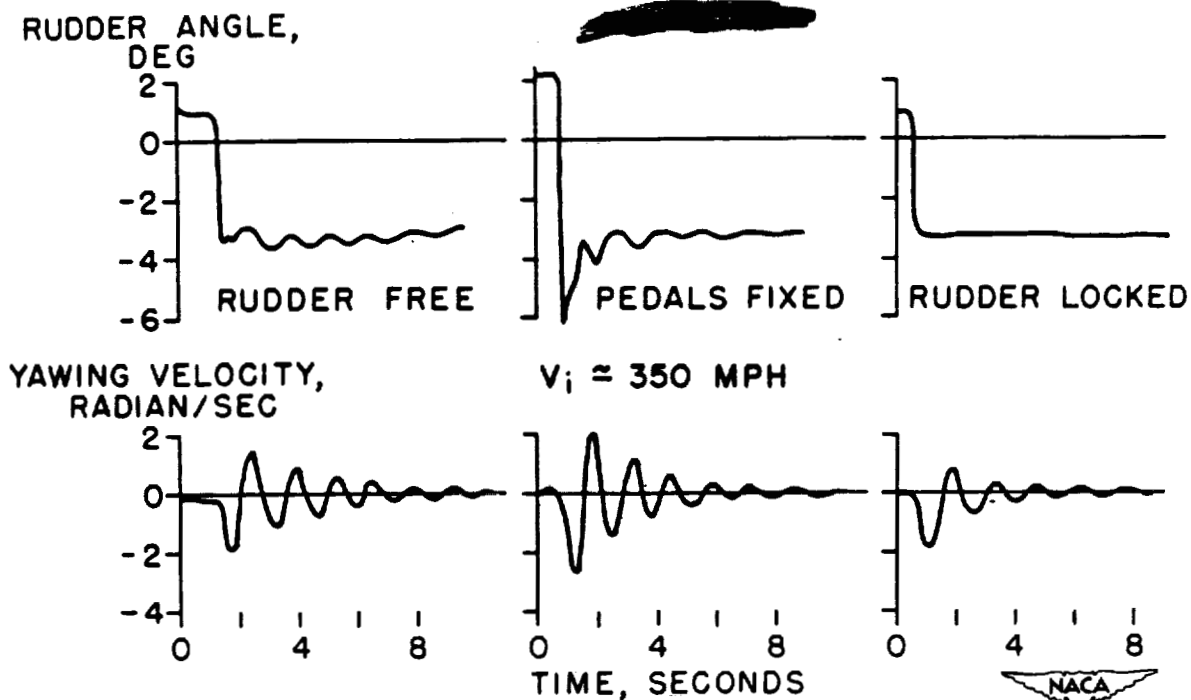


Figure 5.- Time histories of the lateral oscillations of a conventional attack airplane.

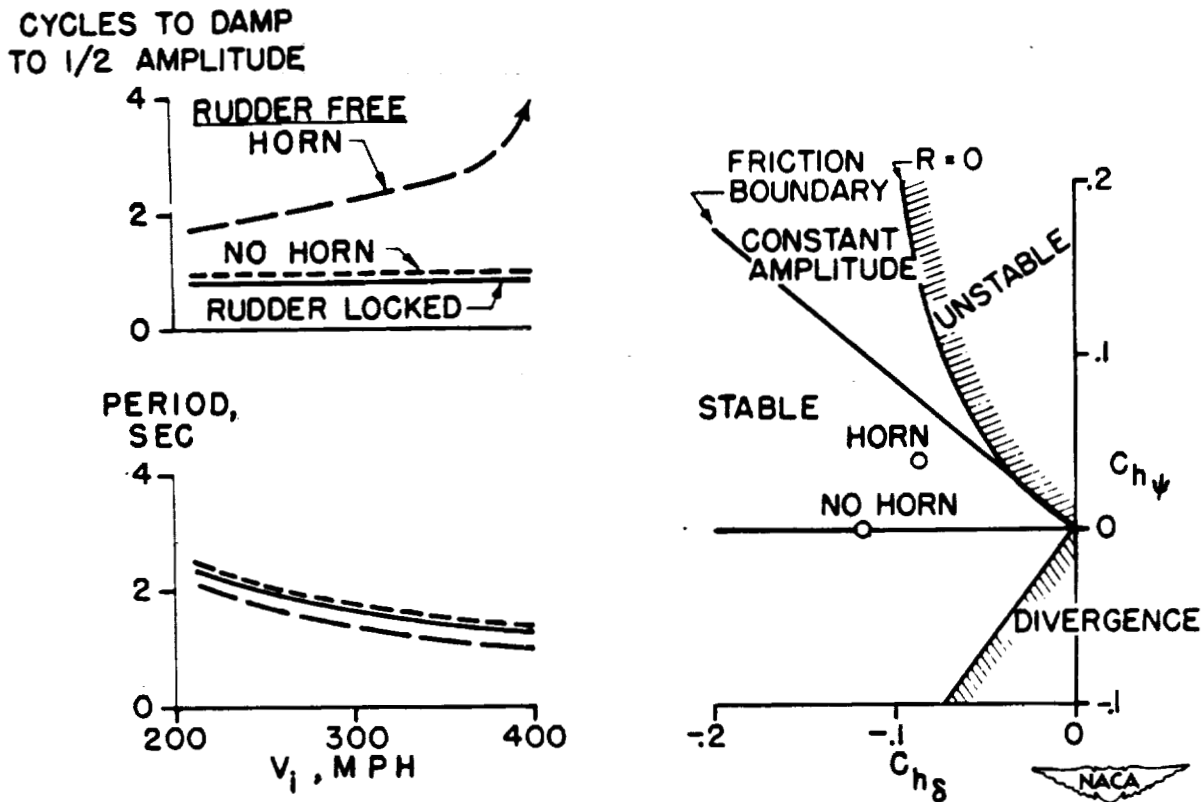


Figure 6.- Period and damping of the lateral oscillation and calculated rudder-free stability boundary for conventional attack airplane.

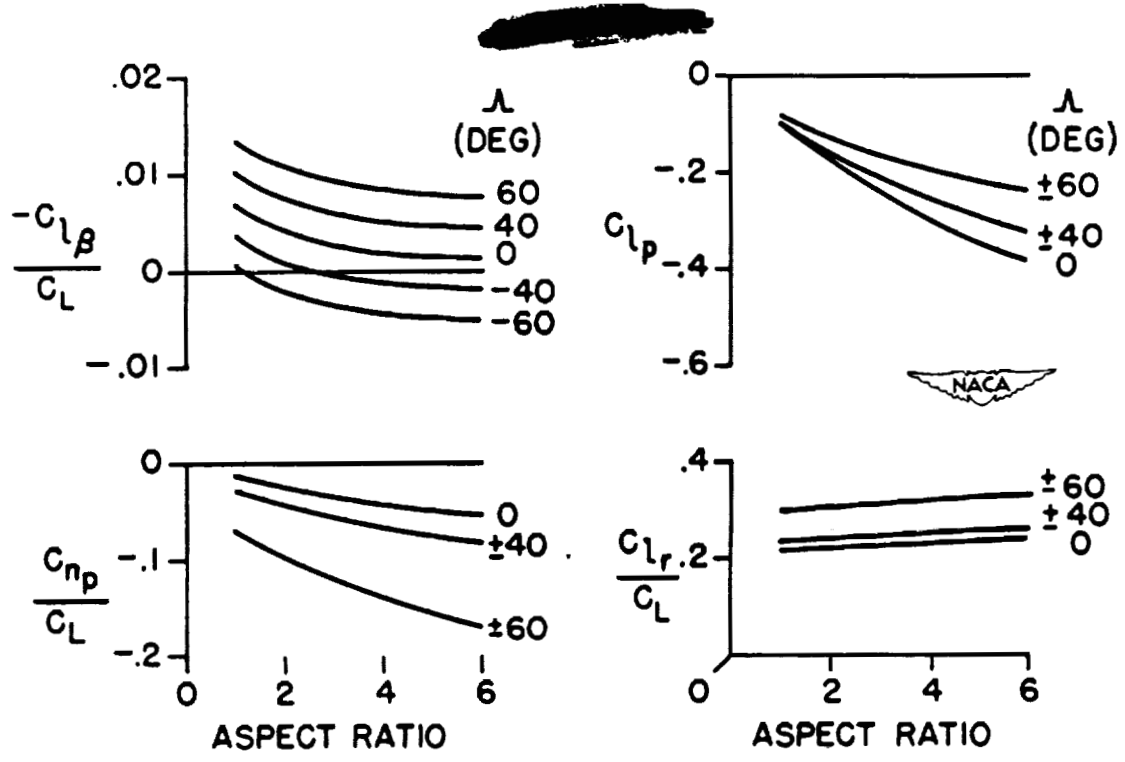


Figure 7.- Lateral-stability derivatives calculated by approximate theory for swept wings with taper ratio of 0.5.

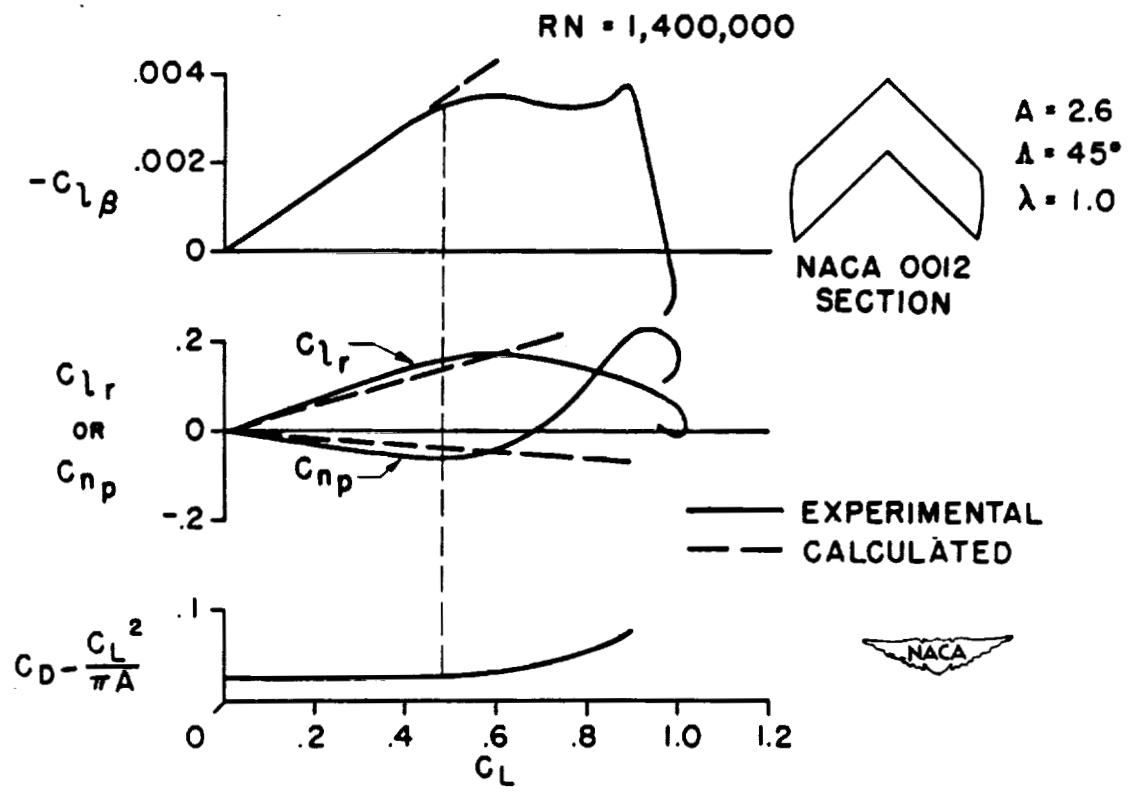


Figure 8.- Comparison of experimental and calculated lateral-stability derivatives.



Campbell

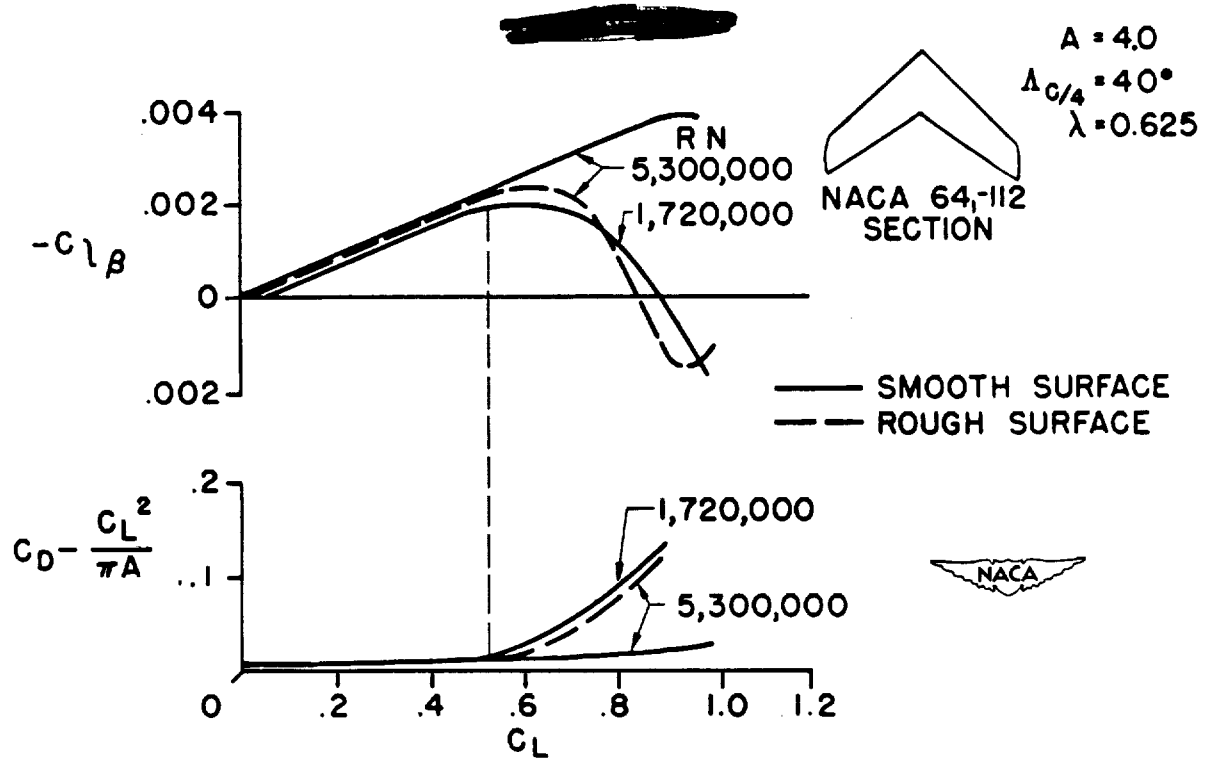


Figure 9.- Effect of Reynolds number and wing roughness on rolling moment due to sideslip.

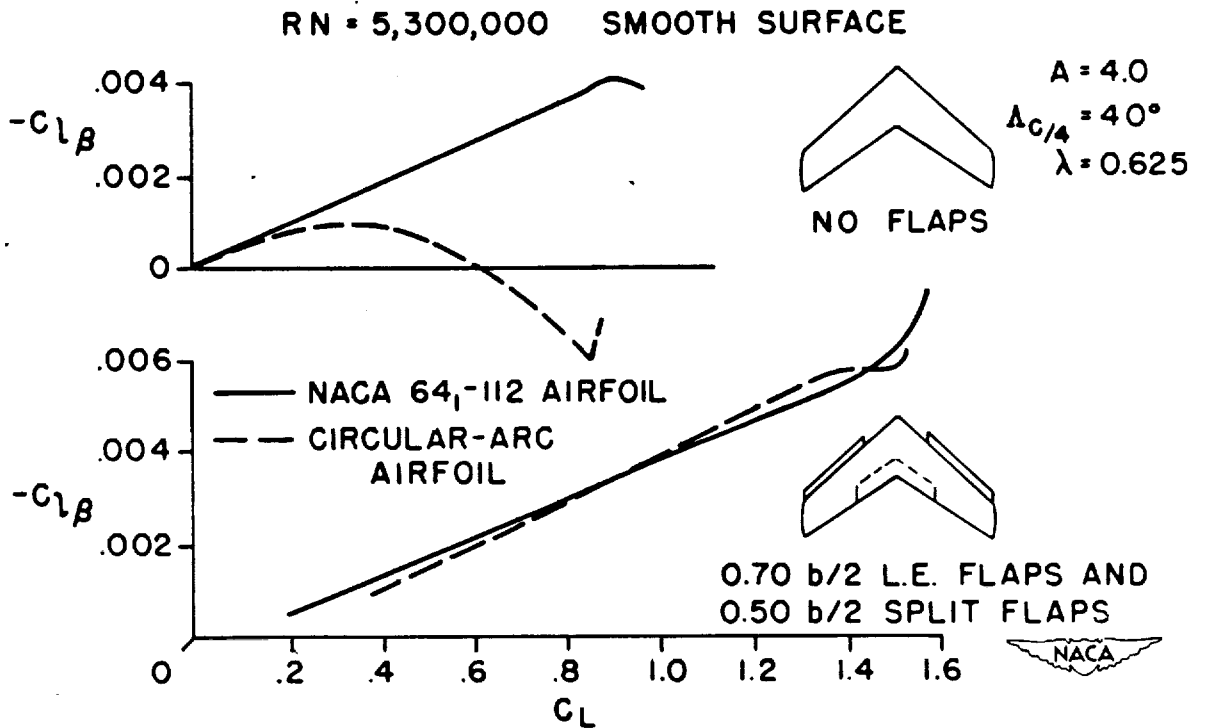


Figure 10.- Effect of airfoil section and flaps on rolling moment due to sideslip.

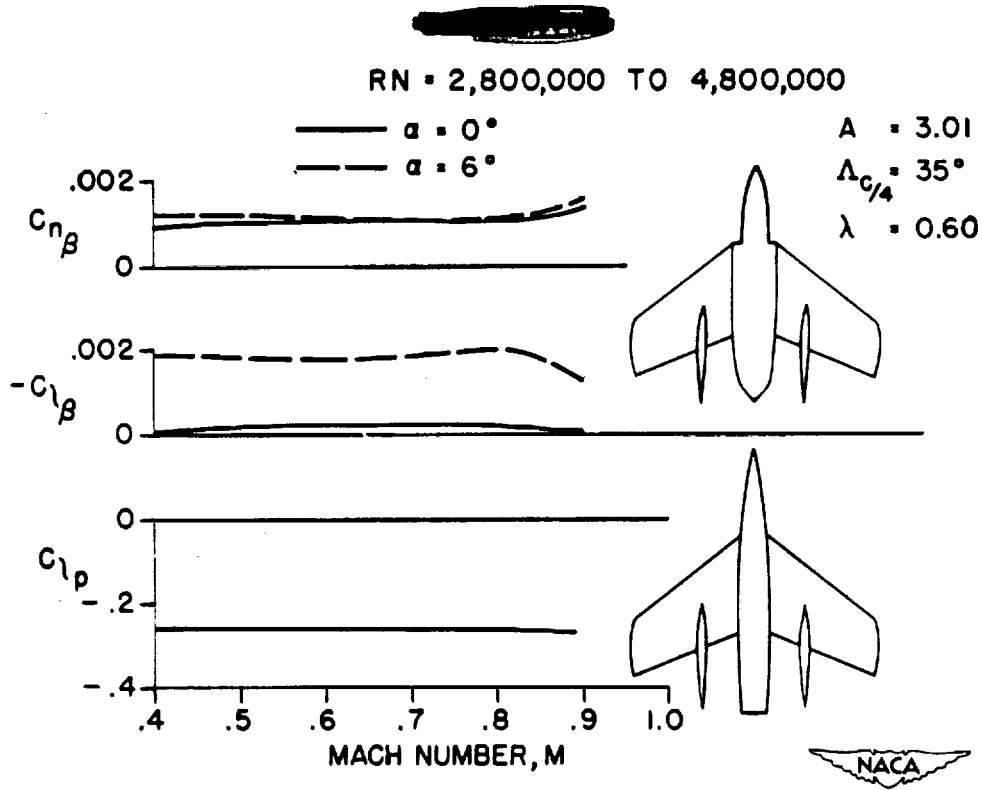


Figure 11.- Effect of Mach number on lateral-stability derivatives.

~~SECRET~~

D17

LOW-SPEED FLIGHT INVESTIGATION OF AN AIRPLANE

WITH SWEEPBACK WINGS

By W. H. Phillips

Langley Memorial Aeronautical Laboratory

Some of the stability parameters of sweptback wings are considerably different from those of conventional straight wings. In order to determine how these different stability parameters would affect the low-speed flying qualities of an airplane, the Navy early in 1946 authorized the Bell Aircraft Corporation to modify two P-63 airplanes to incorporate sweptback wings. The first figure shows a drawing of the modified airplane, which is designated the L-39 airplane. The outer wing panels are swept back 35° along the quarter-chord line. The center section, containing the cooling air intakes, is left unchanged. The main landing gear of the L-39 airplane is fixed. The tail was lengthened after preliminary flight tests at the Bell Company, partly to increase the directional stability but mainly to assist in getting the tail down for landing. The wing leading edge is made of wood and may be modified to incorporate fixed slots covering various portions of the span. Because of the fixed landing gear and the structural features of the wing, the airplane is restricted to an indicated airspeed of 250 miles per hour. Also, because of the fuselage modifications, the sideslip angle is restricted to fairly small values at high speeds. In all cases except those noted, the extension on the ventral fin shown in figure 1 was installed for the flight tests reported herein. Some tests were made with this extension removed, however, to give a condition of reduced directional stability. The flight tests made by the NACA and reported in this paper were all made with the first L-39 airplane, which incorporates conventional airfoil sections, designated NACA 66, 2X116, a = 0.6 measured perpendicular to the quarter-chord line. Tests made by the Bell Aircraft Corporation on this airplane before the NACA investigation are reported in reference 1. The second L-39 airplane had a pointed leading edge, simulating a circular-arc airfoil section 14.3 percent thick. This airplane was tested by the Bell Company but has not been flown by the NACA.

Tests have been made of a 0.22-scale model of the L-39 airplane in the Langley 7- by 10-foot tunnel, so that a comparison between the small-scale wind-tunnel results and the flight results is possible.

Measurements of the longitudinal- and lateral-stability characteristics and stalling characteristics have been completed with

three slot arrangements. These slot configurations will be referred to as the 0, 40-percent, and 80-percent span slots. The 40-percent span slots covered 40 percent of the span of the sweptback outer panels, starting at 40 percent of the span and extending out to 80 percent of the span. The 80-percent span slots extended from 20 percent of the span to the tip. These slot arrangements are shown in the first figure.

All tests were made with power off, because it was felt that the results would be of most interest for application to jet-propelled aircraft where slipstream effects would be absent.

The main item of interest in connection with the longitudinal stability of a sweptback-wing airplane is the stability at low speeds near the stall, because wind-tunnel tests of many swept-back configurations have shown instability at high lift coefficients.

The longitudinal stability of the L-39 airplane was investigated by recording the elevator angles and forces in steady flight at various speeds with two center-of-gravity positions, 20 and 26 percent of the mean aerodynamic chord. The results of these tests are presented in detail in reference 2. Figure 2 shows the variation of elevator angle with speed for the flaps-down condition with the three slot configurations, with the center of gravity at 26 percent of the mean aerodynamic chord. A negative slope of this curve, corresponding to a larger up-elevator angle for trim at lower speed, represents a stable condition.

The results presented show that without slots the stability became neutral near the stall. The stall occurred at the minimum speed plotted. The stability was large in the normal-flight range, where the neutral point was at about 42 percent of the mean aerodynamic chord. The decrease in stability close to the stall was not objectionable to the pilot, because the elevator angle and stick force variations did not become unstable. There was a slight nosing up tendency at the stall but this could easily be controlled by application of down elevator. In an airplane with a smaller degree of stability in the normal flight range, this much loss in stability would result in more serious instability at the stall, which would probably be very objectionable to the pilot. Tests could not be made with a more rearward center-of-gravity position in the L-39 airplane because of the position of the main landing gear.

The use of slots reduced the tendency toward instability at the stall. The slots also improved the stalling characteristics so that the airplane could be controlled to some extent in flight beyond the stall. In this case the elevator had to be pulled up to

prevent the airplane from pitching down when it was in a partially stalled condition. This characteristic is shown by the low-speed end of the curves in figure 2. The pitching moments beyond the stall were, therefore, stable with flaps down when the slots were employed.

The longitudinal stability with flaps up was good all the way to the stall with any of the slot configurations. The tendency toward neutral stability at the stall was not present in this case.

Tuft studies showed that, with flaps up, the wing of the L-39 airplane stalled first at the root, probably because of the leading-edge air intakes and the design of the wing-fuselage juncture. This root stall occurred even without slots in the wing, and probably tended to reduce the unstable pitching tendencies at the stall by reducing the downwash at the horizontal tail at high lift coefficients. With flaps down, the initial stall did not occur at the root.

The most apparent difference expected between the lateral stability characteristics of sweptback and straight wings is the large increase in dihedral effect with lift coefficient for the sweptback wings. The dihedral effect of an airplane is felt by the pilot by the amount of aileron angle required to maintain equilibrium in sideslips. The characteristics of the L-39 airplane in steady sideslips are shown in figure 3. More complete data on the lateral and directional stability characteristics of the L-39 airplane are given in reference 3. This figure shows the total aileron angle and rudder angle as a function of sideslip angle for various values of the airspeed. The variation of rudder angle with sideslip angle was essentially the same for all speeds. At the highest speed tested, 235 miles per hour, a small amount of left aileron angle was required in right sideslips, indicating a slight negative dihedral effect. As the speed was decreased, the dihedral effect became positive and reached a large positive value at 110 miles per hour, the lowest speed tested. At this speed, full aileron deflection was required to hold a steady sideslip with only  $8^\circ$  rudder deflection. Even higher dihedral effect was observed in the flaps-down condition because of the higher lift coefficient which could be reached. The dihedral characteristics in the flaps-up condition for various slot configurations are summarized in figure 4. This figure shows the variation of aileron angle with sideslip as a function of normal-force coefficient for the three slot configurations tested. The effect of slot configuration is not great, but a slightly greater variation of dihedral effect with normal-force coefficient was obtained with the 80-percent span slots.

Some question has arisen as to the ability of small-scale wind-tunnel tests to predict the characteristics of sweptback wings. In order to obtain a comparison between the flight and wind-tunnel measurements of dihedral effect, the airplane was flown with known asymmetric loadings so that the sideslip angle required to balance a given rolling moment could be measured. The variation of rolling-moment coefficient with sideslip  $C_{l\beta}$  as a function of normal-force coefficient for the condition of 80-percent span slots is shown in figure 5. The wind-tunnel measurements are also shown in this figure. The small-scale wind-tunnel results showed somewhat smaller values of effective dihedral than the flight-test results, though the trends are similar. The flight results always showed an increase of  $C_{l\beta}$  all the way to the stall. It should be noted that the maximum value of  $C_{l\beta}$  was about -0.006 per degree, a value corresponding to 30° effective dihedral in a straight wing.

It had been expected that the large dihedral effect obtained with a sweptback wing might lead to objectionable or dangerous flying qualities. The pilots of the L-39 airplane, however, did not consider any of the flying qualities caused by the large dihedral to be dangerous or objectionable. They had only minor objections to a few characteristics. The main difficulty was the considerable reduction in rolling velocities which could be reached in rudder-fixed aileron rolls as a result of the combined effects of the dihedral and the sideslip developed during the roll. The maximum value of  $pb/2V$  obtainable in rolls at speeds approaching the stall with flaps down was 0.035 radians as compared with the value of 0.07 which is considered to be the minimum for satisfactory flying qualities. Also, it was noted that at low speeds the rolling response was oscillatory; that is, the rolling velocity following an abrupt deflection of the ailerons would build up to a maximum and then fall off to zero or even reverse, then build up again.

Although in landing approaches and landings use of the rudder produced large lateral trim changes, this characteristic was not considered dangerous. The pilots considered the slight negative dihedral effect present at low normal-force coefficients to be more objectionable than high dihedral effect present at high normal-force coefficients. The negative dihedral effect leads to an illogical type of control because the rolling velocity due to rudder deflection is in the wrong direction. This is particularly objectionable to the pilot if the airplane changes from a condition of high positive to negative dihedral, so that he cannot become accustomed to either. It appears from these tests that in the design of sweptback-wing airplanes, the use of negative geometric

[REDACTED]

dihedral to reduce the effective dihedral at high lift coefficients should not be carried to the point of producing negative effective dihedral at low lift coefficients.

Another feature of sweptback-wing airplanes which it was thought might prove undesirable was the possibility of poorly damped lateral oscillations. The time history of a lateral oscillation of the L-39 airplane started by abruptly deflecting and releasing the rudder is shown in figure 6. In this case the ventral fin extension was removed. The lateral oscillation at this speed had a period of about 5 seconds and required 1.5 cycles to damp to half amplitude. The oscillations were satisfactorily damped in this case although the rolling motions associated with the oscillation were relatively large in comparison with those of conventional airplanes. The pilot had no objections to the lateral oscillations because he could easily control them. The type of control motions used in recovery from an oscillation is shown in figure 7. It is shown by this figure that, following an abrupt rudder kick, the airplane rolled  $35^\circ$  and started to return to its original attitude. As it was returning, the pilot applied coordinated rudder and aileron control to bring the airplane to the level attitude and then applied a small amount of control in the opposite direction to prevent overshooting. The speed at which the oscillation damped out indicates that an oscillation of such a long period is not likely to cause any difficulty, even if it should be poorly damped or undamped.

The application of the results of the L-39 tests to airplanes of higher wing loading or different size will be considered briefly. The dynamic-stability characteristics of an airplane of similar type will be the same if the value of the relative density factor  $\mu$  is the same. For the L-39 airplane, the value of  $\mu$  (based on wing span) was 14. An approximately equal value of  $\mu$  might be obtained on a larger airplane with higher wing loading. In this case, the damping characteristics of the lateral oscillations in terms of the number of cycles to damp to half amplitude would be the same at a given lift coefficient, but the period of the oscillations would be increased as the square root of the linear dimension. It would be expected that the pilot would have less difficulty in controlling these oscillations than those of the L-39 airplane. If the airplane had the same size as the L-39 but a heavier wing loading, or flew at a higher altitude, the value of  $\mu$  would be increased. As a result, the damping of the lateral oscillations would probably be decreased but the period of these oscillations in flight at a given lift coefficient would be the same. As mentioned previously, reduced damping would probably not be serious for an oscillation of this period.

[REDACTED]

The L-39 results give a good indication of the amount of directional stability that should be provided on an airplane with sweptback wings. With the ventral fin installed, the value of  $C_{n\beta}$  at high lift coefficients was 0.00195 per degree. With this amount of directional stability, the characteristics were fairly satisfactory, as noted previously. This value is about twice that usually present in conventional straight-wing fighter airplanes. With the ventral fin extension removed, the value of  $C_{n\beta}$  was about 0.001 per degree. In this case, the pilot considered the airplane difficult to fly because of the large lateral trim changes produced in any maneuver when inadvertent sideslipping occurred and because of the reversal in rolling velocities in rudder-fixed rolls. In the case of the L-39 airplane, with the fin extension removed, the variation of rudder angle with sideslip in steady sideslips was practically zero even though the directional stability measured in the wind tunnel was comparable with that of a conventional airplane. The loss of stability in steady sideslips is caused by the destabilizing effect of the aileron yawing moments when the ailerons are deflected to offset the high dihedral effect. The pilot's impression of directional stability is obtained from the variation of rudder angle with sideslip. In this case, therefore, the pilot felt that the directional stability was very small.

A larger value of directional stability is therefore required on sweptback-wing airplanes than on straight-wing airplanes for two reasons: First, to maintain adequate aileron effectiveness in rolls, and second, to offset the destabilizing effect of the aileron yawing moments in steady sideslips.

Complete studies of the stalling characteristics of the L-39 airplane were made with flaps up and flaps down and with all slot configurations. Without slots, the stalling characteristics were very undesirable. Figure 8 shows a time history of the rolling velocity during a stall with the flaps up and no slots. Also shown for comparison is a similar record obtained with the 80-percent-span slots. Without slots, there was a small amount of stall warning given by preliminary motion of the airplane but, at the stall, the airplane rolled abruptly because of almost instantaneous stalling of a complete wing panel. With either the 40-percent or 80-percent-span wing slots, the airplane performed increasing lateral oscillations at the stall. The stalling characteristics were considered good with either the 40-percent- or the 80-percent-span slots installed. The rate of increase of the oscillations at the stall was considerably greater when the ventral-fin extension was removed.

In order to obtain a comparison with the wind-tunnel measurements of the lift characteristics of the L-39 model, flight



measurements of the angle of attack of the L-39 airplane were made during stall approaches. The angle of attack was measured by means of a vane located on a boom ahead of the wing tip. The position error of this installation was determined by tests of a similar vane on the wind-tunnel model. A comparison of the flight and wind-tunnel measurements of the variation of normal force coefficient with angle of attack is given in figure 9. These results, which are representative of all the conditions tested, show that the agreement was good.

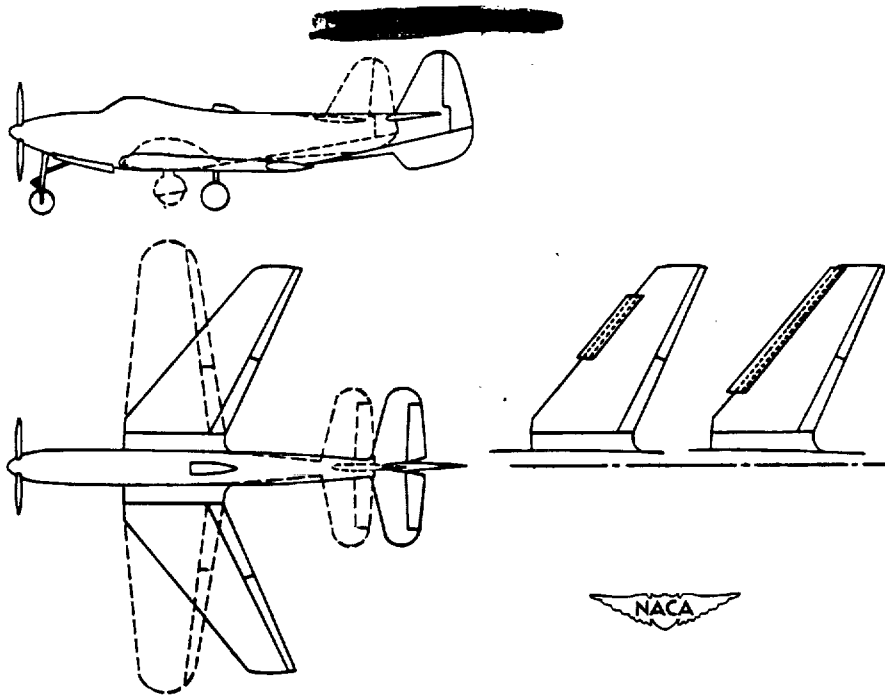
The maximum lift coefficient of the L-39 airplane without slots with flaps up was 1.20 and with flaps down was 1.51. The original P-63 airplane with the unswept wing had essentially the same values of maximum lift. The maximum lift coefficient of the L-39 airplane with slots installed was slightly less than without slots. Tuft studies indicate that this unexpected effect was caused by premature separation of the flow inside the inboard end of the slot. With the plain wing, the stall occurred abruptly over the whole wing at the same instant and therefore steady flight was possible right up to the maximum lift coefficient. With the slots installed, however, the premature separation of flow near the inboard end of the slot caused rolling and pitching motions of the airplane so that higher values of maximum lift coefficients which might have been obtained at high angles of attack were not usable in steady flight.

Though no NACA flight tests have been made on the second L-39 airplane with simulated circular-arc wing sections, a brief summary of the Bell flight test results may be of interest. No quantitative data from the Bell flight tests are available, and these statements are based on pilot's comments. It was found that the longitudinal instability at the stall was somewhat worse than that of the L-39 airplane with normal wing sections. The lateral stability characteristics were similar, but no measurements are available at high lift coefficients. The stalling characteristics were good in that there was no tendency to roll off at the stall. Flow separation started near the leading edge of the wing at speeds below 130 miles per hour, and at 140 miles per hour the flow was turbulent over the entire upper surface of the wing. Control could be maintained to 110 miles per hour, resulting in a normal value of maximum lift coefficient. The drag was very high at low speeds, however, and power-off landings at low speeds were dangerous because of the excessively steep gliding angle and high sinking speed.

## REFERENCES

1. Lambert, Arthur A.: Flight Investigation of a Bell P-63 Airplane with 35° Swept-Back Wings. Rep. No. 33-943-032, Bell Aircraft Corp., Oct. 1, 1946.
2. Sjoberg, S. A., and Reeder, J. P.: Flight Measurements of the Longitudinal Stability, Stalling, and Lift Characteristics of an Airplane Having a 35° Sweptback Wing Without Slots and with 40 Percent Span Slots and a Comparison with Wind-Tunnel Data. (Prospective NACA paper)
3. Sjoberg, S. A., and Reeder, J. P.: Flight Measurements of the Lateral and Directional Stability and Control Characteristics of an Airplane Having a 35° Sweptback Wing with 40-Percent-Span Slots and a Comparison with Wind-Tunnel Data. (Prospective NACA paper)

Phillips



### L-39 AIRPLANE

Figure 1.

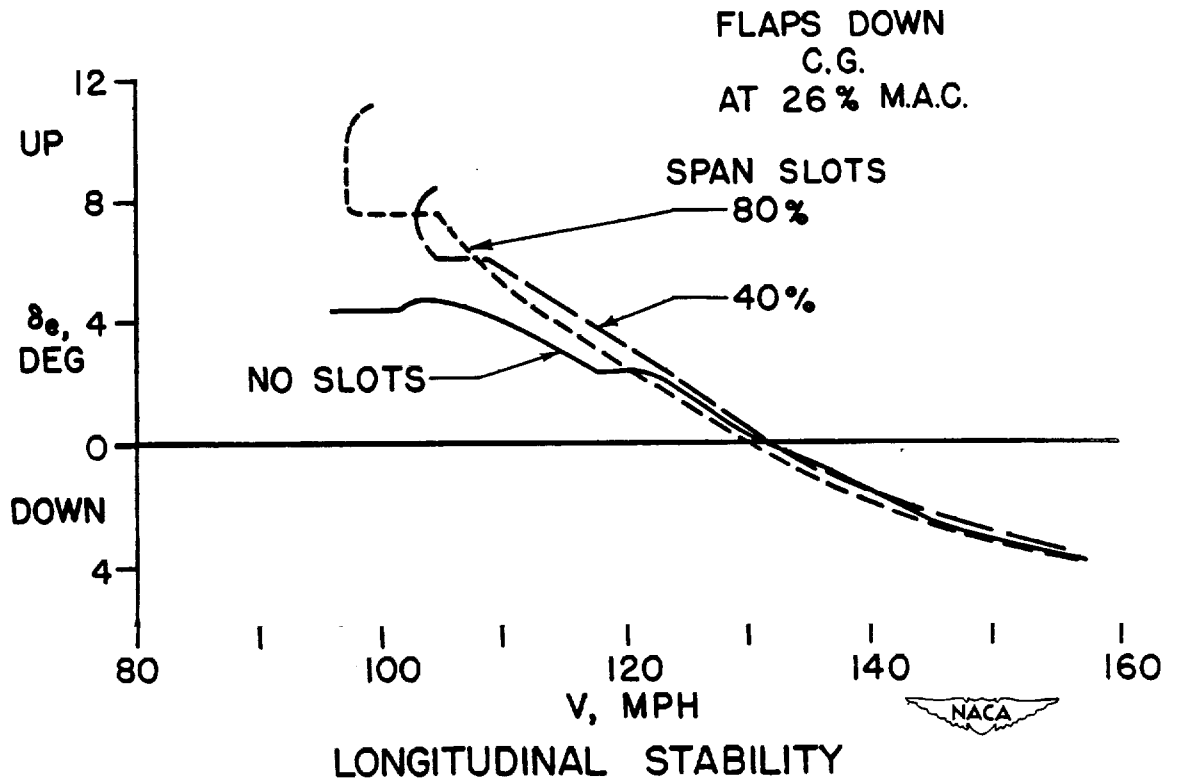


Figure 2.

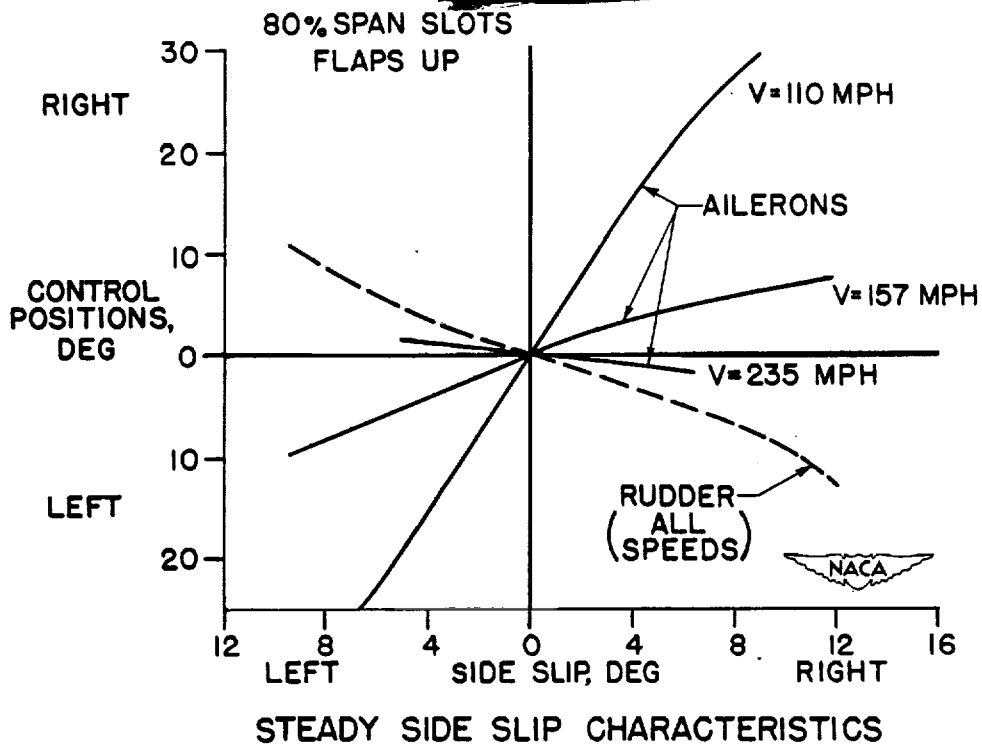


Figure 3.

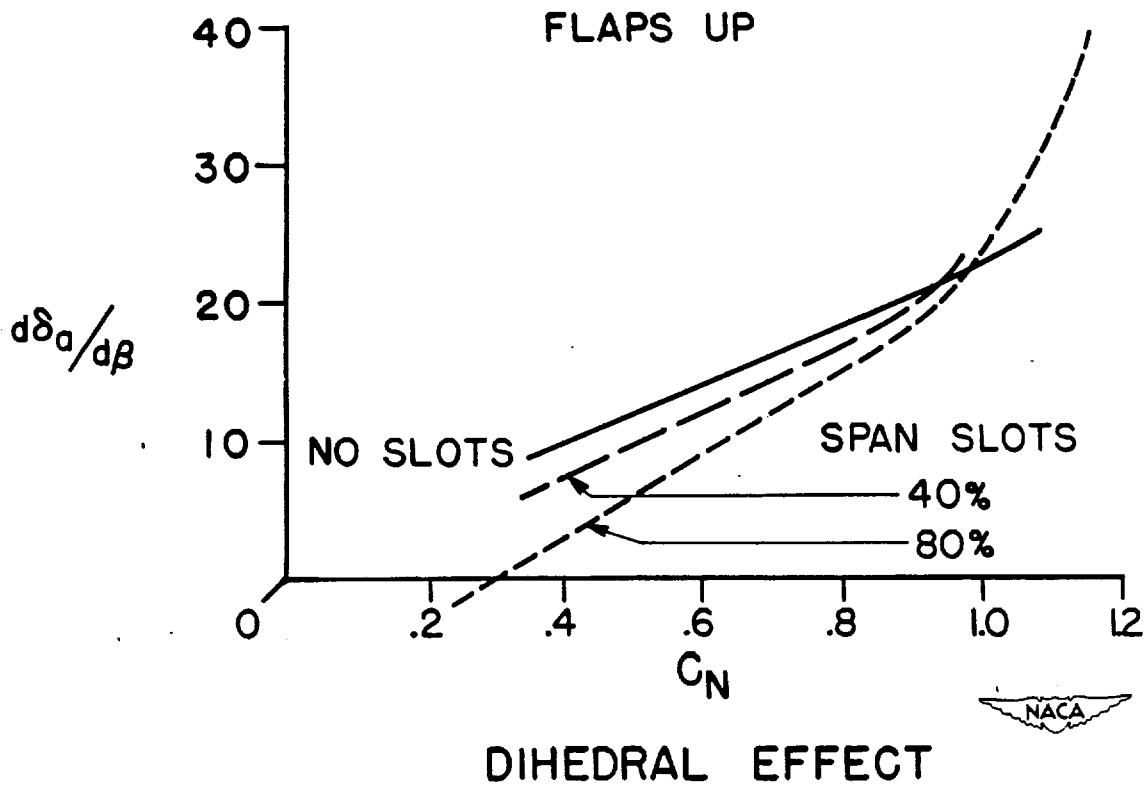


Figure 4.

Phillips

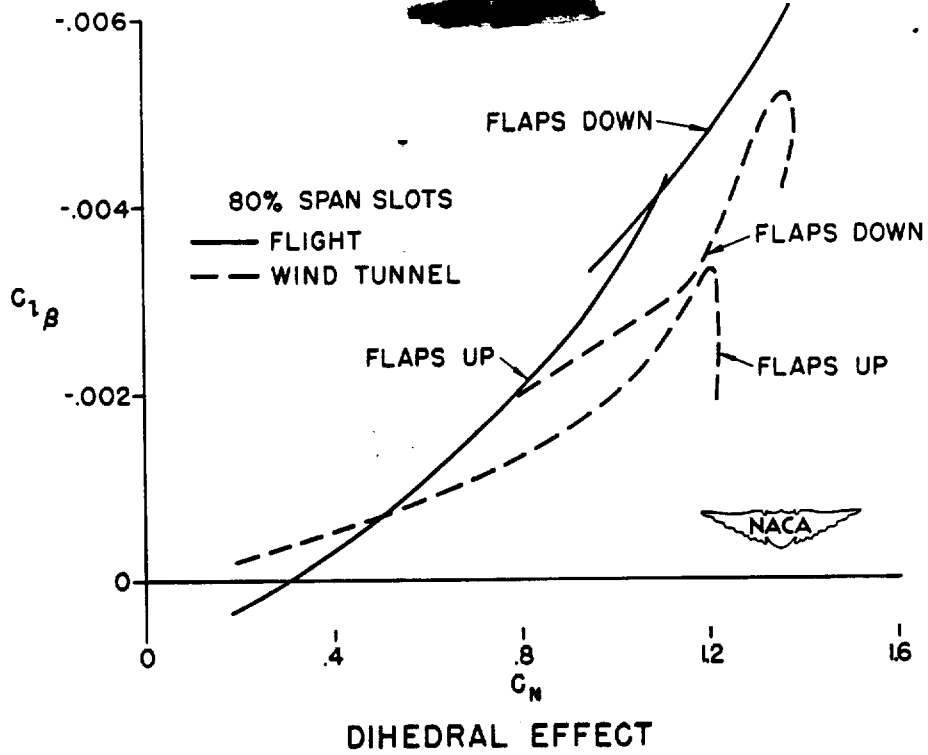


Figure 5.

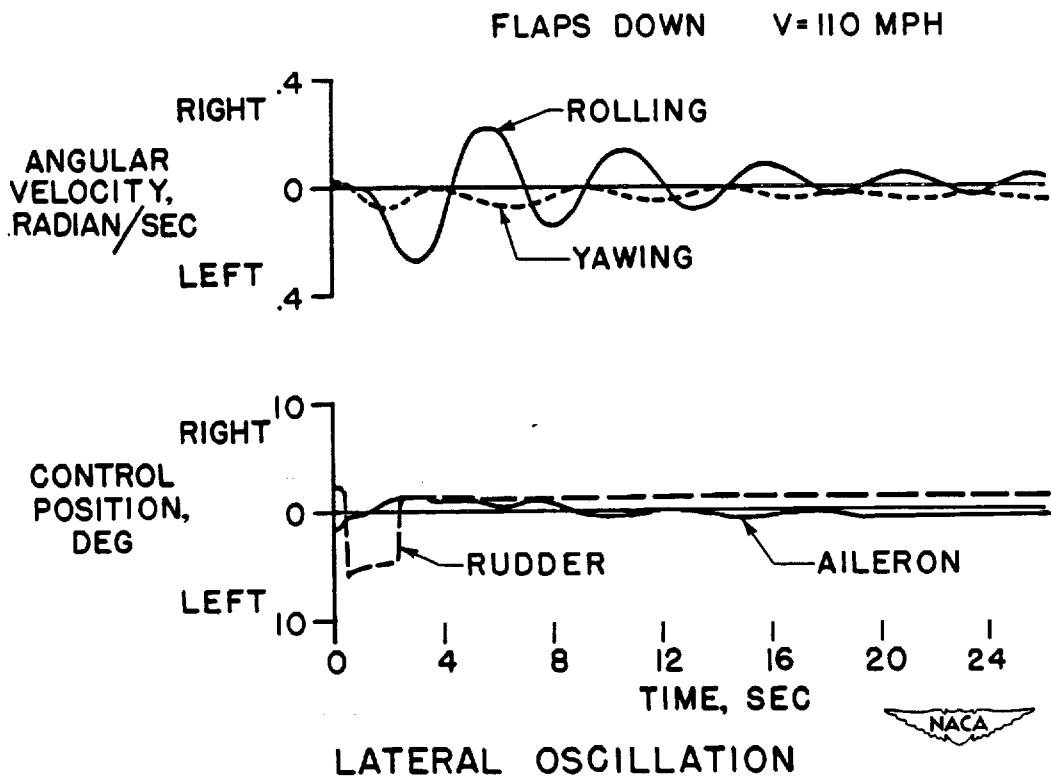


Figure 6.

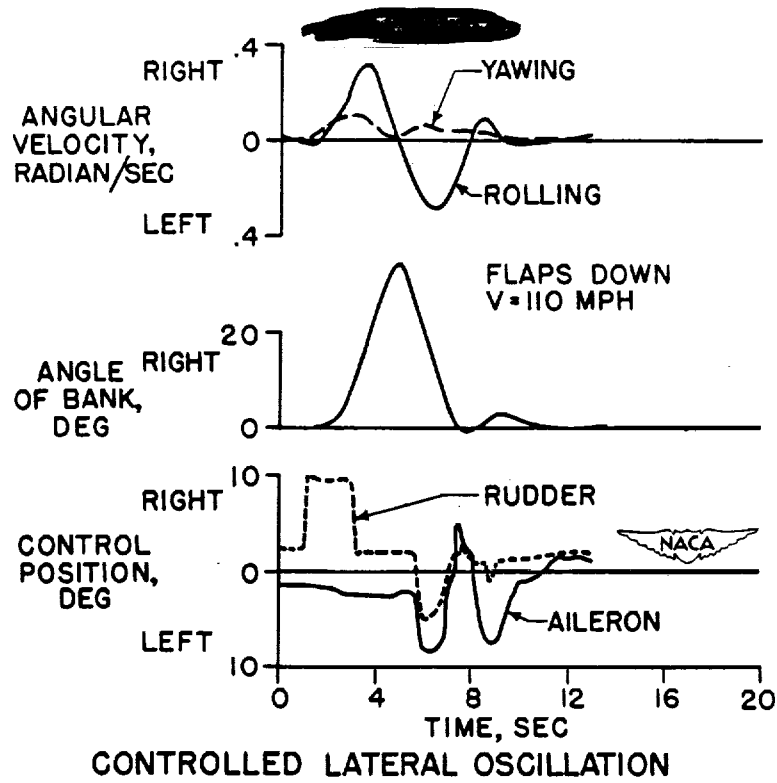


Figure 7.

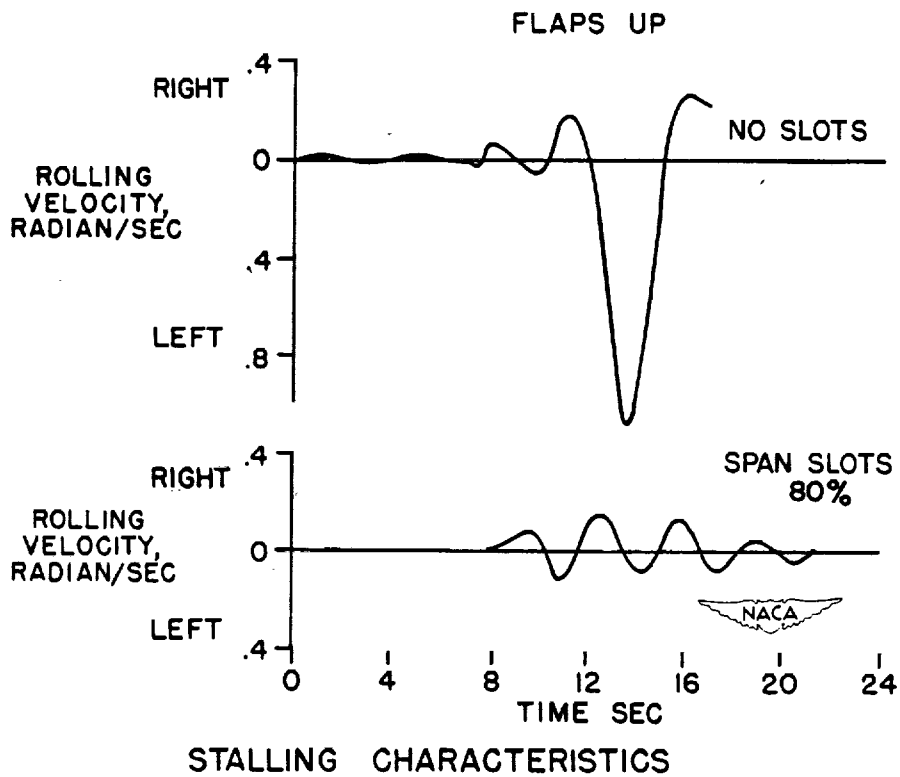


Figure 8.

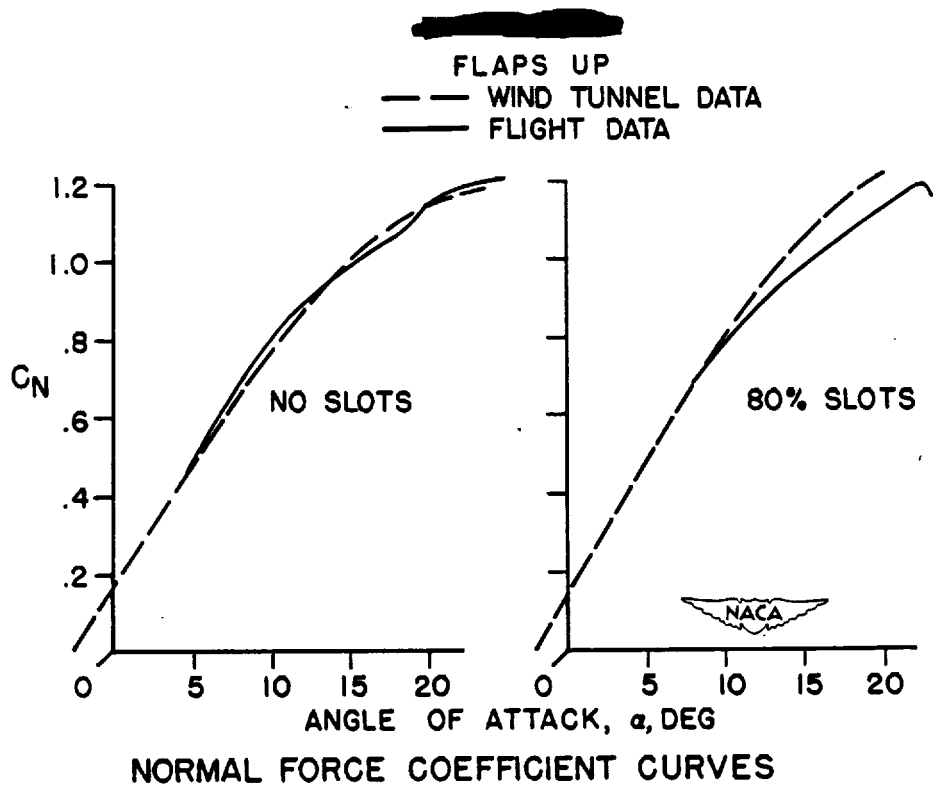
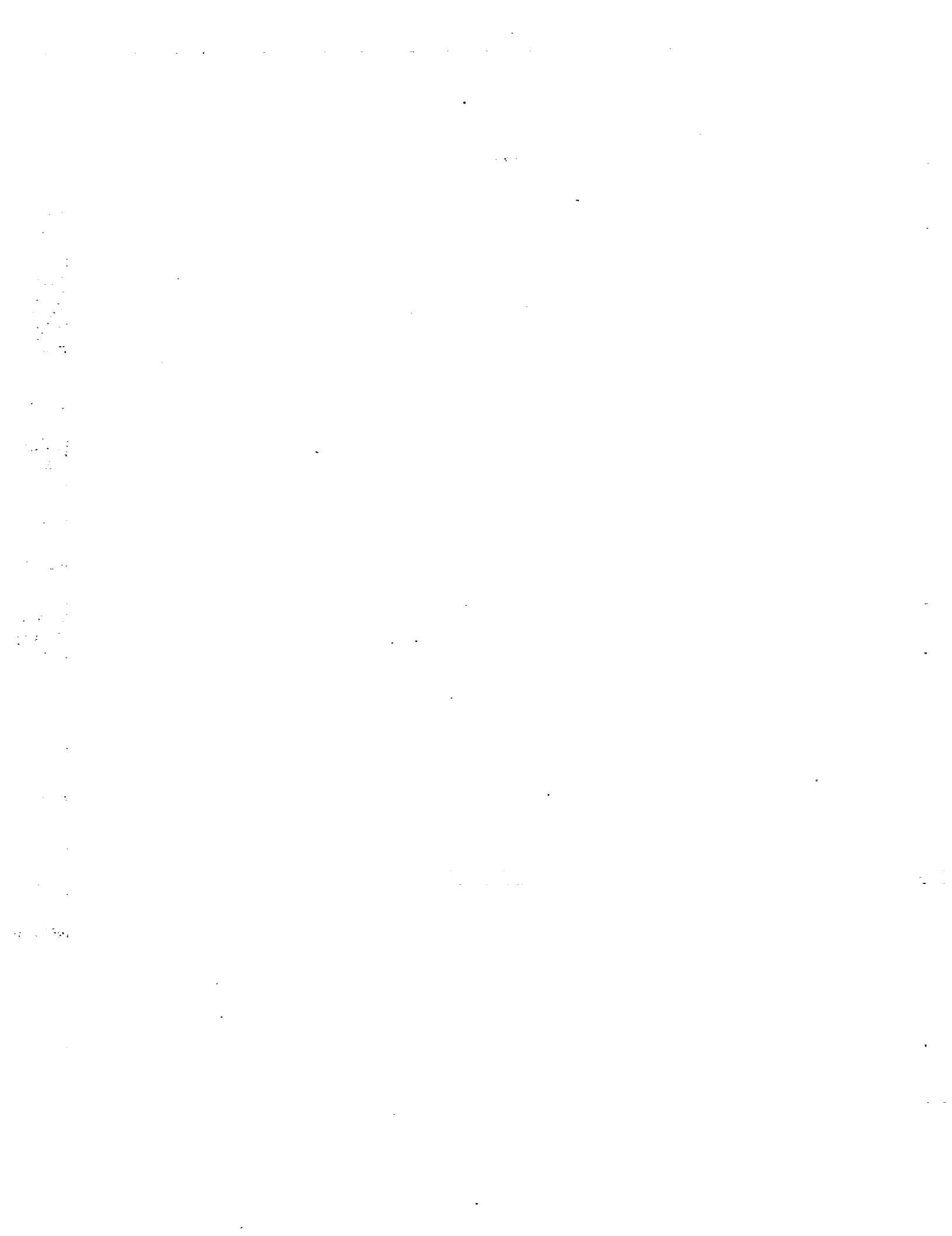


Figure 9.

██████████





D13

FLIGHT CHARACTERISTICS AT TRANSONIC SPEEDS

I - P-80A AIRPLANE INVESTIGATION

By H. H. Brown

Ames Aeronautical Laboratory

Extensive flight tests have been conducted at the Ames Laboratory on the P-80A airplane well up into the transonic range.

Previous to the flight tests, a  $\frac{1}{3}$ -scale model of the airplane was thoroughly tested in the Ames 16-foot high-speed tunnel up to a Mach number of 0.85. Analyses of these test results indicated that the airplane should possess satisfactory stability and control characteristics up to the maximum Mach number tested. The basis for this opinion is the results shown in the first two figures.

Figure 1 presents the elevator angle for trim in level flight at 20,000 feet as a function of Mach number. The solid curve shows the results based on the wind-tunnel tests. For purposes of comparison the flight test results are shown by the dashed curve. The tucking-under tendency as indicated by the increase in up-elevator angle required above a Mach number of 0.70 was not considered serious since the pilot would presumably have ample warning. The change with Mach number of the tucking under was less severe in flight than indicated from the wind-tunnel tests.

Similarly in figure 2 is shown the variation of required elevator angle with acceleration factor for Mach numbers of 0.80, 0.825, and 0.85. The solid curves are based on the wind-tunnel results and the dashed curves on flight tests. There was nothing shown here which would predict a pitch-up.

In spite of the reassuring nature of the wind-tunnel results and the careful manner in which the flight tests were conducted, a condition was encountered during a dive at a Mach number of about 0.85 which produced a violent and inadvertent stall. This particular feature of this airplane remains one of the major factors which limit operation of the airplane to still higher Mach numbers.

Figure 3 shows a time history of some of the quantities evaluated during this dive. The lift coefficient roughly follows the elevator motion up to about 13.25 seconds. At this point the lift coefficient rapidly began to increase with only a small change in elevator angle and no change in stick force.

Reexamination of the wind-tunnel data failed to indicate the cause of the pitch-up for two reasons:

- (1) The strength of the model limited the  $C_L$  to a value of 0.40 at a Mach number of 0.85, which was a lower value than the value encountered during the pitch-up.
- (2) Tunnel conditions at the larger lift coefficients and highest Mach numbers were close to choking.

Combining the data obtained during the dive with the wind-tunnel results did afford a partial solution to the problem. The fuselage due to its high critical Mach number was eliminated as a cause of the pitch-up. The wing pressure distributions made during the dive also enabled the pitching-moment coefficient of the wing to be eliminated as a cause. The spanwise loadings derived from the pressure measurements showed only a minor difference compared to the lower Mach number results and therefore downwash changes were ruled out. Lastly, the effects due to the shift in the angle for zero lift of the wing were obtained from the wind-tunnel data.

In figure 4 the total out-of-trim pitching-moment coefficient of the airplane during the pitch-up is shown with  $C_M$  as the abscissa. Also shown is the out-of-trim pitching-moment coefficient furnished by the negative shift in the angle for zero lift as the airplane decelerated. The difference between these two curves represents the destabilizing influence that must be attributed to something other than the wing and fuselage.

In order to determine whether the flow conditions at the tail or whether the tail characteristics were responsible, the isolated horizontal tail was tested in the Ames 16-foot high-speed tunnel at the Mach numbers and over the angle of attack and elevator angle range reached during the dive.

The results showed large changes in effectiveness of the tail, especially at the high elevator deflections encountered in the dive. This change in effectiveness, plus the immersion of the tail in the wake at higher lift coefficients, which tends to accentuate its effect, accounts for the unstable action of the airplane in the pull-up.

On the left side of figure 5 the variation of tail pitching moment has been plotted against the Mach number determined from the isolated tail tests. The elevator deflection, which was used in the dive, is  $12^\circ$ , and the tail angles of attack were those which would be encountered by the tail in the process of the pitch-up.

If it were presumed that the pull-up were made at a constant Mach number of 0.87 and that the tail operated at free-stream Mach number, a crossplot along the vertical line at a Mach number of 0.87 would give the tail contribution to the pitching moment of the airplane. The result is shown by the solid line on the right side of figure 5 with the  $C_N$  of the airplane as the abscissa. It can be seen that the tail contribution is stabilizing.

An estimation based on wind-tunnel results of the wake location shown in figure 6 shows, however, that the tail was in all probability passing into the wake as  $C_N$  increased.

In the upper part of figure 6, sketch A represents conditions at a low lift coefficient (about 0.10) and the tail is practically out of the wake. Sketch B shows conditions at a lift coefficient of about 0.50, and sketch C shows conditions at a lift coefficient of 0.80 when the tail was well into the wake. The lower part of figure 6 shows the values of  $q_H/q$  and decrement in Mach number at the tail corresponding to the upper sketches. Thus as the airplane lift coefficient changed from 0.5 to 0.8 at a constant free-stream Mach number, the tail Mach number decreased by about 0.08.

Figure 5 shows the effect of this Mach number decrease on the tail contribution to the airplane pitching moment.

In this case as the normal-force coefficient  $C_N$  at a constant Mach number is increased at a constant Mach number the values shown by the dashed curve are produced taking into account the decrease in Mach number at the tail. This results in a tail contribution to the airplane pitching moment which is neutral or destabilizing above a lift coefficient of 0.7.

Adding this type of tail pitching-moment contribution to the change in trim which occurred due to the decreasing Mach number during the dive means an apparent instability of the entire airplane above a lift coefficient of 0.5.

It is to be emphasized that this instability did not exist at all other elevator deflections. For example, figure 7 shows the results of a similar analysis for an elevator angle of  $4.4^\circ$ , which was required for trim in level flight at a Mach number of 0.87. In this case the influence of the wake is considerably less important and the tail contribution is stabilizing throughout the angle-of-attack range. This accounts for the normal variation of elevator angle against Mach number and elevator angle against acceleration of

gravity  $g$  over the limited range for which it was possible to derive these results from the wind-tunnel tests of the complete model.

Since the airplane is unstable at high Mach numbers, it becomes of interest to determine what rates of elevator response are required of the pilot to forestall such a pitch-up as did occur. By using the conditions at the start of the pitch-up, the change in the normal acceleration factor with time was determined with various rates of elevator motion using a step-by-step solution of the equations of motions. The results are shown in figure 8. With no time delay in the pilot response a rate of elevator motion of  $2^\circ$  per second was sufficient to prevent the acceleration building up to a stall. With a quarter-second time delay, which is about the best response which can be expected from a pilot, a rate of elevator motion of almost  $4^\circ$  per second was needed to prevent a stall. For time delays much longer than a quarter of a second, the required rates became unreasonably large. Actually a pilot responds to a change in acceleration and since the pitch-up motion at first produced only a small acceleration change, the pilot's response time was quite long. As a result, it is improbable that a pilot will be able to prevent such a stall.

The fact that airplanes with higher critical Mach numbers have exceeded Mach numbers of 0.85 or 0.86 without similar stability and control troubles may merely indicate postponement of this danger to a higher Mach number. The necessity for testing in the transonic wind tunnels to higher lift coefficients and larger elevator deflections is apparent. If this is not possible because of the limitation of the model or wind tunnel, then recourse can be made to a study based on isolated tail tests and wake profiles similar to that done in this case.

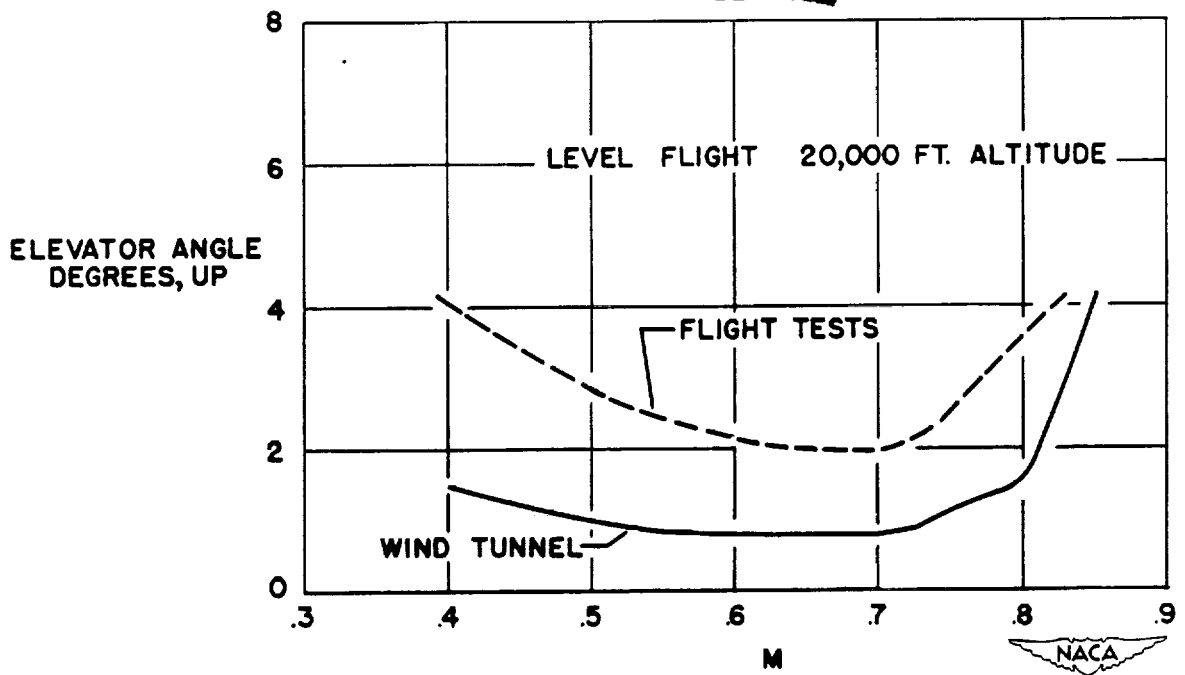


Figure 1.- Variation of elevator angle for trim in level flight at 20,000 feet with Mach number.

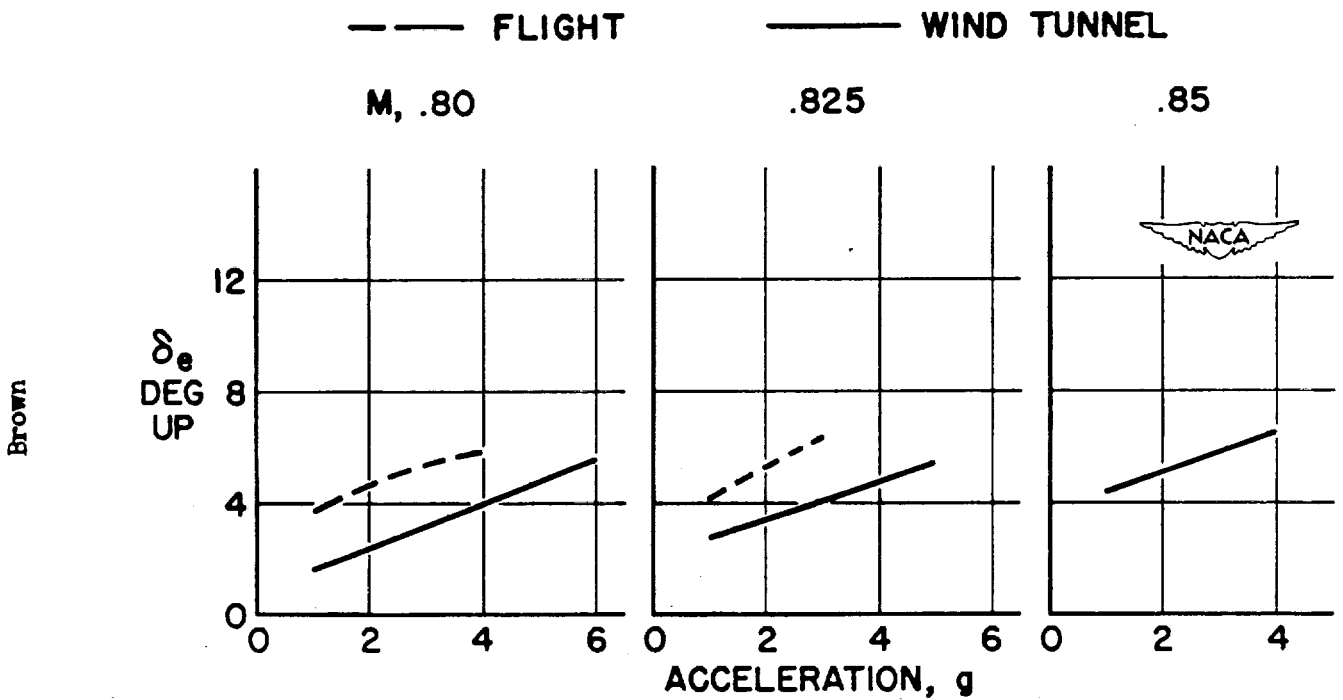


Figure 2.- Variation of required elevator angle with acceleration factor at high Mach numbers.

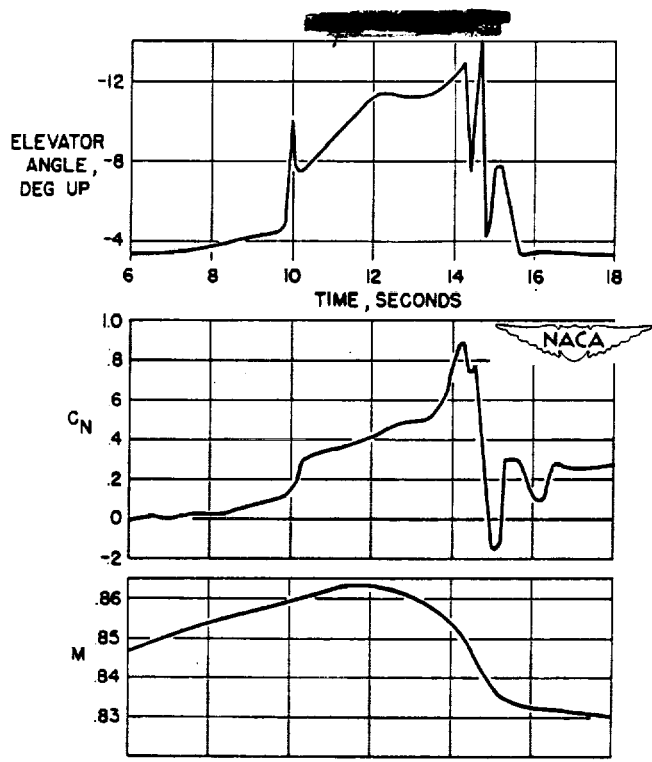


Figure 3.- Time history of dive.

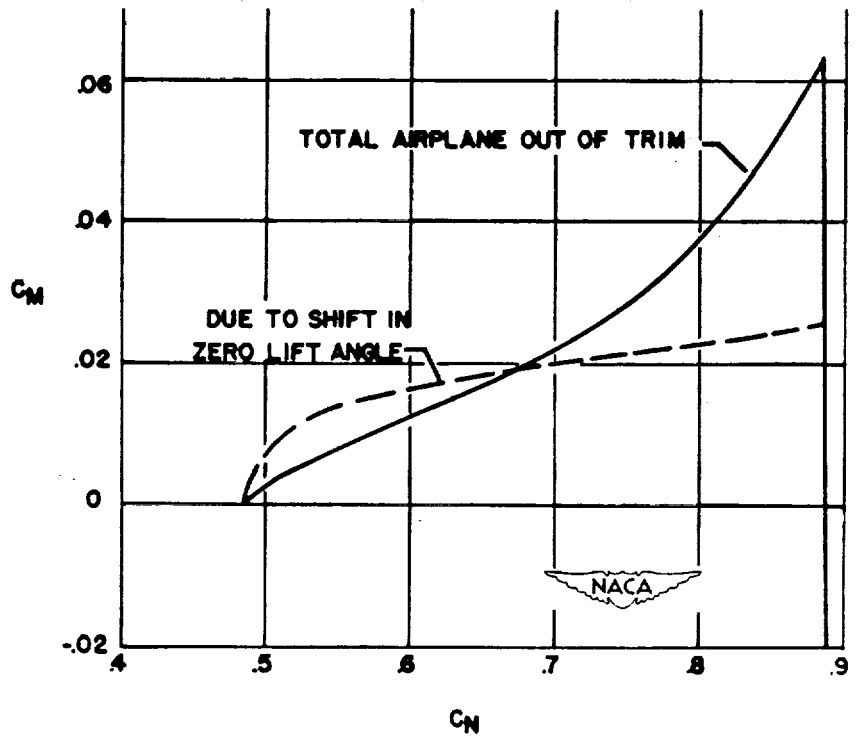


Figure 4.- Out-of-trim pitching-moment coefficients during pitch-up.

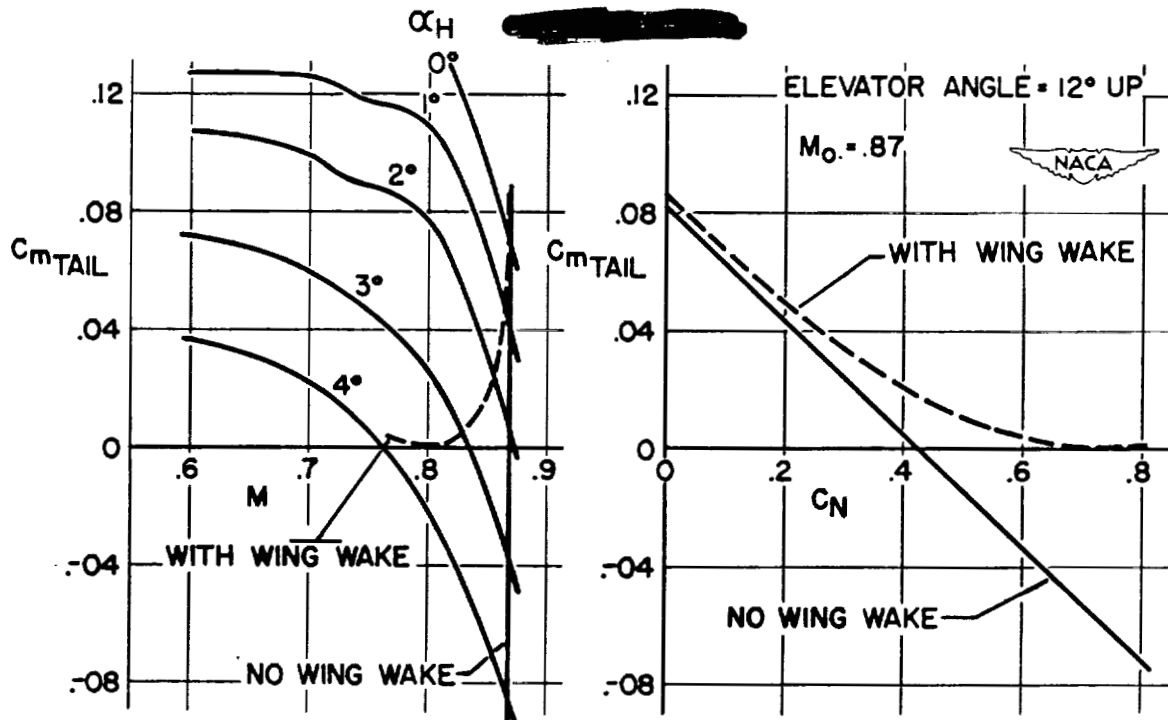


Figure 5.- Tail pitching-moment coefficient with large elevator deflection.

Brown

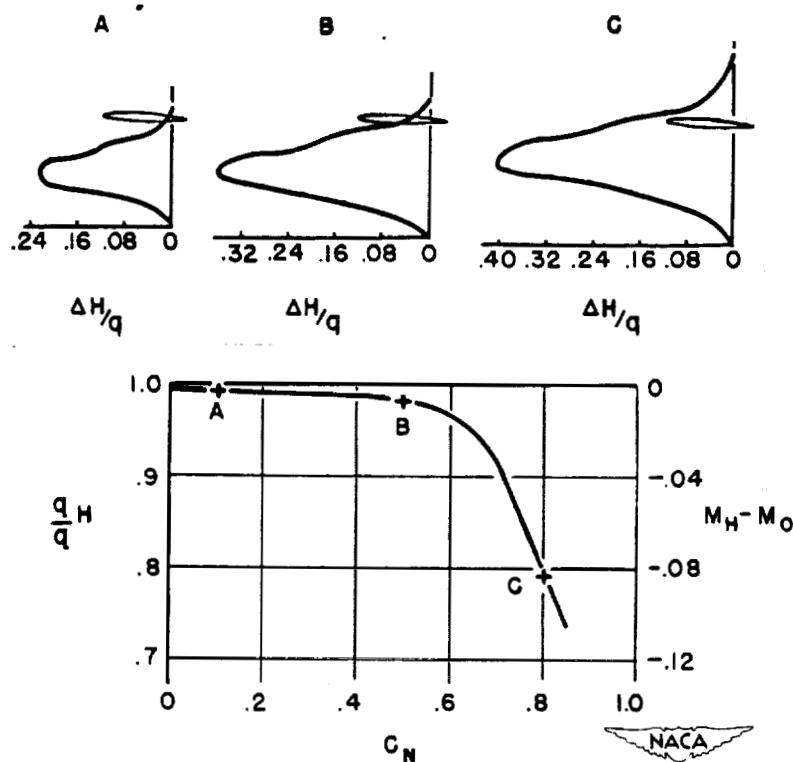


Figure 6.- Estimated wake at the tail and the effect on local Mach number.

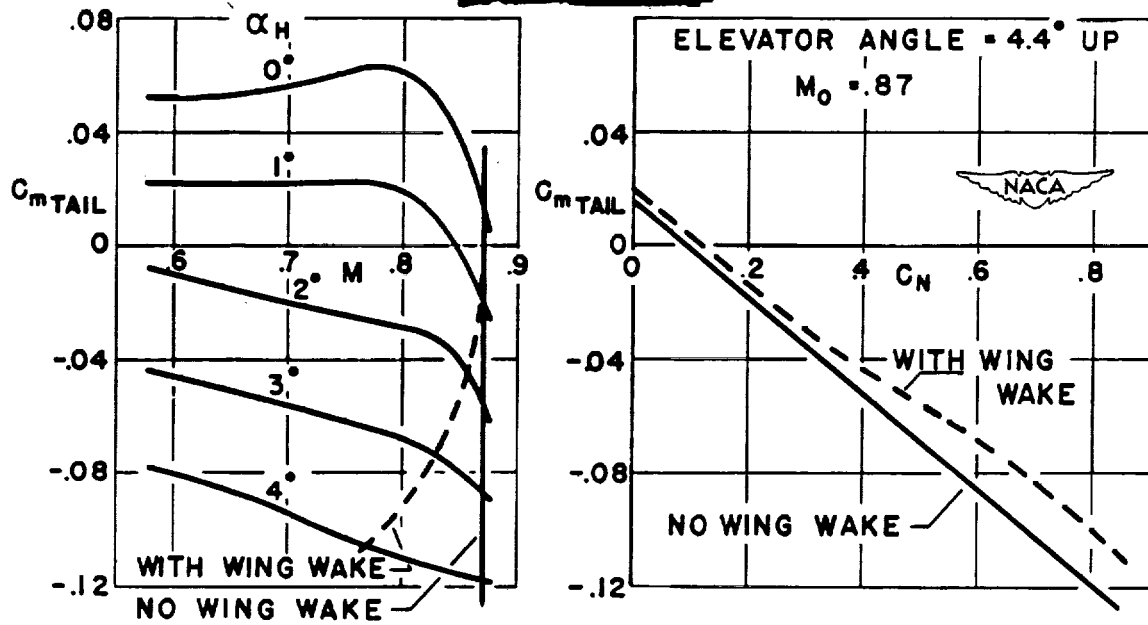


Figure 7.- Tail pitching-moment coefficient with a moderate elevator angle.

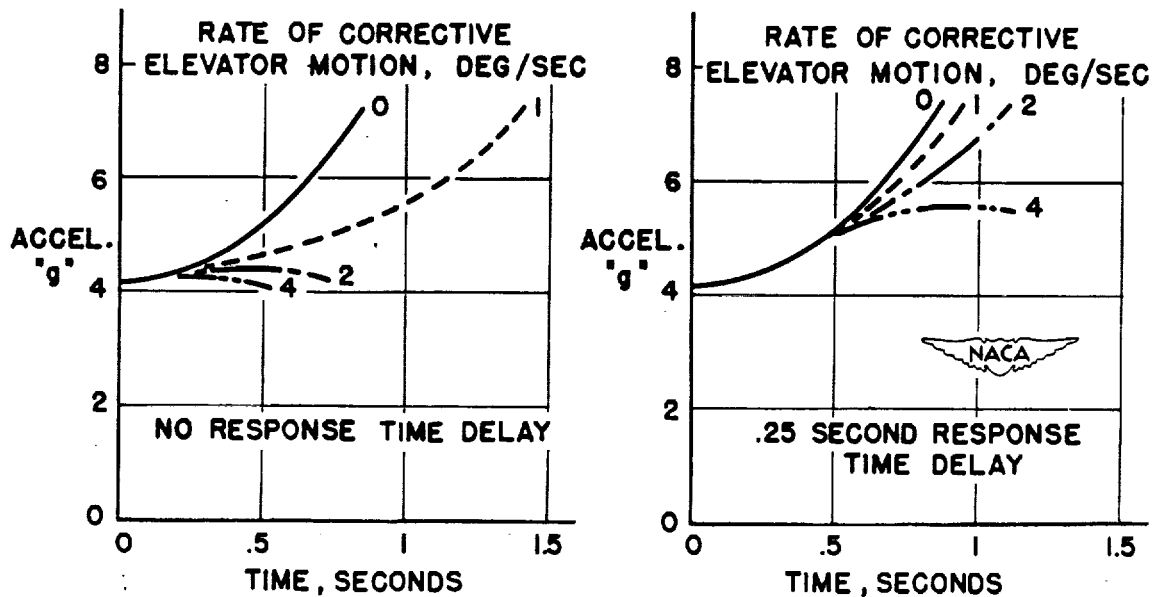


Figure 8.- Effect of rate of response and time delay in preventing a stall.



## FLIGHT CHARACTERISTICS AT TRANSONIC SPEEDS

## II - RESEARCH AIRPLANES

By Walter C. Williams

Langley Memorial Aeronautical Laboratory

## INTRODUCTION

The Air Forces, the Navy, and the NACA have been engaged in a cooperative program for the development and procurement of a series of research airplanes which would have potential characteristics necessary for level flight in the transonic- and supersonic-speed zones. This program was undertaken in anticipation of the increased importance of flight research in the transonic-speed range where the aerodynamic characteristics of airplanes were known to show large and sudden changes. The range of airplane configurations flying or under construction include straight-wing types with conventional airfoil sections, straight-wing types with a supersonic airfoil section, sweptback-wing types, and tailless sweptback-wing types. The manufacturers involved are Bell Aircraft Corp., Douglas Aircraft Co., and Northrup Aircraft Corp. Two types of these airplanes are flying: the Douglas D-558 Phase I airplane procured by the Navy; and the Bell XS-1 procured by the Air Forces. The airplanes represent the first phase of the program and are being used to explore the limits to which an airplane of relatively conventional design can be flown.

The Navy procured from the Douglas Aircraft Co. the D-558 Phase I airplane. This airplane has a 10-percent-thick straight wing with an aspect ratio of 4 and an 8-percent-thick horizontal tail. The power plant is a TG-180 turbojet engine. The Douglas Aircraft Co. recently turned one of these airplanes over to the NACA at Muroc, Calif. The installation of NACA recording instrumentation has been completed and flight tests of this airplane are expected to begin this week. This airplane will be used for the measurement of stability and control characteristics and over-all aerodynamic loads by use of strain gages throughout the allowable speed range of the airplane. It is expected that a second D-558 Phase I airplane will be delivered to the NACA within the next several weeks and this airplane will be used for detailed measurements of the pressure distribution on the wing and on the horizontal tail.

The Bell XS-1 airplane was procured by the Air Forces. This airplane has a straight wing with an aspect ratio of 6 and is powered by an RM-1 liquid oxygen-alcohol rocket engine. Two of these airplanes have been completed. One airplane has a 10-percent-thick wing

and an 8-percent-thick horizontal tail; whereas, the other airplane has an 8-percent-thick wing and a 6-percent-thick tail.

The acceptance tests on the XS-1 airplane conducted by the Bell Aircraft Corp. have been completed. During these tests NACA instruments were installed to measure stability and control characteristics and aerodynamic loads up to a Mach number of 0.8 which was the contractual limit of the tests. These tests showed that the airplane had good handling qualities with no unusual characteristics.

Upon completion of the acceptance tests, one XS-1 airplane (with a 10-percent-thick wing and an 8-percent-thick horizontal tail) was assigned to the NACA for a systematic step-by-step investigation of flight to exploit the full capabilities of the type in the transonic-speed range. The same instrumentation used in the acceptance tests will be used in the early phase of these tests. Later tests will include detail pressure-distribution measurements. These tests are just getting under way having been delayed by mechanical difficulties. The other XS-1 airplane (with an 8-percent-thick wing and a 6-percent-thick horizontal tail) was taken over by the Flight Test Division at Wright Field for use in an accelerated transonic-flight program. These tests would differ from NACA tests in that no detailed investigations would be made, and as large an increase in Mach number as compatible with safety would be made in each flight. If necessary, flight would be made at extreme altitudes (50,000 to 60,000 ft). This is a cooperative program between the Wright Field Flight Test Division and the NACA. NACA instrumentation is used on all flights, data reduction and analysis are performed by NACA personnel, and the flying is done by a Wright Field Flight Test Division pilot. The instrument installation, however, is not as comprehensive as in the NACA XS-1. Telemetering and recording instruments are used to measure airspeed altitude, elevator, right aileron and stabilizer position, normal, transverse, and longitudinal acceleration, shear and bending moment on the right horizontal tail, and bending moment on the right wing. These tests have been in progress several months and the data presented herein are results obtained in the accelerated transonic program up to a Mach number of 0.92.

#### TESTS, RESULTS, AND DISCUSSION

A preliminary airspeed calibration was made during the acceptance tests. These results showed the static-pressure error to be of

the order of 1/2 percent up to a Mach number of 0.8. As the flights of the airplane progressed to higher speeds, calibration of the static-pressure error of the airspeed head was made. The calibration was made using radar to obtain true altitude. The results of the calibration up to a Mach number of 0.92 are given in figure 1 where the error is expressed as the ratio of error in Mach number to corrected Mach number and is plotted as a function of corrected Mach number. Figure 1 shows that below a Mach number of 0.83 the airspeed head is indicating static pressure lower than true static pressure; whereas above a Mach number of 0.83, an increasing error in static pressure above true static is indicated. It is believed that this variation in static-pressure error above a Mach number  $M$  of 0.8 is caused by the formation of a shock on the airspeed head itself and the shock is moving back on the head towards the static holes. No correction was applied to the total-head measurement since the total-head measurement is not expected to be affected by shock-wave formation until a free-stream Mach number of at least unity is reached. The airspeed head used in this case is a Kollsman Type D-1 high-speed head mounted on a boom 1-chord length ahead of the left wing tip.

Most transonic flight tests have been limited by the changes in longitudinal stability and trim, and these data have been of primary concern in the XS-1 tests. The results obtained are presented in figure 2 where elevator position and force are plotted as functions of Mach number for two stabilizer positions. The elevator positions shown here are measured relative to the stabilizer, and the stabilizer positions are relative to the fuselage reference line. With the stabilizer set at an angle of incidence  $i_t$  of  $1.0^\circ$ , the pilot stopped at a Mach number of about 0.88 because of the large trim forces required and the forward position of the stick. A nose-down trim change is indicated at the highest Mach number. With the stabilizer set at an angle of incidence of  $2.2^\circ$  the pilot continued flight up to a Mach number of 0.92. In going to this speed, three trim changes were encountered. The first, which began at a Mach number of about 0.8 was in the nose-down direction which the pilot corrected with up elevator. Above a Mach number of about 0.87, the nose-down trim condition is alleviated and the airplane tends to pitch upward, and then, the pilot corrected with down elevator; at the highest Mach number the airplane is again showing a tendency toward nose-down trim position. Most tests have terminated somewhere in the region of the first trim change because with conventional fighters the control forces involved are large. In the present case the range of forces in the trim changes is of the order of 10 pounds. The changes in elevator angle for trim were also not large (of the order of  $4^\circ$ ). Because of the small control forces and motions, the

pilot did not object to the unusual trim changes. The forces are low in this case because the tests were run at a moderately high altitude (about 30,000 ft) and because the elevators are very small. With a larger airplane or at a lower altitude these control characteristics would probably be objectionable. Data from the Langley 8-foot high-speed-tunnel tests and from wing-flow tests of XS-1 models are in general qualitative agreement with flight data.

From the elevator positions required for trim with two stabilizer positions, a measure of the relative effectiveness of the elevator was obtained. These data are shown in figure 3 where the ratio of the change in stabilizer incidence  $\Delta\alpha_t/\Delta\delta_e$  to change in elevator position is plotted as a function of Mach number  $M$ . Between a Mach number of 0.72 and 0.87 the relative elevator effectiveness is reduced by more than 50 percent.

This reduction in elevator effectiveness in the speed range tested affects the magnitude of the trim changes as noted by the pilot, but in figure 4, where the pitching-moment coefficient of the wing-fuselage combination is plotted as a function of Mach number, it can be seen that the trim changes are being caused by changes on the wing. These data were obtained by using measured values of horizontal tail loads. Very little data have been obtained to show the longitudinal stability in accelerated flight but it is indicated that the stability as evidenced by the pilot, that is the elevator motion required to produce a given acceleration, is greatly increased above a Mach number of 0.85. Some of this increase in the elevator angle per lift coefficient  $C_L$  is caused by the decrease in elevator effectiveness, but the data though meager, indicate that the airplane is becoming more stable. These characteristics will be investigated in detail during the NACA tests of the XS-1.

Difficulties have been experienced in recent tests at transonic speeds with one-dimensional flutter or buzz. There has been no evidence of buzz in the data of the XS-1 tests. One probable contributing factor to the absence of this oscillation in addition to the thin wing section is the large amount of friction in the aileron control system. The friction in the ailerons is of the order of 20 foot-pounds. The aerodynamic hinge-moment coefficient for the dynamic pressure  $q$  corresponding to a Mach number of 0.85 at 30,000 feet and neglecting the effects of Mach number on the hinge-moment coefficient is of the order of 6.9 foot-pounds per degree. Hydraulic dampers are installed but have not been used. There has been no evidence of abrupt changes in the floating tendencies of the ailerons. The pilot did report a right wing heaviness which he noticed at a Mach number of about 0.88 and which continued up to a

Mach number of 0.92. Figure 5 shows that the right aileron angle for trim increased in the downward direction with increasing Mach number.

An unusual unclamped lateral oscillation has occurred in some flights. Because of the usual stability boundaries it would be expected that the airplane would be stable because the directional stability is very high and the lateral stability is moderate. The oscillations have occurred in steady gliding flights and in turns from a Mach number of 0.7 to a Mach number of 0.85. It was thought that these oscillations were possibly caused by fuel sloshing. A series of tests was made therefore with varying amounts of fuel on board. These tests showed that the fuel had little effect on the damping of the short period oscillation.

Another difficulty which has limited the Mach number at which airplanes are flown has been buffeting. The buffet boundary and the limit lift for the XS-1 are shown in figure 6 as a function of Mach number. These data were obtained in level flight or in gradual turns with the stabilizer set at an incidence angle of  $2.2^\circ$ . Limit lift has been determined from measurements where lift ceased to increase although increasing up elevator was being applied. Although buffeting has been experienced in level flight, it has not been disconcerting to the pilot because the buffeting is not severe. The maximum buffeting tail loads were obtained at limit lift from a Mach number of 0.76 to a Mach number of 0.80 and were of the order of  $\pm 400$  pounds. At Mach numbers above 0.80 the buffeting tail loads decreased, and up to a Mach number of 0.92 the buffeting tail loads were less than  $\pm 250$  pounds.

## CONCLUSIONS

The data obtained for the XS-1 airplane show that most of the difficulties expected in the transonic range have been experienced, and although conditions are not normal, the airplane can be flown satisfactorily at least to a Mach number of 0.92. The following results have been noted in detail:

1. The airplane has experienced longitudinal trim changes in the speed range from a Mach number of 0.8 to a Mach number of 0.92, but the control forces associated with these trim changes have been small. The pilot has been able, therefore, to control the airplane.
2. The elevator effectiveness has decreased by more than 50 percent in going from a Mach number of 0.7 to a Mach number of 0.87.

This loss in elevator effectiveness has affected the magnitude of the trim changes, but the actual trim changes have been caused by changes in the wing-fuselage moment.

3. No aileron buzz or associated phenomena has been experienced up to a Mach number of 0.92. The airplane becomes right wing heavy but can be trimmed with aileron.

4. Buffeting has been experienced in level flight but has been very mild up to a Mach number of 0.92. The tail loads associated with the buffeting have been small.

Williams

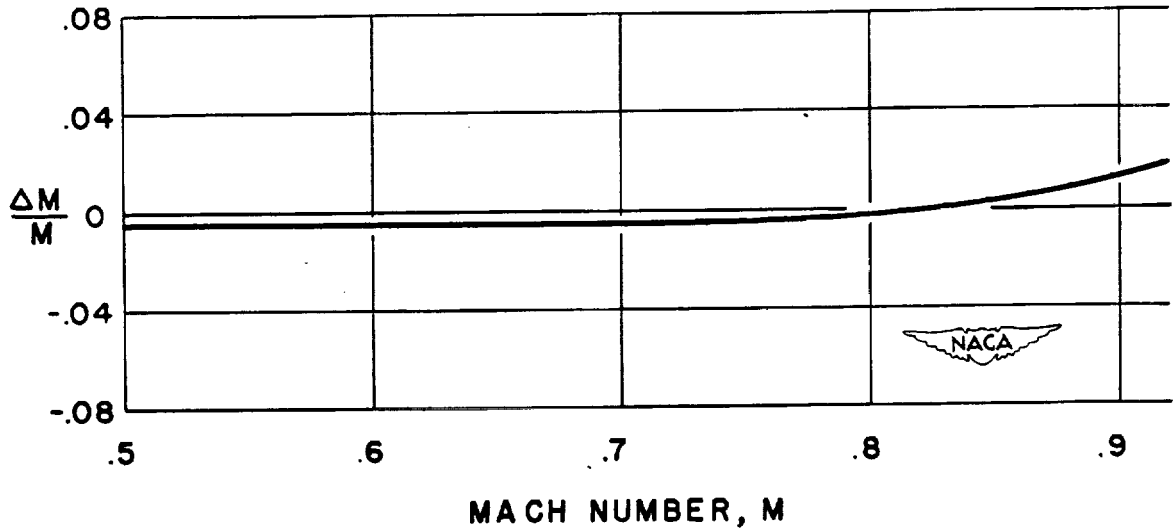


Figure 1.- Variation of Mach number error  $\Delta M/M$  with corrected Mach number. XS-1 airplane.

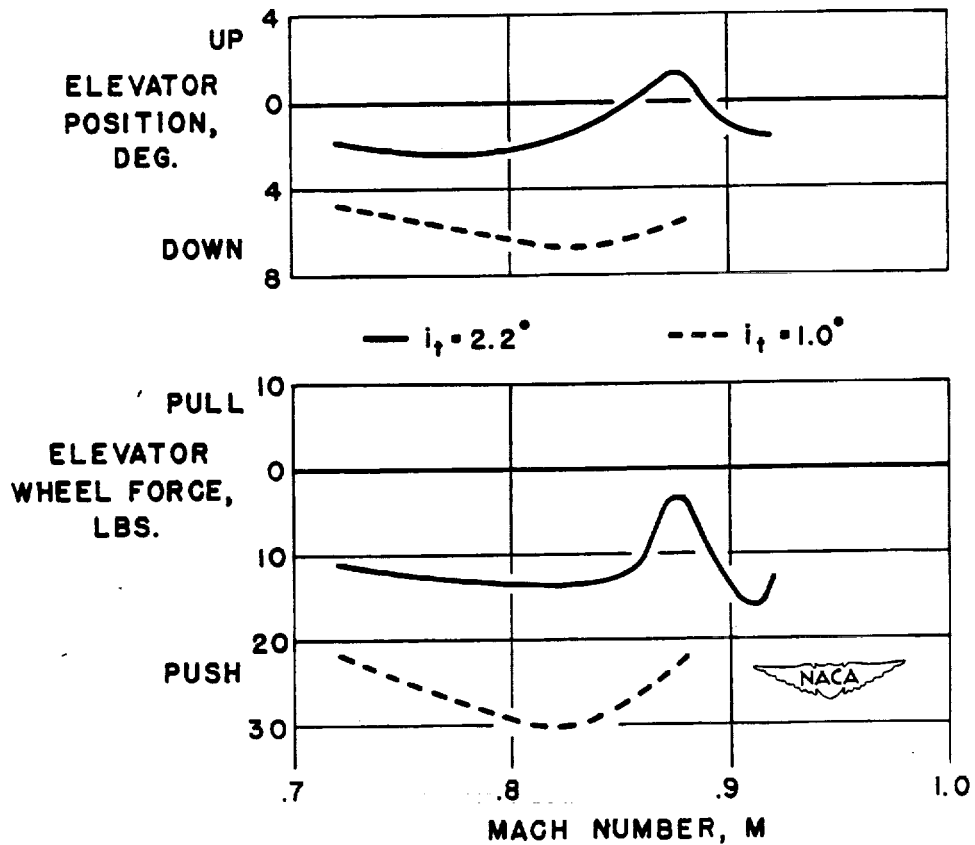


Figure 2.- Variation of elevator position and force with Mach number. XS-1 airplane.

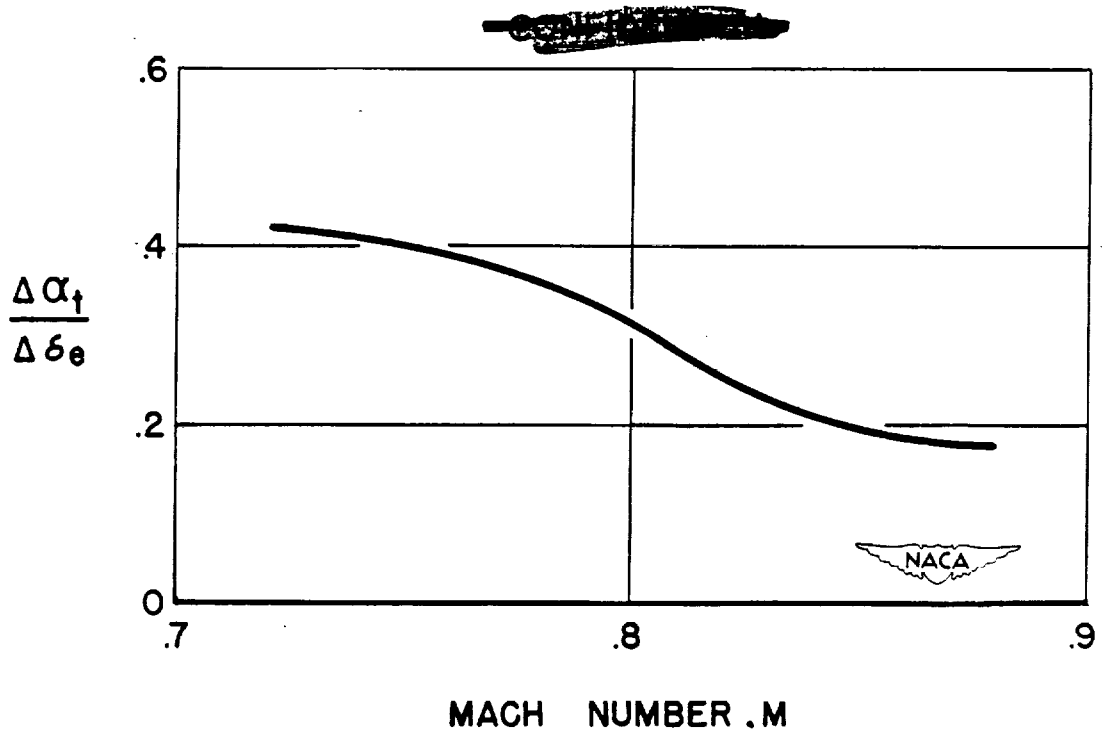


Figure 3.- Variation of elevator effectiveness factor  $\Delta\alpha_t/\Delta\delta_e$  with Mach number.

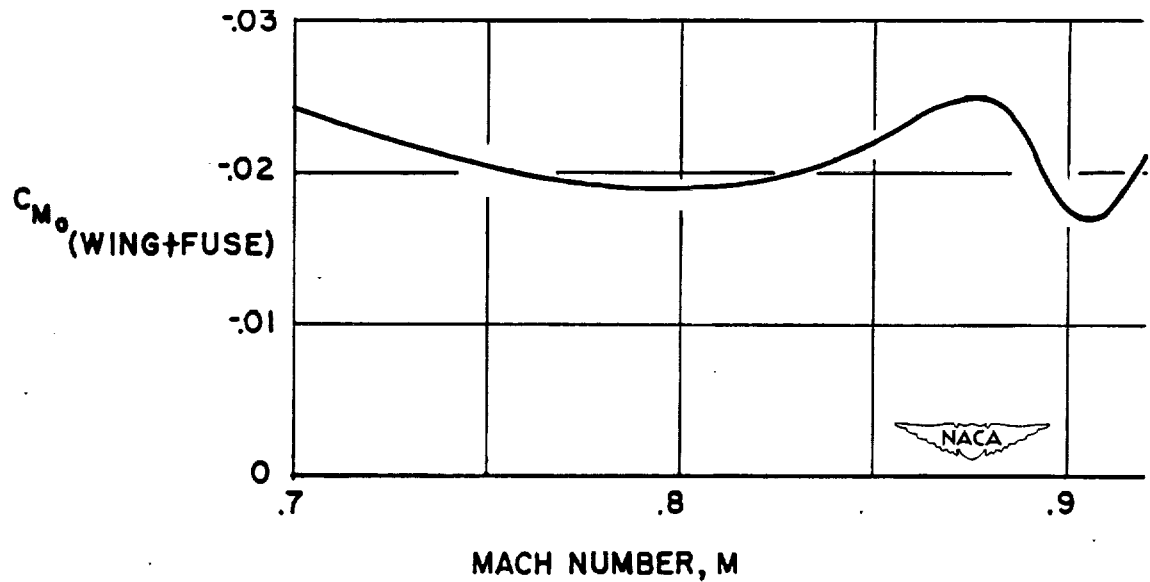


Figure 4.- Variation of wing-fuselage pitching-moment coefficient with Mach number. XS-1 airplane.



Williams

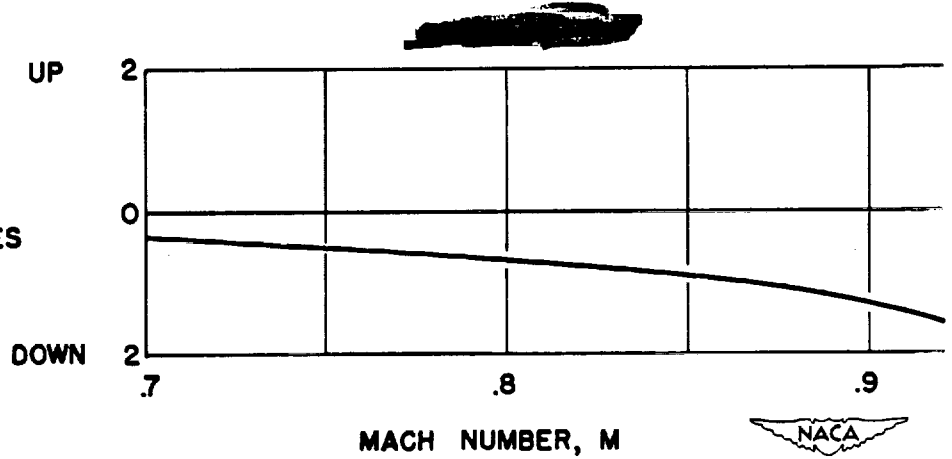


Figure 5.- Variation of right aileron angle with Mach number. XS-1 airplane.

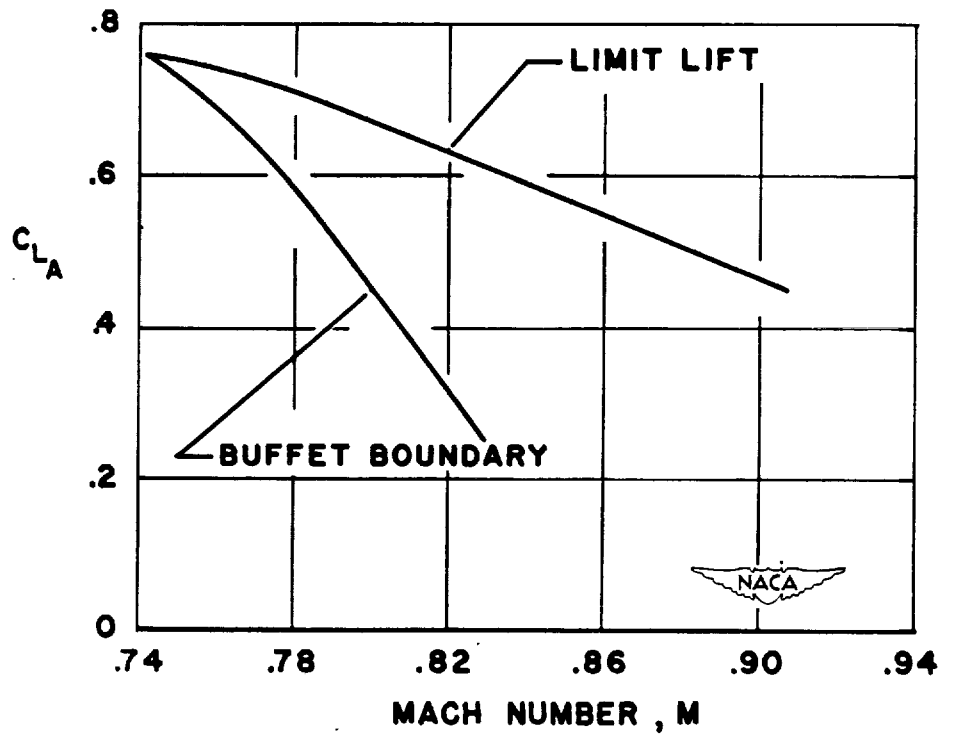
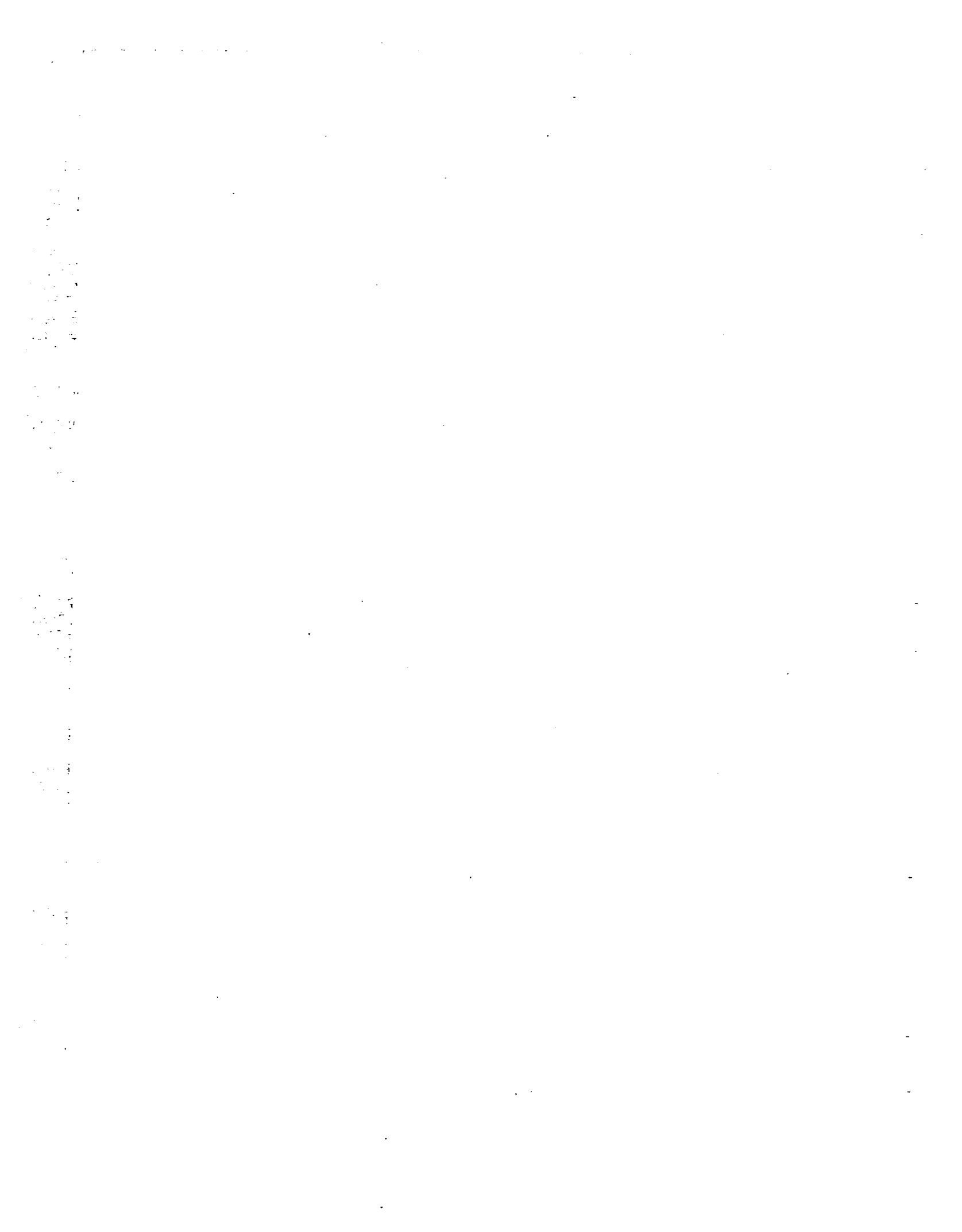


Figure 6.- Buffet boundary and limit lift. XS-1 airplane.

162(c)



CONFIGURATIONS WITH EXTREME SWEEP

CHARACTERISTICS OF A CONFIGURATION WITH A  
LARGE ANGLE OF SWEEPBACK

By Robert T. Jones

Ames Aeronautical Laboratory

A brief discussion is given of some recent experimental results obtained on a supersonic transport-type airplane for a large range of Mach numbers. The theoretical arguments which led to the configuration of this airplane were brought out at the NACA Conference on Supersonic Aerodynamics at the Langley Laboratory, June 19-20, 1947; hence, it will not be necessary to dwell on them herein. Briefly, our calculations showed that a reasonably good lift-drag ratio and, hence, reasonably good fuel economy, could be maintained up to a Mach number of 1.5. The configuration required would incorporate a long slender body and wings having a large angle of sweepback together with the highest practicable aspect ratio.

Figure 1 is a photograph of the model, designed to incorporate these features, tested in the Ames 1- by 3-foot supersonic tunnel and the Ames 1- by  $3\frac{1}{2}$ -foot tunnel. A maximum lift-drag ratio of better than 10 to 1 was expected with this configuration. The first experiments in the Ames 1- by 3-foot supersonic tunnel showed lower values but in these experiments there were indications of laminar separation over an appreciable portion of the wing surface at zero lift, a condition attributed to the low Reynolds number of the test and an effect of the sweepback. Since these first tests, lift-drag ratios as high as 9 to 1 at the low Reynolds numbers have been obtained by the use of some modifications of the original design. Instead of a flat symmetrical wing the revised model had a cambered, twisted wing designed to support a nearly uniform lift distribution at the cruising lift coefficient. Both the original and the revised model showed highest lift-drag ratio with the leading edge of the wing at  $67^\circ$  sweepback.

Figure 2 shows lift-drag ratio  $L/D$  plotted against lift coefficient  $C_L$  for the revised model in the Ames 1- by 3-foot supersonic tunnel. It will be noted that the characteristics are varying fairly rapidly with Reynolds number at the scale of these tests. At both Reynolds numbers, surface flow studies show regions of laminar separation on the wing at zero angle of attack. However, some recent experiments on a larger wing in this tunnel show that the laminar separation phenomenon disappears at higher Reynolds numbers; hence, it is believed that the calculated values can be reached or exceeded at full scale.

In addition to tests of the revised model in the Ames 1- by 3-foot supersonic tunnel we have continued a variety of experiments on the original model. The object of the experiments is to define the behavior of this airplane over as wide a range of Mach numbers and Reynolds numbers as possible. This program is quite new and some of the preliminary results shown herein may be subject to later correction.

The most interesting result is the variation of drag coefficient  $C_D$  with Mach number  $M$  obtained in the Ames 1- by  $3\frac{1}{2}$ -foot tunnel and shown in figure 3. In these tests no drag rise occurred throughout the range of Mach numbers up to 1.5. Actually, of course, the supersonic drag is expected to be somewhat higher than the drag at subsonic speeds as indicated by the dashed-line curve, but the difference is small and in these tests might have been masked by Reynolds number effects. Although no claim is made for great accuracy of measurement in these tests, the value at  $M = 1.5$  is in agreement with that obtained in the Ames 1- by 3-foot supersonic tunnel on the same model.

Although the minimum drag coefficient showed no appreciable change with Mach number, the lift-drag ratios obtained at supersonic speed were less than the subsonic values. Figure 4 shows the variation of maximum lift-drag ratio throughout the Mach number range as obtained from the Ames 1- by  $3\frac{1}{2}$ -foot tunnel. One fact brought out in these tests is that at low Reynolds numbers the lift-drag ratio values at subsonic speeds fall considerably below the usual estimates. At all speeds the rate of increase of drag with lift coefficient was greater than that indicated by the induced drag theory - a characteristic of separated flow. Evidently the laminar separation phenomenon noted earlier is not an effect of supersonic speed but is to be associated with the Reynolds number and the sweepback. Tests of the wing alone in the Ames 12-foot low-turbulence pressure tunnel at a higher Reynolds number showed values from 16 to 1 to 18 to 1, in the subsonic range.

The stability and control characteristics of this model are of great interest. One important question is to find how far the aerodynamic center travels within the range of flight Mach numbers. Unfortunately, data from different sources are not in very good agreement on this point as figure 5 indicates. This diagram shows the fore and aft location of the neutral-stability point superimposed on a plan view of the airplane drawn to the same scale and plotted against Mach number. The two test points at the ends of the curves are calculated values for the wing alone. The wing-flow tests

showed a pronounced backward shift of the aerodynamic center, or, in other words an increase in stability, near a Mach number of 1; whereas the Ames 1- by  $3\frac{1}{2}$ -foot-tunnel tests indicated a gradual variation. Neither the Ames 1- by  $3\frac{1}{2}$ -foot tunnel nor the wing-flow tests indicated any rapid variation of lift in this region and their lift curves are in good agreement throughout. The reasons for the disagreement in pitching moment are not yet understood.

It seems to be a generally applicable rule that the wing forms designed for highest efficiency at supersonic speed show the poorest lifting qualities in the landing condition. High efficiency at supersonic speed is the result of achieving insofar as possible a two-dimensional flow over the oblique wing. In a perfect two-dimensional flow the stalling lift coefficient is reduced by the cosine-squared of the sweep angle. With  $60^\circ$  sweep this means that the wing sections will stall at one-fourth their normal lift coefficient.

Figure 6 is taken from data obtained on a large model in the Ames 40- by 80-foot tunnel and illustrates this stalling behavior. A peculiarity of the behavior of these wings is that the initial flow separation is not accompanied by a loss in lift - in the present case the lift kept increasing up to nearly  $45^\circ$  angle of attack. This increasing lift can hardly be utilized in practice, however, because of the high drag and the erratic center-of-pressure travel associated with the separated flow. It will be noted that in the full-scale tests the drag curve follows the normal induced drag law up to a lift coefficient  $C_L$  of about 0.3. Beyond 0.3 the resultant force begins to fall back toward the normal to the chord, indicating a loss in the suction force at the leading edge as a result of separation. At this point,  $C_L = 0.3$ , also the pitching-moment coefficient  $C_M$  begins to depart from the values calculated for a potential flow. Other characteristics of the wing show similar nonlinear behavior beginning at this point, which corresponds approximately to the section  $c_{l_{\max}} \cos^2 \Lambda$ .

Because of the high sinking speed, or the large amount of power required for level flight, and because of the nonlinear stability characteristics, the airplane could probably not be flown safely above this initial stalling lift coefficient. The obvious remedy for this situation is of course to straighten out the wings for landing. However, the low useable lift coefficient and higher landing speed of the sweptback wing are not believed to present

any unsurpassable difficulty. Through the use of Handley Page slots or nose flaps the landing lift coefficient can probably be increased to 0.5 or 0.6. Higher lift coefficients than this do not result in any decrease of the power or thrust required to maintain a given sinking speed unless the aspect ratio is increased. Conventional airplanes have already exceeded the speed at which landings can be made safely without power. In the present case a wing loading of 40 pounds would result in a landing speed of 165 miles per hour and a relatively small amount of thrust would be required to maintain a sinking speed below 20 feet per second.

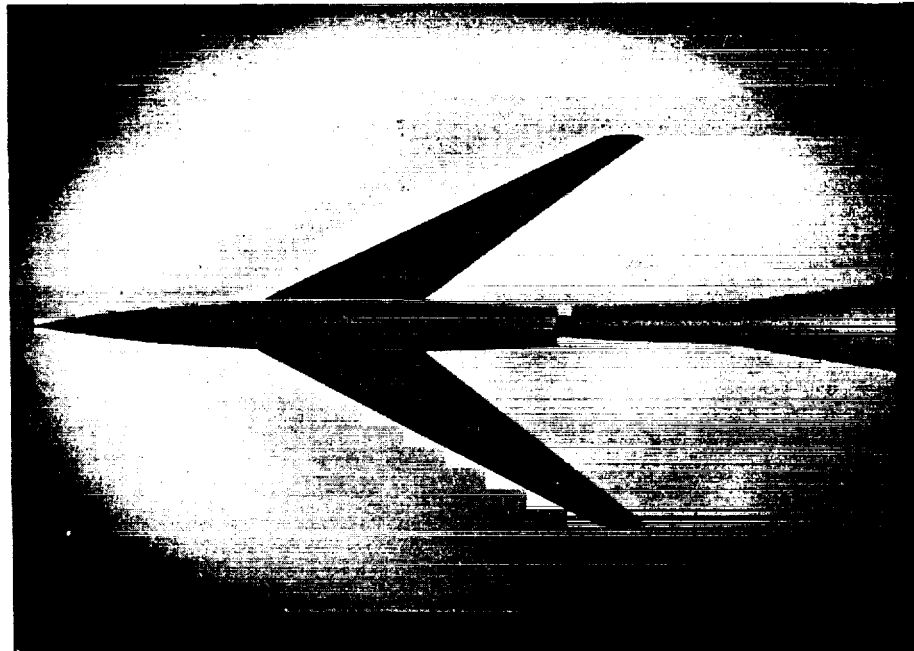


Figure 1.- Original model tested in Ames 1- by 3-foot supersonic tunnel and Ames 1- by 3  $\frac{1}{2}$ -foot tunnel.

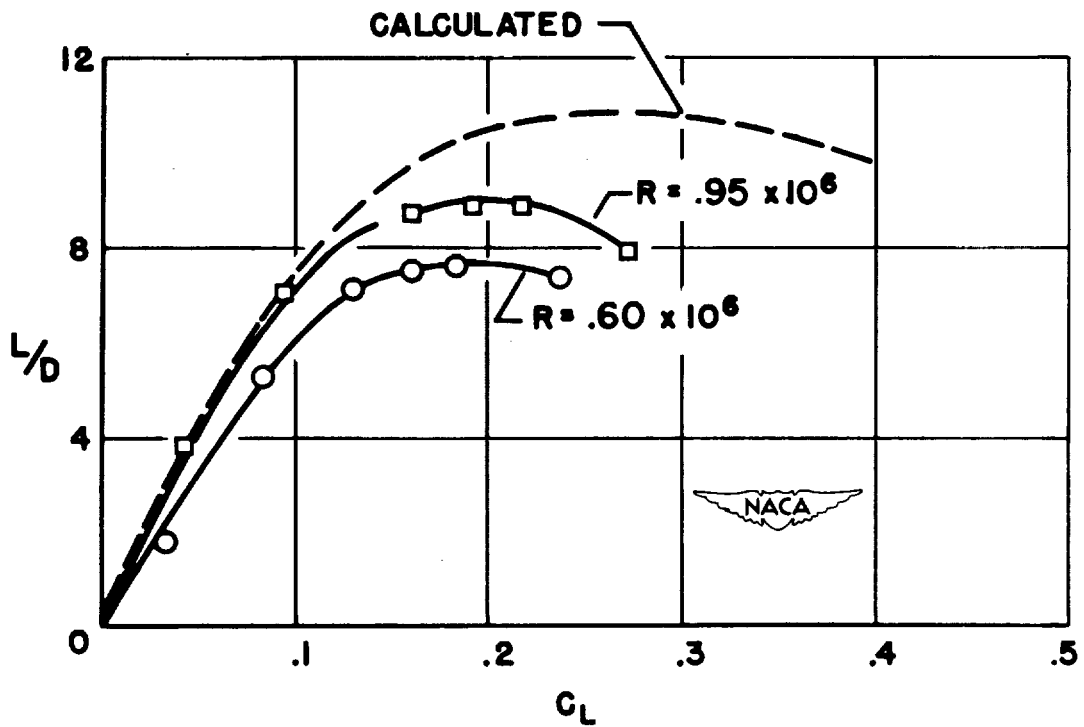


Figure 2.- Lift-drag ratio plotted against  $C_L$  for revised model in Ames 1- by 3-foot supersonic tunnel.



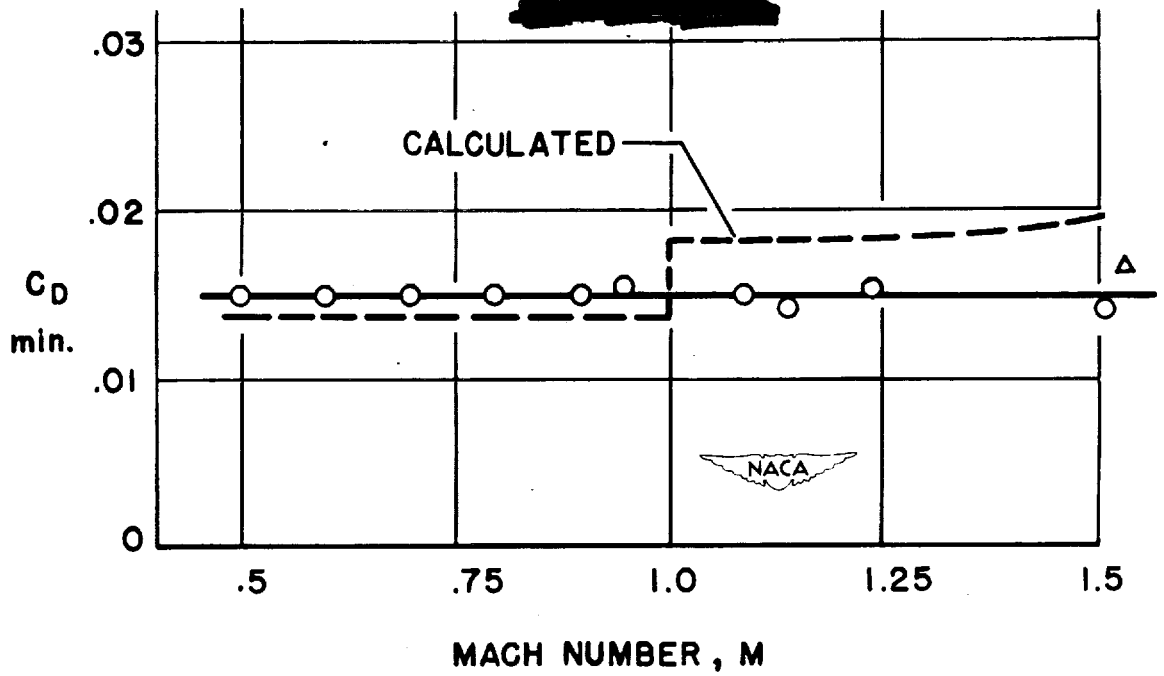


Figure 3.- Variation of drag coefficient with Mach number for original model.

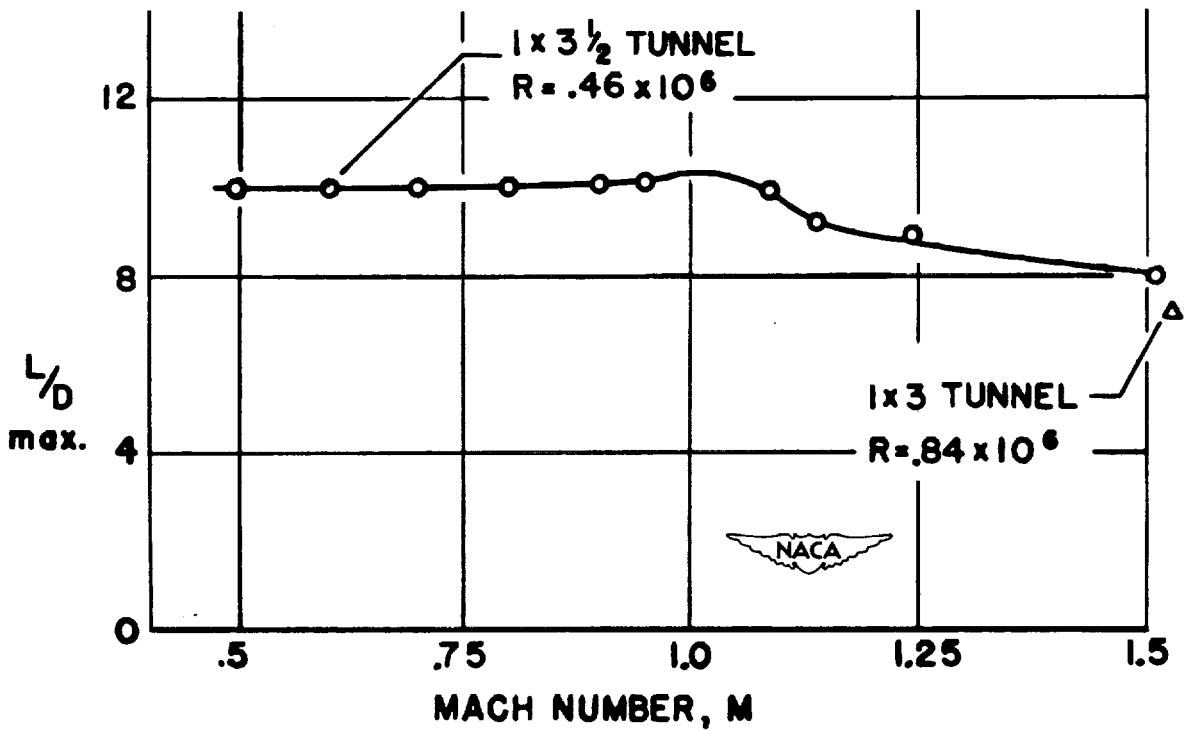


Figure 4.- Maximum lift-drag ratios plotted against Mach number for original model.

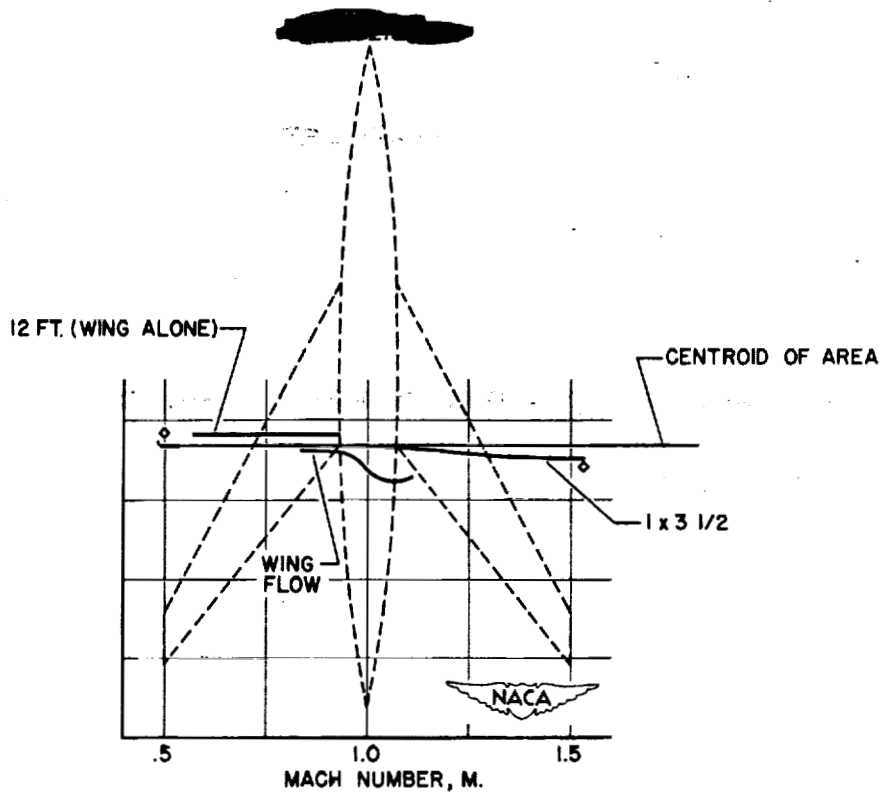


Figure 5.- Positions of aerodynamic center at various Mach numbers.

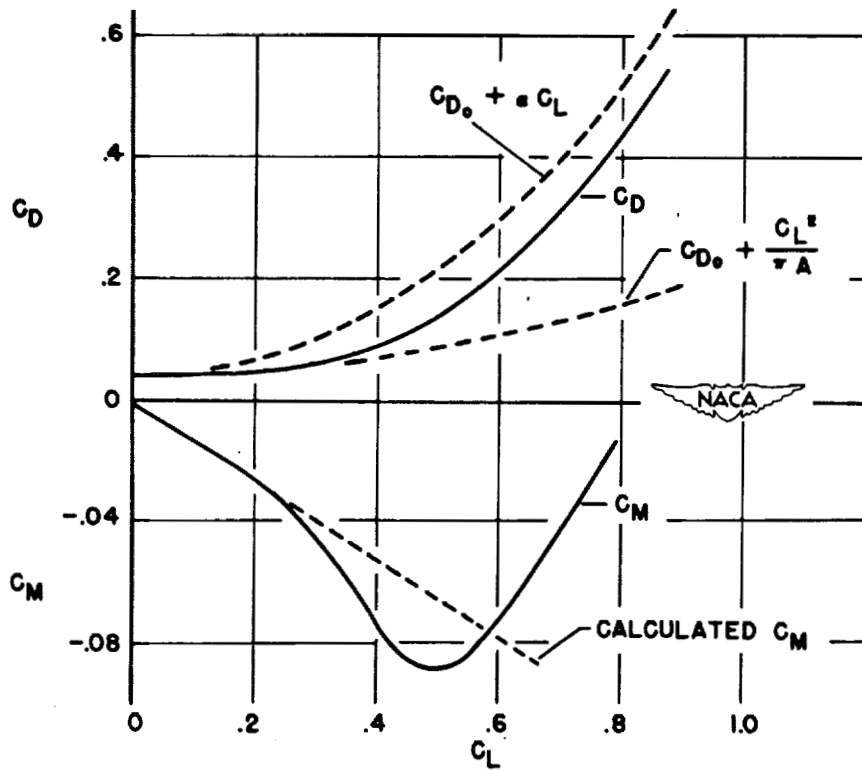


Figure 6.- Variation of drag and pitching-moment coefficients with lift coefficient from tests in Ames 40- by 80-foot tunnel.

## CHARACTERISTICS OF A TRIANGULAR-WINGED AIRCRAFT

## I - PERFORMANCE DATA

By Donald J. Graham

Ames Aeronautical Laboratory

Approximately a year ago a research program was formulated at the Ames Aeronautical Laboratory aimed at investigating the possibilities of employing a wing of low aspect ratio and triangular plan form on a transonic or moderately supersonic aircraft. A wing was selected to be investigated concurrently in the subsonic, transonic, and supersonic wind-tunnel facilities of the laboratory and, in addition, at transonic speeds by means of the NACA wing-flow method. It was planned to determine thereby the effects of wide variations in both Reynolds number and Mach number upon the characteristics of the subject configuration.

The choice of wing was made on the basis of the best existing predictions of the pressure-drag characteristics of triangular airfoils in the moderately supersonic-speed region. The wing was of 5-percent-chord-thick symmetrical double-wedge section with maximum thickness at 20 percent of the airfoil chord and had an aspect ratio of 2 with a vertex angle of  $53^\circ$ . The sweep of the leading edge thus amounted to approximately  $63^\circ$ .

In figure 1 is pictured the model, which was tested in the Ames 1- by  $3\frac{1}{2}$ -foot tunnel and the 1- by 3-foot supersonic tunnel, and the smallest scale model tested. The wing was mounted on a slender cylindrical body which was sting supported from the rear.

Figure 2 is a photograph of the model in the Ames 12-foot low-turbulence pressure tunnel and shows the semispan configuration mounted on a turntable in the tunnel floor.

Aerodynamic characteristics of this wing were determined for Mach numbers from 0.1 to 1.5 and for Reynolds numbers from  $0.7 \times 10^6$  to  $27 \times 10^6$ . The Reynolds number variation was confined to the subsonic tests, all of the supersonic tests having been made for Reynolds numbers of the order of  $1 \times 10^6$ .

A considerable portion of the results of this investigation will be published shortly. The object of the present paper is to summarize the principal results which are involved in a prediction of the performance and the stability and control characteristics of a low-aspect-ratio triangular-wing aircraft.

The variation of the minimum drag coefficient with Mach number for the triangular wing is shown in figure 3. It will be noted that the results from the Ames 1- by  $3\frac{1}{2}$ -foot tunnel (unpublished data) presented for Mach numbers from 0.5 to 1.5, indicated by the solid line, appear to reasonably bridge the gap between the low-speed value from the Ames 7- by 10-foot tunnel (reference 1) and the value for a Mach number of 1.5 from the Ames 1- by 3-foot supersonic tunnel (reference 2). The higher Reynolds number data from the Ames 12-foot low-turbulence pressure tunnel (reference 3) are not in such close agreement with the high subsonic Mach number data from the Ames 1- by  $3\frac{1}{2}$ -foot tunnel as could be desired despite allowance for the difference in scale. It should be emphasized, however, that the respective test conditions were dissimilar. The wing in the Ames 1- by  $3\frac{1}{2}$ -foot tunnel was mounted on a thin body, the drag of which could not readily be separated from that of the combination; whereas, the data from the Ames 12-foot low-turbulence pressure tunnel shown are for the wing alone. The effect of adding a fuselage to the model wing in the Ames 12-foot low-turbulence pressure tunnel was to displace the curve of minimum drag coefficient above that of the wing in the Ames 1- by  $3\frac{1}{2}$ -foot tunnel. No satisfactory explanation has yet been forthcoming for the seemingly early rise in the drag coefficient with Mach number evidenced by the results from the Ames 12-foot low-turbulence pressure tunnel.

Also shown for comparison in figure 3 are minimum drag coefficients for a 6-percent-chord-thick symmetrical double-wedge airfoil section from two-dimensional tests in the Ames 1- by  $3\frac{1}{2}$ -foot tunnel. The favorable effects of sweep and aspect-ratio reduction are apparent here.

It was inferred at the beginning of the paper that the present wing was selected because, from theoretical considerations, it had the lowest pressure drag for the practicable thickness distributions of the given triangular plan form at moderately supersonic speeds. Subsequent tests, however, in the Ames 1- by 3-foot supersonic tunnel and the Ames 1- by  $3\frac{1}{2}$ -foot tunnel showed lower actual minimum drag coefficients at a Mach number of 1.5 for a wing of the same plan form with the maximum thickness at 50 percent of the airfoil chord, an effect traced to the differences in the friction drag of the two surfaces. Hence, if any useful function such as structural convenience were to be served by locating the maximum thickness in the vicinity of the midchord, there would apparently be no associated penalty in minimum drag.

In figure 4 the variation of maximum lift-drag ratio with Mach number is presented. The differences in the subsonic-speed characteristics as determined in the various facilities appear to be consistent with the corresponding differences in the Reynolds numbers of the respective tests. The subsonic-speed lift-drag ratios, although seemingly low, might reasonably be expected to improve somewhat with increasing Reynolds numbers, as was observed in the case of the subsonic speed characteristics.

Furthermore, for these tests, the wing had sharp leading edges and, hence, did not realize an appreciable amount of the possible leading-edge suction which would further boost the maximum lift-drag ratios in the speed range under consideration.

Previously reported tests (reference 4) in the Ames 1- by 3-foot supersonic tunnel at a Mach number of 1.5 with the leading edges of this wing rounded have indicated the attainment of a significant but by no means major portion of the theoretical leading-edge suction. Figure 5, the material for which was presented at the NACA Conference on Supersonic Aerodynamics at the Langley Laboratory, June 19-20, 1947, illustrates the variation of lift-drag ratio with lift coefficient at a Mach number of 1.5 for the wing with sharp leading edge and with the leading edge rounded to approximate the nose radius of a 5-percent-chord-thick NACA 65-series airfoil. Rounding the leading edge, while raising the maximum lift-drag ratio by decreasing the drag due to lift, did not affect the minimum drag. These results should not be taken as evidence of the maximum gain to be expected from leading-edge shape modification because the subject wing section was not selected with this objective in mind. It appears likely that at full-scale Reynolds numbers the use of airfoil sections with rounded nose contours of the subsonic type on wings with highly swept leading edges would, by realizing a greater part of the possible leading-edge suction, afford considerably higher maximum lift-drag ratios at low supersonic Mach numbers than those indicated in figures 4 and 5.

An additional fact of interest is that the lift coefficients corresponding to the maximum lift-drag ratios were found to be sensibly independent of Mach number, having varied but inappreciably from a value of about 0.2 over the range of the tests.

The slope of the lift curve of the triangular wing as a function of Mach number is shown in figure 6. Satisfactory agreement is evident both between the results of the various wind-tunnel tests and the calculated subsonic and supersonic values. The variation with Mach number is regular and apparently free from abrupt discontinuities at transonic speeds.

From the standpoint of performance at transonic Mach numbers the results of research to date indicate the low-aspect-ratio triangular wing to be a practicable lifting surface for a short-range interceptor aircraft. Were a wing section to be selected at this date for an aircraft designed to fly at transonic or moderately supersonic Mach numbers with the type of wing plan form under discussion, a profile having the general shape of the NACA 64-series or 65-series airfoil sections would be recommended because of the higher maximum lift-drag ratios afforded.

#### REFERENCES

1. Rose, Leonard M.: Low-Speed Investigation of a Small Triangular Wing of Aspect Ratio 2. I - Effect of Combination with a Body of Revolution and Height above a Ground Plane. NACA RM No. A7K03, 1947.
2. Vincenti, Walter G., Nielsen, Jack N., and Matteson, Frederick H.: Investigation of Wing Characteristics at a Mach Number of 1.53. I - Triangular Wings of Aspect Ratio 2. NACA RM No. A7I10, 1947.
3. Edwards, George G., and Stephenson, Jack D.: Tests of a Triangular Wing of Aspect Ratio 2 in the Ames 12-Foot Pressure Wind Tunnel. I - Effect of Reynolds Number and Mach Number on the Aerodynamic Characteristics of the Wing with Undelected Flap. NACA RM No. A7K05, 1947.
4. Vincenti, Walter G.: Experimental Characteristics of Finite-Span Wings. NACA Conference on Supersonic Aerodynamics. June 19-20, 1947.

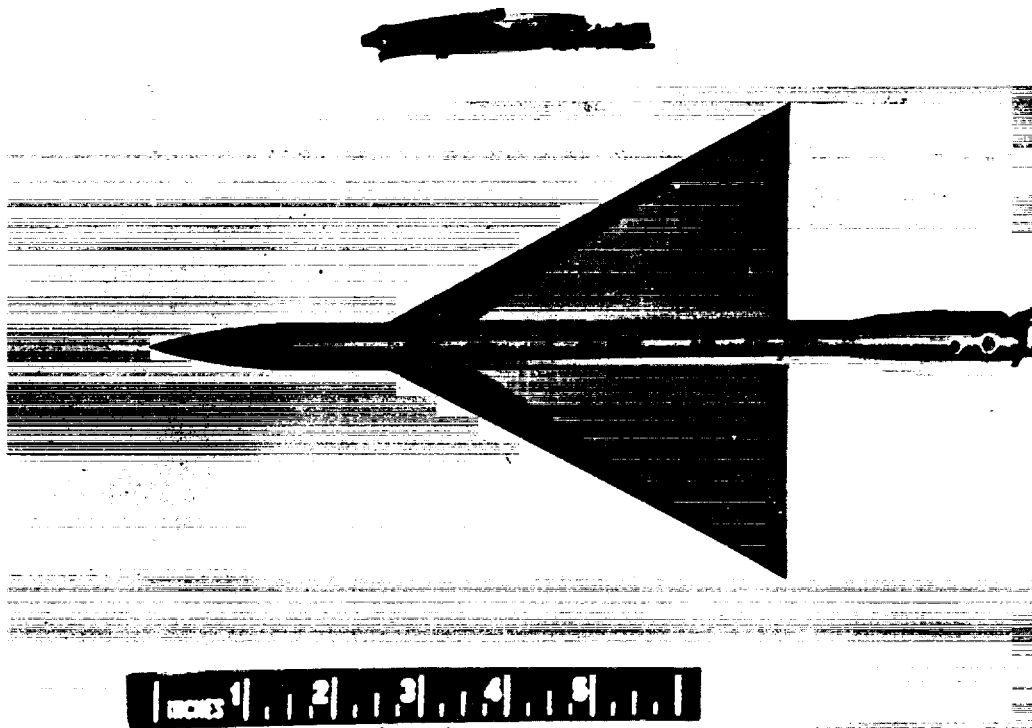


Figure 1.- Model tested in the Ames 1- by  $3\frac{1}{2}$ -foot tunnel.

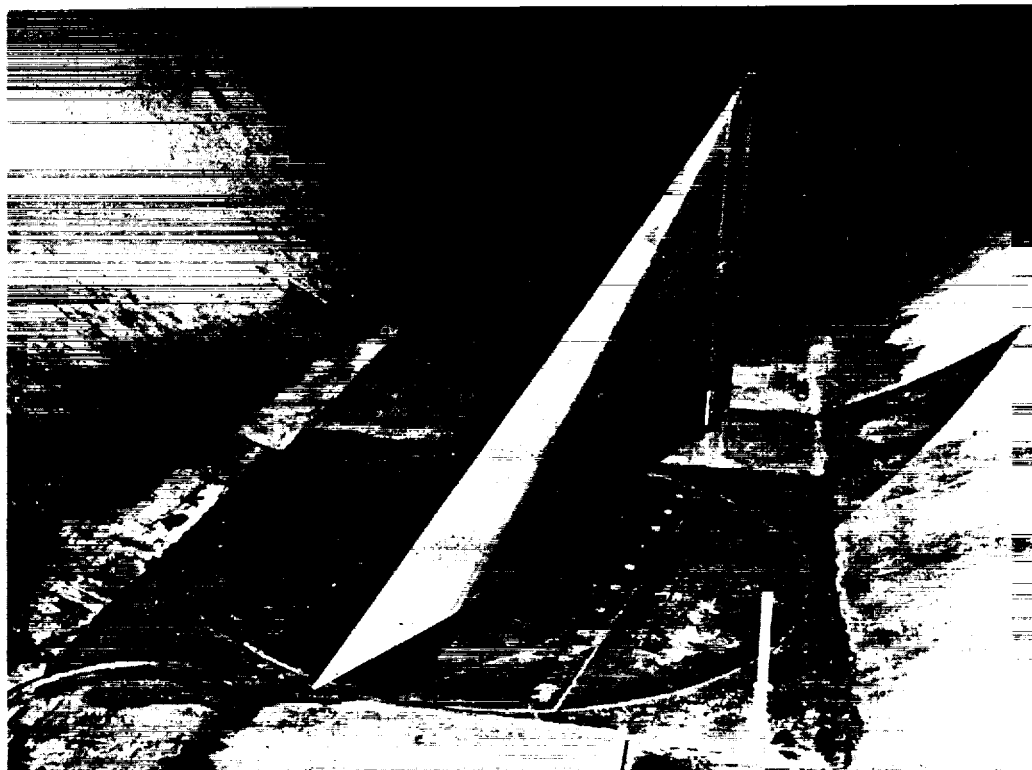


Figure 2.- Model tested in the Ames 12-foot low-turbulence pressure tunnel.

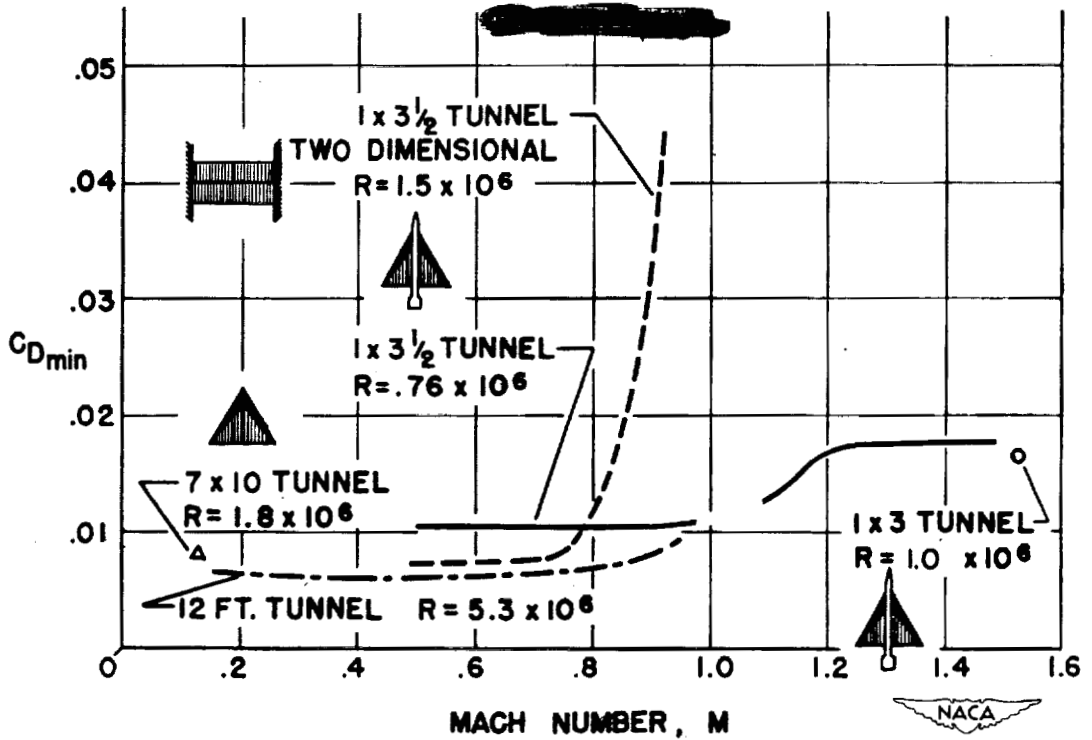


Figure 3.- The variation with Mach number of minimum drag coefficient for triangular wing.

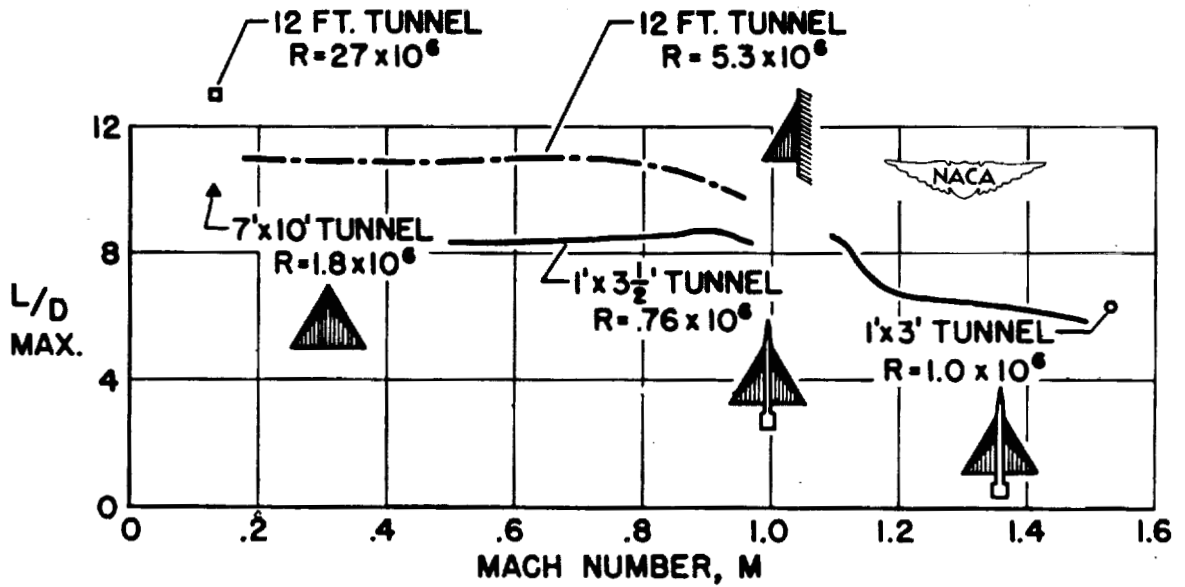


Figure 4.- The variation of Mach number with maximum lift-drag ratio for the triangular wing.



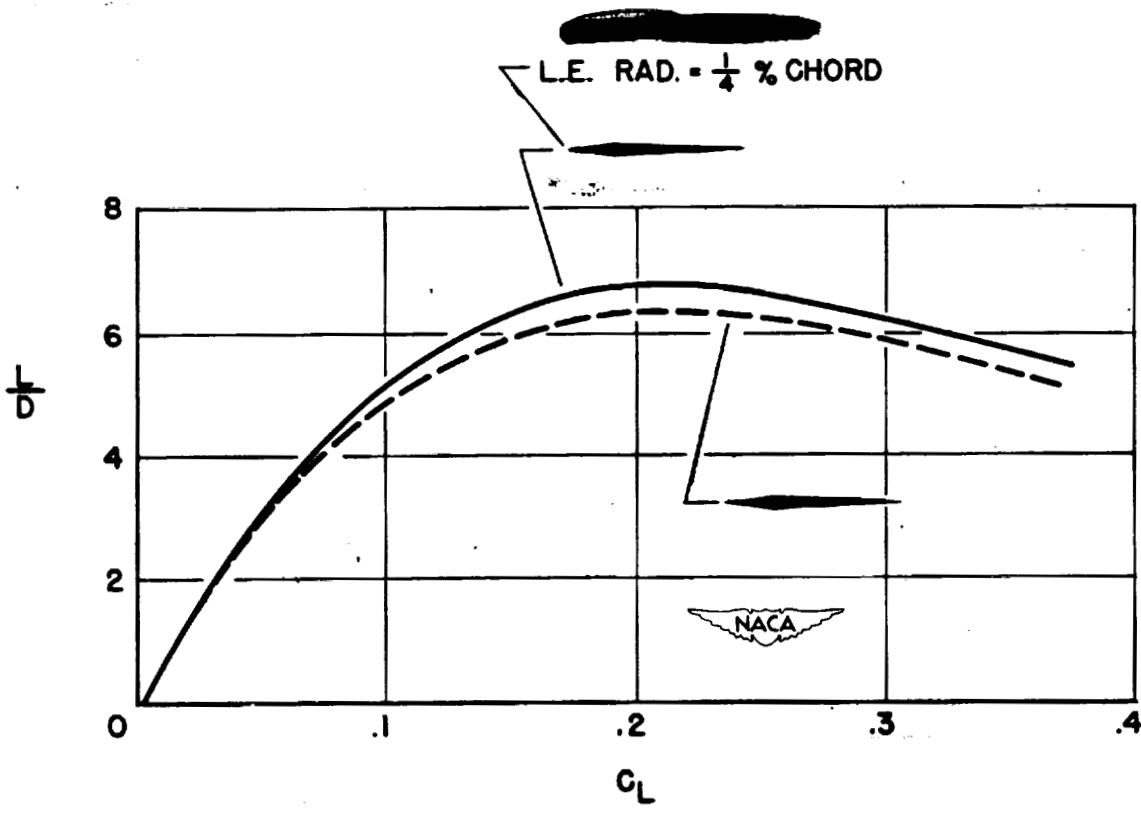


Figure 5.- The effect of leading-edge radius upon lift-drag ratio of triangular wing at a Mach number of 1.53 and a Reynolds number of  $1 \times 10^6$ .

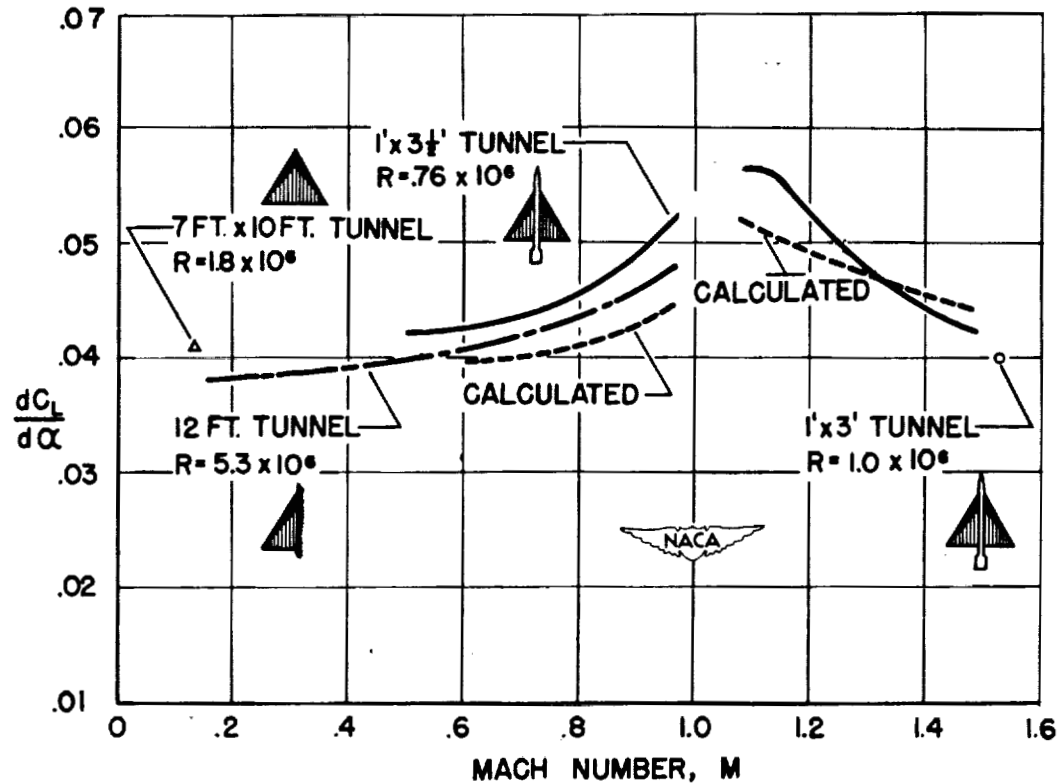


Figure 6.- The variation of Mach number with lift-curve slope of the triangular wing.

D21

CHARACTERISTICS OF A TRIANGULAR-WINGED AIRCRAFT

II - STABILITY AND CONTROL

By Robert M. Crane

Ames Aeronautical Laboratory

The stability and control problems associated with wings of triangular plan form have recently been the subject of an intensive research investigation at the Ames Laboratory. Tests have included the measurement of effectiveness and hinge moment for a constant-chord trailing-edge control at Mach numbers up to 0.95 (reference 1), effectiveness of a similar control at a Mach number of 1.53 (reference 2), and directional characteristics at low subsonic speeds and at a Mach number of 1.53 of an aircraft using a single vertical tail and using twin vertical tails (references 2 and 3). Low-speed flight tests using a constant-chord trailing-edge control have also been made in the Langley free-flight tunnel (reference 4). Some of these results relating to static longitudinal stability and control will be presented in this report.

The wing model used in these tests had a triangular plan form and an aspect ratio of 2. The control surface investigated had a constant chord and an area equal to 20 percent of the wing area. When tested with a fuselage, the fuselage was a body of revolution with a fineness ratio of 12.5 and a frontal area equal to  $5\frac{1}{4}$  percent of the wing area. The effect of Mach number on the lift-curve slope and the location of the aerodynamic center are presented in figure 1. Data are included from tests of a semispan model in the Ames 12-foot low-turbulence pressure tunnel and tests of a small-scale complete-wing model in the Ames 1- by  $3\frac{1}{2}$ -foot tunnel and the Ames 1- by 3-foot supersonic tunnel. The results from the various test facilities show reasonable agreement, considering the large differences in Reynolds number and minor differences of model configuration.

Slope parameters of this type may often be very misleading because they fail to show the linearity or nonlinearity of the various coefficients. Figure 2 presents lift and moment data at Mach numbers up to 0.95 and more clearly illustrates the excellent linearity of the characteristics of a triangular wing at high subsonic speeds. While these data only extend up to  $M = 0.95$ , data obtained at transonic speeds by the wing-flow method on a free-floating model indicate none of the erratic disturbances which are associated with a straight wing in passing through a Mach number of unity.

The influence of Mach number on the effectiveness of the constant-chord plain flap is shown in figure 3. The theoretical effectiveness

at supersonic speeds is based on linearized theory. The experimental point at a Mach number of 1.53 was obtained from tests of an airplane model having a triangular wing of aspect ratio 2.31 with a 21.3-percent-area constant-chord control. For the theoretical calculation it was assumed that there was no carry-over of elevon lift across the fuselage. The agreement between the experimental value and the theoretical value indicates that the assumption of no-lift carry-over is valid. The effectiveness data from the wing-flow method were obtained on a sharpened flat plate using the free-floating technique (reference 5). The Reynolds number for these tests was about 1 million compared to 5.3 million for the data obtained in the Ames 12-foot low-turbulence pressure tunnel. It is not completely understood whether the lack of agreement between these data is due to the difference in airfoil section, the difference in Reynolds number, or to shortcomings of the free-floating technique. Further tests are scheduled in an attempt to determine the exact reasons for these discrepancies. Figure 4 presents elevon effectiveness for several angles of attack at five different Mach numbers, the highest being 0.95. This figure illustrates again the linearity of the data from which the slope parameters have been obtained.

The hinge-moment characteristics of the constant-chord elevons are shown in figure 5. The supersonic values are computed from linearized theory and no experimental verification is available. Note the large rapid rise in  $C_{h\delta}$  at Mach numbers approaching unity. If a constant-chord control with an unswept hinge line is to be used, the necessity for some type of power-operated irreversible control mechanism is obvious. Note also the large negative values of  $C_{h\alpha}$  which will have a profound influence on the control forces in steady flight.

These data have been used to predict the static longitudinal stability and control characteristics of a hypothetical aircraft employing the wing and fuselage previously described. This aircraft is shown in figure 6. In order to permit the reduction of the hinge-moment data, a wing area of 500 square feet has been assumed. The span is thus 31.6 feet. In order to fulfill its assumed mission, the aircraft must be capable of engaging in tactical maneuvers at a Mach number of 1.5 and an altitude of 60,000 feet with wing loadings of at least 60 pounds per square foot.

The variation with Mach number of the elevon angle and the elevon hinge moment required to balance the aircraft in level flight at an altitude of 30,000 feet is shown in figure 7. The airplane center of gravity has been assumed at 32 percent of the M.A.C. Note in particular that, due to the large negative value of  $C_{h\alpha}$ , the

variation of stick force with speed is neutrally stable over most of the speed range. Note also that despite the large distance between the center of gravity and the aerodynamic center at supersonic speeds, the elevon angle required to balance the airplane at supersonic speeds is essentially independent of the Mach number. This neutral stick-fixed stability is due to the loss in elevon effectiveness associated with increasing supersonic Mach numbers.

The variation with normal acceleration of the elevon angle and elevon hinge moment in steady turning flight at two high subsonic Mach numbers is shown in figure 8. For these computations it is assumed that the elevon is used for both balancing the aircraft and as the maneuvering control. The rapid changes in control forces at large normal accelerations is due to nonlinearity of the elevon hinge moments at these high Mach numbers.

The effect of the location of the center of gravity on the maneuverability of the aircraft at a Mach number of 1.5 is shown in figure 9. In all cases the elevator deflection has been limited to  $12^\circ$  which is the critical-flow deflection angle for this Mach number.

It is apparent that if the aircraft is to produce a normal acceleration of  $4g$  at an altitude of 60,000 feet with a wing loading of 60 pounds per square foot, the center of gravity must be at about 45 percent M.A.C. However, with the center of gravity this far aft, the aircraft will become longitudinally unstable at subsonic speeds. If the airplane center of gravity is not permitted to move aft of 32 percent M.A.C., the most aft center of gravity for stability at landing, the maximum normal acceleration which can be produced by the elevons for the above condition is only  $0.2g$ . It is obvious that the maneuverability of the airplane would be enhanced if some auxiliary trimming device were available so that the elevon power could be reserved for maneuvering.

The effect of static margin on the theoretical increment in elevon hinge moment per  $g$  of normal acceleration is shown in figure 10 for flight at a Mach number of 1.5 at an altitude of 60,000 feet. It is seen that the control forces will become enormous unless the static margin is maintained between 5 and 12 percent. At lower supersonic speeds, the control forces are even higher due to the very rapid rise of negative  $C_{hg}$  with decreasing supersonic Mach numbers.

The landing characteristics of the triangular-winged aircraft have been computed for wing loadings of 20, 30, and 40 pounds per square foot. The data used for these computations were all obtained at a Reynolds number of 15,000,000 and a Mach number of 0.13. The variation with landing speed of the elevator angle, control hinge moment, sinking speed,

and angle of attack is presented in figure 11. For all of these computations the only longitudinal control is the constant-chord trailing-edge elevator, and landing is assumed to be accomplished with power off. It is observed that a push force is required to land the airplane and that the variation of elevon force with speed is unstable over most of the speed range. Note that for a landing speed of 140 miles per hour with a wing loading of 40 pounds per square foot, the sinking speed is in excess of 60 feet a second and the airplane angle of attack is greater than  $20^\circ$ . The lift-drag ratio for this condition is only 3.0. These values indicate the necessity of applying power if a safe landing is to be accomplished.

Recent tests of a similar wing and control have been made in the Langley free-flight tunnel. These tests indicated that the airplane was controllable up to a maximum lift coefficient of 1.0. A moderate amount of difficulty was observed in trying to fly the model at these high lifts due to the large sinking speeds. The tests did indicate, however, that slow-speed flight could be achieved despite the large angle of attack and the high drag.

Examination of the preceding data permits several interesting observations regarding the performance of a triangular-wing aircraft with a constant-chord control. In the first place, the elevator is not adequate for both trimming and maneuvering the aircraft at high altitudes with large wind loadings, and the elevon forces are such as to require an irreversible power control. Second, the sinking speed and landing attitudes of the aircraft are excessive when the flap is used as a longitudinal control. Third, the variation of aerodynamic center with Mach number, although much less than for a straight-wing configuration, is sufficient to complicate severely the problem of longitudinal control. If the center of gravity is permitted to move aft as fuel is consumed in supersonic flight so as to keep the supersonic static margin down to a reasonable figure, there must be some method of moving the center of gravity forward or the aerodynamic center aft to permit stability at low speeds for landing. A possible solution to these problems is presented in the following discussion.

Consider a second small triangular wing mounted far forward on the fuselage as shown in figure 12. For landing, permit this auxiliary wing to float freely about its 30 percent M.A.C. with its floating angle determined by the deflection of constant-chord trailing-edge flap connected to the pilot's control. This freely floating wing will not affect the aerodynamic center of the airplane but will serve as a very powerful longitudinal control. For the present analysis, this trimmer wing is considered to have an area equal to 8 percent of the wing area and a distance from the one-quarter M.A.C. of the main wing of 1.5 mean aerodynamic chord lengths.

The trimmer configuration for which the present computations have been made has not been tested at transonic or supersonic speeds. Downwash from the trimmer may have a sizeable effect on the airplane characteristics, but for the present analysis no interference effects between the trimmer and the wing or between the fuselage and the trimmer have been considered.

The landing characteristics for this configuration with the wing flaps deflected  $10^\circ$  are presented in figure 13. The sinking speed and ground angle for landing with the elevons is shown for comparison. For both sets of calculations, the center of gravity is at 32 percent M.A.C. Note that the floating trimmer reduces the sinking speed of the aircraft for a given contact speed by more than 25 percent and, equally important, reduces the ground angle by as much as  $11^\circ$ . The sinking speeds are still of such magnitude, however, that power will have to be applied for landing.

At a Mach number of 1.5 the trimmer is very ineffective. This results directly from the fact that, if the trimmer pivot is placed far enough forward to insure free-floating stability at the landing condition, the trimmer stability is so large at supersonic speeds that its control is ineffective in producing lift.

The fact that the floating trimmer does not affect the aerodynamic center, while locking the trimmer will move the aerodynamic center forward by 12 percent M.A.C., suggests a method of reducing the static margin at supersonic speeds without causing instability at landing. If the disposable load is so arranged that the center of gravity continually moves aft as fuel is consumed, take-off, climb, and supersonic flight can be accomplished with the trimmer locked and landing can be made with the trimmer floating.

Thus at take-off with the trimmer locked, the aerodynamic center will be at approximately 26 percent M.A.C. and the center of gravity may be at 20 percent M.A.C. As fuel is consumed, the center of gravity may be permitted to move aft to 32 percent M.A.C., resulting in a 6-percent static margin at a Mach number of 1.5. As speed is reduced for landing, the trimmer may be unlocked at a Mach number of about 1.1, permitting the landing to be made with a static margin of 6 percent with the same center-of-gravity position as at the termination of supersonic flight. With the trimmer locked, it may be used as a trimming device at high speeds and take-off, using the trailing-edge elevators on the wing as a maneuvering control. The maneuverability with this arrangement at a Mach number of 1.5 and an altitude of 60,000 feet is shown in figure 14. It is observed that with this arrangement if the center of gravity is not permitted to move aft of 32 percent M.A.C. (the center-of-gravity position for stability at landing), the elevons

are capable of producing a maneuvering normal acceleration of 3.75g compared to 0.2g with the elevons alone (fig. 9). This increased maneuverability over that with the plain elevons is due not only to the increase in elevon power resulting from the use of the trimmer but also the permissible reduction in static margin resulting from the ability to control the aerodynamic center for landing by allowing the trimmer to float at low speeds. If the disposable load can be arranged close to the center of gravity, it may be feasible to take off and climb with the trimmer free floating, locking it only after supersonic flight has been attained. This should not modify in any way the flight characteristics previously presented.

In summary, it may be stated that, with the exception of the exceedingly large hinge moments, the longitudinal stability and control of triangular wings presents no severe difficulties for level flight at Mach numbers up to 1.5. Constant-chord trailing-edge elevons provide adequate control to balance the aircraft throughout the speed range; but if a large degree of maneuverability is required of a highly loaded aircraft, some auxiliary trimming device should be incorporated in the design. One possible configuration employs a trimmer wing placed far forward on the nose of the aircraft. Use of this trimmer permits landing at moderate ground angles and modest sinking speeds, and greatly enhances the maneuverability of the aircraft at large lift coefficients. The hinge-moment characteristics of a constant-chord trailing-edge elevon are such as to require an irreversible control mechanism with the boost power dictated by the hinge moments which occur near a Mach number of unity.

While the efficiency of a triangular wing at supersonic speeds is inferior to that of a highly sweptback wing, the increased structural strength, the increased maneuverability, and the greater freedom from landing problems certainly warrant careful consideration of this plan form for aircraft designed for pursuit and interception at transonic and supersonic speeds.

## REFERENCES

1. Stephenson, Jack D., and Amuendo, Arthur R.: Tests of a Triangular Wing of Aspect Ratio 2 in the Ames 12-foot Pressure Wind Tunnel. II - The Effectiveness and Hinge-Moment Characteristics of a Constant-Chord Plain Flap. (Prospective NACA paper)
2. Scherrer, Richard, and Wimbrow, William R.: Wind-Tunnel Investigation at a Mach number of an Airplane with a Triangular Wing. NACA RM No. A7J05, 1947.
3. Anderson, Adrien E.: An Investigation at Low Speed of a Large-Scale Triangular Wing of Aspect Ratio 2. III - Characteristics of Wing with Body and Vertical Tail. (Prospective NACA paper)
4. McKinney, Marion O., Jr., and Drake, Hubert M.: Flight Characteristics at Low Speeds of Delta-Wing Models. NACA RM No. L7K07, 1947.
5. Rathert, George A., and Cooper, George E.: Wing Flow Tests of a Triangular Wing of Aspect Ratio 2. I - Effectiveness of Several Types of Trailing-Edge Flaps on Flat Plate Models. NACA RM No. A7G18, 1947.



Crane

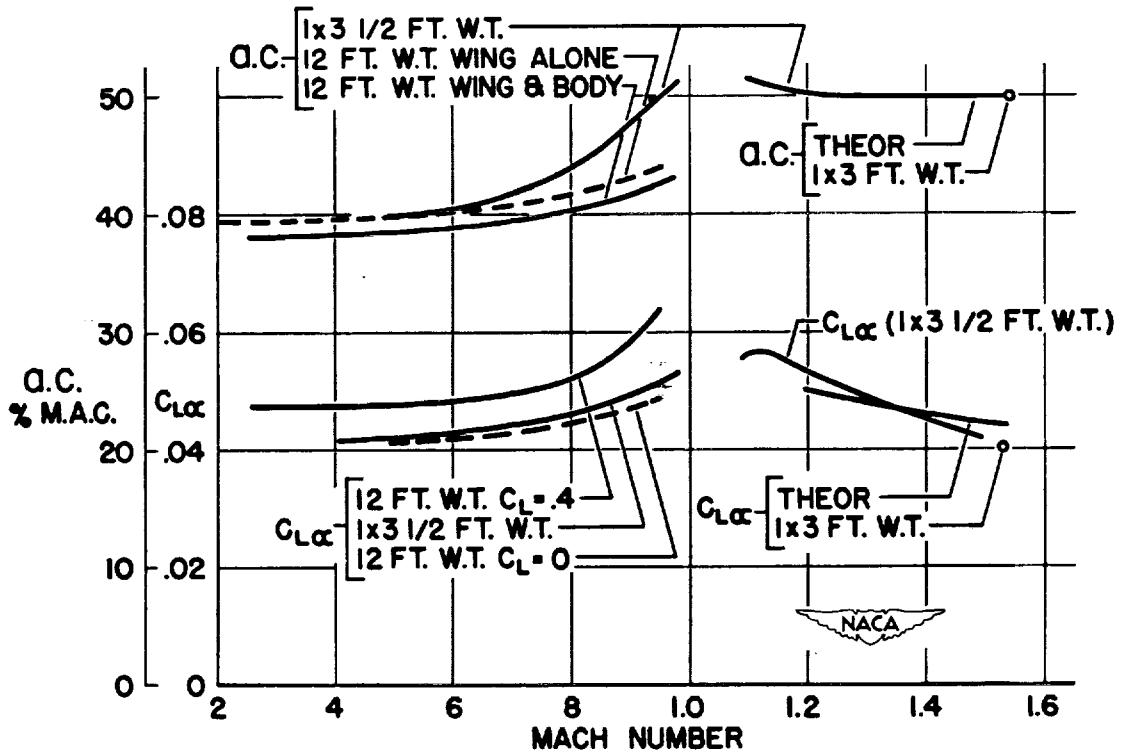


Figure 1.- The effect of Mach number on the lift-curve slope and the location of the aerodynamic center for a triangular wing of aspect ratio 2.

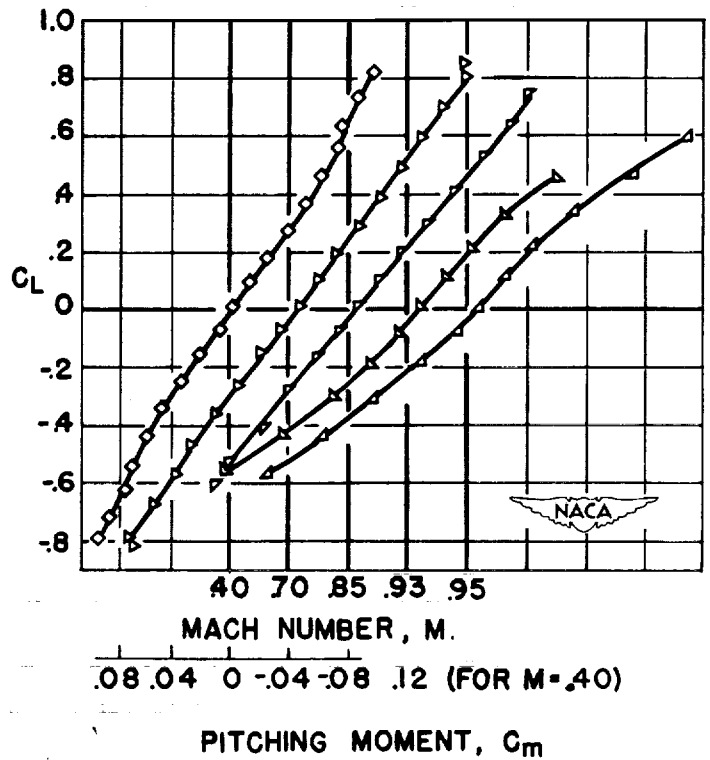
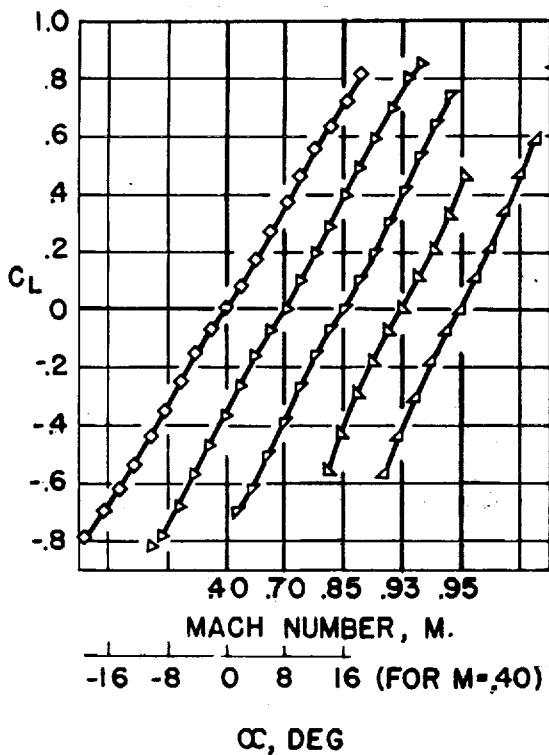


Figure 2.- The effect of Mach number on the lift and pitching-moment characteristics of a triangular wing of aspect ratio 2.

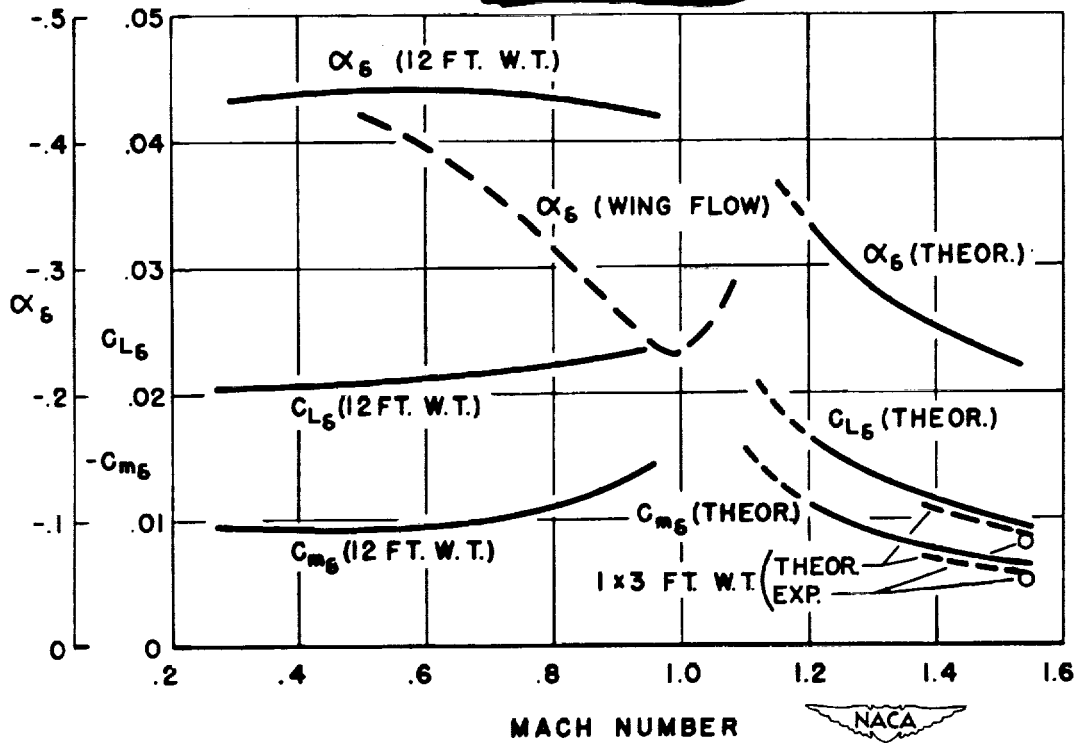


Figure 3.- The effect of Mach number on the effectiveness of a constant-chord plain flap on a triangular wing of aspect ratio 2.

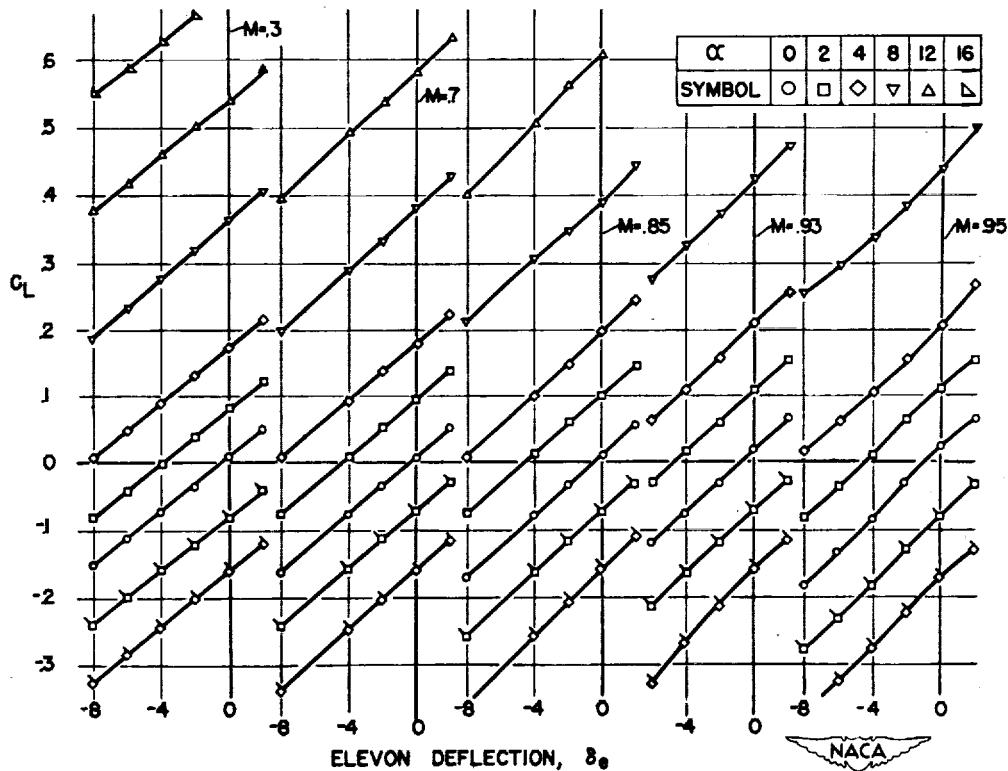


Figure 4.- The effect of Mach number on the lift effectiveness of a constant-chord plain flap on a triangular wing of aspect ratio 2.

Crane

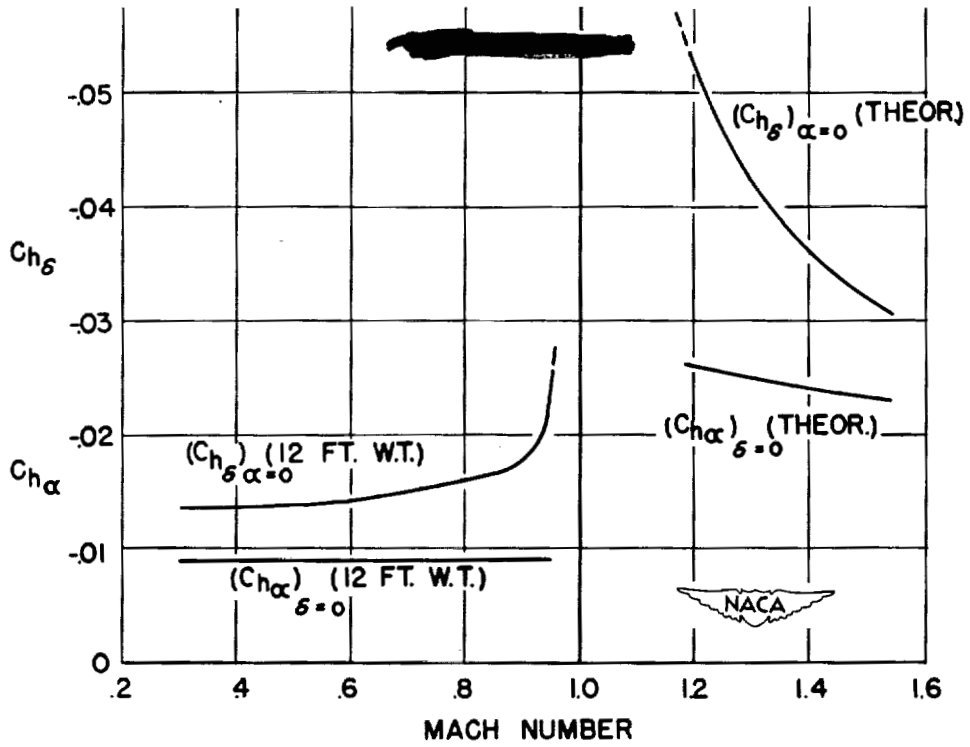


Figure 5.- The effect of Mach number on the hinge-moment characteristics of a constant-chord plain flap on a triangular wing of aspect ratio 2.

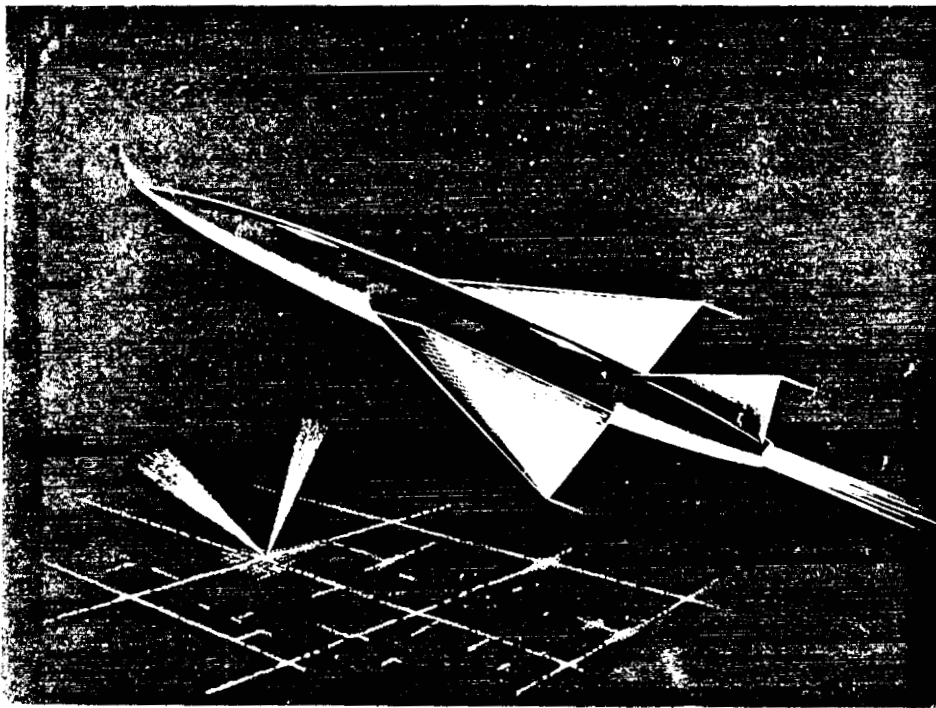


Figure 6.- Interceptor-type aircraft using a triangular wing with a constant-chord control.

Crane

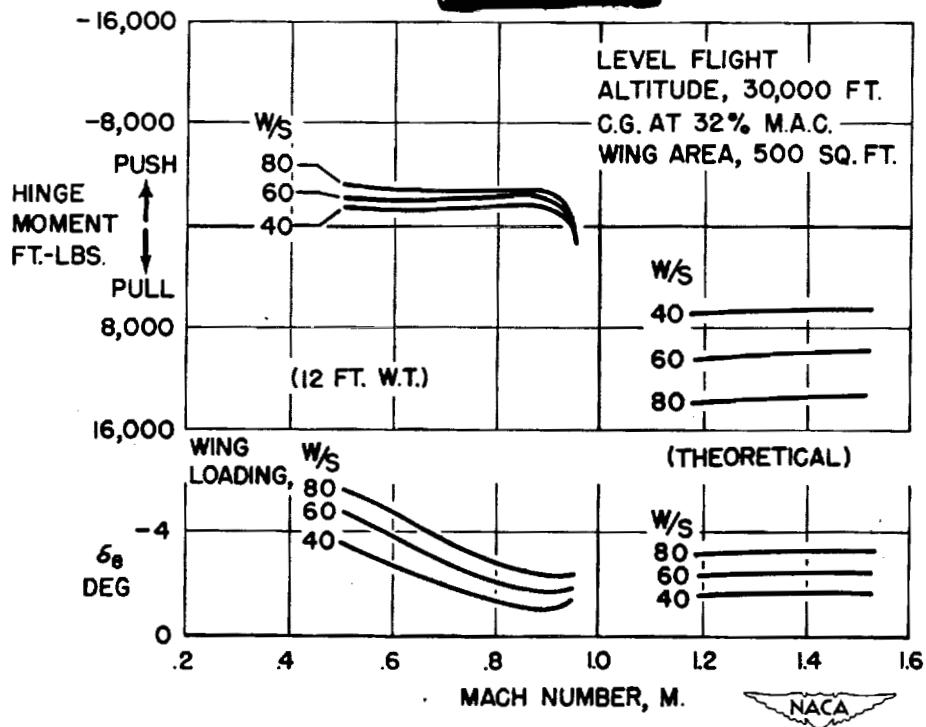


Figure 7.- The estimated variation with Mach number of the elevon angle and the elevon hinge moment required to balance a triangular-winged aircraft in level flight at an altitude of 30,000 feet.

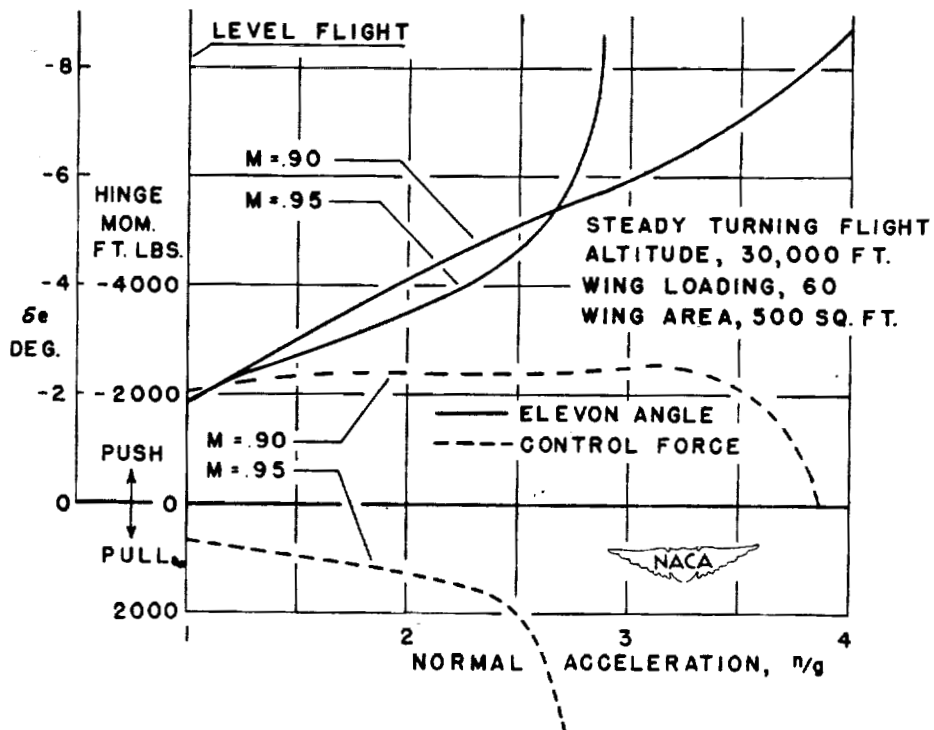


Figure 8.- The estimated variation of elevon angle and elevon hinge moment with normal acceleration for a triangular-winged aircraft in steady turning flight at an altitude of 30,000 feet.

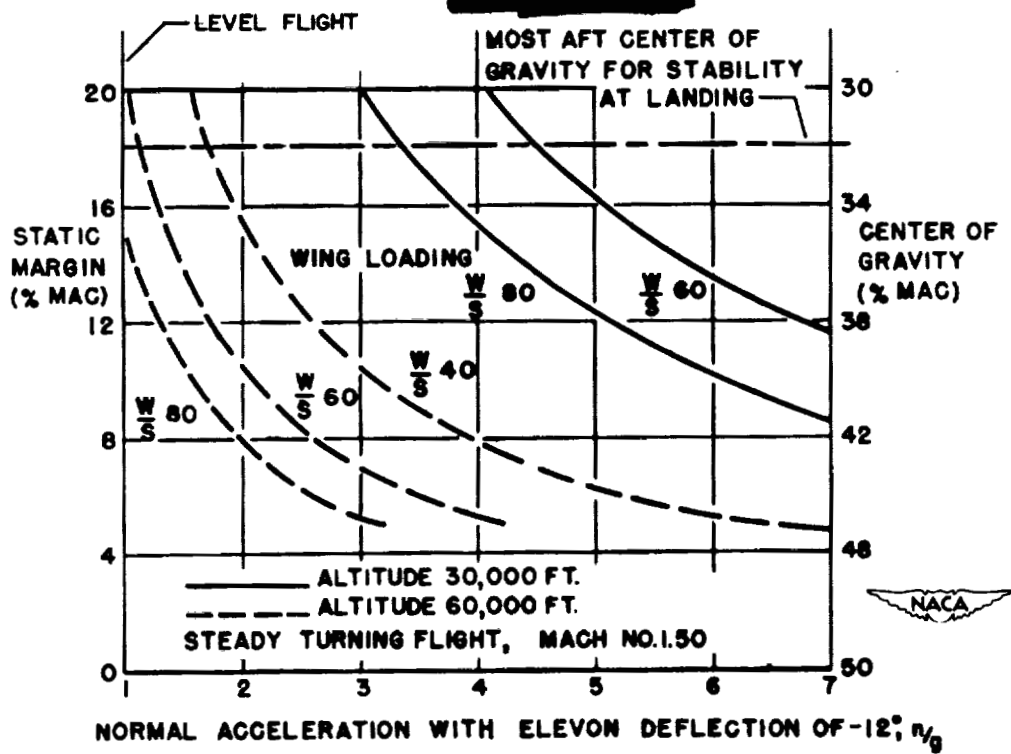


Figure 9.- The effect of static margin on the estimated maneuverability of a triangular-winged aircraft at a Mach number of 1.50.

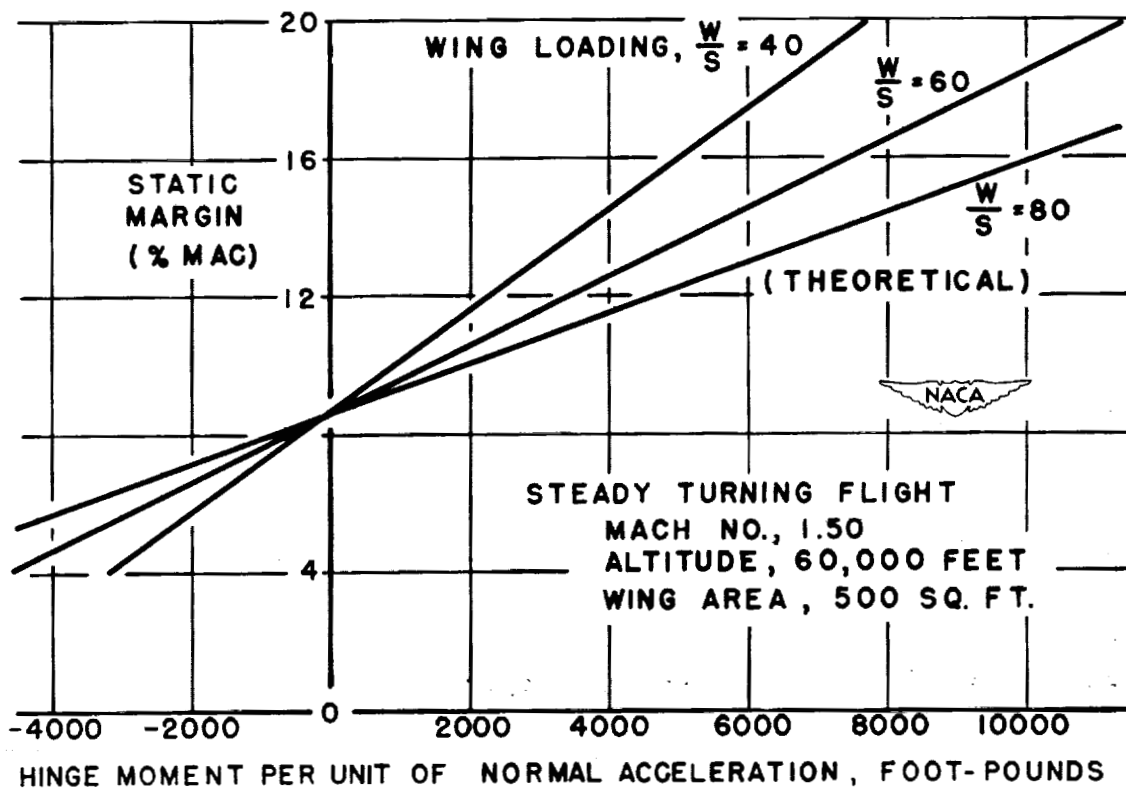


Figure 10.- The effect of static margin on the estimated elevon hinge moment per g of normal acceleration for a triangular-winged aircraft at a Mach number of 1.50.

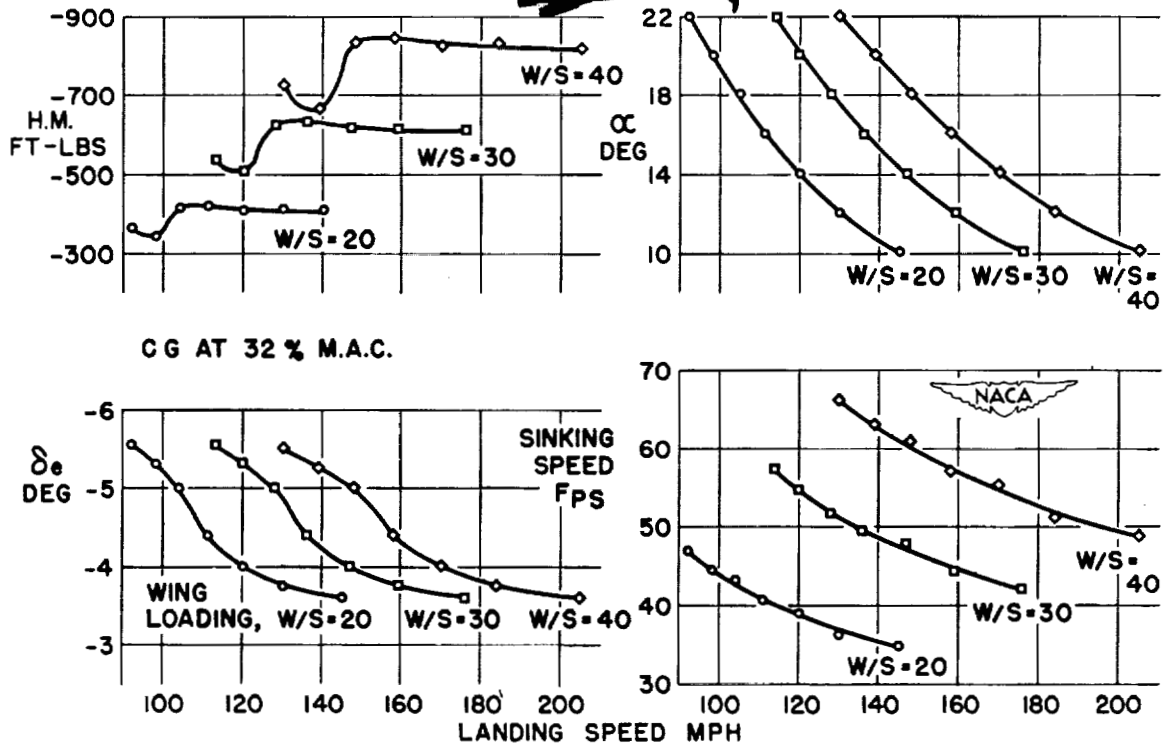


Figure 11.- The estimated landing characteristics of a triangular-winged aircraft with constant chord elevons. Center of gravity at 32 percent M.A.C.

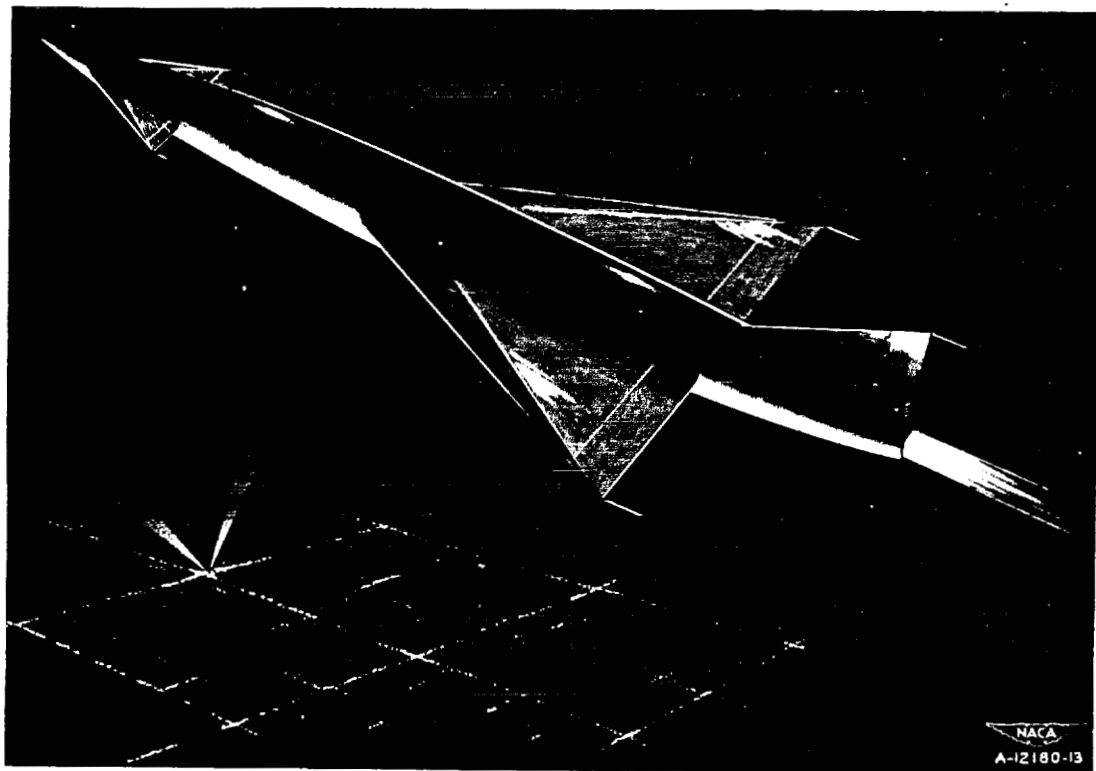


Figure 12.- Interceptor-type aircraft using a triangular wing with a constant-chord control and a trimmer wing.

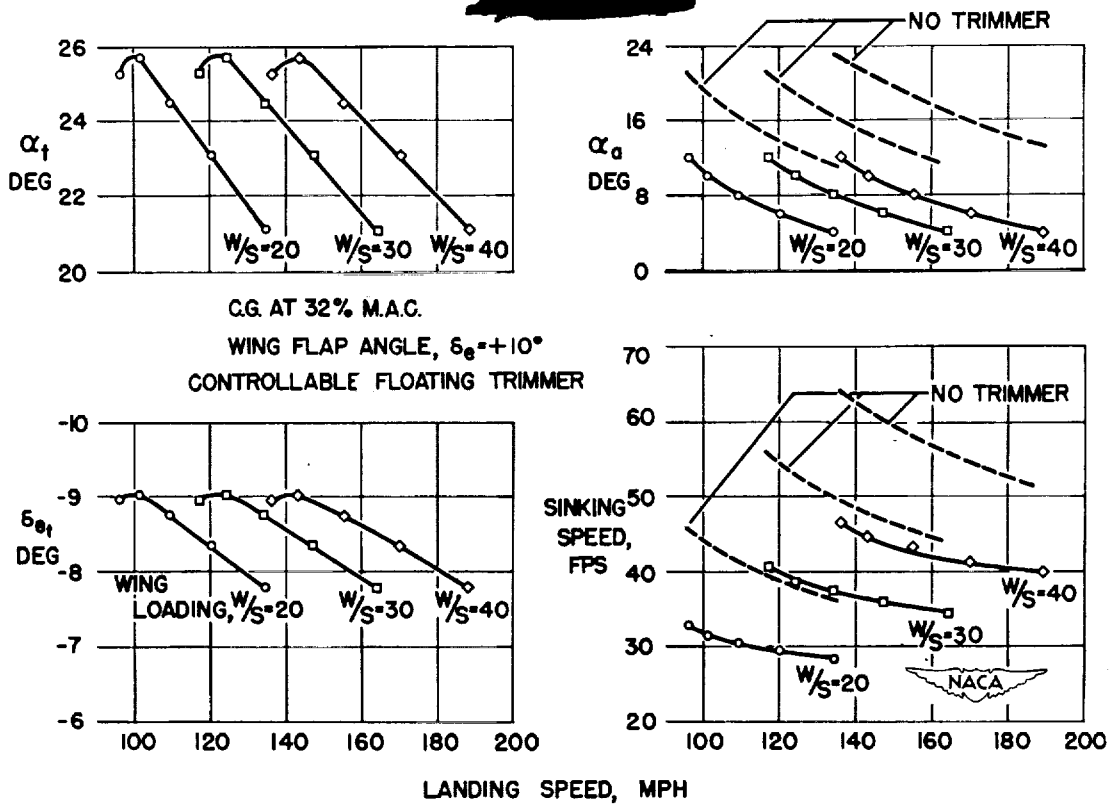


Figure 13.- The estimated landing characteristics of a triangular-winged aircraft equipped with a floating trimmer.

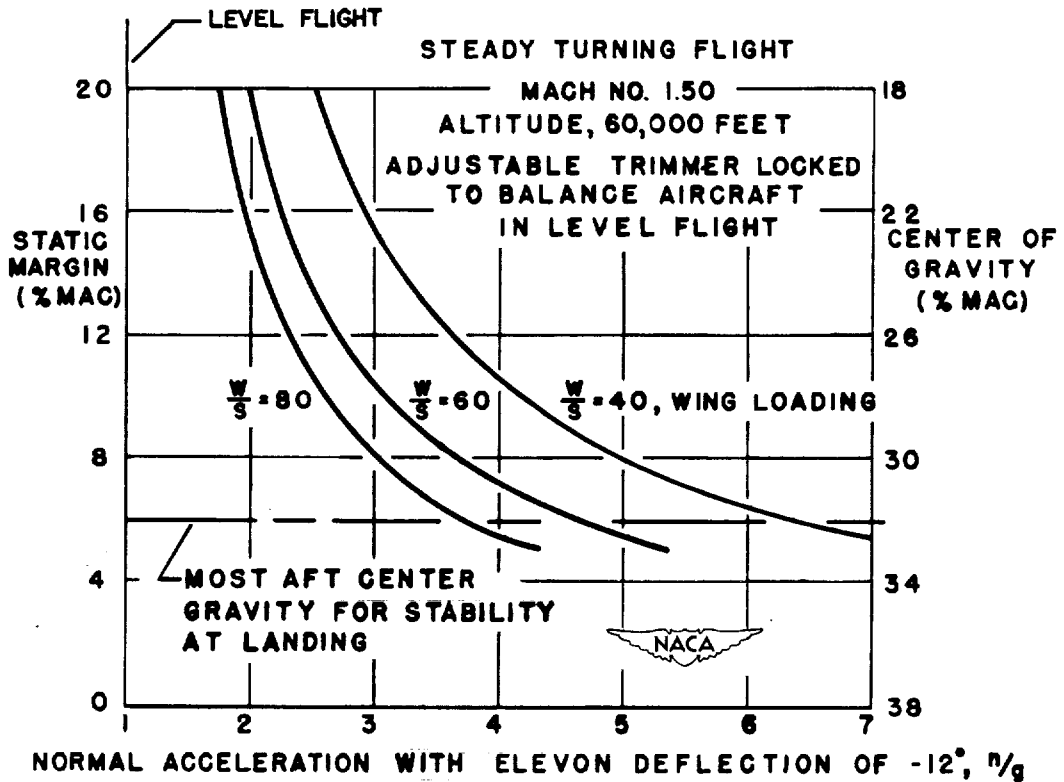


Figure 14.- The effect of static margin on the estimated maneuverability of a triangular-winged aircraft equipped with a trimmer wing. Trimmer locked to balance aircraft in level flight at a Mach number of 1.50.

UNCLASSIFIED

UNCLASSIFIED